Polymer Mediated Growth and Morphology in Thermoplastic Composites

THESIS
SUBMITTED TO THE
UNIVERSITY OF PUNE
FOR THE DEGREE OF
DOCTOR OF PHILOSOPHY
IN CHEMISTRY

BY

C. SAUJANYA

POLYMER SCIENCE & ENGINEERING GROUP
DIVISION OF CHEMICAL ENGINEERING
NATIONAL CHEMICAL LABORATORY
PUNE-411 008, INDIA

NOVEMBER 1998

DEDICATED

TO MY

PARENTS

CERTIFICATE

Certified that the work incorporated in this Thesis entitled "***Polymer Mediated Growth and Morphology in Thermoplastic Composites***" submitted by **Ms. C. SAUJANYA**, was carried out by her under my supervision at the Polymer Science & Engineering Group, Chemical Engineering Division, National Chemical Laboratory, Pune-8. Such material as has been obtained from other sources has been duly acknowledged in the thesis.

S. Radhakrishnan

Dr.S. Radhakrishnan
Research Guide

November 1998
Pune

ACKNOWLEDGEMENTS

I take this opportunity with deep sense of gratitude to record my sincere thanks to my guide ***Dr. S. Radhakrishnan,*** *for his keen interest, valuable guidance, drive towards perfection and constructive criticism during the course of this investigation. The fruitful scientific discussions with him have taught me the method of designing, executing and analysing the problems in a true scientific spirit.*

I am very much thankful to ***Ms. A.Mitra, Dr. S.R. Sainkar and Dr. Gopal Pathak,*** *for the instrumental analysis of various samples.*

The assistance provided by the library and drawing office is gratefully acknowledged.

I wish to thank ***Dr. B.S.Rao,*** *for the help rendered during the final stages of this investigation.*

Thanks are due to my close friends and colleagues for the willing co-operation extended to me at various difficult stages of this work.

Last, but not the least, I would like to thank my ***parents, brother and sisters*** *who have enabled me to see the light of this day.*

I wish to thank the ***Director, National Chemical Laboratory, Pune,*** *for permitting me to submit this work in the form of a Ph.D. thesis.*

Financial assistance from the ***Council of Scientific & Industrial Research, New Delhi,*** *is gratefully acknowledged.*

National Chemical Laboratory,
Pune – 411 008.

C. Saujanya

(C. Saujanya)

CONTENTS

LIST OF ABBREVIATIONS

ABS	acrylonitrile-butadiene- styrene
DSC	differential scanning calorimetry
EO	electro-optic modulation
EPDM	ethylene-propylene-diene-monomer
EPM	ethylene- propylene- monomer
EPR	ethylene- propylene rubber
HDPE	high density polyethylene
IR	infrared spectroscopy
ITO	indium tin oxide
LCP	liquid crystalline polymer
MA	maleic anhydride
MC	melt crystallized samples
MFI	melt flow index
MNA	meta nitroaniline
magn.	Magnification
NLO	nonlinear optical property
NYBR	nylon-butadiene-rubber
NY	nylon (grade)
PA	polyamide
PBu	polybutadiene
Pc	polycarbonate
PC	powder blend composite
PE	polyethylene
PEK	polyether ketone
PEEK	polyether ether ketone
PEO	polyethylene oxide
PET	polyethylene terephthalate
PIB	polyisobutylene
PNA	para nitroaniline

POM	polyoxymethane
PP	polypropylene
PPDT	poly(p-phenylene terethalamide)
PPS	polyphenylene sulphide
PS	polystyrene
PTFE	polytetra fluoroethylene
PVA	polyvinyl alcohol
PVAc	polyvinyl acetate
PVDF	polyvinylidieneflouride
SBR	styrene-butadiene-rubber
SBS	styrene-butadiene-styrene
SC	solution crystallized samples
SEM	scanning electron microscopy
SHG	second harmonic generation
TCNQ	tetracynoquinodimethane
TEM	transmission electron microscopy
TGA	thermogravimetric analysis
TTS	triisostearoylisopropyl titanate
WAXD	wide angle X-ray diffraction
wt.	weight

LIST OF SYMBOLS

A	absorbance
A_r	a constant area of the rod
A_v	a constant in the Avrami equation
B	constant
C_i	crystallinity
d	diameter
d(obs)	observed interplanar distance
d(cal)	calculated interplanar distance
D	thickness of the disc
E_c	modulus of the composite
G	linear growth rate
ΔG^*	Gibbs free energy
h	fraction of fibres parallel to the direction of measurement
ΔH	heat of fusion
I_m	intensity at time t=m
I_t	intensity at time t=t
I_o	intensity at time t=0
k	Boltzmann constant
l_c	critical fibre length
L	crystallite size
l_s	lattice parameter of the substrate
l_g	lattice parameter of the growing media
l/d	length to diameter ratio
m	mass fraction of a material
n	Avrami exponent
N	nucleation rate
N_d	nucleation density
R	gas constant
t	time

$t_{1/2}$	crystallization half time
T	temperature
T_c	crystallization temperature
T_g	glass transition temperature
T_m	crystalline melting point
X(t)	mass fraction of a crystal at time t
β_e	nonlinear electronic susceptibility
δ_l	lattice mismatch parameter
$\Delta\theta$	breadth of the diffraction peak
η	reinforcement efficiency factor
ξ	strength efficiency factor
λ	wavelength
$\Delta\mu$	birefringence of a spherulite
μ_r	refractive index along the radial direction
μ_t	refractive index in the tangential direction
ϕ_m	volume fraction of the matrix
ϕ_f	volume fraction of the filler/fibre
ψ_c	area under the crystalline curve
ψ_a	area under the amorphous curve
σ_c	tensile strength of the composite
σ_m	tensile strength of the matrix material
σ_θ	tensile strength of the randomly oriented composite
σ_c'	longitudinal strength of a continuous fibre composite
τ_m	shear strength of the matrix
ε_m	dielectric constant of the matrix
ε_c	dielectric constant of the composite
ω	frequency

LIST OF TABLES

LIST OF FIGURES

Abstract

There has been a tremendous surge of activity in the recent years for synthesis of novel materials through modification of crystal structure, domain size and morphology. The polymer induced crystallization or structure development in composites has become an important area in the context of smart materials, high performance composite, nanotechnology , etc. In the present studies, we have investigated the role of polymer matrix on the structure development in conventional composites such as polypropylene (PP) filled with $CaSO_4$, glass fibres, thermoplastic elastomers and polyester fibres as well as novel composites containing (NLO) crystals.

In all these systems, the matrix plays a very important role in controlling the structure, growth habit and morphology of the crystallites of the additives. Also, these show the effect of additives on the crystallization behaviour of the polymer matrix itself. These various changes in the supermolecular structure give rise to prominent changes in the mechanical, optical and other properties of these composites.

Chapter 1

Introduction

"New high -tech materials are being developed all over the world for wide ranging applications from optoelectronics to space vehicles." New materials technology is being adopted for the improvement of properties in existing materials and better utilization of available resources. One of such techniques is the polymer induced crystallization of additives and matrix mediated growth in composites. The main theme of the present studies is the role of polymer matrix in this type of structure development.

1.1 Importance of Composites

Composites, an important class of engineering materials, are used in a wide variety of applications as there is a considerable scope for tailoring their structure to suit the service conditions together with other advantages such as high strength to weight ratio, low cost, etc. The composite materials combine beneficial properties of its component materials, which is not possible with one- component materials.

1.1.1 Definition of a Composite

Composites can be defined as materials consisting of two or more distinct phases with a recognizable interface or interphase boundary. In other words, it is a combination of two or more materials (reinforcing elements, fillers and composite matrix binder), differing in form or composition on a macroscale. The constituents retain their identities; they do not dissolve or merge completely into one another.

1.1.2 Classification of Composite Materials

The composite materials can be classified broadly by their form or their constituent components. There are mainly three categories of composites.

(a) Natural composite materials: These include wood, bone, bamboo, muscle and other tissues.

(b) Micro composite materials: These comprise of metallic alloys (for example steel), toughened thermoplastics (example impact polystyrene, ABS) sheet moulding compounds and reinforced thermoplastics.

(c) Macro composites (Engineering materials): These include galvanized steel, reinforced concrete beams, helicopter blades etc.

The polymeric composites are mainly micro-composites. The micro-composites may be further classified according to the reinforcement forms into particulate reinforced, fibre reinforced and laminar composites.

(a) Particulate reinforced composites: These include materials reinforced by spheres, rods, beads, flakes and many other shapes of roughly equal axes. The examples of these are polymeric materials incorporating fillers such as glass spheres or finely divided powders, polymers with fine rubber particles, etc.

(b) Fibre reinforced composites: These contain reinforcements having much greater length than their cross-sectional dimensions. They may be continuous (with lengths running the full length of the composite) or discontinuous (of short lengths). These fibres may be unidirectional, cross woven or random. Typical examples are glass fibre reinforced plastics, carbon fibres in epoxy resins, wood (a composite of cellulose in a matrix of lignin), vehicle tyres in which rubber is reinforced with nylon cords.

(c) Laminar composites: These are composed of two or more layers held together by the matrix binder. These have two of their dimensions much larger than the third. Wooden laminates, plywood and some combinations of metal foils, glasses, plastics, film and papers are laminar composites. Some ceramic and metallic composites also fall into this category.

Composites are sometimes also classified according to the nature of the matrix. Thus, composites can be classified as metal, ceramic or polymer matrix based. Or else, composites can be called inorganic or organic matrix based. Metal matrices of iron, nickel, tungsten, titanium, aluminium and magnesium are generally used for high temperature usage in oxidising environment. Ceramic matrices are often used with carbon, ceramic, metal and glass fibres. These are used in rocket engine parts and protective shields. Glass matrices are mostly reinforced with carbon and metal oxide fibres. Heat resistant parts for engine, exhausts and electrical components are their primary applications. Carbon matrices with carbon whiskers or fibres as reinforcement are used for desired properties. Carbon in the form of diamond and graphite have a high heat capacity per unit weight and therefore selected as ablative materials.

Polymer matrix composites are the subject of the present investigations and hence are discussed in greater detail in the following paragraphs.

Polymers are a logical choice for matrices in many applications as these are easily processable and offer good mechanical and dielectric properties. Although, polymers have lower softening points than metals, it is because of the relatively low processing temperatures that many organic reinforcements can be used. Natural and synthetic fibres including silk, cotton, wool, polyester and various inorganic, non-metallic fibres of glass, carbon, asbestos and oxides are widely used in industrial and automotive applications. The polymer matrix can

be thermoplastic or thermoset. However, thermoplastics are often considered superior to thermosets because they are easier to handle, have better ductility, hot-wet performance, damage tolerance and can be recycled.

Fibrous fillers are the most common forms of reinforcement in reinforced thermoplastics. A spherical filler particle or a particulate filler with reasonable sphericity has an aspect ratio (length to diameter ratio) of 1. On the other hand, fibres are characterised by high aspect ratios. The main functions of the fibres are to carry most of the load applied to the composite and provide stiffness. The fibres used may be continuous or discontinuous. Aligned fibres give better reinforcement efficiency and high modulus.

For a composite with uniaxially oriented continuous fibres and a uniform elastic matrix tested in the direction of orientation, the modulus or tensile strength of the composite (polymer matrix and reinforcement fibres)[1-3] are given by

$$E_c = E_f \phi_f + E_m (1-\phi_f) \tag{1.1}$$

$$\sigma_c = \sigma_f \phi_f + \sigma_m (1-\phi_f) \tag{1.2}$$

where E_c, E_m and E_f are the moduli of composite, matrix polymer and reinforcing fibres respectively; σ_c, σ_m and σ_f are the corresponding tensile strengths; ϕ_f = volume fraction of fibre, ϕ_m $(=1-\phi_f)$ is the volume fraction of matrix polymer. Equations 1.1 and 1.2 can be generalized to accommodate the effect of orientation by introducing an alignment factor (η) of reinforcement efficiency factor as

$$E_c = \eta E_f \phi_f + E_m(1-\phi_f) \tag{1.3}$$

$$\sigma_c = \eta \sigma_f \phi_f + \sigma_m(1-\phi_f) \tag{1.4}$$

The values of reinforcement efficiency factor for different type of fibre orientation are given in Table 1.1.

Table 1.1 Alignment factor or orientation efficiency factor for different cases.

Orientation type	Efficiency factor
Unidirectional parallel to stress	1
Unidirectional at angle θ to stress	$\cos^4 \theta$
Bidirectional fraction (P) parallel to stress	P
Random distribution in a plane (two dimensional)	3/8
Random distribution in three directions	1/5

Where θ is the angle between the fibre and direction of stress

For discontinuous fibres of finite length[2,4] the load is transferred from the matrix to the fibre via the interfacial shear stress at the polymer/fibre interface.[2,4-6] Thus, the actual fibre length and the interfacial adhesion between the fibre and matrix become important parameters. The tensile strength of a composite with randomly oriented discontinuous fibres has been given by Chen[5] as

$$\sigma_\theta = 2\tau_m / \pi \ (2 + \ln \xi \sigma_c' \sigma_m / \tau^2_m) \qquad (1.5)$$

Where σ_θ is the tensile strength of the randomly oriented composite, τ_m is the shear strength of the material at the weakest interface, ξ is the strength efficiency factor (= 1 for continuous fibre composite), σ_c' is the longitudinal strength of a continuous fibre composite, and σ_m is the strength of the matrix material.

For fibres of finite length, stress is assumed to be transferred from the matrix to the fibre by a shear transfer mechanism. The critical fibre length (l_c) which is the shortest length of the fibre necessary for the stress in the fibre to build up to the value equal to the tensile fracture stress[7] of the fibre is given by

$$l_c = (d \sigma_f / 2 \tau_m) \qquad (1.6)$$

where d is the diameter of fibre, σ_f is the tensile strength of the fibre and τ_m is the strength of bond between fibre and matrix (often assumed equal to the strength of matrix polymer).

For example, the critical fibre length for discontinuous glass and carbon fibre reinforcement is typically about 1-2 mm.[8] Ample practical data are available on the effect of fibre length on tensile strength, modulus, impact, shear strength, mould shrinkage and other properties of various reinforced thermoplastic materials.[3,8-11]

For mechanical and electrical properties of the composites, the shape and size factors of the fillers play a significant role. For example the Young's modulus (E_c) of the composite[12] is given by

$$E_c = E_m [1+ 0.67 (S\phi_f) + 1.62 (S\phi_f)^2] \quad (1.7)$$

where E_m is the modulus of the matrix,ϕ_f is volume fraction of the filler and S is the shape factor or aspect ratio of the filler. Similarly, tensile strength also depends strongly on the aspect ratio. Figure 1.1 summarizes these various results. Large improvement in this property is expected for high aspect ratio filler.[13-15] Similarly, the dielectric constant (ε_c) is given by Nielsen's formula[16]

$$\varepsilon_c = \varepsilon_m [1 + (PQ\phi_f / 1-Q (1-\phi_f)] \quad (1.8)$$

where ε_m is the dielectric constant of the matrix polymer, P and Q depend on the aspect ratio, packing (hexagonal, square or other types) and dielectric constant of the filler and ϕ_f is the volume fraction of the filler.

1.1.3 Applications of Composites

The composites have various applications. For example, in aircraft, automobile, chemical, furniture and equipment, electrical and sports, etc. They exhibit different properties such as high strength and stiffness, improved torsional stiffness, outstanding corrosion resistance, good dimensional stability, impact and damage tolerance characteristics, unique coefficient of thermal expansion and significant weight savings and lastly easy portability. Many thermoplastic composites are made up of semicrystalline polymers, which can develop different types of morphological features. These also affect the properties of the composites.

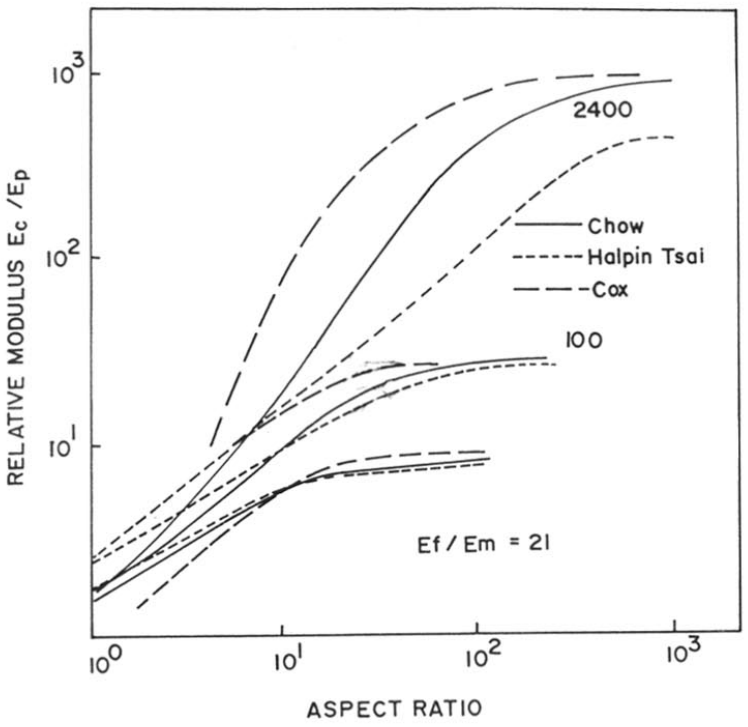

Figure 1.1 Effect of morphology on properties

1.2 Crystallization and Morphology in Semicrystalline Polymers

1.2.1 Morphology of Semicrystalline Polymer

The early studies on the crystalline structure of polymers carried out using X-ray diffraction indicated the existence of both crystalline and amorphous regions. As the chain molecules were much longer than the crystalline micelle, it was assumed that the polymeric chain had to take part in several crystalline and non-crystalline regions. This first concept underwent a serious revision in 1957, with the studies of single crystals of PE crystallized from dilute solutions. It was found that these were composed of thin flat platelets (lamellae) about 100 Å thick and often many micrometers in lateral dimensions.[17-19] The electron diffraction measurements indicated that the polymer chains were oriented normal to the plane of lamellae. Since the polymer molecules were 1000 Å long and the lamellae only about 100 Å thick, it was concluded that they must be folded as shown in Fig. 1.2. This gave the folded chain model for development of crystalline ordered structure in the polymers.

The evolution of the supermolecular order is depicted in Fig. 1.3. The primary lamellae formed initially grow into branched crystals, which further form the spherulitic structure in the polymer. Most semicrystalline polymers exhibit the spherulitic morphology.

1.2.2 Epitaxial Crystallization

The word epitaxy was introduced by Royer from the Greek word epi (which means 'on') and taxos (which means 'organized deposition'). Epitaxy is the oriented growth of a crystal upon a foreign crystal that resembles the deposit structurally. For example, the epitaxial crystallization of synthetic polymers on inorganic substrates has been reported before.[20] The epitaxial crystallization of guest materials on polymeric substrates is discussed in section 1.6.3.

1.2.3 Transcrystallinity

When fibres are embedded in a thermoplastic melt, they may act as nucleants for the growth of spherulites. If there are many nucleation sites along a fibre's surface then the resulting spherulitic growth will be restricted in the lateral direction. This results in a columnar layer of crystals known as transcrystallinity, which surrounds the fibre. Transcrystalline morphology has been explained with examples in the later section (1.4).

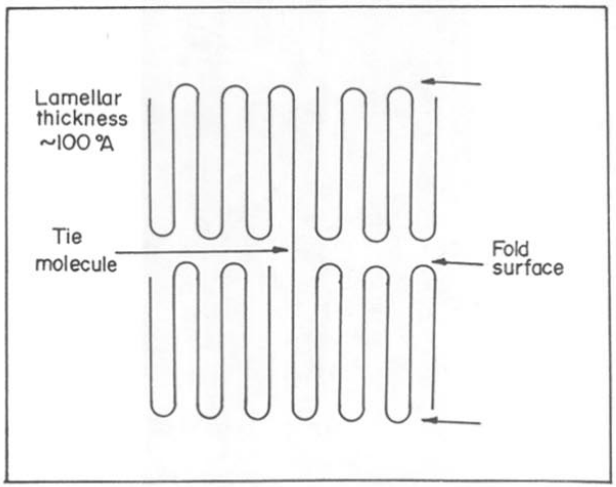

Figure 1.2 A chainfolded conformation (schematic).

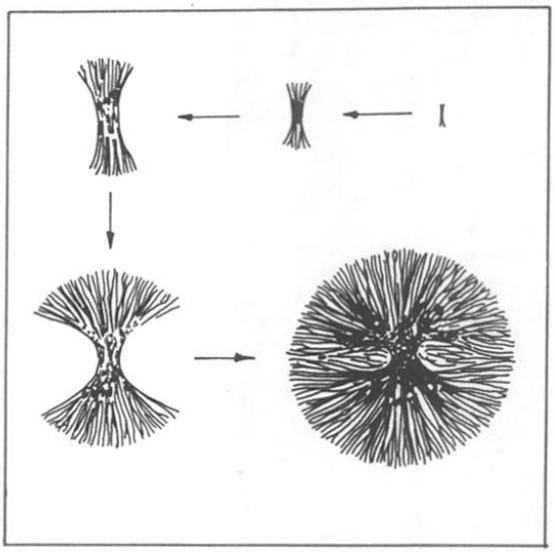

Figure 1.3 Stages in the formation of a spherulite.

1.2.4 Birefringence of a Spherulite

Under a polarising microscope, a spherulite shows a central dark cross (maltese cross) with wings coincident with respective planes of polariser and analyser. The birefringence of a spherulite is defined by equation

$$\Delta\mu = \mu_r - \mu_t \qquad (1.9)$$

where μ_r and μ_t are the refractive indices along the radial and tangential direction of the spherulite respectively. Depending on the birefringence, spherulites are called optically positive or negative.[21] The sign of birefringence of the spherulites can be determined by using gypsum plate located diagonally between crossed poles. A spherulite is positive when its first and third quadrants are blue and second and fourth ones are yellow whereas a reverse arrangement of quadrants is observed for a negative spherulite.

1.2.5 Factors Affecting Crystallization Process

Polymers with ordered stereo-regular structures with no bulky side groups and a minimum of chain branching will usually crystallize. The following sources of irregularity discourage crystallization:

(a) random copolymerization

(b) bulky side groups

(c) chain branching

(d) lack of stereo-regularity such as tacticity

(e) certain geometrical isomers

Orientation is also a dominant feature, which affects crystallization. Crystallization can be induced by orientation as seen in polymers at large elongations where the alignment of the chain occurs. This was first observed in case of natural rubber. Orientation can occur in two ways : (i) orientation of the polymer chains in the melt; for example, on extrusion from a nozzel or (ii) deformation of the crystallized polymer by stretching/drawing. The stretching of already crystallized polymers during fibre and film production is of considerable practical importance where the subsequent orientation can substantially modify the crystalline structure.

1.2.6 Crystallization Kinetics in Semicrystalline Polymers

The crystallization of polymers proceeds through a series of stages: melt, nucleation, lamellar growth, spherulite growth and aggregation growth. The melt crystallizes when the system is cooled below the equilibrium melting point (T_m) to the crystallization temperature (T_c) which is usually midway between T_g and T_m ($T_g < T_c < T_m$). The difference $\Delta T = T_m - T_c$ is a measure of supercooling that in turn depends on the cooling rate and the nucleation mechanisms.[22-24]

Nucleation: Primary nucleation is a process by which a new phase is initiated within a parent phase. Under isothermal conditions, the number of nuclei is either constant (athermal nucleation) or increasing linearly in time (thermal nucleation). There are various types of nucleation processes.

(a) Homogeneous nucleation: This occurs by statistical fluctuations in the parent phase i.e. chains in a melt are considered to be in a dynamic equilibrium. This involves continuous aggregation and disaggregation of chains until the aggregate formed exceeds a certain critical size, which leads to nucleation. After this, further growth can take place and aggregate increase in size.

(b) Heterogeneous nucleation: This is catalysed by the presence of heterogeneity. It brings into focus the role of nucleating agents as structure modifiers in polymers. There are substances which when incorporated in the polymer melt promote abundant crystallization. They increase the rate of crystallization leading to shorter processing cycles. In heterogeneous nucleation, the total interfacial free energy of the crystalline embryo is reduced by a foreign phase which already provides a part of the interface to be formed, thus reducing the activation energy and hence the degree of supercooling required for nucleation. The higher the preference of the crystalline phase to adsorb at the foreign phase rather than the liquid phase, the lower is the activation energy for nucleation.

(c) Orientation induced nucleation: This is caused by macromolecular alignment and spontaneous crystallization.

(d) Self nucleation: The term self nucleation was coined by Blundell, Keller and Kovacs[25] to describe nucleation of folded crystals grown from solution on high molecular weight remnants of its own crystals which remained through the dissolution step. In other words, it is the nucleation of a macromolecular melt or solution by its own crystals grown previously in it.

The steady state nucleation rate per unit volume and time can be expressed by

$$N = N_0 \exp(-E_D/RT - \Delta G^*/RT) \quad (1.10)$$

where N_0 is a constant, E_D in the energy of transport in the solid-liquid interface and ΔG^* is the free energy of formation of a stable nucleus. As ΔG^* is a function of the temperature, the nucleation rate is also a function of temperature in accordance with the above equation. The nucleation rate is zero at or above the melting temperature and at absolute zero and reaches a maximum value at an intermediate temperature. Below the melting temperature (T_m) the nucleation rate has a high negative temperature coefficient, thus as the temperature decreases further, the rate increases until it reaches a maximum and then decreases. At temperatures below the maximum, the temperature coefficient is positive as a result of the influence of the transport term.

For most thermoplastic polymers, the spherulite radial growth rate from the melt is linear and it is usually described by

$$G = dr/dt \quad (1.11)$$

where r is its radius.

1.2.7 Overall Crystallization Process

For crystallization to occur, considerable molecular mobility is necessary. Thus, the temperature range for crystallization is between the glass transition temperature T_g and the crystalline melting point T_m. The overall formation rate of crystals is equal to the product of the nucleation rate N and the growth rate G. The growth rate is diffusion controlled and is maximum just below T_m. The nucleation rate is maximum just above T_g. Therefore, the overall crystallite formation rate is maximum at temperature about half way between T_g and T_m as shown in Fig. 1.4. Increasing the molecular mass of a polymer decreases its rate of crystallization because the diffusion rates in the melt/solution are reduced. In many polymers, the progress of crystallization from the melt is described by the Avrami equation.[26,27] This takes into account the different nucleation mechanisms and the impingement of crystals during the later stages of crystallization. It is expressed as

$$X(t) = 1 - \exp(-A_v t^n) \quad (1.12)$$

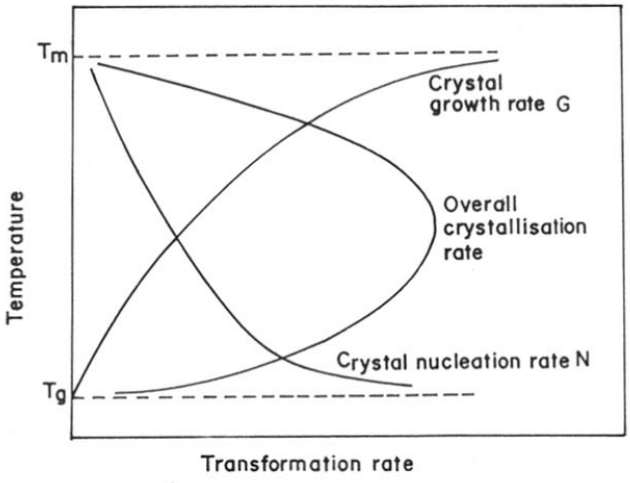

Figure 1.4 Plots showing the growth rate, the nucleation rate and the overall rate of crystallization verses temperature for a polymer.

X(t) is the mass fraction of crystals at time t, A_v is a constant describing the rate of crystallization and n is the Avrami exponent. In general n and A_v characterise the nucleation type and crystal growth geometry.

Table1.2 Theoretical values of constants n and A_v in the Avrami equation (eqn.1.12) for different morphologies and nucleation mechanisms

Crystal growth shape	Nucleation mode	Avrami exponent (n)	Avrami constant (A_v)
Rod	Heterogeneous	1	N_dGA_r
	Homogeneous	2	$N_dGA_r/2$
Disc	Heterogeneous	2	πN_dG^2D
	Homogeneous	3	$(\pi/3) N_dG^2D$
Sphere	Heterogeneous	3	$(4\pi/3) N_dG^3$
	Homogeneous	4	$(\pi/3) N_dG^3$
Sheaf	Heterogeneous	5	-
	Homogeneous	6	-

Where A_r is a constant area of the rod; D is the thickness o f the disc; G is the linear growth rate, N_d is the nucleation density; A_v is the nucleation rate and n is the Avrami exponent.
The half life of bulk crystallization process is given by

$$t_{1/2} = (\ln 2^{1/n}/ A_v) \qquad (1.13)$$

It should be noted that the crystallization process characterised by the Avrami equation with constant coefficient (n) is termed primary crystallization and is associated with the growth of spherulites at the expense of matrix. The crystallization that takes place over and above the Avrami value is termed secondary crystallization. Primary crystallization is steeply temperature dependent and also on molelcular weight of the polymer. The secondary

crystallization is associated with two processes (i) additional crystallization within the boundaries of the spherulites (ii) crystallization of the material trapped between mature spherulites. The former occurs by incorporation of intra-spherulitic non-crystalline regions into existing or new crystals.

1.3 Crystalline Structure and Crystallization kinetics in Polypropylene (PP)

1.3.1 Crystalline Structure

Isotatic polypropylene (iPP) is a semi-crystalline polymer. Its high tendency for crystallization is due to its regular chain structure. It is an important polymer not only commercially but also scientifically because of its polymorphic behaviour and wide range of properties.

At the crystal lattice level, iPP exhibits different morphological forms: Monoclinic (α) form, hexagonal (β) form, triclinic (γ) form and the quenched mesomorphic form. Some reports have also proposed the existence of a δ form having a high percentage of amorphous material. Among these crystal structures, the monoclinic (α) form is by far the most common one that is usually formed in melt crystallized and solution crystallized iPP samples. The α, β, and γ form can be identified using specific peaks seen in the X-ray diffraction pattern as shown in Fig. 1.5.

The iPP exhibits a variety of spherulite types classified typically on the basis of the sign of the birefringence. The first attempt to describe the different morphologies of melt crystallized iPP was carried out by Padden and Keith in 1959.[28] When iPP was crystallized in the temperature range 110 - 148° C, five distinct types of spherulites exhibiting different optical properties were identified (Table 1.3). Among these, three types exhibiting slightly positive, negative and mixed birefringence revealed an X-ray diffraction pattern typical of α iPP crystal form. The other two types which are less frequent and display negative birefringence revealed an X-ray diffraction typical of β iPP crystal form. Among the latter two types of spherulites, one is a radical type while the other is a ringed type of spherulite.

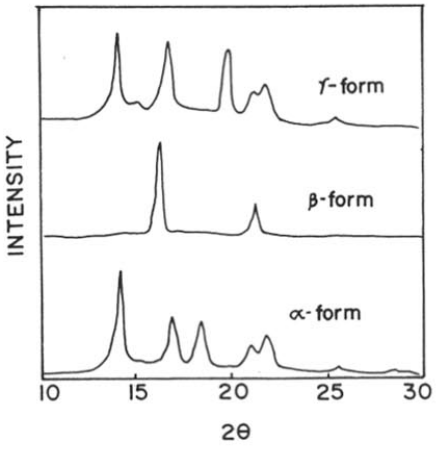

Figure 1.5 WAXD patterns for different forms in iPP crystals

Table 1.3 Different types of polypropylene spherulites

Type	Crystal phase	Spherulite birefringence	Crystallization temperature range (°C)
I	α	Weakly positive	< 134
II	α	Weakly negative	> 138
Mixed	α	Mixed	134 - 138
III	β	Negative	110 - 128
IV	β	Negative	128 - 132

(a) The α form of PP:

The predominant crystal structure of pure iPP at atmospheric pressure is the monoclinic α structure.[29] The unit cell parameters of monoclinic α iPP were calculated by Natta and Corradini in 1960. It contains four 3-fold helical chains with a = 6.65 Å, b = 20.96 Å, c = 6.5 Å and β = 99.3°C. The melting point of iPP is between 168-174°C.

(b) The β form of PP:

This form of iPP crystallizes in a hexagonal[29-32] unit cell with a = 19.08 Å, c = 6.49 Å, γ = 120° and α = β = 90°. The (300), (301) reflections in X-ray diffraction patterns are assigned to these two d spacings. The melting point of β spherulite is between 150-154°C. The β form in iPP can be obtained through rapid quenching, zone solidification, crystallization in a temperature gradient or through use of selective nucleating agent such as quinacridone dyes or triphenodithiazine. The transition of β form to α form can be carried out by various ways. The β form in iPP can be transformed into the α form by drawing at high temperatures. Melt crystallization at elevated temperature close to the melting temperature of the bulk samples also transforms the β form to the α form.

c) The γ form of PP:

This form of iPP was first noted during the 1960s and can be generated by several methods. It is largely produced by crystallization at elevated pressures.[33,34] The second route to γ iPP is from the crystallization of low molecular weight fractions produced by pyrolysis[35,36] or by special synthesis[37]. Yet another route to γ iPP[30] is by crystallization from the melt of stereo-block fractions extracted from a commercial homopolymer using petroleum ether or xylene extraction in the 35-70°C temperature range. The fourth route is crystallization of copolymer of iPP with small amounts (4 -10%) of ethylene or butene[38]. The γ form crystallizes in orthorhombic[39,40] structure with a = 8.54 Å, b = 9.93 Å, c = 42.41 Å. It shows negative birefringence. The melting point of γ form is reported in the range of 125 to 150°C. The transformation of γ form to α form occurs when it is quenched from very high temperatures.

The studies of Marrow and Newman[41] of low molecular weight (≈ 1260) show that solution crystallized iPP gives rise to needle like crystals with the presence of both α and γ form structures. A common crystallographic direction was found in both phases i.e. b* direction was conformed to be shared α and γ phase crystals when γ lamellae crystallized epitaxially on the lateral edges of iPP parent lamellae. This was proved from electron diffraction patterns.

(d) The smectic form of PP:

The smectic form has an intermediate crystalline order[29]. This mesomorphic form was first named by Natta et al. and was later assigned different names. Miller suggested that the order existing in this form might be of the type described in general terms by Hosemann as paracrystalline[42,43]. This term was also used by Zannetti et al.[44,45] Wonderlich and Grebowicz who proposed the term Condis crystal[46] which means conformationally disordered crystal. It is prepared by quenching thin sheets of iPP from the melt using ice water. Two broad maxima in the X-ray diffraction- one at 14.8° and the other at 21.2° (2θ, Cu Kα) are assigned to this mesomorphic form.

There are reports also on the existence of a δ form [47] of iPP having a high percentage of amorphous material.

1.3.2 Crystallization Kinetics in Polypropylene

Avrami equation is often used to describe isothermal polymer crystallization kinetics. Isothermal crystallization is a process by which a polymer is cooled rapidly from its melting temperature to a constant temperature (T_c) that is below the melting but above the T_g. Over time, the polymer transforms (crystallizes) from a liquid to a solid. The time needed for this process is determined by the Avrami equation as mentioned in section 1.2.7. For example, PE crystals are two dimensional. The value of n can be changed from 1-4 by molar mass nucleation and secondary crystallization.[48,49] For iPP which has a three dimensional spherulitic crystal growth, the value of n is rather stable. Experimental data gives n~ 3. Analysing iPP's mass fraction of crystallinity, Hoshino et al.[50] reported values of 4 for n at low conversion to less than 2 for n at high conversion. In most cases, the isothermal crystallization kinetics are discussed using a constant 'n' value. The equation accurately fits the experimental data only during the early stage of the crystallization process and unsuccessfully describes the entire process because it does not account for the secondary crystallization. Some have tried to improve the Avrami equation. Gordon and Miller introduced a model in which the crystalline solids were considered single crystal lamellar growing by a chain folding mechanism to explain the observed kinetics of PE.[51] Miller explained the fractional values of the Avrami exponent in terms of constant growth of spherulites followed by further crystallization within the spherulites which obeyed a first order law[52]. Other researchers have also studied the secondary crystallization[51,53,54] Recently, Perez-Cardenas et al[54] established a model to obtain the Avrami equation by considering the primary and secondary crystallization.

1.4 Effect of Additives on Morphology and Properties of PP

Fillers have been used as additives for plastics in order to reduce the cost, improve some properties as well as impart some special attributes to the product. In filled semi-crystalline thermoplastic polymers, both the polymer as well as filler contribute to the desirable properties of the composite. The filler can be solid, power -like, fibrous or laminar in shape. In a few cases, the filler may possess different crystalline phases as for example, anatase and rutile forms of titanium dioxide, calcite and vaterite forms of calcium carbonate. In the past the additives such as pigments and particulate fillers were routinely added to polymers to impart colour or to reduce the cost of the product. The morphology and properties of polymers

can be modified by a variety of additives i.e. mineral fillers such as talc, calcium carbonate, wollastonite, mica, kaolin, etc. These mineral fillers show reinforcing effect, nucleation of certain crystalline form, and even epitaxial growth/transcrystallinity in PP. Detailed studies of the effect of additives on the polymers have shown that these additives can themselves affect the crystallization and induce structural or morphological features, which can produce modification in many properties such as impact and mechanical strengths.

Talc is considered as reinforcing filler due to its plate like form or high aspect ratio. It is also an active nucleant in polyolefins. Under favourable conditions, the polymer-filler interaction leads to epitaxial crystallization. The epitaxial polymeric overgrowth is prominent in polyethylene containing talc.[55] When PP is filled with talc, its rigidity, heat distortion temperature, tensile and flexural strengths and thermal conductivity increases while its thermal expansion coefficient, mould shrinkage and impact strength decreases because of flaky shape and nucleation ability of talc particles.[56]

The influence of polymer orientation especially with fillers of anisometric shape was investigated by Rybnikar.[57] In PP-talc, both the crystals and anisometric talc sheets were preferentially oriented. Unlike PP, the orientation of talc particles in the composite remains practically unaffected even at temperatures far above the PP melting point because of high melt viscosity. On cooling, PP melt crystallized on oriented talc sheets in an ordered fashion due to the high talc nucleation efficiency and far reaching orientation action. Calcite[58] and mica[59] also have a slight nucleation effect on PP crystallization. Their particles are oriented in the PP matrix but they are unable to produce an oriented PP structure upon cooling the molten composite.

During the investigation of crystallization, nucleation and morphology in PP containing calcite[60], the calcite particles increased the number of heterogeneous crystallization nuclei, which resulted in a high crystallization rate. The addition of 10% $CaCO_3$ particles led to an increase in the density of heterogeneous nuclei from about 10^5 to $10^6/cm^3$ at $T_c = 138^{\circ}C$. Thus, a small fraction of filler particles acted as nuclei without influencing the crystal structure of PP which was the stable monoclinic α modification. Morphological studies examining the PP-calcite interface demonstrated the tendency of PP to epitaxial order in parallel lamellae growing out from the calcite cleavage face oriented in significant substrate crystallographic directions. The studies on the preparation and thermal conditions of manufacture of filled compositions based on β PP showed that chalk induced a β phase in PP with a weak α

nucleating activity while talc showed a strong α nucleating activity. However, the chalk filled compositions recrystallized into the α modification during drawing thus showing high tensile strength than the corresponding talc filled composition.

Calcium carbonate is available in various forms such as fibrous, needles, whiskers, etc. The whiskered variety[61] of $CaCO_3$ exists as single crystals in a filament form. When nylon-6 was filled with such $CaCO_3$ whisker (diameter of 0.2 - 10 μm and length of 10-30 μm) in the ratio 70 is to 30, excellent mechanical properties were obtained. PP filled with whiskers having diameter 0.5 - 4 μm and length 10-100 μm showed excellent improvements in flexural strength and impact strength.

Radhakrishnan et al.[62] have reported large changes in the crystallization rate and spherulite size for PP filled with $CaCO_3$. The use of stearic acid in PP-$CaCO_3$[63] prevented particle agglomeration and acted as a plasticiser for PP thus increasing the ductility of the matrix. There are also various reports on the use of maleated PP[64] for the enhancement of interfacial adhesion and good mechanical properties.

The mineral wollastonite has also been used as a filler for plastics. It has been incorporated into polymers such as nylon 6 and 66 to produce composites with improved properties.[65] In the case of nylon 6 filled with wollastonite, the tensile modulus of the composite, containing silane coated acicular wollastonite, increased by 122% with respect to unfilled nylon 6. It has improved the impact strength of nylon 6. Further nylon 66 - wollastonite offered advantages of better mechanical and thermal properties compared to nylon 6 - wollastonite composite. Some reports[66] indicate that the use of azidosilane coupling agents substantially increase the tensile and flexural strengths of wollastonite containing composites. SEM of fracture surfaces of PP-wollastonite[67] prepared by silane treatment show a good adhesion between the wollastonite and the PP matrix. Fibre pullout was seen in the composite without silane treatment.

Jasvela et al.[68] have also studied the mechanical properties of PP-wollastonite. They observed that at 25-30wt.% wollastonite improved the hardness, stiffness, flexural strength and flexural modulus of PP but caused small decreases in impact and tensile strength at higher filler content level which could be due to poor interfacial adhesion.

A large amount of work has been reported on the structure and properties of PP-mica composites. Xavier and Sharma[69] while studying the structure and morphology of PP-mica composite observed the occurrence of transcrystallinity in PP in presence of mica flakes.

Transcrystallinity or the columnar growth has been described in section 1.2.3. These authors also studied the effect of coupling agent and the influence of transcrystallinity on the interfacial bonding between the polymer and mica. The SEM of tensile fracture surface of 50% titanate coated mica showed flake pullout thus indicating poor interfacial bondage between mica coated TTS (triisostearoylisopropyl titanate) and PP. The optical micrographs revealed transcrystalline growth along the surface of mica flakes for both uncoated mica as well as that coated with titanate coupling agent. A recent investigation by Garton[70] showed that when mica was treated with silane coupling agent, the nucleation effect was greatly diminished and no transcrystallinity was observed. On the other hand, the uncoated mica was found to induce transcrystalline morphology. Boira and Chaffey[71] found that interfacial bondage was non-existent when transcrystalline morphology was seen. However, when mica was treated with silane coupling agent, the interfacial bondage was extremely good with no transcrystallinity. Thus, although there was transcrystalline structure with both coated as well as uncoated mica, the interfacial bondage was been found to be poor which could be due to low forces of interaction between the polymer and mica. In case of mica coated with silane coupling agent, no direct link seemed to exist between the disapperance of transcrystallinity and the improvement in the thickness of the interfacial region. Busigin et al.[72] while studying the injection moulded PP-mica specimens observed an increase in flexural and tensile modulus in proportion to the aspect ratio of the filler. The modulus varied over a range from 30 to 60 Gpa to a maximum of 8 GPa.

Amongst the various fillers, glass fibres are the most extensively used and studied. Misra et al.[73] studied the transcrystallinity in PP/glass fibre composites during injection moulding. The observed transcrystalline regions in the injection moulded samples were attributed to the availability of sufficient inherent internal stresses. Moreover, an increase in fibre concentration was found to enhance transcrystallinity. This indicated that internal stresses increased with increasing fibre population.

Morphological aspects of β transcrystalline interphase in glass reinforced PP where glass fibres were coated with quinacridone pigment have been studied.[74] IR dichroism confirmed the anisotropy in mechanical properties of the directionally solidified samples in the β form. The anisotropy was rationalized using crystallization, kinetics argument.

There are many reports on the mechanical properties of glass reinforced PP composites but only a few on the nucleation and crystallization behaviour of PP in glass filled PP

composites. It should be noted that due to high aspect ratios, glass fibres impart great mechanical strength to a polymer composite. Iroh et al.[75] studied the crystallization behaviour and mechanical properties of glass reinforced PP. The short glass fibres nucleated the PP matrix to the extent that the crystallization and morphology of the matrix differ appreciably from the homopolymer. The ultimate strength and the Young's modulus of PP also increased in presence of short glass fibre. Devaux et al.[76] investigated the non-isothermal crystallization of glass fibre and also jute fibre reinforced PP. It was found that in the presence of jute fibre transcrystalline morphology was obtained. However, when the jute fibres were covered by silicon oil, no transcrystalline phase was observed. In case of glass fibre reinforced PP, subjecting the composite to shear stress during crystallization resulted in a superstructure similar to transcrystallization adjacent to the fibre. Both glass and jute fibres acted as nucleating agents for PP and increased the rate of crystallization. Fernanda et al.[77]studied the structure development of wood fibre in PP using maleated PP and silane treatment. Maleated PP gave improved adhesion and caused a significant increase in strength and modulus. The use of A 172 silane treatment improved adhesion still further.

Similarly, transcrystalline phase has been reported to occur in PP crystallized in contact with various other fibres such as carbon[78], aramid[79], kevlar[80] and inorganic fibre basalt[81], copper fibre[82] and organic fibre cotton[83], etc.

Thus, it can be concluded that the effect of filler/fibre on PP is determined by the characteristics of the filler such as shape of the particles, particle size and size distribution, surface area, particle packing, chemical composition and so forth. This can give rise to different morphological features, which depend not only on the characteristics of the filler and its surface treatment but also on the processing parameters. These in turn modify the various properties of the composites. Orientation of fibres also play a role in the modification of properties.

1.5 Novel Composites

As compared to conventional materials such as particle filled, fibre reinforced or glass reinforced polymers, etc., some composites contain very fine domain size of the dispersed phase giving rise to better flexibility and optical properties. Some other composites can contain two materials dispersed in a third matrix material resulting in synergistic improvements in properties. Such new types of composites are termed 'novel composites'.

One of the routes to prepare novel composites is by polymer induced crystallization which is a method that has been recently introduced in the area of materials science. This method is discussed in detail in the following section.

1.6 Polymer Induced Crystallization

Polymer induced crystallization/or polymer mediated growth of the dispersed phase is a new observation made only recently.[84-86] This has become an increasingly important area of research especially in the context of production of smart materials, high performance composites and nanotechnology. In this method, the polymer plays a significant role in controlling or modifying the morphology or growth habit of the additive or dispersed phase. The dispersed phase can be organic, inorganic, metal or another polymer in the polymer matrix. The *in situ* growth and modification of the crystalline phase, orientation, morphology and crystallite size of the additive result in special properties.[87-90] This novel idea of using synthetic polymers as crystallization media first arose from the studies on biomineralization or biocomposites formed by *in situ* precipitation which has received attention from material scientists in recent years.[90-92]

1.6.1 Biomineralization

Many biological composite materials such as bones, teeth and shells have a polymer matrix reinforced by a mineral hydroxyapatite or $CaCO_3$, which forms in this matrix. As compared to synthetic materials where the filler is normally blended into the polymer, in biological materials, the particles are grown *in situ* within the polymer matrix and under the control of the matrix. Thus, as compared to synthetic materials, the biological materials have two striking characteristics. Firstly the shape, size, orientation and organization of the mineral in the matrix shows a high degree of sophistication when compared to random dispersion of particles in a filled polymer composite. Secondly, the structures formed by the growth of mineral phase in the polymer are more ordered than the structure formed by the synthetic route of dispersion of particles in a liquid resin.

There are many reports, which highlight the role of macromolecules in the mediation of mineral deposition. At low concentrations, the polymers in the solution act as habit modifiers for crystal growth. For example, NaCl crystallization is affected in the presence of low concentration of polysaccharides[93] by selective adsorption and prevention of specific growth faces. The growth habit is affected by polarity and adsorption properties of the growth

medium. These processes are important in the biological mineralization of bones and shells. It has also been reported that proteins rich in aspartic acid found in mollusc shells, affect the habit of calcite crystals.[94,95] The authors explained that there are three key features which biology adopts in the controlled deposition of mineral particles within polymer matrices (i) non-flux regulation at the matrix interface, (ii) growth and habit modification by soluble molecules present within the matrix and (iii) crystallochemical mediation of nucleation and growth by molecular specific interactions at the polymer surface. Calvert and Mann[91] have classified the biocomposites according to the combination of matrix mediated processes exhibited by the system. In type I (matrix-inert) biocomposites, passive molecular interactions at the matrix-mineral interface results in non-specific nucleation and spatially restricted growth. For example, this type of biocomposite has been found in radular teeth of chitons.[96] Here, magnetic mineralization in chiton teeth occurs with magnetic crystals deposited in a fibrous organic framework. Its primary function lies in specialised cutting action required to remove algae from the rock surface. The type II (nucleation) biocomposites combine the matrix-mediated processes of site directed and spatially organized nucleation. For example, in case of an eggshell, the inner surface of the shell comprises a mesh of fibrous disulphide linked proteins intimately associated with polysaccharide material. The boundary of the membranes with the shell contains regiospecific loci of spherulitic protein mats (cores) which provide the active sites for calcite nucleation. The type III (amorphous) biocomposites comprises amorphous mineral phases from active matrix-mediation in both nucleation and vectorial growth processes. As amorphous materials have no intrinsic crystallographic habit, they can be moulded into a myriad of shapes. This has been highlighted in the complex structures of the silica shells of diatoms.[97] The major functions of these matrices include selective stabilization of amorphous phases, particle growth control and mechanical support. In plant silica, the deposition of type III biocomposites is associated with precise morphological order at the microscopic level.[98] The type IV (oriented) biocomposites are the most complex and highly organized biominerals known. They combine the processes of site-directed and regiospecific nucleation with vectorial growth regulation. In addition the processes are coordinated spatially and temporarily such that oriented composites are constructed. For example, growth surface of the nacreous layer from the mollusc shells shows a stacked arrangement of aragonite crystals.[99] Lowenstam and Westbrook et al.[100,101] reported that precipitated and/or clustered inorganic compounds play important roles in biology. Such

structures are a part of bones and teeth. These structures in bones and teeth are involved in storage and direction finding as magnetic and gravity devices. These latter functions require extremely fine spatial and geometrical tuning of the clusters. Biological control of inorganic cluster formation - biomineralization is largely mediated by cellular membranes. The physico-chemical bases for mineralization have only been examined recently. The reports also suggested that compartmentalization provided by membranes and cells is responsible for the inflow of ionic precursors and imposes size and shape limits on particle growth. Interaction with cell matrix induces orientation of crystal growth. Magnetic bacterium is the living example of stringent biomineralization where spherical, single domain Fe_3O_4 particles are longitudinally aligned in the cytoplasmic membrane. This molecular organization imparts a magnetic moment parallel to the axes of motility.

Thus, studies on biomineralization or biocomposites, have drawn considerable interest among the various material scientists because of fascinating features observed such as growth of certain inorganic compounds, calcium carbonates, phosphates, iron oxides, etc. by biological systems in most unusual morphological forms which at the same time show single crystal type diffraction pattern.[102,103] Proposed by biological composite materials, scientists have tried to synthesize synthetic composites by *in situ* precipitation mimicing the biosynthetic mechanisms as closely as possible. A wide range of synthetic composites have been prepared by inducing precipitation within a polymer.

1.6.2 Synthetic Composites

Studies on precipitation from a glassy polymer have shown that the morphology of the precipitate can be modified in the case of a viscous polymer but not in a solvent. This aspect was studied by various authors during the precipitation of nitroanilines from polymers for second harmonic generation (SHG).[104] The normal morphology of meta nitroaniline (MNA) showed long needles. However, when dispersed in polystyrene (PS), it formed spherulites with 1 to 10 μm fibres. Also 2-methyl-4-nitroaniline which normally formed equiaxed crystals showed a very fine particle of 0.5 μm on precipitation from PS. This clearly brings out the effect of polymer matrix on the growth of crystals. Narkis and coworkers[105-108] studied the precipitation from PS of a number of halogen benzenes used as flame retardants. The crystals formed as needles, dendrites or small crystals depending on the conditions. Oriented structures could be produced by shearing the sample during crystallization. Kardos and coworkers[109,110] produced samples of glassy-styrene acrylonitrile and rubbery butadiene acrylonitrile reinforced

with acetanilide or anthracene as models for the reinforcing effect of the crystalline phase in spherulitic polymers. Measurements of crystallization rate showed that crystallization rate increased with increasing degree of supercooling below the solubility line (liquidus) and then decreased again as the glass transition was approached. For a 17% acetanilide - polystyrene system the crystals formed as rods of 20 to 50 μm length and 5 to 20 μm diameter at 90°C. As the crystallization temperature was reduced to 45°C the diameter decreased to 0.1 μm. Similar studies were also reported for precipitation from a crystalline polymer.

There are a number of systems where inorganic salts are soluble in polar polymers. For example, dielectric properties of PEO salt complexes[111,112] have been extensively studied as these are of importance as battery electrolytes.[113] The effect of melting and crystallization behaviour of lithium halides soluble in nylons has also been studied.[114] Such polymeric additive eutectics have been attractive because they allow formation of a finely dispersed and highly oriented crystalline phase reinforcing the polymer. Another approach taken in the literature has been to swell the polymer with an additive solution and then induce precipitation by allowing the solvent to evaporate. Moskvina et al.[115] have produced such composites of oriented tridecanoic acid crystals in drawn polyethylene (PE) and polytetrafluoroethylene (PTFE) films.

Conducting polymer composites prepared by precipitating organic metallic compounds in polymers have also been studied. The conducting salt TCNQ-TTT was cast from solution with polycarbonate in dichlorobenzene.[116,117] The salt formed whiskers and fibrous dendrites that rendered the composite electrically conducting at 1 wt.% salt much below the 20 to 30% that would be expected for spherical particles in a matrix. Similar structures were obtained for thiapyrylium dyes which formed crystals of a complex with polycarbonate. These showed greatly enhanced photoconductivity compared to the pure dye.[118,119]

There are several investigations on precipitation by reaction to form a variety of composites of polymers with metals or metal oxides reported in the literacture.[120,121] A number of groups have explored the production of particles of magnetic metals in polymers by decomposition of metal carbonyls. Hess and Parker[120] prepared cobalt particles of 10 to 100 nm by thermal decomposition of dicobalt octa carbonyl in solutions of various polymers. The polymer promoted formation of single domain particles rather than large multidomain particles. Decomposition of cobalt carbonyl in solid polystyrene produced particles of 10 to 30 nm.

There have also been a number of reports of conducting composites made by the decomposition of metal salts in polymers. Copper sulphide and cadmium sulphide dispersion in polymers have shown high conductivity at 40 wt.%. Sulphide and electrically conducting copper sulphide treated polyacrylonitrile fibre is reported to be commercially available.[122]

Gels have also been used as supports for crystal growth. Gels of all types have been used including synthetic polymers, silica gels and biological polymers. A recent report on iron oxide precipitation in gels argued that they can give a clearer view of the true morphology of colloidal precipitates.

Recently, several authors reported the polymer induced crystallization effects for an inorganic phase controlled by a polymer matrix.[84,123,124] The studies investigated crystallization of copper chloride ($CuCl_2$) calcium chlroide ($CaCl_2$), calcium carbonate ($CaCO_3$), cadmium sulphide (CdS) and calcium phosphate ($CaPO_4$) in polyethylene oxide, polystyrene, nylon and PEO/PS blends.[123,124]

Radhakrishnan et al.[84] and Patricia et al.[125]studied the development of CdS phase in polymer matrix PEO. The PEO matrix was chosen because PEO binds metal ions strongly forming crystalline complexes and resembles biological systems in which inorganic ions interact strongly with an organic matrix. Particles of CdS varying in size from 2 nm to 2 μm were obtained in a PEO matrix by altering the initial $CdCl_2$ concentration.

The formation of calcium carbonate *in situ* from PEO-$CaCl_2$ and PEO-K_2CO_3 matrices was investigated by S. Radhakrishnan et al.[126] The authors showed a mixed phase of vaterite and monoclinic forms with preferential row nucleation along the polymeric fibres. They also investigated the role PEO-$CuCl_2$ as a function of temperature. At concentrations above 1:4 mole/monomer ratio highly crystalline accicular morphology was observed which was attributed to precipitation of the inorganic component. A new hexagonal type structure was seen to occur for high concentrations of copper chloride while orthorhombic phase was observed at high temperatures.

1.6.3 Polymer Induced Crystallization During Epitaxial Crystallization of Guest Materials on Polymeric Substrates

The nucleation and growth of metal particles on certain crystallographic surfaces of molecular metal, ionic and covalent crystals can lead to epitaxial growth. Petermann and Broza[127]studied the epitaxial deposition of metals on uniaxial oriented semicrystalline polymers where they found that the evaporation of certain metals (tin, indium, bismuth and

tellurium) onto uniaxially oriented semicrystalline polymer films leads to strongly textured lattice orientations of the metals. For example, on polybutene, tin crystallites showed a preferred orientation with the (100) axis of the tetragonal tin parallel to the chain direction of the polymer. Schultz[128] et al studied the thin layers of (25-1000-Å) tin evaporated on to a highly oriented PP sheet. At lower thickness a preferred orientation of tin was seen while at higher film thickness, a random orientation of crystallites was observed.

The polymer-polymer epitaxy is considered as a specific interfacial interaction between two distinct macromolecular species as opposed to homoepitaxial behaviour. This has been observed for example in hydrodynamically induced crystalline structures (Shish Kebabs).[129] Willems[130] ,reported the case of interpolymer heteroepitaxy. He succeeded in orienting PE from dilute xylene solution on POM (polyoxymethane). The overgrowth morphology was fibrillar, elongated structures perpendicular to the POM draw axis (molecular axis). A number of polymers were isothermally crystallized from the melt on to uniaxially drawn and annealed polymers by Takashashi et al.[131] Overgrowth morphology and molecular orientation were obtained using electron and optical microscopy and XRD. Favourable orientational behaviour was obtained on linear polyethylene by all the deposited polymers whereas polycaprolactone would orient only on polycaprolactam. Polypropylene proved to be a poor nucleating agent for polycaprolactone and linear polyethylene whereas POM gave opposite results. Comparison of the crystal packing modes of substrate and deposited phase for the successful system suggested that structural similarites are not an important criterion. Another interesting observation was that while polycaprolactam would epitaxially crystallize on LPE, the crystallization of PE on polycaprolactam was of random nature. Willems et al.[132] obtained oriented films of PE and paraffins on uniaxially sketched nylon 6, nylon 11 and nylon 610 substrates. In both cases, the overgrowth long axes were perpendicular to the sketch direction.

Takashashi et al.[133] attempted to orient a number of polymers from the melt on PTFE which was stretched 300% and annealed at 200°C. HDPE, polycaprolactone, nylon 6 and PP crystallized in epitaxial fashion. Electron microscopy, optical birefringence and XRD indicated in rod like crystalline overgrowths perpendicular to the PTFE chain direction and overgrowth molecular axes parallel to those of PTFE. Matching of periodicities along the molecular axes was identified to be a condition for epitaxy.

Wittmann and Smith[134] studied the oriented growth of materials on a highly oriented thin film of PTFE. A thin single crystal like form of PTFE was first deposited mechanically on

a smooth substrate (such as glass). Materials following this showing a remarkable degree of alignment were grown on this coated surface from solution, melt or vapour phases.

1.6.4 Polymer Induced Crystallization Effects of a Polymer on Another Polymer (as in Blends)

The crystallization of a polymer can take place from mixtures, which contain a low molecular weight, diluent as an added ingredient and can also occur from mixtures, which contain another polymer as an ingradient. Recent research on the effect of an amorphous polymer upon the crystallization of a crystalline polymer has reached some importance.[135-140] When two polymers are compatible in the melt, the diffusion of the noncrystallizable polymer plays an important role in the crystallization process. This can determine changes in the morphology, crystallinity and melting behaviour of the crystalline polymer. The polymer pair also provides a suitable system for studying the growth kinetics of spherulites particularly with regard to the influence of an uncrystallizable polymer present in the blend. Such a study has been carried out recently on PEO-PMMA blends.[141] At isothermal crystallization temperature of 44 to 58°C, the introduction of polymethyl methacrylate (PMMA) into polyoxyethylene (PEO) resulted in a reduction of spherulite growth rate as the proportion of PMMA was increased from 0 to 40% by weight. The morphology of PEO/PMMA blend with 10% PEO displayed a well-defined spherulite of melt crystallized PEO. At T_c of 39-56°C, the spherulite showed a regular shape with defined borders. No separated domains of uncrystallizable PMMA component were observed in the intra-spherulitic regions nor in the interspherulitic contact zones. Moreover, after crystallization the PEO/PMMA films appeared completely filled with impinging spherulites. Martuscelli[142] et al. investigated the influence of tacticity of PMMA on the crystallization process of PEO/PMMA blends. The addition of atactic and syndiotactic PMMA at a given T_c showed a drastic depression of the spherulite growth rate of PEO. Thus, the PEO crystals grew in equilibrium with a one phase PEO-PMMA melt. On the other hand, in a blend containing isotactic PMMA, the composition and molecular weight of PMMA did not influence the Gibbs free energy (ΔG^*). Thus, examining the effect PEO crystals grew in the presence of a two phase melt. Similar studies of compatible non-crystallizable polymer on the crystallization behaviour of a crystallizable polymer have been carried out for polyvinyl dienefluoride PVF_2-PMMA[143], PCL-PVC[144] and 2,6-dimethyl phenylene oxide-PS.[137] In all cases, the presence of dissolved noncrystallizable component reduced the overall crystallization rate and the spherulitic growth rate with significant changes

in morphology, crystallinity and melting behaviour. In case of PCL-PVC, the texture of spherulites, crystallized at the room temperature became increasingly coarse and open with increasing PVC concentrations. The value of A_v in the Avrami equation decreased markedly with increase of PVC concentration. The results of elemental analysis using a X-ray spectrometer indicated uniform distribution of PVC molecules in the blends regardless of the composition. The PVC exerted a considerable influence on the melting behaviour of PCL. Pure PCL showed a narrow melting peak but the melting peak moved towards lower temperatures as the PVC concentration was increased. These observations indicated that increasing PVC lowered the crystalline order and/or crystallize size. The X-ray diffraction studies revealed that the unit cell dimensions of PCL remained unchanged with the incorporation of PVC.

Keith and Padden[145] conducted a systematic study on the effect of atactic PP on the crystalline morphology and spherulitic growth kinetics of iPP. It was reported that concentration and molecular weight of polymeric impurity showed a considerable influence on the texture and growth rate of the spherulites. The influence of one crystalline polymer on the crystallization and morphology of another crystalline polymer in a blend have also been investigated. For example, in PP/HDPE and PP/LDPE[146] PE drops were occluded within the growing PP spherulites during the crystallization of PP. When the crystallization was carried out at $T < T_c$ (PE) = 127°C, the PE crystals were found to nucleate PP, increasing the number of spherulites and reducing their size. The finer micromorphology resulted in an improvement of overall mechanical properties.

Compatibilizers can also be used to control the properties of a multiphase blend. It controls the size of the phase domains and the adhesion between them and thus, improves the properties of the blend. The PE/PA (polyamide) blends are normally immscible[147] and are characterised by two distinct phases. Addition of PE based ionomer to the PE/PA blend during melt blending[148] results in smaller dispersed phase sizes with reduced interfacial mobility. It has been found that blends with compatibilizers at the interface shows much greater impact strength than uncompatibilized blends made from the same components and having similar particle sizes. Brown, Kramer and others[149-152] also illustrated the use of block polymers as compatibilizers. Graft polymers have also been used as compatibilizers. In the case of EP-graft- PP blends[153] where maleated PP was reacted with functional versions of EP, the size of dispersed EP phases in the 80:20 PP:EP blend was reduced by adding a small amount of

compatibilizer. The addition of this graft polymer also improved the toughness of these blends.

The *in situ* formation of compatibilizers is also possible. This can be achieved by modifying the mixture's components in such a way that one of the polymers reacts with the other. For instance, a polyolefin resin is immiscible with nylon-butadiene rubber (NYBR) but PP modified by a maleic anhydride in the presence of a decomposing organic peroxide blended with respect to NYBR produces a good oil resistant, elastomeric composition.[154]

1.6.5 Polymer Induced Crystallization During Processing

(a) *In situ* fibre formation in blends

Fibres can be formed *in situ* during (solidification) crystallization to produce materials with enhanced moduli. Under appropriate conditions, the dispersed phase can deform during processing to produce elongated structures such as ellipsoids, or even fibres. This depends upon various factors: (a) Method of preparation (e.g. method of mixing of polymer blends where the components blends could be partially compatible or incompatible. (b) Control of morphology (the state of dispersion, particle size and particle shape of the component). (c) The rheological properties such as melt viscosity, temperature, rate of extrusion, shear stress, etc. These above factors in turn influence the morphology and thus influence the ultimate physical and mechanical properties of the finished product.

Evidence of fibrillation in the flow of molten mixtures of polymers was first presented by Tsebrenko et al.[155] who examined the fibrils of polyoxymethylene in copolyamide matrix during extrusion. The occurrence of fibrillation is shown schematically in Fig.1.6. The formation of fibres occurs as follows. First the dispersed droplets formed during the mixing operation get elongated as they enter the die entrance (region A) due to tensile stresses acting in the direction of converging streamlines. The elongated droplets then recoil as they pass the die entrance. Finally, rearrangement of the elongated droplets occurs at the down stream side of the capillary (region D) giving rise to fibrils parallel to capillary axis. The final extrudate is therefore reinforced with uniaxially aligned fibres. It should be noted that the more viscous component of the blend forms the discrete phase and the less viscous component forms the continuous phase.

Another example of *in situ* fibre formation composites are from blends with thermotropic liquid crystalline polymers.[156] LCPs have sufficient chain stiffness to give high strength and yet have sufficient flexibility to melt. LCP's form fibres where the molecular

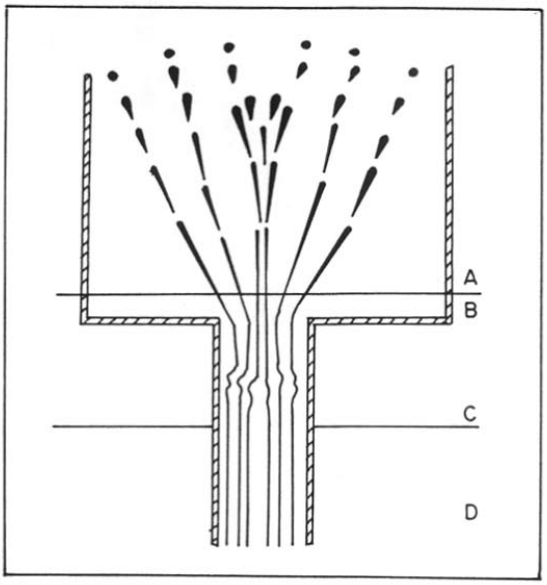

Figure 1.6 Schematic representation of the fibrillation process

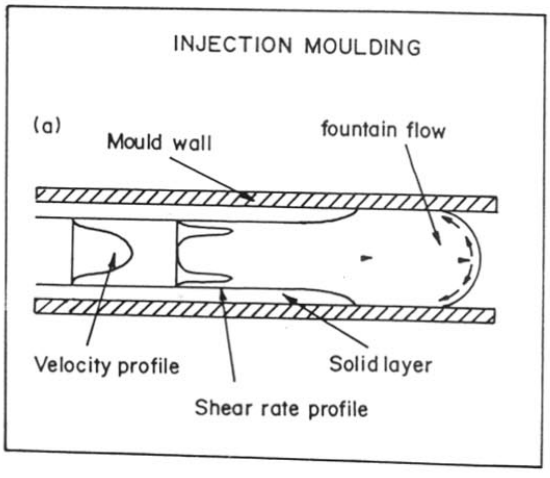

Figure 1.7 Flow profile during mould filling process

orientation occurs. Thus, the physical properties of moulded articles exhibit a high degree of anisotropy and ehnanced mechanical properties.

The evidence of *in situ* fibre formation has also been found in SBS-PS blends and SBS-HDPE blends. Folkes et al.[157] found that in case of SBS-PS, the 10% PS showed no evidence of fibre formation whereas for 50% PS almost perfect fibres were produced. In case of SBS-HDPE the most perfectly formed fibres were produced in the 60/40 blend. The SEM micrograph of this blend showed PE as a series of micro fibrils surrounded by SBS matrix. These various observations were due to lowering of surface energy of the dispersed homopolymer PS or PE by the block copolymer and the formation of PS fibres or PE fibres by a process of elongational flow through the spider holes during extrusion.

(b) Fibre orientation during injection moulding

During the moulding process, the fibres may get oriented in a complex manner. It has been observed that flow geometry is the major parameter affecting fibre orientation.[158] The resin viscosity and flow rate also alter the proportions of the oriented regions. The flow of various reinforced resin systems in injection moulds has been described qualitatively by Folkes. Figure 1.7 shows schematically the flow profile that normally exists through the section of the moulding during mould filling process. As the material reaches the fountain's flow region at the moving melt front, it is first stretched and laid down against the mould surface. This stretching ensures that most of the fibres in the outer layers are aligned in the plane of the moulding. Behind the moving melt front a stationary layer of material builds up on the mould surface, as the mould extracts heat from the melt. This solid layer grows in thickness to an equilibrium value, which then remains constant during the rest of the mould filling phase. The schematic velocity profile is shown below. It illustrates the point that due to nonisothermal nature of flow, the maximum shear rate occurs not adjacent to the solid layer but a small distance inward from it. The thickness of solid layer is determined by the balance between viscous heat generation in the shear layer and conduction heat through the solid layer into the mould. Finally after the mould has been filled, the molten material at the centre of the product section cools and solidifies. As the packing pressure is maintained by the moulding machine during solidification, the thermal and solidification contraction of the moulding can result in some further movement of central core material away from the gate towards the extremities of the moulding. Because of the different mechanical and thermal histories experienced by the material at different points through the cross-section of the part, there is a

considerable gradation of both fibre orientation and matrix orientation and morphology through the thickness. For polypropylene[159], a number of morphologically distinct layers can be identified through the moulding thickness. First, there appears a thin surface layer of 15 μm thick called skin of moulding, which is, unaffected by processing conditions. Followed by this, there occurs a highly birefringent thicker layer whose thickness is markedly dependent on processing conditions (for e.g. as the injection time increases, the layer thickness increases). This layer is called a solid layer. Following this, there is a birefringent region called shear layer associated with the region of high shear in the hot core material. Finally, in the centre of the moulding called core layer, the material is unoriented due to the fact that molecules have considerable time to relax before the material solidifies. The relative thickness of the skin and core regions vary as a function of moulding conditions, the most important parameters being melt temperature, moulding temperature and injection speed. Increasing any of these parameters can be expected to decrease the solid layer thickness and hence the thickness of the skin layers of the moulding.

A second contribution to molecular orientation in fibre-filled thermoplastics is the influence of fibres on the morphology of the surrounding matrix. Studies of the spherulitic growth of nylon 6 around various types of fibre have been reported by Bessell et al.[160,161] The crystallization processes around a single fibre and in composites containing 15% volume function of uniaxially aligned fibres were studied. It was found that columnar spherulitic growth occurred around the fibres, the extent of this depending on the type of fibre and its surface treatment. Associated with this, there was a high degree of chain alignment parallel to the fibre axis. Stressing the composite so as to fracture along the fibre axis results in fibre pull out with a sheath of matrix material adhering to the fibres. Clearly, these effects become significant as the volume fraction of fibres increases.

(c) Orientation induced during poling:

Poling is a method to align the molecules which is accomplished by applying an electric field across a polymer film at a temperature above the glass transition temperature of the polymer matrix. After sometime that is enough to allow the chromophores to orient along the direction of electric field, the film is cooled down in presence of the field so as to freeze in the aligned molecule in place. Poling has been studied extensively by various authors.[162-166] Figure 1.8 shows how the domains get oriented during poling. For e.g. large SHG was obtained in electrically ordered PNA-PEO guest host system.[167] In this system the oriented

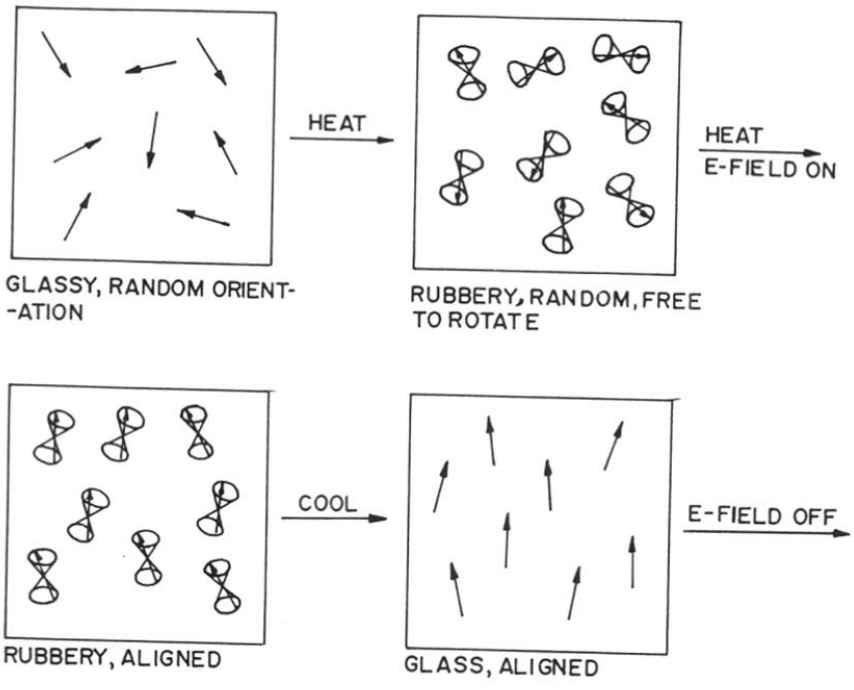

Figure 1.8 Orientation of domains during poling

crystal growth was achieved by applying a low intensity electric field (~ 10^{-2} mV/cm). The azodye disperse Red I [168] in PMMA matrix during poling showed alignment of dopant molecules at electric field of 0.2-0.6 mV cm^{-1}. Several authors studied the orientation and SHG in doped PS and PMMA films. These exhibited better stability of molecular orientation.[169]

1.7 Aim and Scope

In the foregoing discussion, it may be noticed that the novel idea of using synthetic polymers as crystallization media first arose from the studies on biomimeralization or biocomposites. Although many biological composite materials have been studied extensively, many difficulties have been encountered in understanding the crystallization behaviour, characterization, etc. For example, biological materials such as proteins are difficult to characterise by different physico-chemical methods because of their complicated macromolecular or complex structure. Hence, scientists have focussed on synthesis of synthetic composites by *in situ* precipitation that mimic the biosynthetic mechanisms as closely as possible. The simplest route to achieve this was by polymer induced crystallization method.

Polymer induced crystallization using synthetic polymer is easier to characterise or study for morphological changes compared to bio-materials. Secondly, they are easier to handle and process. Thus, this method seems promising for the production of smart materials, high performance composite, nano-technology, etc. By this process, it is possible to control the overall morphology, uniformity of size and dispersion and achieve better interfacial adhesion. However, the literature has only a few scientific reports on this method. Further, there are various aspects, which need to be investigated more in greater detail. For example, the influence of surrounding matrix on orientation, structure and morphology of the additive and its correlation on the properties of the composites has not been considered in the past.

In the present studies, we have investigated the role of the polymer matrix on the structure development in (a) conventional composites such as polypropylene filled with $CaSO_4$, blended with thermoplastic elastomers , glass fibres and polyester fibres and (b) novel composites made with PMMA containing (NLO) crystals. In these studies, the polymer induced structural changes can take place due to: (a) the effect of an additive on the crystallization of a polymer as in conventional composites, (b) effect of one polymer on crystallization of another polymer as in blends and (c) polymer mediated growth in the

molecularly dispersed systems such as NLO guest/host sytems. In all these various systems, a detail study on the structure development and properties of the composites have been carried out in order to understand the exact nature of interaction between the polymer matrix and the guest material leading to polymer mediated growth. This can give a new route for the development of novel materials having improved properties.

1.8 References

1. A. Kelly, Strong Solids, Oxford University Press (1973).
2. J.H. Davis, Plastics and Polymers, **39** (1971) 140,137.
3. J.C. Williams, D.W. Wood, I.F. Bodycot and B.N. Epstein, 23rd ANTEC of SPE. Reinforced Plastics/Composites Division, Proceedings Section, **2C1**(1968).
4. P.E. Chen, Polym. Eng. and Sci., **11(1)** (1971) 51.
5. W.H. Bowyer and M.G. Bader, J. Mat. Sci., **7** (1972) 1315.
6. A. Kelly and W.R. Tyson, J. Mech. Phys. Solids, **13** (1965) 329.
7. F.W. Maine, B.E.Riseborough and J.E. Theberge, SPE RETEC, Polymer Structure and properties , Toronto (1970).
8. M.G. Bader and W.H. Bowyer, Composites **4** (1973) 4, 150-156.
9. W.C. Filbert, SPE Journal, **24** (1969) 65.
10. J.D. Crabtree and D. Pickthall Paper at I.R.I., Conference, Loughborough, 15-17th Sept. (1969).
11. G. Roos, Kunststoffe, **60** (1970) 12, 924.
12. J.E. Ashton, J.C. Halpin and P.H. Pefit, "Primer on Composite Materials" Technomic, Stanford (1969) Chpt. 5.
13. J.C. Halpin, J. Compos. Mater., **35** (1969) 732.
14. P.J. Barham and R.G.C. Arridge, J. Polym. Sci., Polym. Phys., **15** (1977) 1137.
15. T.S. Chow, J. Polym. Sci. Polym. Phys., **16** (1978) 959, 967.
16. L.F. Nielsen, J. Compos. Mater., **1** (1967) 100.
17. A. Keller, Philos. Mag., **2** (1957) 1171.
18. F.W. Fischer, Z. Naturforsch, **12a** (1957) 753.
19. P.H. Till, J. Polym. Sci., **24** (1957) 301.
20. K.A. Mauritz, E. Baer and A.J. Hopfinger, J. Polym. Sci. (D) Macro Mol. Rev., **13** (1978) 1.
21. W.B. Wunderlich, Macromolecular Physics, Academic, New York, NY **1** (1975)
22. L. Mandelkern, Crystallization of Polymers, McGraw Hill, New York (1964).
23. F.P. Price, In Nucleation; A.C.Zettlemoyer Ed., Marcel Dekker: New York (1969).
24. B. Wunderlich, Macromolelcular Physics, Academic: New York, **2** (1976).
25. D.J.Blundell, A.Keller and A.J. Kovacs , J of Polym. Sci. Part $\mathbf{B_4}$ (1966) 481.
26. M.J. Avrami, J. Chem. Phys., **7** (1939) 1103

27. M.J. Avrami, J. Chem. Phys., **8** (1940) 212
28. F.J. Padden, H.D. Keith, J. Appl. Phys.,**30** (1959) 1479
29. G. Natta and P. Corradini, Nuovo Cimento, Suppl., **15** (1960) 40.
30. A. Turner-Jones, J. M. Aizlewood, D.R. Beckett, Makromolekulare Chemie, **75** (1964) 134.
31. H.D. Keith, F.J. Padden, N.M. Walker and H.W. Wyckoff, J. of Apply. Phys., **30** (1959) 1485.
32. A. Turner-Jones and A.J. Cobbold, J. of Polym. Sci. Part B, Polymer Letters, **6** (1968) 539.
33. J.C. Kardos, A.W. Christiansen and E. Baer, J. Polym. Sci., **A-2(4)** (1966) 777.
34. K.D. Pae, D.R. Morrow and J.A. Sauer, Nature, **211** (1966) 514.
35. B. Lotz, S. Graf and J.C. Wittmann, J. Polym. Sci. Polym. Phys. Ed., **24** (1967) 2017
36. M. Kojima, J. Polym. Sci., **(B) 5** (1967) 245.
37. M. Kojima, J. Polym. Sci., **A-2(6)** (1968) 1255.
38. A. Turner-Jones, Polymer, **12** (1971) 487.
39. S. Bruckner, S.V. Meille, Nature, **340** (1989) 455.
40. S.V. Meille, S. Bruckner, W. Porzio, Macromolecules, **23** (1990) 4174.
41. D.R. Morrow, B.A. Newman, J. Appl. Phys., **39** (1968) 4944.
42. R.C. Miller, Polymer, **1** (1960) 135.
43. R. Hosemann, Acta Crystall., **4** (1951) 520.
44. R. Zannetti, G. Celotti, A. Fichera, R. Francesconi, Macromol. Chem., **128** (1969) 137.
45. R. Zennetti, G. Celotti, S. Armigliato, Eur. Polym. J., **6** (1970) 879.
46. B. Wunderlich, J. Grebowicz, J. Adv. Polym. Sci., **60** (1984) 1.
47. E.J. Addink and J. Bienteme, J. Polymer, **2** (1961) 185.
48. E. Ergoz, J.G. Fatou, L. Madelkern, Macromolecules, **5** (1972) 147.
49. A. Booth, J.N. Hay, Polymer, **12** (1971) 365.
50. S. Hoshion, E. Meinecke, J. Powers et al., J. Polym. Sci., **A-3** (1965) 3041.
51. M. Gordon, I.H. Hillier, Trans. Faraday Soc., **60** (1964) 763.

52. I.H. Hillier, J. Polym. Sci., Part **A 3** (1965 3067.

53. A.J. Peterlin, J. Appl. Phys., **35** (1964) 75.

54. F.C. Perez-cardenas, L.F. Castillo, R.J. Vera-Granziano, Appl. Polym. Sci., **43** (1991) 779.

55. F. Rybnikar, J. Macromol. Sci. Phys., **B19(1)** (1981) 1.

56. J. Sveda and R. Evanzin, Int. Polym. Sci. Technol., **11(7)** (1984) T/4.

57. F. Rybnikar, Eur. Polym. J. **27** (1991) 549.

58. T.J. Hutley and M.W. Darlington, Polym. Common., **25** (1984) 226.

59. A.L. Lovinger, Polym. Phy Edn., J. Polym. Sci., **21** (1983) 97.

60. F. Rybnikar, J. Appl. Polym. Sci., **42** (1991) 2727.

61. Fujiwara, Toshio, Jpn. Pat. 03,247,668 (91,247,668), 5th Nov. (1991).

62. A.Khare, A.Mitra and S.Radhakrishnan, J.Mater.Sci. **31** (1996) 5691.

63. B. Pukanszky, E. Fekete and F. Tudos, Makromol. Chem. Macromol. Symp., **28** (1989) 165.

64. J. Jancar and J. Kucera, Polym. Eng. Sci., **30** (1990) 714.

65. Celanese Engineering Resins, quoted in Plast. Rubb. Int., **9(4)** (1984) 22.

66. G.A. McFarren, T.F. Sanderson and F.C. Schappell, Polym. Eng. Sci., **17(1)** (1977) 46.

67. A. Whelan and J.L. Craft, Developments in London Plastic Technology, Elsevier Applied Sci. Pub. **3** (1986).

68. E.J. Paakkonen, P.A. Jarvela, P. Tormala, J.C. LeBell, Kunststoffe, **77(6)** (1987) 602.

69. S.F. Xavier and Y.N. Sharma, Angew Makromol. Chem., **127** (1984) 145.

70. A. Garton, Polym. Comp., **3** (1982) 189.

71. M.S. Boaira, C.E. Chaffey, Polym. Eng. Sci., **17** (1977) 715.

72. C. Busigin, R. Lahtinen, G.M. Martinez, G. Thomas and R.T. Woodhams, Polym. Eng. Sci., **24** (1984) 169.

73. A. Misra, B.L. Deopura, S.F. Xavier, F.D. Hartley and R.H. Peters, Angewandte Makro. Chemie., **113** (1983) 113-120.

74. A. Lustiger, C.N. Marzinsky, R. Mueller, H.D. Wagner, Annu. Techn. Conf. Soc. Plast. 52nd **2** (1994) 2390.

75. J.O. Iroh and J.P. Berry, Euro. Journal, **32** (1996) 1425.

76. E. Devaux and B. Chabert, Polymer Commun., **31** (1990) 391.
77. M.B. Fernanda, T. Coutinho, H.S. Costa, J. Appl. Polym. Sci., **65(6)** (1997) 1227.
78. J.L. Thomason and A.A. Van Rooyen, J. Mater. Sci., **27** (1992) 5.
79. D. Campbell and M.M. Qayyum, J. Polym. Sci. Polym. Phys. Edn., **18** (1980) 83.
80. M. Avella, G.D. Volpe, E. Martuscelli and M. Raimo, Polym. Eng. & Sci., **32** (1992) 377,383.
81. A. Whelan and J.L. Craft, Developments in Plastic Technol.. Elsevier Appl. Publish., **2** (1985) Chapt.5 .
82. M.G. Huson and W.J. McGill, J. of Polym. Sci., Polym. Phy. Edn., **23** (1985)121.
83. R.H. Burton and M.J. Folkes, Mechanical Properties of Reinforced Thermoplastics, Elsevier Applied Sci., London, (1986) 269.
84. S. Radhakrishnan, J. Cryst. Growth, **141** (1994) 437.
85. S. Radhakrishnan and V.M. Nadkarni, Int. J. Polym. Mater., **11** (1986) 79.
86. S. Radhakrishnan and S.G. Joshi, Euro. Polym. J., **23** (1987) 819.
87. D.J. Sandman (Edt.) "Crystallographycally ordered polymers" ACS Sym. Ser., 337, ACS Washington (1987).
88. R.P. Andres et al., J. Mater. Sci., **4** (989) 704.
89. S.N. Black R.J. Daney and T.D. Mclean, Mol. Cryst. Liquid. Cryst., **161** (1989) 283
90. S. Zu, X. Zhao and J.H. Fendler, Adv. Mater., **2** (1990) 183
91. P. Calvert and S. Mann, J. Mater. Sci., 23 (1988) 3801.
92. T. Kokubo, S. Ito, Z. Huang, T. Hayashi and S. Sakki, J. Biomed. Mater. Res., **24** (1990) 331.
93. J.D. Birchall and R.J. Davey, J. Cryst. Growth, **54** (1981) 323.
94. L. Addadi and S. Weiner, Proc. Nat. Acad. Sci. USA, **82** (1985) 4110.
95. A.P. Wheeler, J.W. George and C.A. Evans, Science, **212** (1981) 1397.
96. K.M. Towe and H.A. Lowenstam, J. Utrastruc. Res., **17** (1967) 1.
97. B.E. Volcani and T.L. Simpson, "Silicon and Siliceous Structures in Biological Systems" (Springer, Heidelberg, 1981).
98. S. Mann and C.C. Perry, in "Silicon Biochemistry", Ciba Foundation Symposium, **121** (Wiley, Chichester (1986) p. 40.
99. E.T. Degens, D.W. Spencer and R.H. Parker, Comp. Biochem. Physiol., **20** (1967) 553.

100. H.A. Lowenstam, Science (Washington, D.C.), **211** (1981) 1126

101. P. Westbrook, E.W. deJong, Biomineralization and Biological Metal Accumulation Reidel: Dordrecht, Holland (1983).

102. K. Simkiss and K.M. Wibur, "Biomineralization" Academic Press (1989).

103. P.L. O'Niell, Science, **213** (1981) 646.

104. B.D. Moyle, R.E. Ellul and P.D. Calvert, J. Mater. Sci. Lett., **6** (1987) 167.

105. A. Siegmann, M. Narkis, M. Puterman and A.T. Benedetto, Polymer, **20** (1979) 89.

106. M. Narkis, A. Siegmann, M. Puterman and A.T. Dibenedetto, J. Polym. Sci. Phys., **17** (1979) 225.

107. A. Siegmann, M. Narkis and A. Dagan, Polymer, **15** (1974) 499.

108. M. Narkis, A. Siegmann, A. Dagan and A.T. Dibenedetto, J. App. Polym. Sci., **21** (1977) 989.

109. J.R. Joseph, J.L. Kardos and L.E. Nielsen, J. Appl. Polym. Sci., **12** (1968) 1151.

110. J.K. Kardos, W.L. McDonnell and J. Raisoni, J. Macromol. Sci. Phys., **B6** (1972) 397.

111. R.E. Wetton, D.B. James and F.P. Warner, Amer. Chem. Soc. Adv. Chem., **187** (1980) 253.

112. M. Watanabe, S. Oohashi, K. Sanui, N. Ogata, T. Kobayashi and Z. Ohtaki, Macromolecules, **18** (1985) 1995.

113. M.B. Armand, Ann. Rev. Mater. Sci., **16** (1986) 245.

114. B. Valenti, E. Bianchi, G. Greppi, A. Tealdi and A. Ciferri, J. Phys. Chem., **77** (1973) 389.

115. M.A. Moskvina, A.V. Volkov, T. YeGrokhovskaya, A.L. Volynskii and N.F. Bakeyev Polom. Sci., USSR, **26** (1984) 2648.

116. J.K. Jeska, J. Ulanski and M. Kryszewski, Nature, **289** (1981) 390.

117. J. Hocker, F. Jonas and H.K. Muller, Angew. Makromol. Chem., **145/6** (1986) 191.

118. W.J. Dulmage, W.A. Light, S.J. Marino, C.D. Salzberg, D.L. Smith and W.J. Staudenmayer, J. Appl. Phys. **49** (1978) 5543.

119. J.H. Perlstein, in "Electrical Properties of Polymers", edited by D. Seanor (Academic New York, 19082) p. 59.

120. P.H. Hess and P.H. Parker, J. Appl. Polym. Sci., **10** (1966) 1915.

121. R. Tannenbaum, C.L. Flenniken and E.P. Goldberg, J. Polym. Sci. B (Phys), **25** (1987) 1341.

122. T. Yamamoto, E. Kubota, A. Taniguchi, M. Kubota and Y. Tominaga, J. Mater. Sci. Lett., **5** (1986) 132.

123. S. Radhakrishnan and J.M. Schultz, J. Cryst. Growth, **116** (1992) 378.

124. S. Radhakrishnan and Roy Joseph, Polymer Processing Society Conf. PPS-8, New Delhi (1992).

125. A. Patricia, J.L. Bianconi and R.S. Angela, Nature, **349** (1991) 315.

126. S. Radhakrishnan and D.R. Saini, J. Of Cryst. Growth, **129** (1993) 191.

127. J. Petermann and G. Broza, J. Mater. Sci., **22** (1987) 1108.

128. J.M.Scultz, S.Penava, J.of Polym. Sci., Part B Polym. Phys., **25 (1)** (1987) 185.

129. A.J. Pennings, J.M. Vander Mark, A.M. Kiel, Kolloid Z., **237** (1970) 336.

130. J. Willems, Naturwissenschaften, **50** (1963) 92.

131. T. Takahashi, M. Inamura and I. Tsujimoto, J. Polym. Sci. Polym. Lett. Ed., **8** (1970) 651.

132. J. Willems, Kolloid, **251** (1973) 496.

133. T. Takahashi, F. Teraoka, I. T. Sujimoto, J. Macromol. Sci. Phys., (1976).

134. J.C.Wittmann and P. Smith, Nature, **352** (1991) 414.

135. E. Riande, J.G. Fatou and J.C Alcazar, Polymer, **18** (1977) 1095.

136. G.S.Y. Yeh and S.L. Lambert, J. Polym. Sci., **A-2 10** (1972) 1183

137. H. Berghmans and N.J. Overbergh, J. Polym. Sci., Polym. Phys. Edn., **15** (1977) 1757.

138. T.T. Wang and T. Nishi, Macromolecules, **10** (1977) 2.

139. C.J. Ong and F.P.J. Price, Polym. Sci., **C 63** (1978) 59.

140. A. Aref-Azar, J.N. Hay, B.J. Marsden and N.J. Walker, Polym. Sci., **A-2 18** (1980) 637.

141. E. Calahorra, M. Cortazar and G.M. Gyzman, Polymer, **23** (1982) 1322.

142. E. Martuscelli, M. Dracella and Y. Wangping, Polymer, **25** (1984) 1097.

143. T.T. Wang and T. Nishi, Macromolecules, **10** (1977) 421.

144. C.J. Ong and F.P. Price, J. Polym. Sci., Polym. Symp., **63** (1978) 45.

145. H.D. Keith and F.J. Padden, Jr., J. Appl. Phys., **35** (1964) 1270.

146. Z. Bartczak, A. Galeski and M. Pracella, Polymer, **27** (1986) 537.

147. J. M. Willis, V. Caldas, B.D. Favis, J. of Mater. Sci., **26** (1991) 4742.

148. J. M. Willis and B.D. Fans, Polym. Eng. Sci., **28 (21)** (1988) 1416.

149. H.R. Brown, V.R. Deline, P.F. Green, Nature, **341** (1989) 221.

150. K. Char, H.R. Brown, V.R. Deline, Macromolecules, **26** (1993) 4164.

151. C. Creton, E.J. Kramer, C.Y. Hui et al. Macromolecules, **25** (1992) 3075.

152. J. Washiyama, E.J. Kramer, C.Y. Hui, Macromolecules, **26** (1993) 2928.

153. S. Dotta, D.J. Lohse, Macromolecules, **26** (1993) 2064.

154. D.R. Paul, S. Newman, Polymer Blends, Academic: New York (1978)p. 35.

155. M.V. Tsebrenko, A.V. Yudin, T.I. Ablazova and G. Vinogradov, Polymer, **17** (1976) 831.

156. G.W. Calundann and M. Jaffe, Proc. Robert A. Welsh Conference on Chemical Research XXVI, Synthetic Polymers,(1982) 247.

157. M.J. Fokes and P.W. Reip, Polymer, **27** (1986) 377.

158. L.A. Goettler, Monsanto/Washington University ARPA Report ,HPC (1972) 72-150.

159. D.R. Fitchman and Z. Mencik, J. Polym. Sci., Polym. Phys. Edn., **11** (1973) 951.

160. T. Bessell, D. Hull and J.B. Shortall, Faraday Spec. Discuss. Chem. Soc., **2** (1972) 137.

161. T. Bessell and J.B. Shortall, J. Mater. Sci., **10** (1975) 2035.

162. K.D. Singer, J.E. Sohn, S.J. Lalama, J. Appl. Phys. Lett., **49** (1986) 248.

163. M.A. Mortazavi, A. Knoesen, S.T. Kowel, B.G. Higgins, A.J. Dienes, J. Opt. Soc. Am., **B6** (1989) 733.

164. J.W. Wu, J.F. Valley, S. Frmer, E.S. Binkley, J.T. Kenney, G.F. Lipscomb, R.Lytel, Appl. Phys. Lett., **58** (1991) 225.

165. F. Wan, G.O. Carlisle, K. Koch, D.R. Martinez, J. of Mater. Sci., Mater. In Electronics **6** (1995) 228.

166. G.T. Boyd, Thin Solid Films, **152** (1987) 295.

167. T. Watanabe, K. Yoshinaga, D. Fichou and S. Miyata, J. Chem. Soc., Chem. Common., (1988).

168. K.D. Singer, J.E. Sohn and S.J. Lalama, Appl. Phys. Lett., **99(5)** (1986) 4.

169. H.L. Hampsch, J.Y. Georgek and J.M. Torkelson, Macromolecules, **21** (1988) 528.

Chapter 2

Experimental

2.1 Introduction

In order to study polymer induced crystallization of the composites, various techniques were adopted for making the composites such as powder blending, melt compounding, solution casting of films, etc. The main part of these studies is centered on polypropylene based composites. Polypropylene is readily commercially available polymer (Indothane, SM85N, IPCL) and this grade was chosen because it is an injection moulding grade, it has moderate MFI of 8-12, it is sensitive to crystallization temperature etc. It has a variety of structure that is polymorphism, which can be easily controlled by crystallization conditions. The structure development, morphology and the properties of the composites were investigated by various physico-chemical characterisation techniques, which are described in this Chapter.

2.2 Preparation of Polypropylene Powder (iPP) from Pellets

Polypropylene (Indothane SM85N, MFI-12, IPCL, India) powder was obtained by dissolving it in xylene (5-6% of solution) and then precipitation of the solution in acetone followed by thorough washing with acetone and drying at 75-100°C for half an hour.

2.3 Preparation of Filler by *In situ* Deposition Technique

The filler ($CaSO_4$) was prepared by *in situ* deposition technique which essentially consisted of first forming a complex of calcium chloride ($CaCl_2$) with polyethylene oxide (PEO), (WSR N-750, BDH, MW = $3x10^5$) by dissolving the two components in desired proportions in methanol. This was allowed to react for 10 hours. Appropriate stoichiometric amounts of potassium sulphate (K_2SO_4) dissolved in distilled water were added to the above complex slowly without stirring. The whole mixture was allowed to digest at room temperature for 20 hours when the Cl^- and SO_4^{2-} ions diffused through the PEO and formed a white gel like precipitate which became powdery over a period of time. This was filtered, washed lightly and dried. The $CaSO_4$ powder was characterised for particle size, structure and morphology by various physico-chemical characterization techniques.

2.4 Preparation of Composite by Powder Blending

Composite was prepared by taking desired quantity of filler or fibre and dry mixing it with PP powder in an agate pestle and mortar. A range of composition of filler or fibre with respect to PP was made.

2.5 Melt Compounding of the Composites and Blends

A small quantity (0.25 gm) of the above mixed powder was compression moulded in a single ended compaction die at 29 MPa pressure for 30 seconds to form thin discs (12 mm diameter, 2 mm thickness). These were subjected to isothermal melt crystallization as follows:

The sample was first melted at 200°C in a microscopic slide with cover slip placed on a thermostated hot plate. The slides were then quickly transferred to the hot stage of an optical polarising microscope (Leitz,Germany) which was preheated to the desired crystallization temperature (T_c). The samples were kept at the T_c for at least 15 minutes. These were then quenched in methanol or distilled water so as to prevent the crystallization process at any other temperature during cooling.

For measuring the mechanical properties[1,2] such as impact and tensile strength, PP (commercial grade) was compounded with filler or fibre in desired proportion using single screw extruder[3]. The specification and conditions used were:

Model	Brabender Plasticorder
	Single Screw Extruder R-19
Extruder capacity	5 Kg/hr
Screw diameter	19 mm
Screw l/d	33
Die diameter	3 mm
Temperature set:	
Feed zone	150°C
Transitiion zone	175°C
Metering zone	190°C
Die temperature	210°C

All the above parameters were kept constant during the experiment except for the screw speed which was varied depending upon the materials used.

The extruded samples were then pelletized and injection moulded.[4] The specifications and conditions used during the injection moulding process were as follows:

Model	Arburg Alrounder 220-90-350 machine
Screw diameter	25 mm
Screw l/d	33
Screw speed	200 rpm
Clamping force	350 KN tons
Injection pressure	1905 bar
Temperature set:	
Feed zone	188°C
Transition zone	190°C
Metering zone	195°C
Nozzle temperature	210-215°C

The mould was kept at 30°C by water cooling. It contained multiple segments giving both tensile and impact strength test specimens in single shot.

2.6 Study and Monitoring of Crystallization Behaviour

A few of the premixed polymer samples were isothermally crystallized at a preset temperature as described above and the crystallization behaviour was investigated by continuously recording the growth of spherulites as well as the increase of transmitted light intensity (grey scale) in the cross polar mode of the optical polarizing microscope (Leitz, Germany) coupled with image analyser system (VIDPRO - 32, Leading Edge, Australia). The exact procedure used for studying the crystallization behaviour has been given under section 2.9.2.

2.7 Preparation of Blends

2.7.1 Solution Blending Technique

The blends were obtained by dissolving the two components typically PP and SBS (styrene-butadiene-styrene),(Cariflex, CTR 1102, Shell Corporation) in xylene at 120°C in the desired proportions. After the dissolution of the two components, the mixed solution was allowed to cool to room temperature and subsequently precipitated in methanol with constant stirring. The product obtained was in the form of flakes or powder, which was then filtered and washed thoroughly with methanol and finally dried under vacuum for 24 hours. Different compositions were made by varying the concentration of SBS with respect to major polymer

matrix. The product was in powder form which was compacted and studied for crystallization behaviour as described above.

2.7.2 Preparation of Hybrid Composites

The hybrid composite was prepared by the addition of a third component i.e. glass fibres (FGP Limited, diameter 15μm) of known quantity to the blend which was thoroughly mixed in an agate pestle and mortar. It was finely ground to form a uniform mixture. These were melt crystallized or melt processed/moulded and characterized for structure and morphology by various physico-chemical methods.

2.8 Preparation of NLO Crystals Dispersed Composite Films

2.8.1 Preparation of Solution Cast Films

Different polymers such as polymethyl methacrylate (PMMA), polyethylene oxide (PEO), polyvinyl acetate (PVAc) polyvinyl alcohol (PVA), etc. were dissolved in corresponding solvents such as acetone, methanol or deionized water to which were added para nitroaniline (PNA) or meta nitroaniline (MNA),(10% PNA or MNA solution) and a range of compositions were made. A small quantity of this solution cast was evaporated on microscopic glass slides or (15ml) in flat glass petridishes over 20 hours at room temperature kept in a dry box. These films were then subjected to isothermal melt crystallization process as described in section 2.5.

2.8.2 Preparation of Films Grown Under Electric Field

The solution cast films were first placed between transparent conducting indium tin oxide (ITO) coated glass and sandwiched to form ITO/film/ITO configuration. This was placed on hot plate held at desired temperature (> 110°C or T_g of the polymer). The electric field was applied for 1 hour. The samples were slowly cooled to room temperature over a period of 1 hour in presence of field. The field was switched off and the films were pealed off from the substrate after soaking in water. These were then thoroughly dried and used for structure and morphological studies.

2.9 Characterization Techniques

2.9.1 Melt Flow Index (MFI)

This is a tester supplied by International engineering industries. About 2.5 gm of the sample was placed in a preheated barrel (Temperature 190-200°C) and allowed to melt for 2 minutes. Then a load of 2 kg was applied. The extrudate was collected after discarding the initial output for certain predetermined time (15 seconds). Care was taken to retain certain amount of material in the barrel after the reading (the end portion not included). The MFI was estimated as the weight extruded/10 minutes. The extrudate thus obtained were sectioned in transverse direction and the surface morphology was observed by SEM.

2.9.2 Optical Polarising Microscopy

In order to study the crystallization behaviour, particle size analysis and morphology, a polarising microscope[5] (Leitz LaborLux 12 pol, Germany) coupled to an image analyser system (VIDPRO 32, Leading Edge, Australia) was used in the present work. Most of the analysis was carried out under cross polar conditions.

Figure 2.1 shows the essential parts of the optical polarising microscope. The microscope contains essentially a light source (Tungsten lamp 25 W), a condenser, a polariser, a sample stage with controlled heating arrangement, objective assembly, an analyser and eye-piece/microphotography arrangement. In another arrangement, image analyser was connected in place of microphotography.

The image analysis system contained a video camera connected to a computer via the software which provided image grabbing, image storage and analysis facilities. The images were continuously recorded during the isothermal crystallization process for every 10 seconds or 30 seconds interval and then analysed by recording the spot intensity (grey scale) at any given location of the screen. It was possible to direct small changes (up to 1 pixel) occurring at any chosen point for example, next to a fibre/additive surface during the crystallization of the matrix. The graphics provided in the software was used to plot intensity transmitted under cross polar condition with respect to real time.

Figure 2.2a shows the isothermal crystallization curve for pure PP at T_c =115°C as a graph of intensity verses time in seconds. Pure PP shows a slope of 0.14 at the $t_{1/2}$ point. Figure 2.2b shows a graph of spherulite size verses time in seconds for pure PP. Here it shows a slope of 0.104 at the same $t_{1/2}$ point. It should be noted that although the two graphs are

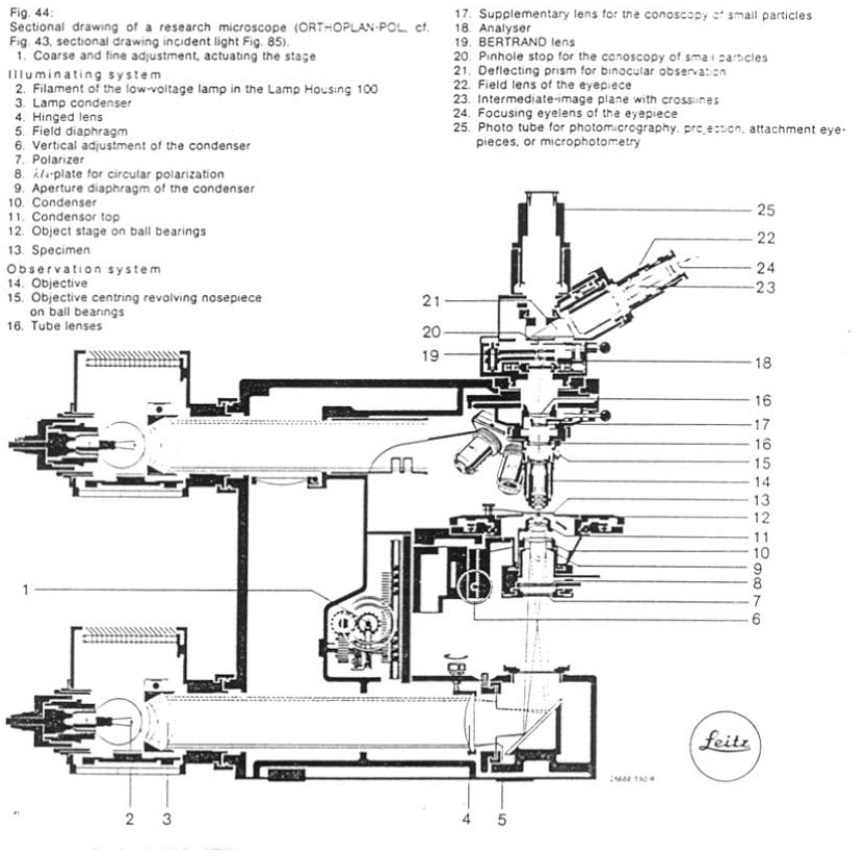

Figure 2.1 Represents the essential parts of the optical polarising microscope

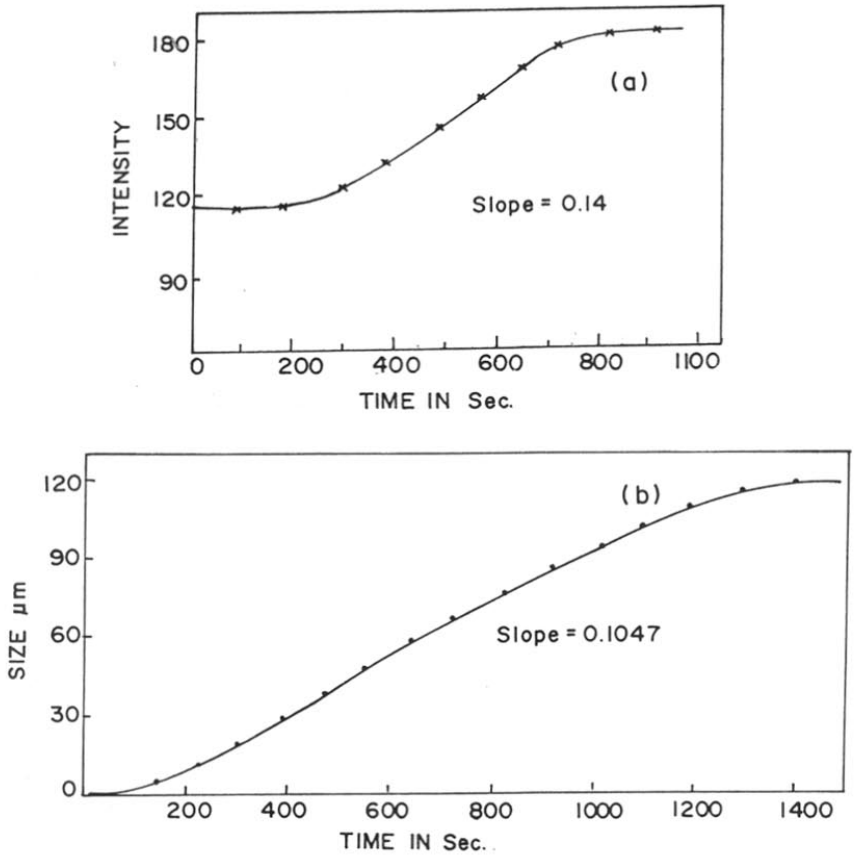

Figure 2.2 Isothermal crystallization curve for pure PP at T_c = 115°C
(a) Graph of intensity as a function of time in seconds
(b) Graph of spherulite size as a function of time in seconds

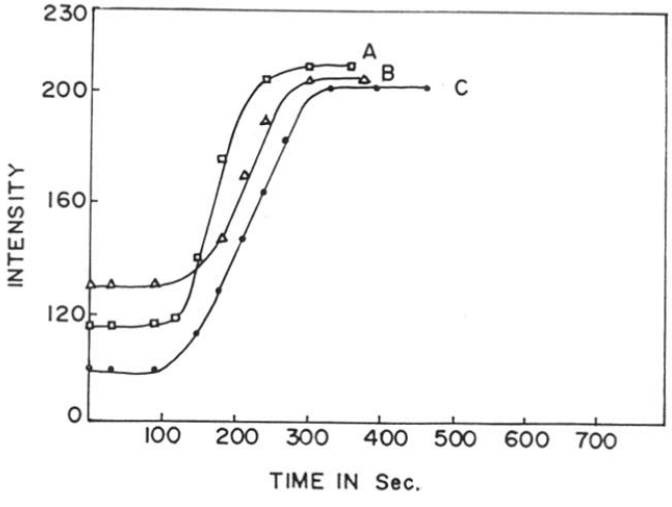

Figure 2.3 Crystallization curve of PP containing additive

similar, intensity measurement is very advantageous as compared to spherulite size measurement with respect to time due to many reasons.

(a) The size can be measured by optical microscope used upto a minimum of 2 microns. While the intensity can be detected on one pixel size on the screen (< 1 μm).

(b) Once the spherulite impinge with the adjacent one, the size of the spherulite remains constant but the internal structure of spherulite may change with crystallization which can be detected by intensity measurements very easily. However, the present measurements have to be compared with the reported ones in terms of spherulite size.

In order to express the growth rate in μm/sec, the growth of spherulites with respect to time for pure PP was first recorded. This same data was used for estimating the crystallization curve in terms of intensity vs time. The slopes of the two curves were compared and the multiplication factor was used to express the data of intensity in terms of μm/sec for the crystallization. This same factor was used for all the samples studied.

Figure 2.3 shows the typical crystallization curve of PP containing additive. It can be seen from the figure that fast crystallization process can be accurately monitored. However, background intensity is varying from sample to sample. This is due to two reasons:

Firstly, the thickness of the sample and secondly, the transparency. Since the present studies are mainly concerned with the crystallization rate and kinetics, the absolute value of intensity are not considered but only change in the intensity with respect to time in the crystallization process is of importance. The main advantage of this technique is that one can accurately determine the growth rate and $t_{1/2}$ values even for fast crystallization process.

2.9.3 X-ray Diffraction

The crystal structure, crystallinity and crystallite size of the samples prepared under various conditions were investigated by wide angle X-ray diffraction technique.[6] X-ray diffraction scans were recorded on a Philips (PW 1730) using the CuKα radiation with β Ni filter. (λ = 1.542 Å). All the scans were recorded in the 2θ range of 6 to 50° at a rate of 4°/min. The samples in the form of powder, thick discs and films coated on glass slides were used for analysis. Care was taken to align the sample surface along the sample holder surface so as to minimise any errors in diffraction angle.

Figure 2.4 shows the typical X-ray diffraction scan of a fibre reinforced polymer sample. Such WAXD patterns were indexed for known crystal structures by comparing the d-

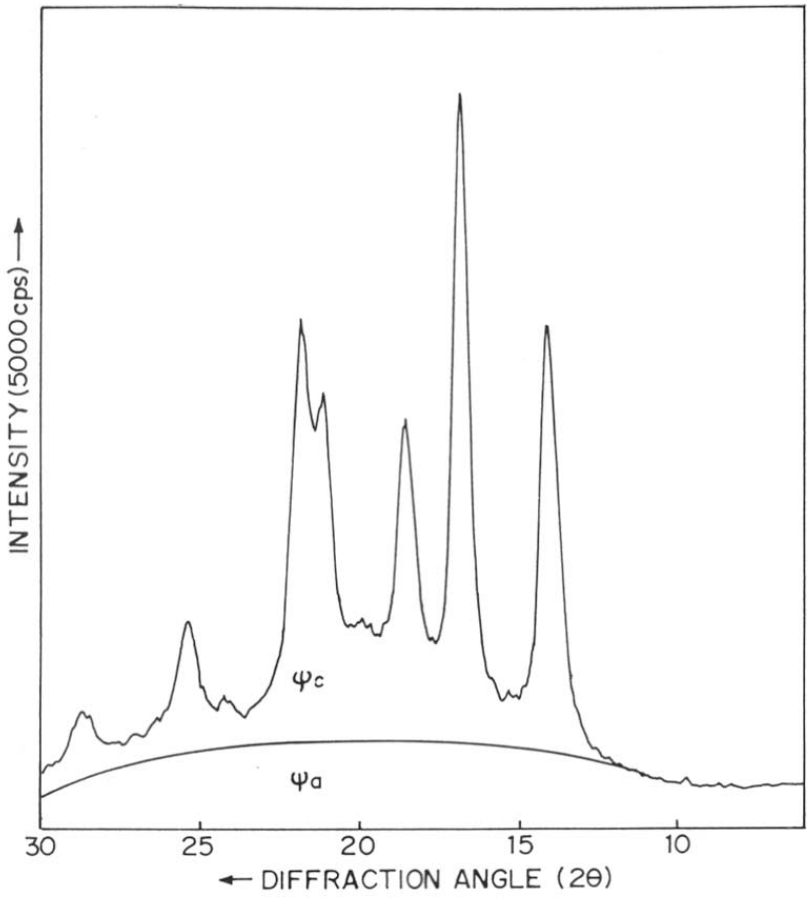

Figure 2.4 X-ray diffraction scan of a fibre reinforced polymer sample

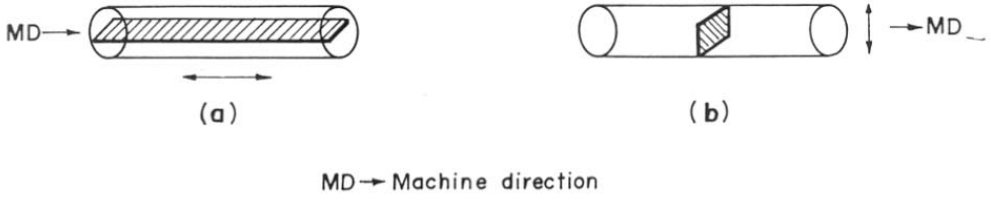

Figure 2.5 Extruded samples sectioned
(a) Parallel to machine direction
(b) Perpendicular to machine direction

values for the various peaks obtained with those expected for the same. The crystal structure of unknown specimen was determined by iterative techniques repeatedly correcting the lattice parameters so as to obtain the d-values closest to the observed ones within second decimal accuracy. The crystallinity (C_i) was determined from the WAXD scan as follows. The amorphous scattering curve was determined first graphically by deconvolution of the experimental curve. The area under the main crystalline peaks (ψ_c) and the area of the amorphous halo (ψ_a) were measured after due correction for the background scattering. C_i was then calculated from the equation

$$C_i = (\psi_c / \psi_a + \psi_c) \qquad (2.1)$$

The crystallite size was also measured using Scherrer's formula by taking the full width at half of the intensity of the peak as

$$L = (B\lambda / \Delta\theta \cos\theta) \qquad (2.2)$$

where B is a constant equal to 1; λ = CuKα is 1.542 Å ; $\Delta\theta$ is the breadth of the peak; θ is the angle and L is the crystallite size.

In order to confirm that the large variations in the intensities of some peaks were due to orientation of the crystallites with respect to film sample surface, the WAXD was recorded for specimens sectioned in different directions. As for example, in extruded samples, specimen were taken from the sections parallel to machine direction and perpendicular to machine direction as shown in Figure 2.5 a and b respectively. The WAXD was recorded from the flat surfaces of these sections. Any change in the intensity of a diffraction peak could then be due to corresponding orientation of crystallites with respect to that direction.

2.9.4 Differential Scanning Calorimetry (DSC)

In order to investigate the melting point, crystallization temperature and phase transitions if any, and also the crystallinity from the ΔH values the samples were analysed for DSC.[7,8] The DSC of Sieko SII SSC 5100 Japan instrument was used in our work. In some cases DSC of Perkin Elmer instrument was also used. The samples were heated at a rate of 10°C/min from RT to 200°C and vice versa.

In some cases (containing elastomers), low temperature range of -40°C to 200°C was used so as to determine change in T_g. The samples used were in the form of powder or film. The crystallinity was determined from the ΔH values by taking into account the heat flux values derived for 100% crystalline material reported in literature.

2.9.5 Thermogravimetric Analysis (TGA)

TGA[9] were investigated to determine the weight loss as a function of temperature and also the degradation temperature if any. The model of the instrument was Seiko II SSC 5100, Japan. The samples in the form of powder were used for analysis under nitrogen atmosphere at a rate of 10°C/minute from RT to 500°C. For example, the TGA of NLO dispersed composite film i.e. MNA (meta nitroaniline) dispersed in PMMA (poly methylmethacrylate) was investigated to determine the actual amount of MNA present in PMMA matrix after solution casting. Figure 2.6 shows the TGA of 50% MNA in PMMA. It can be observed from the figure that for 50% MNA, the data shows 34.1% MNA actually present. Thus, a loss of 16% can be associated due to diffusion of MNA over a period of time. The DSC of this sample gave 27.7 J/g as the heat of fusion ΔH value. The expected ΔH can be calculated for 34.1% MNA from 100% MNA, which shows 144.4 J/g as the ΔH value. Therefore, 49.24 J/g is the expected ΔH value obtained which gives a difference of ΔH of 21.54 J/g remaining. Now since 100% MNA shows a ΔH of 144.4 J/g, 21.54 J/g shows 14.92% of MNA remaining, which is present in the amorphous region. Thus, the actual amount of MNA was determined from both DSC and TGA.

2.9.6 Scanning Electron Microscope (SEM)

SEM[10] studies were performed to investigate the surface morphology or microstructure of the samples. Leica Stereoscan 440 model manufactured by M/s Leica Cambridge Ltd., U.K. was used in our work. The samples were fractured to expose the inside portion and mounted on the standard specimen mounting stubs by silver paste. These were coated with a thin layer of gold in plasma coating unit ES000 to prevent charging of the specimen. The micrographs of the samples with 10 KV EHT and 25 PA beam current were recorded by a 35 mm camera and attached on the high resolution recording unit.

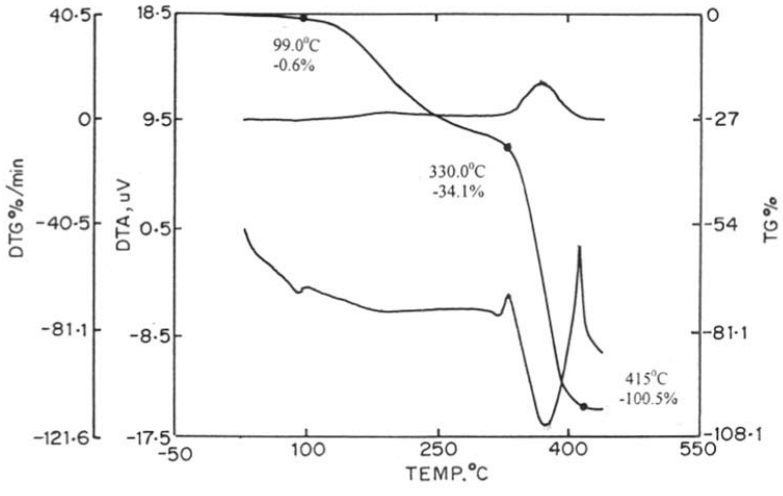

Figure 2.6 TGA of 50% MNA in PMMA composite film

2.9.7 Infrared Analysis

Infrared analysis[11] was carried out in order to determine the complex formation and/ or hydrogen bonding. The Perkin Elmer (16PC) FTIR spectrophotometer was used in our work. The samples were in the form of thin films while in some cases KBr pellet was used. These were scanned in the complete range from 450 to 4000 cm^{-1}.

2.9.8 Tensile Testing

For measuring tensile strength of the dumbell shaped specimens Instron Corporation series IX automated material testing system 1.04 machine was used. The specification and conditions used were:

Temperature	73°F
Humidity	50%
Specimen	ASTM D-638[12]
Crosshead speed	50 mm/min.
Extensometer gauge length	50 mm
Grip distance	115mm
Thickness	3.0 to 3.5 mm
Width	12.5 to 13 mm

Tensile strength was calculated by the following equation:

$$\text{Tensile strength} = \frac{\text{Force (load) N}}{\text{Cross sectional area (mm}^2\text{)}} \qquad (2.3)$$

Figure 2.7 shows the dumbell shaped specimen used for tensile testing.

It can be seen from the figure that W - Width of narrow section = 13mm

L - Length of narrow section = 65mm

Wo - Width over all = 19mm

Lo - Length over all = 215mm

G - Gauge length = 50mm

D - Distance between grips = 115mm

R - Radius of fillet = 76mm

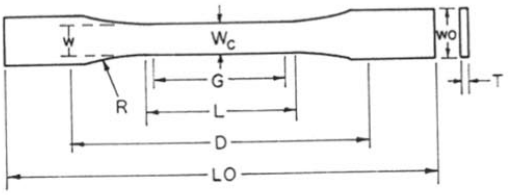

Figure 2.7 Represents the dimensions of dumbell shaped tensile specimen

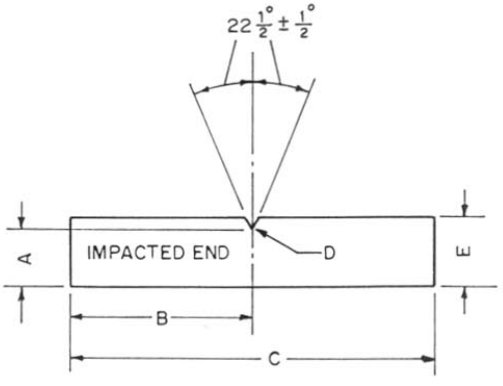

Figure 2.8 Shows the dimensions of Izod type notched impact specimen

2.9.9 Impact Testing

Impact tests were carried out on an Izod impact testing machine of model CEAST 6545/000 using notched specimens. The impact energy was obtained by the difference in the potential energy of falling hammer before and after impact. The specification and conditions used were:

Specimen	ASTM D-256[13]
Hammer	7.5 J
Temperature	Room temperature
Humidity	50%
Sample thickness	3 to 3.25 mm

Figure 2.8 shows the dimensions of Izod type notched impact specimen.

Where A = 10.16 ± 0.05mm

B = 32.20 mm

C = 63.50 mm

D = $0.25\ R \pm 0.05$ mm

E = 12.70 ± 0.15 mm

2.10 References

1. I.M. Ward, Mechanical Properties of Solid Polymers, John Wiley and Sons Ltd . (1983).
2. J. V. Schmitz, Testing of Polymers, John Wiley and Sons Ltd. **2** (1996).
3. Brabender Plasticcorder, PLE-330, OHG, Duisburg - Germany (1983).
4. Arburg, Maschinen Fabrik, Hehl and Soehne. Gmbh & Co. KG (1985).
5. G.H. Meeten ,Optical Properties of Polymers, Elsevier Applied Sci. Publishers London (1986).
6. L.E. Alexander, X-ray diffraction methods in Polymer Science, Wiley-Intersci. John Wiley and Sons, Inc. (1969).
7. W.M. Wendlandt , Thermal Methods of Analysis, John Wiley & Sons, Inc. (1974).
8. B.R. Currell , Thermal Methods, John-Wiley and Sons Ltd., London (1987).
9. T. Hatakeyama and F.X. Quinn, Fundamentals and Applications of Polymer Science, John Wiley and Sons, Japan (1974).
10. J. I. Goldstein and H. Yakowitz, Practical Scanning Electron Microscopy , New York Plenum Press (1975).
11. J.F. Rabek, Experimental Methods in Polymer Chemistry, John Wiley and Sons, New York (1980).
12. Annual Book of ASTM Standards, Part 27 (1973) p. 192.
13. Annual Book of ASTM Standards, Part 27 (1973) p. 72.

Chapter 3

Structure and Properties of PP/$CaSO_4$ Composites

3.1 Introduction

Polypropylene (PP), can be filled with various types of mineral fillers which have been sufficiently described and classified in many technical references.[1-7] These mineral fillers show reinforcing effect, nucleation of certain crystalline form and even epitaxial growth/ transcrystallinity in PP as described earlier in section 1.4. The effect of a filler on PP is determined by the characteristics of the filler such as shape of the particles, particle size and size distribution, surface area, particle packing, chemical composition and so forth.

M. Fujigama and T. Wakino[8] have studied the crystalline structure of injection mouldings of talc filled polypropylenes and found that these had a peculiar crystal orientation in which c and a*-axes were bimodally oriented to the flow direction while the b-axis was oriented to the thickness direction. According to them, this peculiar orientation originates from the flaky shape and nucleation ability of talc particles. In a mould cavity, talc particles are aligned parallel to the cavity wall by the action of flow. The crystallization proceeds with the (040) plane of PP crystal piling on the platy surface o f talc particles leading to b-axis being aligned parallel to the thickness and the cooling direction of injection moulding. The crystal orientation in injection moulding of unfilled PP is basically similar to that of talc filled PP although, the b-axis orientation to the thickness direction is much weaker. Varga et al.[9] while studying the crystallization and melting of PP observed remarkable differences in the effects of chalk and talc fillers. Chalk had a weak α nucleating activity whereas talc was considered as an effective α nucleating agent having a strong effect on the course of crystallization and polymorph composition. This filler, even at the concentration of 1%, suppressed the formation of β phase and in the presence of talc alone the products having high α phase content could be prepared.

During the investigation of structure development in polymer/solid filler systems, Rybnikar et al.[10] found that some sheet silicates such as kaolin and talc under favourable conditions have the character of epitaxial crystallization of polyolefins. The epitaxial polymer over-growth was very well formed in polyethylene-talc while not being well developed in PP-talc.

In the present scope of work, we have investigated the structure, morphology and properties of calcium sulphate filled polypropylene composite.

Calcium sulphate exists in various forms such as dihydrate $CaSO_4 2H_2O$, hydrate $2CaSO_4.H_2O$, sub-hydrate $CaSO_4$. $0.1\ H_2O$, hemi-hydrate $CaSO_4\ 0.5H_2O$ and anhydrite $CaSO_4$ respectively. The most common variety of calcium sulphate is dihydrate form having monoclinic crystal structure with $a_o = 5.68$ Å, $b_o = 15.18$ Å, $c_o = 6.51$ Å and $\beta = 118°.23'$. The anhydrite form crystallizes in orthorhombic system with a = 6.238 Å, b = 6.991 Å and c = 6.996 Å. The anhydrite $\gamma\ CaSO_4$ crystallizes in hexagonal system with a = 6.99Å and c = 8.34Å. The $\gamma\ CaSO_4$ anhydrite phase occurs at high temperature above 300°C. Thus the morphology of $CaSO_4$ depends very much upon the synthesis route.

From the literature survey on the studies of $CaSO_4$ filled plastics, it was found that $CaSO_4$ as filler in plastics has not been studied in depth. A few authors have reported the improvements in mechanical properties of $CaSO_4$ containing polymers. However, they have not looked at the structure, and morphology together with its effect on the mechanical properties of these composites.

Some authors[11] have used calcium sulphate mainly as an additive for building material which improved strength and appearance while others[12] have used $CaSO_4$ along with polyol-polyether mixture which has been recommended as a binder for coatings and sealants. These show resistance to mechanical stress, radiation, heat, etc.

In some of the patents[13], the authors have reported the use of $CaSO_4$ in glass fibre based reinforcing materials with good bending strength for use in building materials. The $CaSO_4$ was also used in PE fibres[14], which improved their tensile strength and modulus. $CaSO_4$ has been used in phenolic resin compounds[15] where the amino or epoxysilane treated gypsum fibres gave a molded specimen with heat resistance of 210°C compared with 190°C for the control containing untreated gypsum fibres.

$CaSO_4$ has been prepared in various forms such as fibres, whiskers, needles, particulates etc. by conventional hydrothermal methods. The high aspect ratio is particularly useful for increasing the reinforcement efficiency.

Winslow and Jerry[16] have prepared a fibrous calcium sulphate of anhydrite: hemi-hydrate form showing markedly improved dispersability for reinforcing purposes. It was prepared in an autoclave by maintaining constant pressure and temperature at or just above the minimum fibre forming conditions. Dispersants such as tannic acid were added to prevent clumping or balling. Crystals with average fibre lengths 100-300 μm and aspect ratio of 25-60 were obtained.

In some cases $CaSO_4$ was used in vinyl chloride polymer compositions[17] along with mica, polyethylene, polymethyl methacrylate, epoxy resin, polyster wax and fatty acid salt which gave good impact strength and appearance.

Recently Franklin[5] prepared a new form of calcium sulphate viz. β anhydrite fibre which is referred to as Franklin fibre. This fibre has a white, lustrous appearance with a silky, soft feel. Microscopic examination shows fibrous crystals with average length of 80 μm and a very uniform diameter of about 2 μm. It is chemically stable. It has low water solubility and exhibits no toxic effects in handling or production. It has high temperature resistance and possesses good insulating qualities. Its use as reinforcing filler in plastics improved tensile strength and in most cases dramatically increased the modulus of elasticity. It was observed that, with improved tensile and flexural behaviour a decrease in impact resistance was often obtained.

Franklin fibre was produced using a single batch reactor system, where a water slurry of gypsum was first preheated and then pumped to a steam jacketed reactor. The reaction product was gravity fed to a holding tank, and then to a filter press, which removed most of the water. The resulting fibrous cake was then heated in an oven to remove the remaining surface moisture. Thereafter the fibrous cake was calcined to form dead burnt, and preferred form of Franklin Fibre.

The use of additives as flame retardants[18-22] in plastics has drawn considerable attention. The considerations of safety in use and in particular the need for low flammability of reinforced thermoplastics have grown in importance with the increasing application of these materials in the building industry, in electrical components, portable tools, domestic and office appliances. Amongst the many flame retarding agents which are being used in various polymers such as polyethylene, polypropylene, polyvinyl chloride, polyesters, etc. are sulphates such as ammonium sulphate, barium sulphate, calcium sulphate, etc. Recently, the use of anhydrous calcium sulphate filler as a flame retardant is gaining interest in plastics.[23] It can be used in plastics processed at over 300°F without releasing water. Apart from flame retardancy, increased interest has been drawn in its use in rigid and flexible polyvinyl chloride and as a TiO_2 extender in colour concentrates.

It is seen from the above survey that $CaSO_4$ can play an important role as a filler in plastics. The advantages of $CaSO_4$ as filler can be summarized as follows:

(a) The fibrous or whisker form of $CaSO_4$ offers high aspect ratio providing increased stiffness without degrading impact strength when used as a filler in plastics.

(b) Flame retardancy as described above.

(c) $CaSO_4$ is an effective additive for many paint and coating formulations especially the aqueous based ones.

(d) Because of its setting properties, it is used along with other building materials.

Although it has the above-mentioned advantages there are very few detailed reports in literature on $CaSO_4$ filled composite system. Hence, it was proposed to investigate the possibility of synthesis of $CaSO_4$ with modified morphology. The main advantage of use of $CaSO_4$ lies in the fact that it can be grown in fibrous morphology leading to better reinforcements and use the same as filler in polypropylene. The accompanying changes in the crystallization behaviour of PP are also of interest since these would govern the various properties of resulting composite.

In the present scope of work, we have investigated the structure, morphology and properties of $CaSO_4$ filled PP composite.

It has been seen from the survey that shape, size, crystalline phase and orientation of the filler play a vital role in deciding the properties of the final product. A number of naturally occurring minerals are used as fillers as described earlier and conventional methods of size / shape selection were limited to their natural availability. Synthetic fillers made by conventional routes also have limited range of morphology. Further, many of the additives have to be treated with surface modifier, coupling agents, wetting agents etc. to enhance interfacial adhesion, dispersability, etc. Conventional compounding techniques often destroyed the original aspect ratio or sizing of the fillers. Hence, it would be advantageous if a process is developed for incorporation of filler by *in situ* deposition within the polymer matrix. The main advantages would be, control of overall morphology; uniformity of size and dispersion, generation of orientation and better interfacial adhesion which can be achieved by shorter direct route. The influence of surrounding matrix or polymer induced crystallization is a new observation reported only recently.[24-26] For example, inorganic salts such as $CuCl_2$, K_2CO_3, $CaCO_3$, Cds, etc. have been grown in polymer matrix *in situ* of polyethylene oxide (PEO). The influence of polymer on the crystallization of the added salt was found in either new features of its morphology or change of its crystalline phase. This has been attributed to

the strong tendency of PEO for complexation with a number of inorganic salts or ions and the subsequent crystallization governed by the template formed by these complexes.

Hence, it was thought that it could be possible to grow $CaSO_4$ crystals by this *in situ* deposition technique under controlled conditions and use the same for making PP-$CaSO_4$ composites. The preparation of the filler i.e. $CaSO_4$ by this polymer mediated technique and formation of composite are described in experimental section while the effect of $CaSO_4$ on crystallization and properties of PP are described in subsequent sections of this chapter.

3.2 Experimental

(a) Preparation of $CaSO_4$ filler by *insitu* technique

The calcium sulphate was prepared by *in situ* deposition technique as described in section 2.3. This essentially consists of first forming a complex of $CaCl_2$ ($CaCl_2$ S.D. Fine Chemicals, India) with polyethylene oxide (PEO; WSR -N-750, BDH, England, MW - $3x10^5$) by dissolving the two components in the range 20% $CaCl_2$ and 3%to 25% PEO in methanol. This was allowed to remain for few hours. Appropriate stoichiometric amounts of potassium sulphate (K_2SO_4, BDH, England) dissolved in distilled water was added to the above complex slowly without stirring. The whole reaction mixture was allowed to digest at room temperature for 20 hours, when the ions diffused through the PEO and formed white gel like precipitate, which was filtered, washed lightly and dried. The formation of $CaSO_4$ can be represented by the following equation:

$$CaCl_2 + PEO \rightarrow \underset{\text{(Complex)}}{CaCl_2 \text{ - } PEO} \qquad (3.1)$$

$$CaCl_2 \text{ - } PEO + K_2SO_4 \rightarrow CaSO_4 \text{ - } PEO + 2KCl \qquad (3.2)$$

Two types of $CaSO_4$ designated as $CaSO_4$ (IS) and $CaSO_4$ (ISW) were synthesized by above method with varying concentrations of PEO from 10 to 50 wt.% in both the cases. The first case i.e. $CaSO_4$ (IS), PEO was firmly bound to $CaSO_4$ whereas in $CaSO_4$ (ISW), PEO was thoroughly washed out of the resulting precipitate during filtration. These were compared with commercial $CaSO_4$ designated as $CaSO_4$ (CM). All the three grades were characterised for structure and morphology by X-ray diffraction and optical polarising microscopy in the manner described in section 2.9.

In another set of experiments, $CaSO_4$ (ISW) variety in which the PEO was thoroughly washed after deposition, PEO was added externally in different concentrations from 10 to 50 wt.%. Thick wet slurry was made and these were subjected to shearing between the glass slides. The samples were allowed to dry and particle size and shape analysis was carried out using the optical microscope coupled to the image analyser system. The $CaSO_4$ (IS) synthesized *in situ* using different concentrations of PEO varying from 10 to 50 wt.% were also characterised by thermogravimetric analysis (TGA) in order to determine the PEO content and moisture in the final product.

(b) Preparation of Composite

Polypropylene (Indothane, SM85N, MFI-12, IPCL, Baroda, India) powder was obtained after precipitation of its xylene solution in acetone followed by thorough washing with acetone and drying. The composite was made by taking desired amount of $CaSO_4$ in PP powder and dry mixed in an agate mortar. Both $CaSO_4$ (IS) and $CaSO_4$ (ISW) prepared with 10% PEO were used for making PP-$CaSO_4$ composite by varying the additive concentration ranging from 10, 20, 30 and 40% by wt. respectively with respect to PP in each case. A small quantity of each of the above mixed PP-$CaSO_4$ composition was also isothermally melt crystallized on the hot stage of the microscope and the crystallization behaviour of these samples investigated in the same manner as described in section 2.6 by observing the intensity under cross polar condition.

The PP-$CaSO_4$ powder samples of different compositions containing 10, 20, 30 and 40 wt.% of both varieties were also compression moulded in a single ended die at 29 MPa pressure for 30 seconds to form thin discs (12 mm diameter, 2 mm thick). These were subsequently subjected to the same melt crystallization as before (melt temperature 190°C, crystallization at 115°C, time 15 minutes). The structure of these melt-crystallized samples was also investigated by X-ray diffraction technique. Some of the PP-$CaSO_4$ powder samples of additive concentration of 20 and 30wt.% were extruded at a mild extrusion rate from a melt indexer and these were analysed for orientation by X-ray diffraction by sectioning the samples parallel and perpendicular to the direction of extrusion. These sectioned samples were observed under microscope in the reflection mode in order to study the orientation of the additive. The melt compounded and injection moulded PP-$CaSO_4$ were also similarly examined. Some of the PP-$CaSO_4$ composites were also analysed by DSC and TGA in order

to determine various phase transitions, crystallization and melting behaviour of PP and the amount of $CaSO_4$ actually present.

The injection-moulded specimens of PP-$CaSO_4$ composites were prepared to measure the mechanical properties. Four compositions of each variety ranging from 5, 10, 15 and 25 wt.% respectively of $CaSO_4$ were made by mixing with commercially available PP pellets (grade IPCL). These were compounded using Brabender-Plasticorder single screw extruder. The temperature conditions set were same as given in section 2.5. The screw speed was maintained in the range of 16-18 rpm. These samples were then pelletized and injection moulded and tested for impact and tensile strength. The instrument details and specifications of single screw extruder and injection moulded machine and also the details of impact and tensile testing have been discussed in sections 2.5 and 2.9.

The various grades of $CaSO_4$ prepared and the PP-$CaSO_4$ composites made from each of them have been designated by certain nomenclature for ease of discussion. These are indicated in Table 3.1A and B.

Table 3.1A gives the list of symbols designated for *in situ* formed filler hereafter in the discussion.

$CaSO_4$(IS)	*In situ* formed $CaSO_4$ containing PEO
$CaSO_4$(ISW)	*In situ* formed $CaSO_4$ after washing out PEO
$CaSO_4$(CM)	Commercial variety of $CaSO_4$

Table 3.1B refers to the list of symbols abbreviated for PP-$CaSO_4$ composite system referred to hereafter in the discussion.

PP-CaS(IS)	*In situ* formed $CaSO_4$ containing PEO mixed with PP powder samples
PP-CaS(ISW)	*In situ* formed $CaSO_4$ without PEO mixed with PP powder samples
PP-CaS(ISWE)	Extruded pellets of PP with *in situ* formed $CaSO_4$ after washing out PEO
PP-CaS(ISJ)	Injection moulding specimen of PP with *in situ* formed $CaSO_4$ containing PEO
PP-CaS(ISWJ)	Injection moulding specimen of PP with *in situ* formed $CaSO_4$ after washing out PEO

3.3 Results and Discussion

3.3.1 Preparation of $CaSO_4$ by Polymer Induced Crystallization Technique

The white precipitate obtained after the reaction of $CaCl_2$ with potassium sulphate in presence of different concentrations of polyethylene oxide (PEO) was analysed for crystal structure by XRD. Figure 3.1 shows the XRD scans for the $CaSO_4$ prepared by *in situ* technique (Curve A) containing 30% PEO together with that of commercially available $CaSO_4$ (Curve B). It is evident from the figure that $CaSO_4$ (IS) is distinctly different from the commercial grade $CaSO_4$ (CM). The detailed analysis of the XRD and assignment of various reflections is given in Table 3.2. There are a number of crystalline forms reported for $CaSO_4$ existing in both anhydrous and hydrated states. Amongst these, the anhydrite and dihydrate forms are the most commonly found ones.[27-29] It is interesting to note that commercial $CaSO_4$ shows a highly intense peak at 2θ of 25.4° which corresponds to (002/020) reflection of monoclinic phase. This peak intensity is suppressed in case of $CaSO_4$ (IS) containing 30% PEO. Also some of the weak reflections observed in $CaSO_4$ (CM) have become enhanced in $CaSO_4$ (IS) with 30% PEO. From the differences observed in the relative intensities of the two, it appears that the commercial $CaSO_4$ contains mainly the anhydrite form (88%) with a small amount of dihydrate $CaSO_4.2H_2O$ as well as hemi-hydrate $CaSO_4$ $0.5H_2O$ present in it. The hydrated forms may have been formed due to absorption of moisture in these commercial samples over a long period of storage. On the other hand, the *in situ* deposition technique with 30% PEO yields exclusively the dihydrate form of $CaSO_4$. The major reflections of $CaSO_4$ (IS) of dihydrate form corresponds to monoclinic crystal structure having the lattice parameters of a= 5.67 Å, b = 15.15 Å, c = 6.51 Å and $\beta = 118.23°$.[30] There are some very weak reflections which may be assigned to the complex of PEO with $CaCl_2$ for which the structure was reported by us.[31] The presence of this very small unreacted component of the complex in these samples could be attributed to strong coupling between the calcium ions and oxygen moieties of PEO which could not be totally dissociated by the sulphate ions within the period of reaction due to slow diffusion of bulky SO_4 groups in the polymer matrix.

In order to understand the effect of PEO on the structure and morphology of $CaSO_4$ formed *in situ*, different concentrations of PEO ranging from 10 to 50 wt.% were used and the reaction was carried out as before after complexation with $CaCl_2$. Figure 3.2 shows the XRD scans for $CaSO_4$ (IS) sample prepared with different concentrations of PEO. The curves A to E correspond to PEO concentrations of 10, 20, 30, 40 and 50 wt.% respectively. It is evident

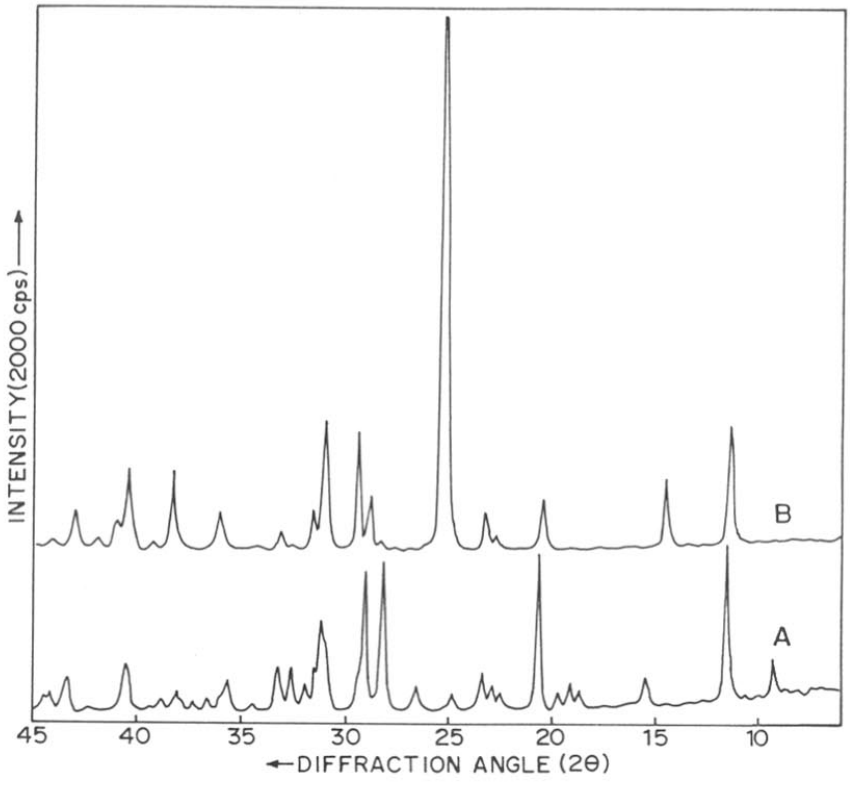

Figure 3.1 X-ray diffraction scan for different grades of calcium sulphate: (A) prepared by *in situ* technique and (B) commercially available grade.

Table 3.2 XRD analysis of $CaSO_4$ prepared by *in situ* technique

Commercial $CaSO_4$		Assignment	$CaSO_4$ (IS) containing 30% PEO		Assignment
d (obs)	I/I_0	(hkl)	d (obs)	I/I_0	(hkl)
7.62	22		7.59	<u>100</u>	dihydrate (020)
6.03	13	hemi-hydrate			
4.31	8	dihydrate ($12\bar{1}$)	4.30	96	dihydrate ($12\bar{1}$)
3.90	3	anhydrite (111)			
3.82	7	dihydrate (031/040)	3.82	25	dihydrate (031/040)
3.52	<u>100</u>	anhydrite (002/020)			
3.13	2	anhydrite (200)	3.16	92	dihydrate ($11\bar{2}$)
3.08	10	dihydrate ($14\bar{1}$)	3.07	85	dihydrate ($14\bar{1}$)
3.02	21	hemi-hydrate			
2.87	23	anhydrite (210), dihydrate (002)	2.86	56	dihydrate (002)
2.82	8	anhydrite (121), dihydrate ($21\bar{1}$)			
2.70	4	dihydrate (022/051)	2.69	26	dihydrate (022/051)
2.48	7	anhydrite (022)			
2.34	14	anhydrite (202/220)			
2.22	15	anhydrite (212)	2.23	30	dihydrate ($15\bar{2}$)
2.19	6	anhydrite (103)			
2.09	7	anhydrite (113)			
1.87	12	anhydrite (230)			

Ref. Anhydrite diffraction file (ASTM) 6-0226 ,
Dihydrate diffraction file (ASTM) 1-0385,
Hemi-hydrate diffraction file (ASTM) 1-0999.
Underlined reflections to bring out the comparison of d-values for strongest peak.

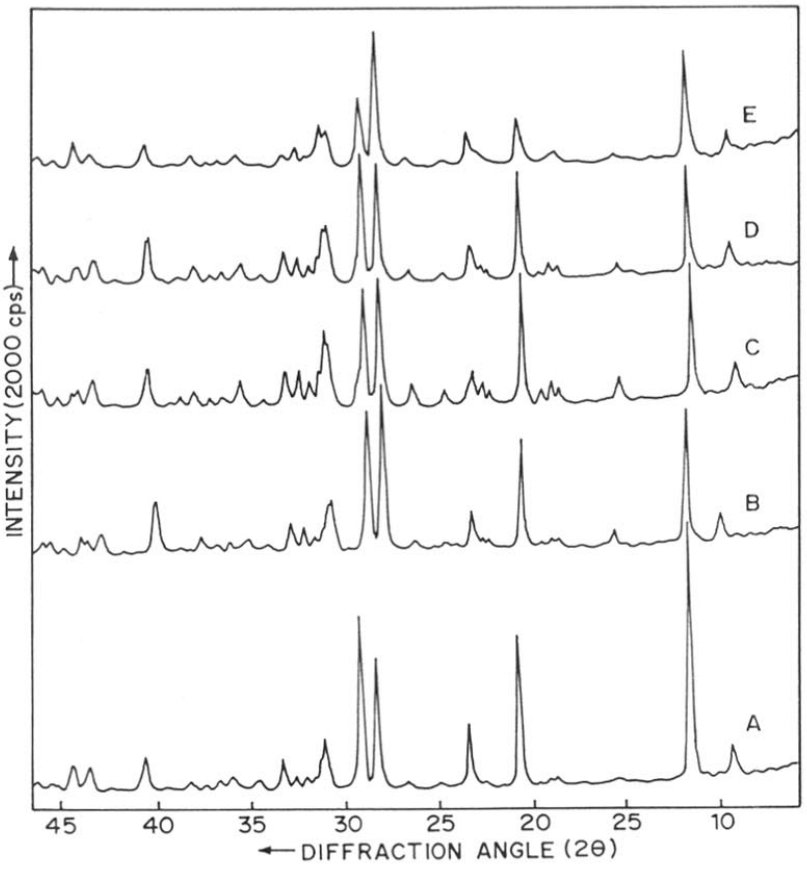

Figure 3.2 XRD scans for $CaSO_4$ prepared by *in situ* method with different concentrations of PEO. Curves (A) to (E) correspond to PEO concentrations of 10, 20, 30, 40 and 50 wt.% in solution respectively.

from the figure that the basic structure of $CaSO_4$ formed is the same i.e. monoclinic in all cases. However, the relative intensities of peaks change considerably especially in the 2θ region of 10 to 30° with the increase of PEO concentration. Thus, the reflections corresponding to (020), $(12\bar{1})$, $(11\bar{2})$ and $(14\bar{1})$ show large variations with the increase of concentration of PEO. The relative intensity ratios and the various assignments of peaks are represented in Table 3.3.

The morphology of $CaSO_4$ prepared by *in situ* technique was compared with commercial variety of $CaSO_4$ and it was found that $CaSO_4$ (IS) sample showed distinctly different morphology from that of the commercial variety. Figure 3.3 shows the optical micrographs for these samples. It is obvious from the figure that $CaSO_4$ (IS) has long needle shaped morphology with aspect ratio of 9 to 10 (Fig.3.3a) whereas the commercial sample consists of small globular shaped particles with aspect ratio of almost 1(Fig.3.3b). Another interesting observation is that the $CaSO_4$ (IS) showed two types of needles in which one was highly birefringent than the other suggesting that there could be two different crystalline phases obtained in these samples.

In order to study the effect of shearing on the $CaSO_4$ needle shaped crystals the $CaSO_4$ (ISW) samples were used to which PEO was added externally in the range 10 to 30 wt.%. These were sheared in the semi-wet state (made wet by few drops of water) and sheared between two glass slides. The structure and morphology of these samples were investigated as before. Figure 3.4 shows the XRD scans for these sheared samples. Curves A, B and C correspond to PEO concentrations of 10, 20, and 30wt.% respectively. It is interesting to note that the intensities of some reflections increase enormously while for others there is decrease in intensity after shearing with the increase in PEO content. The detailed analysis and the assignment of the XRD peaks is given in Table 3.4. It is seen that the intensity of (020) reflection (which is of medium intensity in ordinary hydrated $CaSO_4$) increases tremendously while those of $(12\bar{1})$ and $(14\bar{1})$ reflections decrease considerably in sheared samples. These changes in the intensities of XRD peaks can be associated with the orientation of crystals with respect to the substrate surface during the shearing of samples. Figure3.5 shows the optical micrographs of the sheared samples. It is evident from the figure that $CaSO_4$ crystals are aligned such that their long axis is parallel to the direction of shearing of the polymer.

The particle size analysis of these sheared samples containing different concentrations of PEO were measured using optical microscope coupled to an image analyser (Leitz/VidPro).

Table 3.3 XRD analysis of $CaSO_4$(IS) containing different concentrations of PEO ranging from 10 to 50 wt.%

$CaSO_4$(IS) containing PEO concentration						
	10%	20%	30%	40%	50%	Assignment (hkl)
d (obs)	I/I_o	I/I_o	I/I_o	I/I_o	I/I_o	
9.51	16	24	32	30	28	PEO-$CaCl_2$ (002)
7.56	100	87	100	86	84	dihydrate (020)
5.68	4	13	21	15	10	PEO-$CaCl_2$ (013)
4.74	5	8	13	12	12	PEO-$CaCl_2$ (023)
4.62	3	7	18	15	9	PEO (120/111)
4.27	56	64	94	84	36	dihydrate ($12\bar{1}$)
3.93	3	6	11	8	7	PEO-$CaCl_2$ (130)
3.88	3	7	16	12	10	PEO-$CaCl_2$ (131)
3.78	25	24	24	29	26	PEO (112)
3.33	3	7	16	10	7	PEO (131)
3.15	48	100	89	92	100	dihydrate ($11\bar{2}$)
3.05	65	85	83	100	54	dihydrate ($14\bar{1}$)
2.86	19	29	55	45	33	dihydrate (002)
2.78	5	14	18	14	14	dihydrate ($21\bar{1}$)
2.74	5	8	26	19	15	PEO-$CaCl_2$ (233/300)
2.68	12	15	26	25	10	dihydrate (022,051)
2.59	4	17	6	6	2	dihydrate (150,202)
2.50	3	4	19	16	11	dihydrate (060)
2.49	5	-	-	-	7	dihydrate (200)
2.45	4	8	8	10	6	dihydrate ($22\bar{2}$)
2.40	2	7	-	7	5	dihydrate (141)
2.36	2	4	6	8	10	PEO-$CaCl_2$ (330)
2.35	4	9	12	15	3	PEO-$CaCl_2$ (332)
2.22	12	3	29	34	21	dihydrate ($15\bar{2}$)
2.08	9	12	21	21	12	dihydrate ($12\bar{3}$)
2.04	10	8	13	14	19	PEO-$CaCl_2$ (400)
1.99	3	4	6	8	5	dihydrate (170)
1.96	3	8	13	14	10	dihydrate (211)
1.95	3	8	11	10	12	dihydrate ($\bar{2}11$)
1.90	11	16	19	21	14	dihydrate (080/062)
1.88	5	7	9	12	7	dihydrate ($14\bar{3}$)

Underlined reflections to bring out the comparison of d-values for strongest peak.

(a)

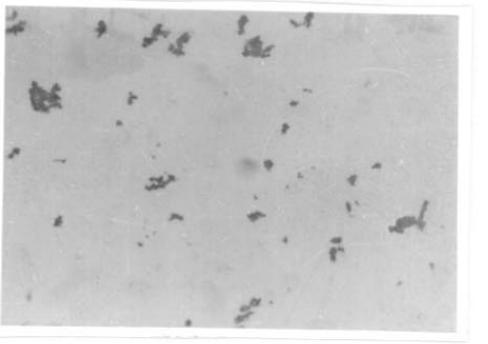

(b)

Figure 3.3 Morphology of $CaSO_4$ particles prepared by *in situ* method (a) and that of the commercial grade (b)

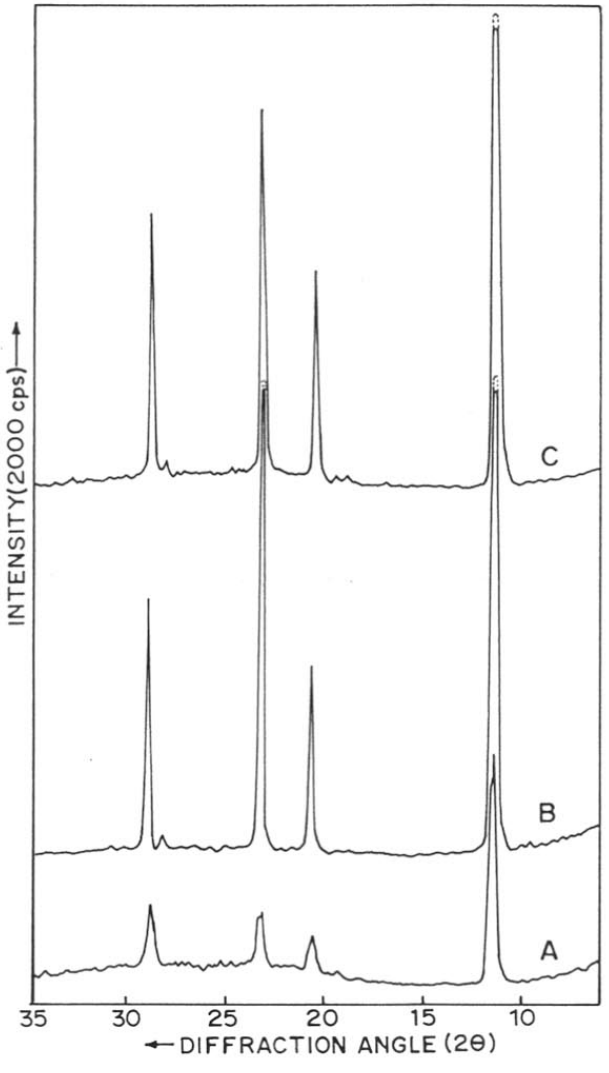

Figure 3.4 XRD scans for $CaSO_4$ prepared by *in situ* method using PEO after shearing between glass slides. Curves A , B and C correspond to PEO concentrations of 10, 20 and 30 wt.% respectively.

Table 3.4 XRD analysis of sheared samples (PEO-$CaSO_4$) containing different concentrations of PEO ranging from 10 to 30 wt.%

10%			20%		30%		$CaSO_4.2H_2O$[a]		
2θ	d (obs)	I/I_o	d (obs)	I/I_o	d (obs)	I/I_o	d (cal)	hkl	I/I_o
11.5	7.69	<u>100</u>	7.69	<u>100</u>	7.69	<u>100</u>	7.70	020	50
20.6	4.33	23	4.31	7	4.31	15	4.29	$12\bar{1}$	<u>100</u>
23.2	3.85[b]	22	3.82	23	3.82	27	3.81	031/ 040	15
28.9	3.11	35	3.08	9	3.08	20	3.06	$14\bar{1}$	63

[a]as per monoclinic crystal structure of $CaSO_4.2H_2O$ Ref. ASTM 1-0385
[b]also 112 reflection of PEO (d = 3.81)
a = 5.76 Å, b = 15.15 Å, c = 6.51 Å β = 118.23°
Underlined peaks represent reflection of maximum intensity

Figure 3.5 Optical micrographs of $CaSO_4$ samples after shearing. (a), (b) and (c) correspond to PEO concentrations of 10, 20 and 30 wt.% respectively. (net magn. =100x)

Figures 3.6a, b, c, d and e represents the histograms of size distribution of the particles of $CaSO_4$ (IS) sheared samples ranging from 10 to 50 wt.% PEO. In 10% concentration of PEO (see Fig.3.6a) there are large number of particles having sizes ranging from 20 to 60 μm. There are a few which have size greater than 70 μm. Thus, the size distribution is quite broad in this case. With increase in PEO concentration to 20%, as can be seen in Fig. 3.6(b), decrease in the number of particles having size greater than 50 μm and increase in the number of particles in the region between 20-30 μm are seen. Here, the size distribution curve has become narrower compared to that of 10% PEO. With further increase of concentration of PEO to 30% (see Fig.3.6c) the size distribution becomes still narrower with greater number of particles between 10 to 30 μm and the formation of some particles having small size less than 10 μm. Figure 3.6d and e show the micrograph for 40% and 50% PEO in which the distribution curve has become very much narrow and the number of particles having size below 10 μm are also increased. Thus, it is clear that with increase in concentration of PEO, the particle size distribution becomes narrower and the peak shifts towards smaller particle size.

These various results explained above clearly bring out the influence of the role of PEO in the formation of $CaSO_4$. The various processes involved in this *in situ* deposition technique can be explained as follows. Firstly, the calcium salt forms a complex with the polymer (PEO) in which the calcium ions are bound within the helical chain of oxygen atoms of the polymer.[32,33] This is then reacted with potassium sulphate during which the sulphate ions diffuse into the polymer. Since the calcium ions are bound by the polymer chain, the formation of $CaSO_4$ can take place only at certain sites which are dependent on the relative concentrations of the polymer. The distance between these sites would depend upon the type of PEO-$CaCl_2$ complex, which must be in the ratio of 2:1, 4:1 or 16:1 etc. with respect to monomer unit of PEO. The proximity of such molecules would ultimately decide how the crystals would grow. Thus the polymer matrix surrounding the $CaSO_4$ moieties influences their growth behaviour. This justifies the presence of some weak reflections corresponding to unreacted PEO-$CaCl_2$ complex. Also, the decrease in the particle size with the increase of PEO content and the variation in the intensities of certain reflections suggest that the growth of certain crystalline face has been inhibited. Thus, these various results obtained are in good agreement with the above hypothesis that the polymer induced crystallization can be used for modifying the characteristics of the additive such as $CaSO_4$.

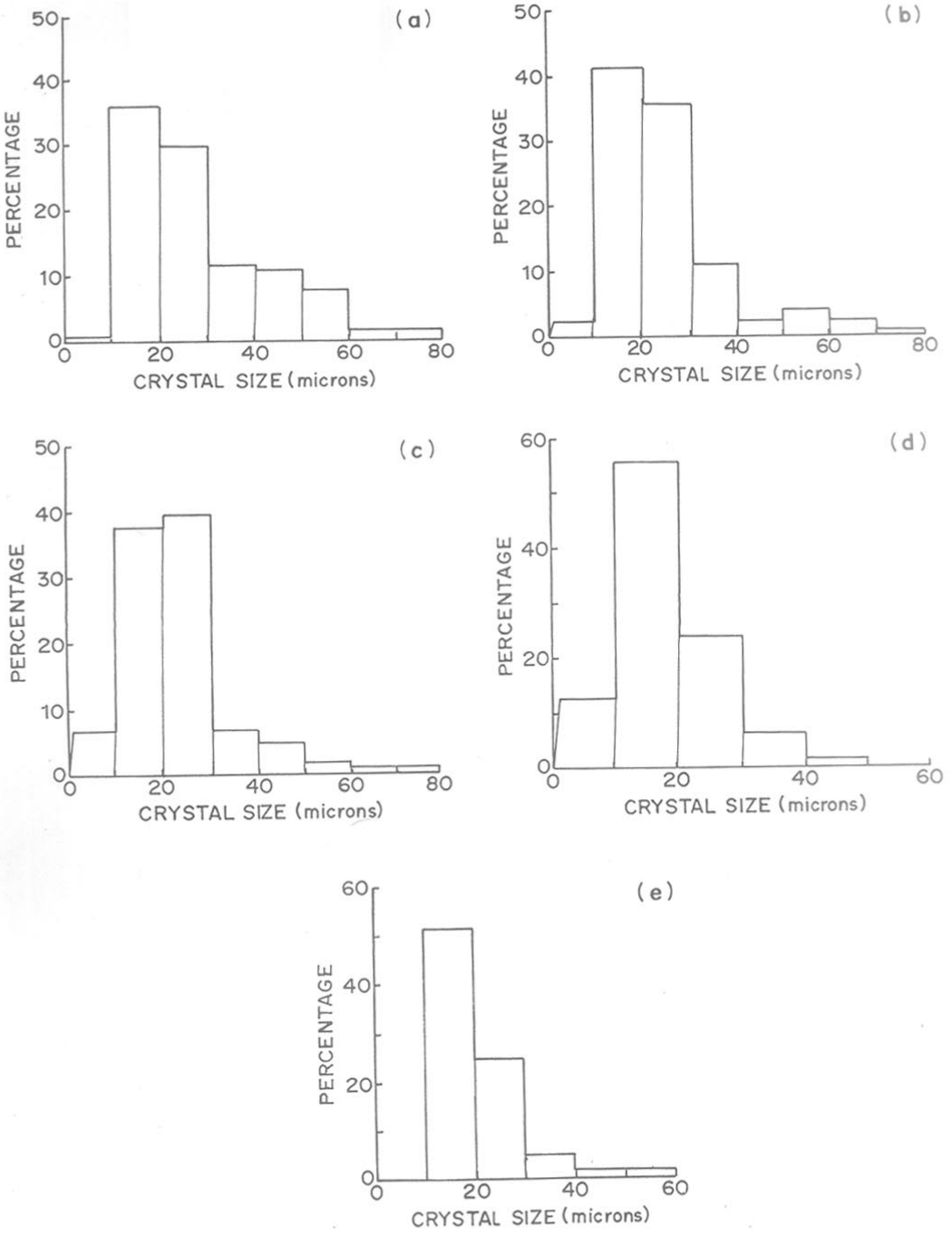

Figure 3.6 Histograms of crystal size distribution of $CaSO_4$(IS) sheared samples a, b, c, d and e correspond to PEO concentrations of 10, 20, 30, 40 and 50 wt.% respectively.

The thermal analysis i.e. TGA of the $CaSO_4$ (IS) samples with different concentrations of PEO were studied for determining the PEO content and possibly the presence of moisture. Figures 3.7a ,b, c and d show thermograms of $CaSO_4$ (IS) containing 10, 20, 30 and 40 wt.% PEO. The thermograms shows two well separated transitions. The weight loss commences just above 100°C. The first transition corresponds to moisture and the second transition to that of PEO content. It is thus confirmed from XRD that $CaSO_4$ (IS) samples have dihydrate form and in addition to this, these may contain small amounts of hemi-hydrate. With this supposition and by knowing the amount of $CaSO_4$ and the corresponding water of crystallization, it has been possible to derive the moisture content in the ratio dihydrate:hemi-hydrate from the thermograms. These have been represented in Table 3.5 below.

Table 3.5 TGA analysis of $CaSO_4$ (IS) prepared with different concentrations of PEO

$CaSO_4$(IS) prepared with PEO concentration	Dihydrate: Hemi-hydrate	Amount of $CaSO_4$ (%)	Remaining PEO (%)
10%	1:1	97.7	2.3
20%	1:5	92.6	7.4
30%	1:10	91.5	8.5
40%	1:5	88.5	11.5

From the above table it is obvious that with the increase of PEO concentration the dihydrate formation is decreasing while that of hemi-hydrate formation is increasing. This rise in hemi-hydrate formation could be due to the presence of PEO, which is capable of holding the water molecules within itself and does not allow the calcium sulphate to crystallize with water of crystallization. Hence, the proportion of hemi-hydrate formation was more at high concentration of PEO. We have also calculated the amount of PEO present for all the compositions from the figure. It was found that approximately one fourth of PEO was remaining from the actual amount added during the *in situ* deposition process, the rest being washed off.

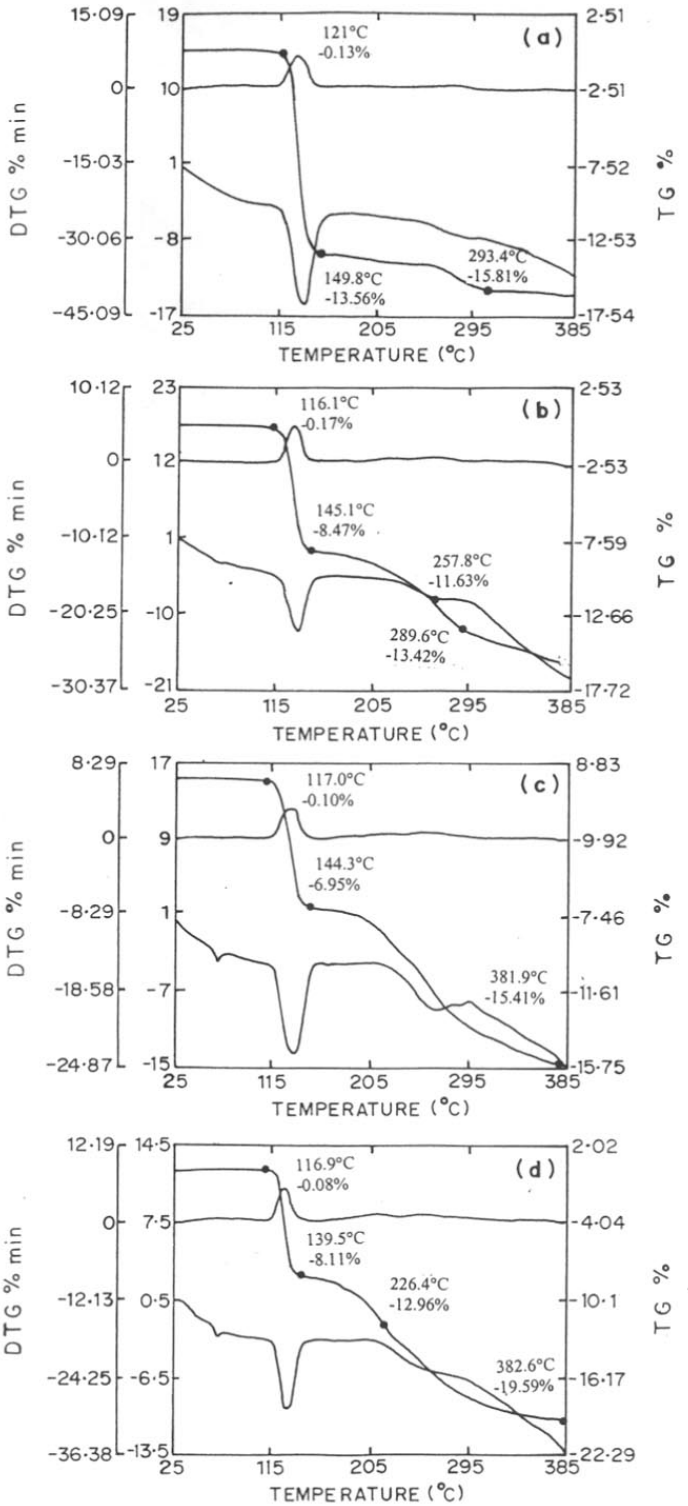

Figure 3.7 Thermograms of $CaSO_4$(IS). Symbols a, b, c and d correspond to PEO concentration of 10, 20, 30 and 40 wt.% respectively.

3.3.2 Effect of $CaSO_4$ on Crystallization and Morphology of PP

After the complete elucidation of preparation and characterisation of $CaSO_4$ (IS) containing different concentrations of PEO, now we shall discuss the effect of this additive on the structure morphology and crystallization in polypropylene.

Figure 3.8 represents the XRD scans for PP containing commercial $CaSO_4$ (10%). It can be seen that major reflections of PP are same as known to be observed in the region 2θ of 5° to 30°. There are five prominent peaks seen in this region which corresponds to the α form of PP.[34] The detailed analysis of XRD data is given in Table 3.6. On the other hand, most interesting results were obtained in the case of PP containing $CaSO_4$ (ISW) prepared by *in situ* method of 10% PEO where the PEO was thoroughly washed out during filtration. The additional peak at 2θ of 26° corresponds to the reflection of anhydrite form of $CaSO_4$. Figure 3.9 shows the XRD scans for these melt crystallized samples at $115^{\circ}C$ containing different concentration of $CaSO_4$ (ISW). Curves A to D represent the additive concentration of 10, 20, 30 and 40 wt.% respectively. The dramatic changes in the XRD pattern are evident especially at 2θ of about 16° where a sharp and intense peak appears. It may be noted that $CaSO_4$ does not exhibit any reflection in this region and all the changes can be attributed to the structure modification of PP itself. The detailed analysis of XRD data is given in Table 3.7 from which it can be concluded that β phase of PP was developed in these samples. Also, another interesting feature to be noted is that $CaSO_4$ (ISW) also gets transformed from its monoclinic dihydrate form to the hexagonal γ phase which is the anhydrite form during the melt crystallization of these composites.

The effect of PEO surrounding the $CaSO_4$ on structure development of PP was also investigated. Figure 3.10 shows the XRD scans for PP-$CaSO_4$ (IS) composites with different concentrations of $CaSO_4$ ranging from 10 to 40 wt.% respectively. Here the 10% of PEO was used during the preparation of filler and it was allowed to be retained in the filtered product without washing it out. The curves A to D correspond to $CaSO_4$ (IS) content of 10, 20, 30 and 40 wt.% respectively. It can be observed that there are some minor changes in the intensities of various reflections but the overall patterns remain more or less same for the additive content upto 30 wt.%. A new peak was observed at $2\theta \approx 16^{\circ}$ only in the curve D which corresponds to $CaSO_4$ (IS) content of 40%. This may be compared with the results depicted in the Fig. 3.9 wherein dramatic changes were observed even at low concentration of $CaSO_4$. The detailed analysis of these XRD peaks is given in Table 3.8. From the various results observed, it can be

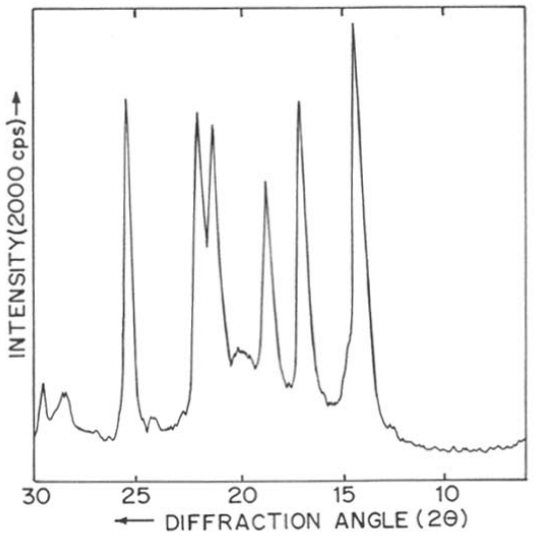

Figure 3.8 XRD of PP containing commercial $CaSO_4$ (10 wt%) sample isothermally crystallized from melt at 115°C.

Table 3.6: XRD analysis of PP containing 10% commercial $CaSO_4$

PP+10% $CaSO_4$ (commercial) d(obs)	I/I_0	Assignment (hkl)
6.32	<u>100</u>	α PP (110)
5.31	82	α PP (040)
4.82	64	α PP (130)
4.23	77	α PP (131)
4.10	79	α PP (041)
3.53	83	α PP (060)
		$CaSO_4$ anhydrite(002/020)
3.14	15	α PP (220)
3.04	17	$CaSO_4$ anhydrite (102)
2.88	13	α PP (161)
		$CaSO_4$ anhydrite (210)

Underlined reflections to bring out the comparison of d-values for strongest peak.

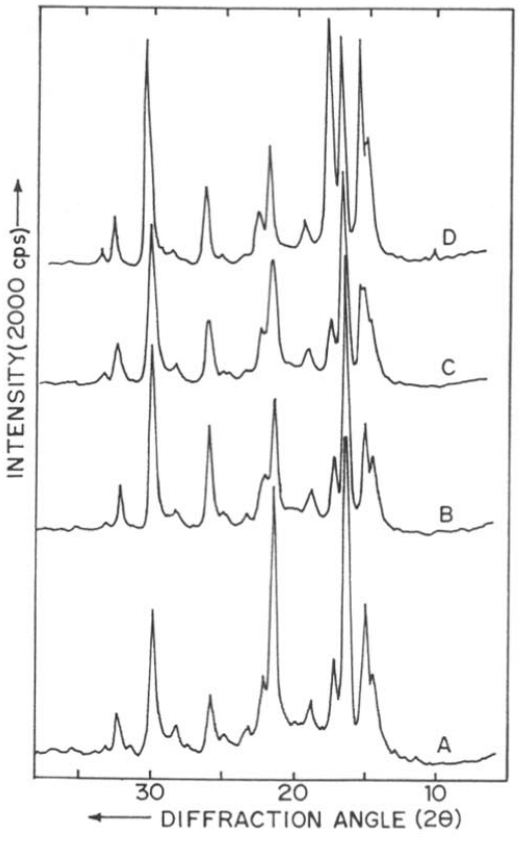

Figure 3.9 XRD scans for PP containing $CaSO_4$ (ISW) prepared by *in situ* method. Curves (A) to (D) correspond to additive concentrations of 10,20,30 and 40 wt.% respectively (melt crystallized at 115°C).

Table 3.7 XRD analysis of PP-CaS(ISW) containing additive concentrations of 10,20,30 and 40 wt.% respectively

10%		20%		30%		40%		α			β			γ-$CaSO_4$		
d (obs)	I/I_o	d(obs)	I/I_o	d(obs)	I/I_o	d(obs)	I/I_o	d(cal)	I/I_o	hkl	d(cal)	I/I_o	hkl	d(cal)	I/I_o	hkl
6.32	17	6.32	27	6.32	33	6.32	51	6.34	100	110	-	-	-	-	-	-
6.11	29	6.11	39	6.11	48	6.11	91	-	-	-	-	-	-	6.05	100	100
5.57	100	5.61	100	5.62	100	5.61	93	-	-	-	5.56	100	300	-	-	-
5.31	19	5.31	28	5.31	32	5.31	100	5.32	70	040	-	-	-	-	-	-
4.82	11	4.84	17	4.82	19	4.82	21	4.84	56	130	-	-	-	-	-	-
4.25	50	4.25	47	4.27	61	4.27	48	4.25	40	131	4.25	28	301	-	-	-
4.10	16	4.11	21	4.10	29	4.11	23	4.10	58	041	-		-	-	-	-
3.51	12	3.49	37	3.52	32	3.52	33	3.50	20	060	3.56	4	410	3.48	60	110
3.21	7	-	-	-	-	-	-	-	-	-	3.19	-	411	-	-	-
3.04	27	3.02	65	3.04	75	3.04	90	-	-	-	3.09	-	112	3.01	60	111
2.81	8	2.82	17	2.83	20	2.83	20	-	-	-	2.78	-	600	2.80	90	102

Underlined peaks represent reflection of maximum intensity

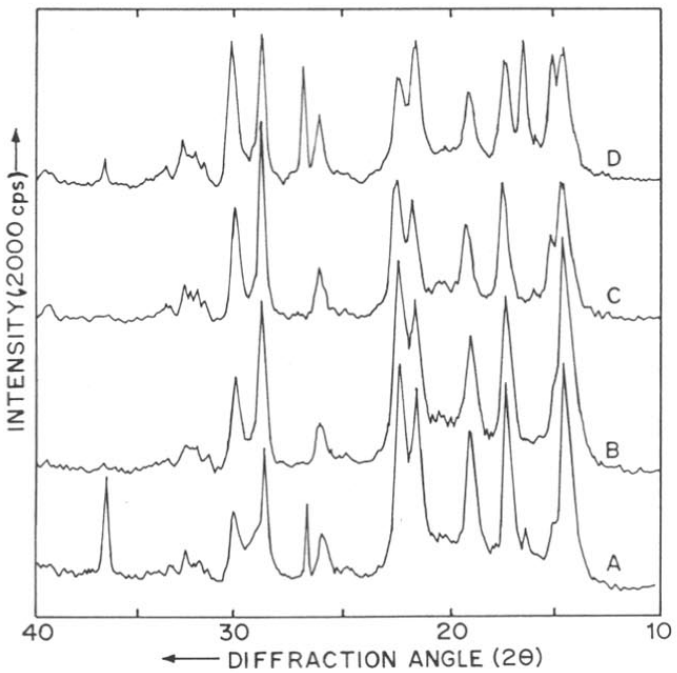

Figure 3.10 XRD scans for PP containing $CaSO_4$(IS) with PEO (wt.%). Curves (A) to (D) correspond to PEO concentrations of 10, 20, 30, and 40% respectively melt crystallized at 115°C.

Table 3.8 XRD analysis of PP-CaS(IS) containing additive concentrations of 10, 20, 30 and 40 wt.% respectively.

Additive concentration								(hkl)			
10%		20%		30%		40%					
d (obs)	I/I_o	d(obs)	I/I_o	d(obs)	I/I_o	d(obs)	I/I_o	d(cal)	α	β	γ $CaSO_4$
6.37	100	6.32	100	6.32	69	6.37	92	6.34	100	-	-
6.10	40	6.10	41	6.10	44	6.15	89	6.05	-	-	100
5.60	29	-	-	5.75	17	5.60	100	5.56	-	300	-
5.34	92	5.30	76	5.30	68	5.30	86	5.32	040	-	-
4.84	71	4.82	60	4.79	49	4.82	66	4.84	130	-	-
4.25	90	4.23	73	4.23	60	4.25	18	4.25	131	301	-
4.09	100	4.07	90	4.09	71	4.09	75	4.10	041	-	-
3.52	28	3.49	23	3.50	29	3.50	48	3.50	060	410	-
3.42	40	-	-	-	-	3.41	82	3.48	-	-	110
3.19	64	-	-	3.17	100	3.18	56	3.19	-	411	-
-	-	3.16	74	-	-	-	-	3.16	220	330	-
3.04	36	3.03	41	3.04	57	3.03	18	3.05	-	-	111

Underlined peaks represent reflections of maximum intensity

noticed that in this case the PP is crystallized in α form with hardly any β content. Thus, it can be pointed out that the presence of PEO surrounding the $CaSO_4$ crystals prevents the nucleation of β phase of PP in the PP-$CaSO_4$ (IS) composites. A small quantity of β phase was generated at or above 40% of $CaSO_4$ (IS) in PP. This can be explained on the basis of actual amount of PEO present in these samples. From the 10% PEO-$CaSO_4$ (IS) sample used, the actual quantity of PEO was found to be nearly 2.5% as confirmed from TGA results discussed earlier. At high concentration of $CaSO_4$ (IS), the PEO is not sufficient to cover all the crystals of $CaSO_4$ and hence a few sites are available for nucleation of the β phase.

The β content in total crystallinity of the polymer was determined from the ratio of the intensities of the major reflection from the β phase to those from α-phase ($I_\beta/I_\alpha + I_\beta$). Table 3.9 indicates the β content with reference to composition for PP-$CaSO_4$ composites with different grades of additive. It is seen that the β content is very high in the case of $CaSO_4$ (ISW) as compared to $CaSO_4$ (IS) or $CaSO_4$ (CM). The reason for this has been discussed above.

The crystallization behaviour of PP containing $CaSO_4$ (IS) prepared with 10% PEO and $CaSO_4$ (ISW) (10% PEO fully washed) were monitored by observing the growth of spherulites. This would be carried out by observing the transmitted intensity through the specimen under cross-polar condition in the microscope. Figures 3.11a and b represent the plots of intensity as a function of time obtained from image analysis for pure PP and PP containing 10 wt.% $CaSO_4$ (IS) and $CaSO_4$ (ISW) (PEO fully washed) respectively. These samples were isothermally crystallized at 115°C. It is well known that at this T_c in pure PP, the spherulites grow to a large size over a long period of time (10 minutes) to attain an ultimate size of 90.5 μm. However, it is evident that for PP containing $CaSO_4$ the growth is rapid in a much shorter duration and the ultimate size obtained is also reduced. The crystallization half times i.e. the time required to attain a spherulite size of half its ultimate value and the growth rates were derived from such curves and these were plotted with reference to composition of $CaSO_4$. This is shown in Figs. 3.12a and b. From Fig. 3.12a it is seen that for both PP-CaS(IS) and PP-CaS(ISW) the crystallization half time show a decrease with the increase of additive content and exhibits a plateau above 8 wt.%. It is interesting to note that the crystallization half time decreases much more rapidly for $CaSO_4$ (ISW) as compared to $CaSO_4$ (IS). Figure 3.12b represents the plot of growth rate vs concentration of $CaSO_4$. High growth rates are observed for PP-Cas(ISW) compared to PP-Cas(IS). These various observations can be explained on the basis of

Table 3.9 shows the β-phase content in PP-$CaSO_4$ composites

Composition $CaSO_4$ (wt.%)	β content (%)		Ci (%)	
	containing PEO	After washing out PEO	Containing PEO	After washing out PEO
10	17	85	77	77
20	-	79	75	80
30	13	75	75	79
40	51	65	71	71

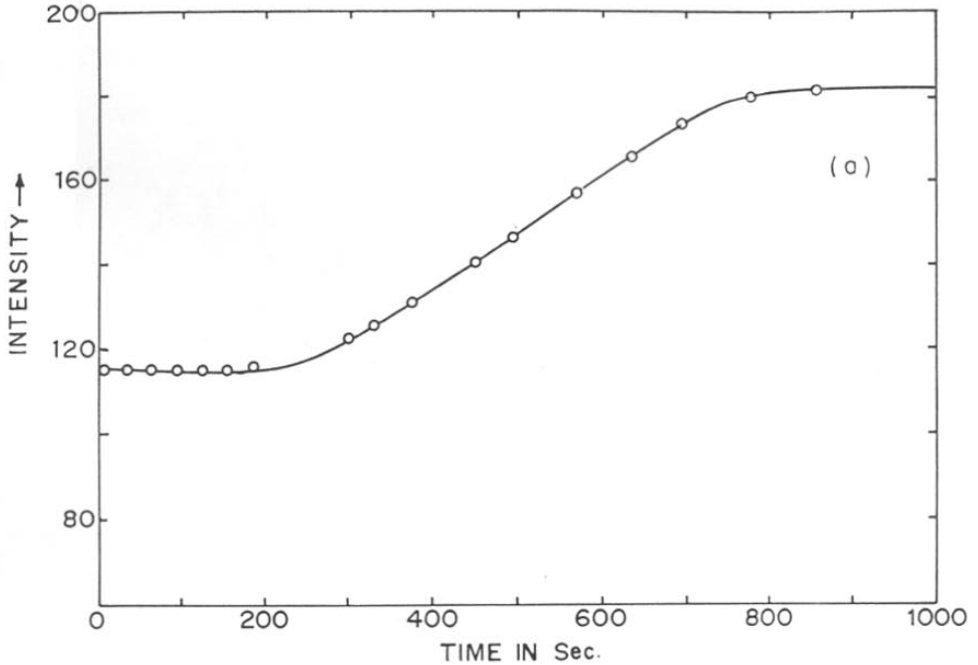

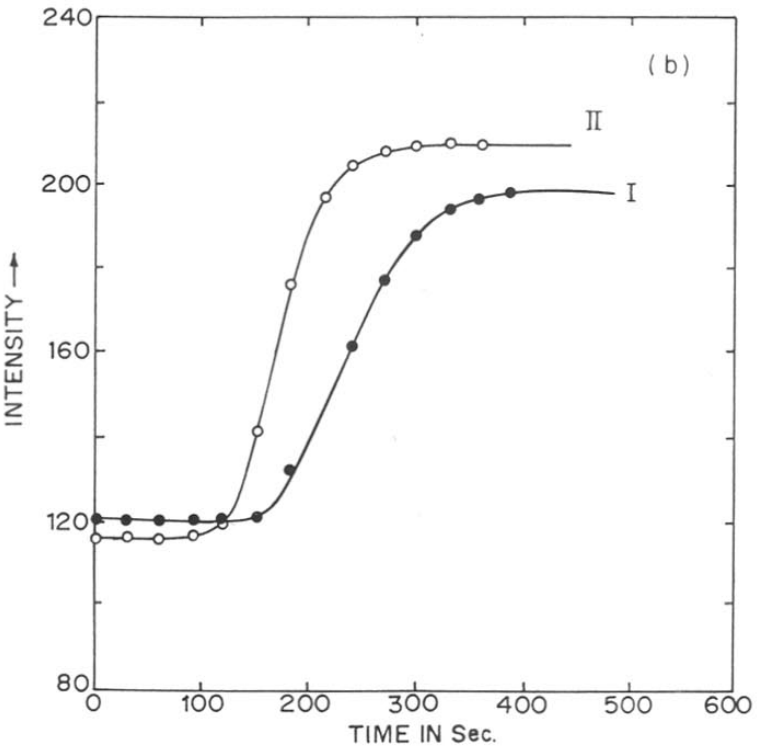

Figure 3.11 (a) The plot of intensity as a function of time for pure PP
(b) Plot of intensity as a function of time for PP containing 10% $CaSO_4$(IS) and $CaSO_4$(ISW) designated as I and II

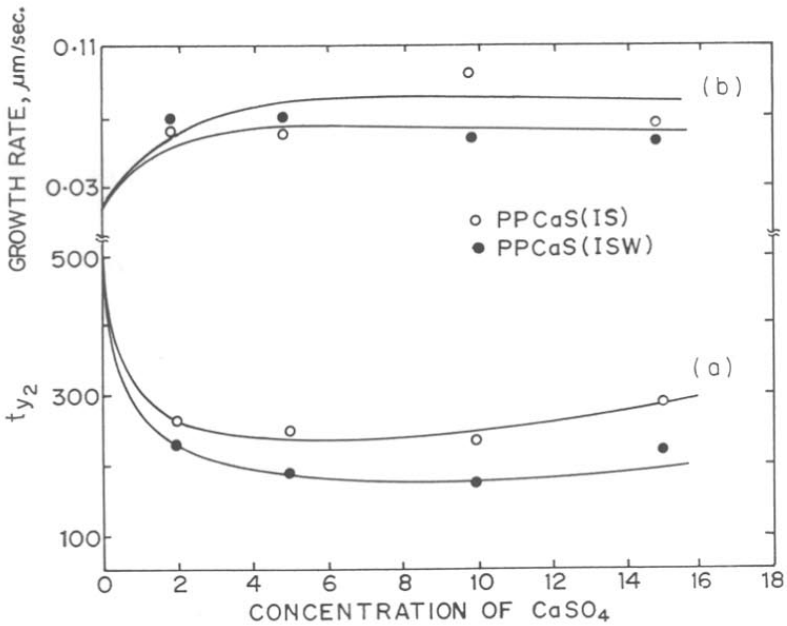

Figure 3.12 (a) Crystallization half time as a function of concentration of $CaSO_4$ for both PP-CaS(IS) and PP-CaS(ISW)
(b) Plot of growth rate vs concentration of $CaSO_4$

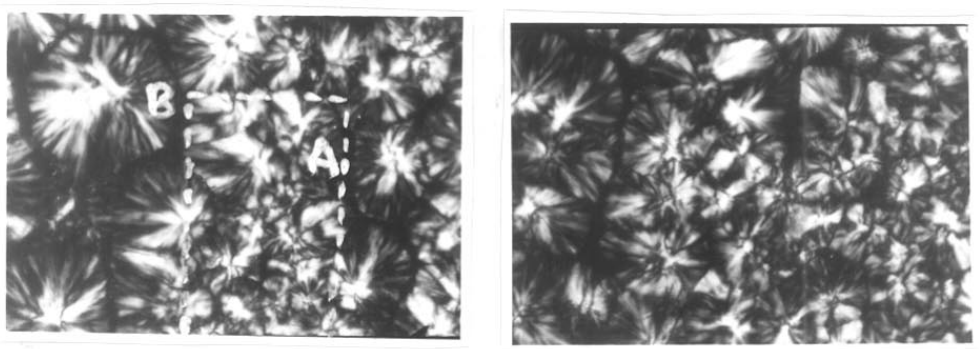

Figure 3.13 Optical micrograph of melt crystallized (a) PP-CaS(ISW). The white dotted line is drawn to delineate the portion nucleated on $CaSO_4$ needle (A) and that away from it (B).(net magn.450x)
(b) Optical polarising micrograph of melt crystallized PP-CaS(IS).

crystallization phenomena in polymers which consists of two processes, namely, nucleation and growth which are both dependent on temperature of crystallization and exhibit maxima at a certain value of temperature (T_c) which exists between the T_g and T_m. The T_g and T_m values together decide the ultimate crystallinity value, spherulitic size etc. It is well known that for high nucleation rate, the crystallization rates are high and $t_{1/2}$values are low leading to decrease in spherulitic dimensions. Hence, one expects the spherulite size to decrease with an increase in the concentration of the additive as observed above. However, with the further increase in the concentration of additive, increase in $t_{1/2}$ values with slow growth rates may be observed. This is because at this high concentration of additive, agglomeration may occur giving rise to reduction in active surface area for the spherulites to nucleate. The enhancement of rate or considerable decrease in $t_{1/2}$ values for PP-CaS(ISW) as compared to PP-CaS(IS) is due to higher nucleation efficiency by $CaSO_4$(ISW) as compared to $CaSO_4$(ISW). Also, nucleation of another crystalline phase (β) that has different morphology as compared to normal α PP takes place for $CaSO_4$(ISW), whereas in PP-$CaSO_4$(IS), the presence of PEO surrounding the $CaSO_4$ particles prevents the interaction between PP and $CaSO_4$ and decreases the nucleation efficiency of filler for generation of β phase of PP.

Figure 3.13 shows the morphology of these samples. It is interesting to observe that (Fig. 3.13a) PP-$CaSO_4$ (ISW) shows transcrystallinity which consists of a set of closely nucleated small spherulites (β) along the $CaSO_4$ crystals giving rise to row nucleation represented by symbol A. These small β spherulites show the dimensions of the order of 6 - 8μm. Large spherulites are observed spaced far from these crystals which are normal α type represented by symbol B. The morphology of PP-CaS(IS) in Fig. 3.13b shows no distinct transcrystallinity, but a decrease in spherulite dimensions (15-16μm) is observed. These observations are in agreement with the above findings in XRD data viz. the existence of β phase of PP for *in situ* $CaSO_4$ (ISW) and α phase of PP for *in situ* $CaSO_4$ (IS) containing PEO which have been discussed earlier.

The effect of processing on the orientation of the additive such as fibres in thermoplastic composites is known and reported for a few systems in the past.[35,36] In the present case, even at a mild extrusion rate, as obtained in a melt indexer, the extrudate were found to consist of $CaSO_4$ crystals oriented with their needle axis parallel to extrusion direction. Figure 3.14 shows the XRD of 20% $CaSO_4$ (IS) sample containing 10% PEO which was sectioned parallel and perpendicular to the direction of extrusion. There are appreciable

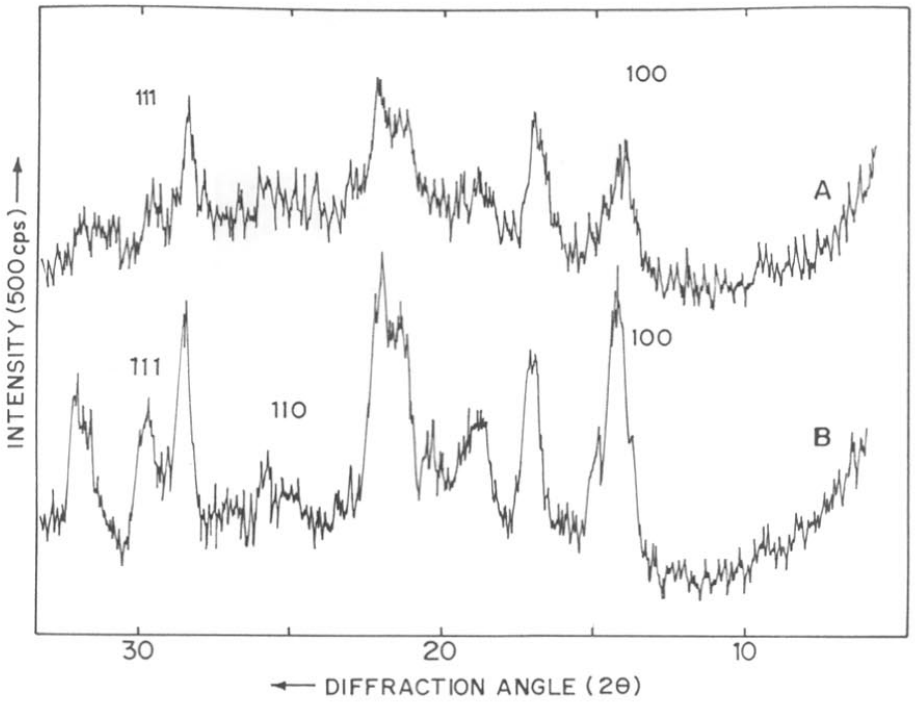

Figure 3.14 XRD scans for the melt extruded PP-$CaSO_4$ (IS) composite.
(A) Samples sectioned perpendicular
(B) Sectioned parallel to the machine direction

Figure 3.15 Optical micrograph of the melt extruded PP-$CaSO_4$ samples sectioned parallel to the extrusion direction taken in reflection mode from top surface. (net magn. = 450x)

changes in the intensities of reflections corresponding to (100) and (111) from $CaSO_4$ crystals of γ phase when the direction of section is changed. This is mainly due to the orientation of $CaSO_4$ crystal parallel or perpendicular to the sectioned surface. Similar variation in the intensities of samples were observed in the case of shear oriented samples as discussed earlier. These sectioned samples were observed under the optical polarizing microscope in reflection mode and it revealed the needle shaped $CaSO_4$ crystals most of which were oriented with their long axis lying along the direction of extrusion as can be seen from Fig.3.15.

The analysis of orientation was also carried out for injection moulded specimens along the surface of machine direction for both PP-CaS(ISJ) and PP-CaS(ISWJ) samples and also for pure PP sectioned near the skin as well as the core. Figures 3.16 to 3.18 shows the XRD scans of skin and core layer of injection molded specimens. From the comparison of XRD for skin and core layer of pure PP, it is interesting to note that the former shows sharp peak intensities than the core layer. There is an appreciable increase in the intensity at 2θ of 16.7°C, which corresponds to (040) reflection of α phase of PP. A small additional peak was also observed at $2\theta = 16^{\circ}$, which corresponds to (300) reflection from β phase.

Marked differences were found in the case of WAXD patterns of skin layer of PP-CaS(ISW) as compared to PP-CaS(IS) (Fig.3.17a and b). A considerable decrease in the peak intensity at 2θ of 14.2 ° of (100) reflection of γ phase of $CaSO_4$ and increase of intensity at 2θ of 29.4° of (111) reflection of γ phase of $CaSO_4$ was observed for PP -CaS(ISW) with increase in the additive concentration from 5% to 25 wt.%, whereas in PP-CaS(IS) there was no peak found at 2θ of 14.2° and peak intensity at $2\theta \approx 29.4^{\circ}$ was significantly low. From these results it is apparent that there is a high degree of molecular orientation induced in the skin layer. It is well known that the skin layer solidifies first and all the molecular orientations are in the frozen state. Whereas in core layer there is random orientation of crystallites due to the presence of small shear stresses, so that nucleation occurs in an essentially quiescent state allowing the random growth of crystallites. The oriented state of skin layer is due to high shear forces/pressure developed during melt flow in the injection molding. This high shear stress is also responsible for change of crystalline phase in pure PP to predominantly β type. Hence, there is a significant amount of β crystallites seen even in pure PP. Also, it should be noted that the high intense peak of α (040) corresponds to the uniaxial orientation of b- axis of α PP. It should be noted that normal γ $CaSO_4$ shows major intense peak at 2θ of 14.2°, which corresponds to (100) reflection randomly distributed crystallites. In PP-CaS(ISW) this

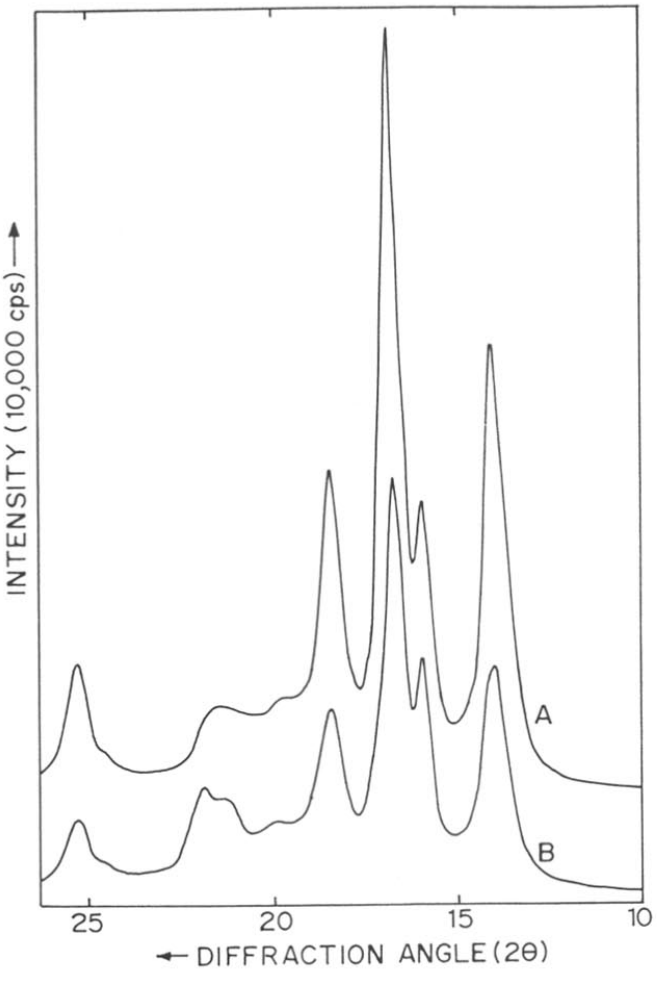

Figure 3.16 XRD scans of skin (A) and core layer (B) of pure PP.

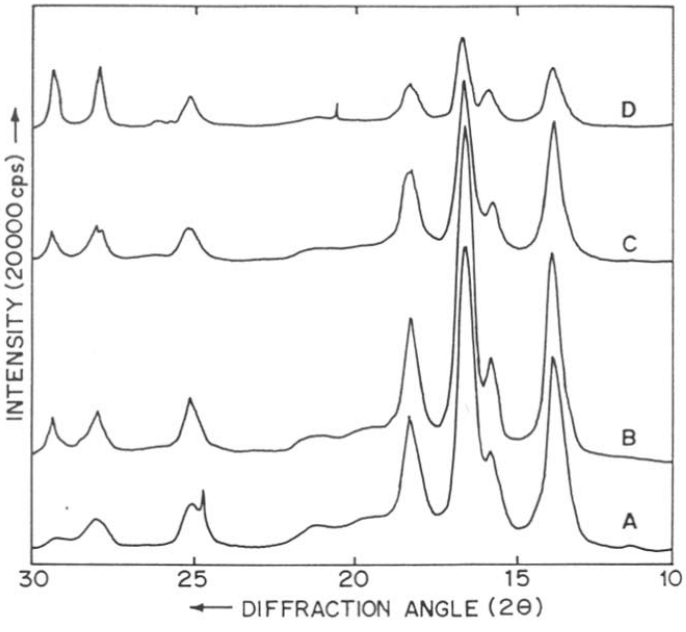

(a)

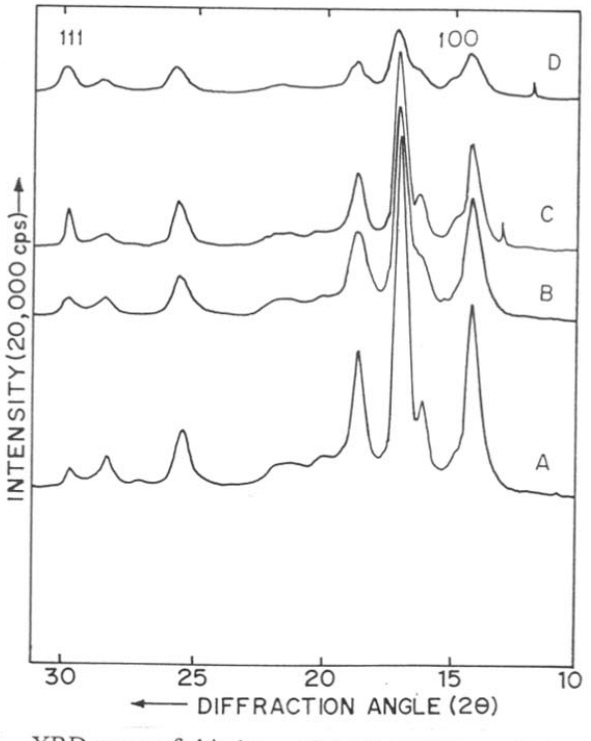

(b)

Figure 3.17 XRD scans of skin layer of PP-CaS(IS) (a) and PP-CaS(ISW) (b) Curves A,B,C and D correspond to additive concentrations of 5, 10, 15 and 25 wt.% respectively.

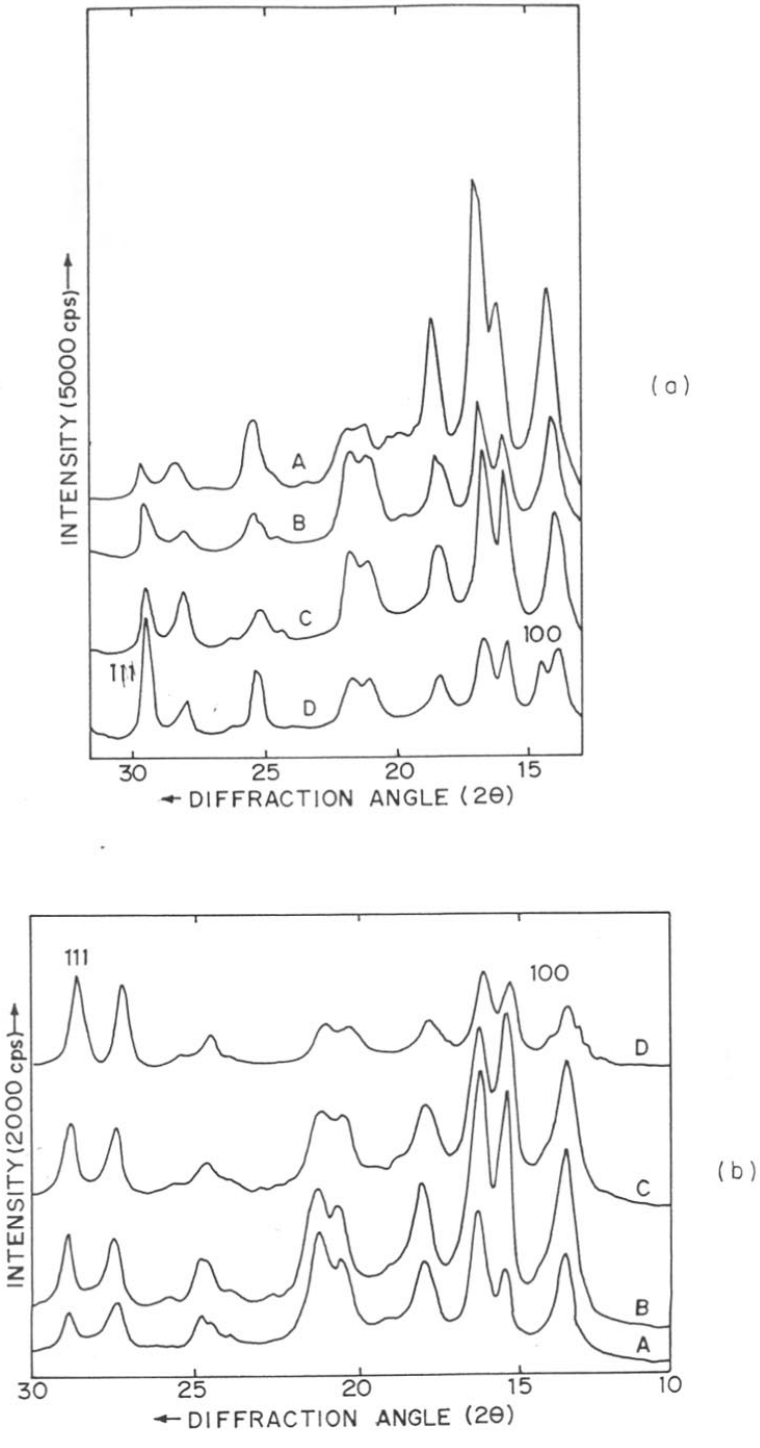

Figure 3.18 XRD scans of core layer of PP-CaS(ISW) (a) and PP-CaS(IS) (b) Curves A,B,C and D correspond to additive concentrations of 5,10, 15 and 25 wt.% respectively.

reflection decreases considerably and the (111) reflection becomes enhanced which suggests preferential orientation of $CaSO_4$ crystallites along perpendicular direction with a-axis pointing away from surface.

Interesting observations were also found when the core layer of PP-CaS(ISW) were compared with PP-CaS(IS). From these figures the β content was determined and these were plotted with respect to additive concentration.(see Fig.3.19). In PP-CaS(IS) one does not expect any β phase formation but some β content is seen in melt processed samples. The reason for this could be high shear flow rates in the injection moulding during which there is partial removal of PEO surrounding the $CaSO_4$ crystals which then behave as that of PP-CaS(ISW) type. Hence, a slight increase in β content is observed. Even in the core layer the preferential orientation of (111) reflection of γ $CaSO_4$ of PP-CaS(ISW) was observed as compared to PP-CaS(IS). This was also evident when optical micrographs of PP-CaS(ISJ) and PP-CaS(ISWJ) containing 15%additive were taken in the reflection mode. The PP-CaS(ISWJ) showed a good alignment of crystallites or in other words strong orientation of $CaSO_4$ crystals which were parallel with reference to each other. In case of PP-CaS(ISJ) sample, presence of some agglomerates were seen and hence no distinct orientation was observed.

These various results on the structure development in PP-$CaSO_4$ composites can be understood in terms of nucleation, growth and crystallographic interaction between the polymers and the additive. According to the crystal lattice mismatch theory, the substrate influences the growth of another substance on it if the lattice parameters for the substrate and the growing phase are close to each other. The lattice mismatch (δ_l) is defined as [37,38].

$$\delta_l = | pl_s - ql_g | / | l_s | \times 100 \qquad (3.3)$$

Where l is the lattice parameter along any axis; p and q are the integers and the subscripts s and g represent substrate and growing media respectively. If the mismatch parameter is below 15% (i.e. $\delta_l << 15\%$) then the substrate can influence the growth of the crystals in the medium in contact with it. Such an influence can give rise to nucleation of certain crystalline phase as for example in polyvinylidiene fluoride or PP wherein certain additives alone give the β phase.[39,40] In the present case, $CaSO_4$ exists in a number of crystalline phases and those obtained in the commercial as well as *in situ* grade have been identified by us. The commercial grade is mostly the anhydrite type with a = 6.238 Å, b = 6.991 Å and c = 6.996 Å while that prepared by

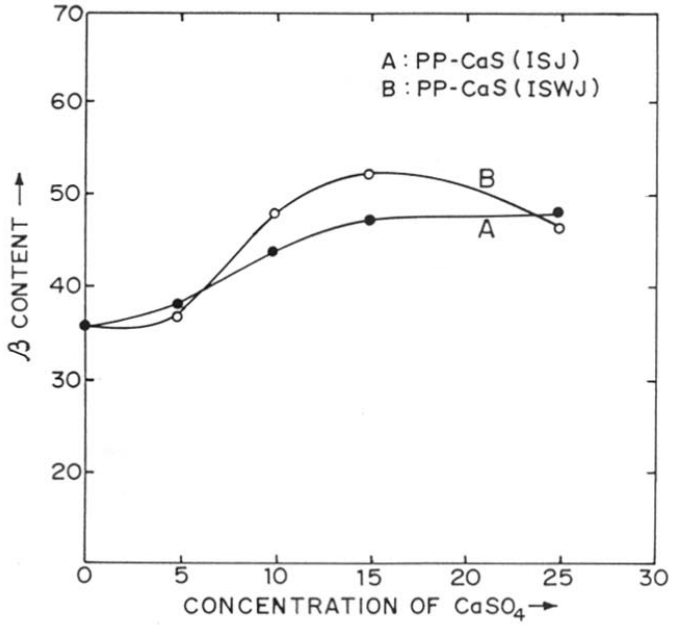

Figure 3.19 β content of PP-CaS(ISJ) and PP-CaS(ISWJ)

in situ technique is dihydrate type with a = 5.67 Å, b = 15.15 Å, c = 6.51 Å, β = 118.23°. The γ $CaSO_4$ has hexagonal configuration with a = 6.99 Å and c = 6.34 Å. The polypropylene has four types of crystallographic forms in which the α and β are most common. The α type PP has monoclinic configuration with a = 6.65 Å , b = 20.98 Å, c = 6.5 Å and β = 99.3 Å. On the other hand, β PP has hexagonal one with lattice parameters of a = 12.74 Å and c = 6.35 Å. If one compares the lattice parameters between the commercial grade $CaSO_4$ and α PP the lattice mismatch is δ_l = 6.2% for a-axis and 7.83% for c-axis. On the other hand, the lattice mismatch between β PP and commercial grade $CaSO_4$ is greater than 10% for all axes. Hence, the PP-$CaSO_4$ containing the commercial grade additive is not likely to contain the β phase PP. If similar comparison is made between γ phase of $CaSO_4$ and β-PP which are both hexagonal one obtains the lattice mismatch of 0.15% for c axis and $| l_g - 2l_s | / | l_s |$ as 9.7%. This clearly suggests that the γ-$CaSO_4$ can nucleate the β phase of PP. The dihydrate $CaSO_4$ also has smaller lattice mismatch values with β PP. Thus it appears that in PP-$CaSO_4$ (ISW) composite containing $CaSO_4$ prepared by *in situ* technique, the melt crystallization process (melt temp. 190°C crystallization at 115°C) gives rise to first the formation of γ $CaSO_4$ which in turn nucleates the β phase of PP. This close crystallographic interaction is essential for the formation of β phase as can be surmised from the crystalline content of PP-CaS(IS) composite made with the additive containing PEO. The surrounding PEO prevents the interaction between PP and $CaSO_4$ and decreases the nucleation efficiency of filler for the generation of β phase of PP (see Fig.3.10). The slight reduction in the β content at high concentration of the additive can be understood in terms of filler particle aggregation giving rise to smaller effective surface area for nucleation. The high degree of orientation of the $CaSO_4$ crystals of PP-$CaSO_4$ composite from a melt indexer and those from the injection moulded specimens also confirms the close crystallographic interaction between the additive and the polymer.

In order to determine the crystallization and melting behaviour of PP-$CaSO_4$ composites and its correlation with structure and morphology DSC were recorded for both PP-CaS(IS) and PP-CaS(ISW) samples. Figures 3.20a and b represent the DSC curves for powder samples of PP-CaS(ISW)and PP-CaS(IS) ($CaSO_4$ 10%) respectively. The curves have been recorded for two heating and cooling cycles. The first heating corresponds to the composite undergoing initial melting as in the extrusion melt (mixing) process, while the first cooling can be related to that of initial crystallization process of the product emerging out of the plasticorder extruder. On the other hand, the second heating cycle represents the composite

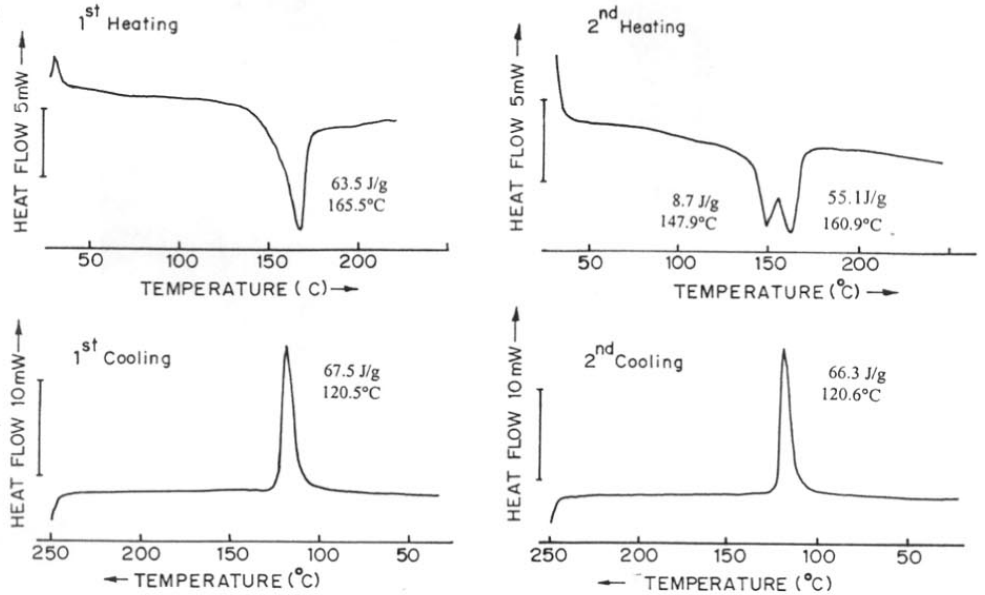

(a)

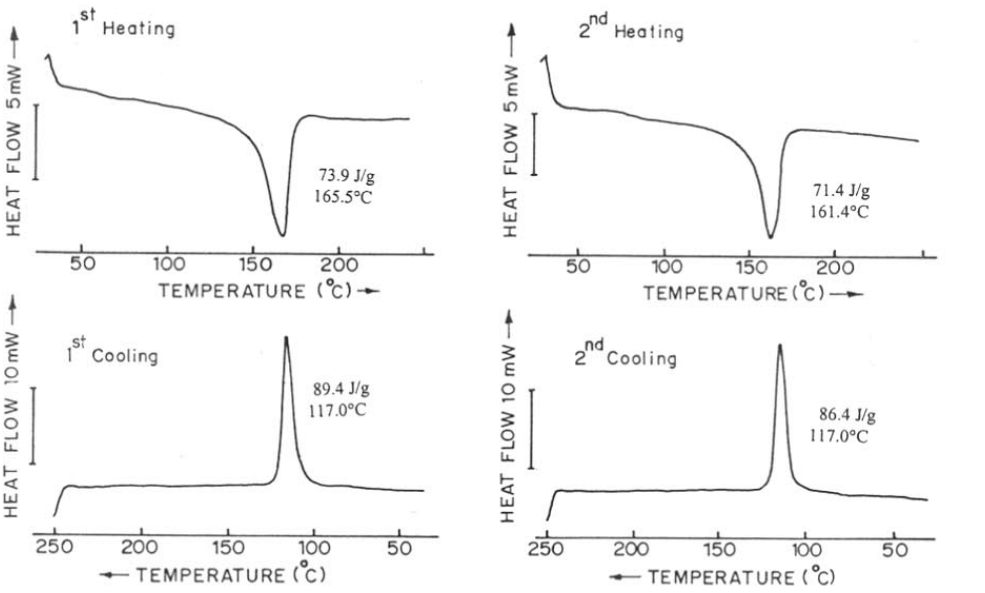

(b)

Figure 3.20 DSC curves for powder samples (a) PP-CaS(ISW) (b) PP-CaS(IS) containing 10% additive concentration.

undergoing melting as in the injection moulding process and the second cooling represents the crystallization process of the product emerging out of the injection mould cavity. In the case of PP-CaS(ISW), the initial heating represents the melt mixing of PP with additive and the cooling curve exhibits crystallization peak at 120.5°C which is much higher than that for pure PP (115°C). This is due to nucleation effect of $CaSO_4$. In the second heating for PP-CaS(ISW) sample it can be seen that two clear endothermic peaks were observed at 147.9°C and 160.9°C and on cooling the crystallization peak appears at temperature of 120.6°C. On the other hand, the PP-CaS(IS) samples showed a prominent endothermic peak at 160°C and a crystallization peak at 116°C in the second cooling cycle. These results can be attributed to high nucleation efficiency exhibited by $CaSO_4$ crystallites in PP-CaS(ISW) giving rise to a new crystalline phase of PP i.e. β phase which has melting point at 147.9°C and increase of temperature of crystallization peak to higher value (120.6°C). In case of PP-CaS(IS) samples, the presence of PEO inhibits the nucleation as explained earlier and hence lower value for temperature of crystallization peak was observed as well as a single melting point.

Figures 3.21a and b illustrate the DSC thermograms of extruded pellets of PP-CaS(ISW) and PP-CaS(IS) having 10% additive respectively. From these figures, the presence of slight amount of β-phase is seen in both the first and second heating cycle for PP- CaS(ISW) samples due to high nucleation efficiency of CaS(ISW) as explained earlier. However, it should be pointed out that the temperature of crystallization peak was slightly higher than that for PP-CaS(IS) in both first and second cooling cycle. This can be explained as follows: Normally the presence of PEO in the unwashed $CaSO_4$ containing samples inhibits the growth of β phase which has been noted for isothermally crystallized samples. On the other hand, in the case of extrusion and injection moulding the melt is subjected to shear stress, PEO having much lower melting point than PP tends to flow more than PP at the processing temperature. Hence, during processing some of the filler particles become free from the PEO surrounding them and give rise to nucleation effects in the same manner as that of washed $CaSO_4$ particles. However, the β phase content is much lower in this case than in the fully washed $CaSO_4$.

In order to determine the content of $CaSO_4$ in the melt-extruded samples thermogravimetric analysis was carried out for various samples. Figures 3.22a, b and c show the thermograms of PP-CaS(ISWE) having additive concentration of 9, 13 and 20 wt.% respectively. The TGA curve shows the polymer degradation taking place at about 325°C, PP is seen to degrade completely in the temperature range of 457-460°C and the remaining filler

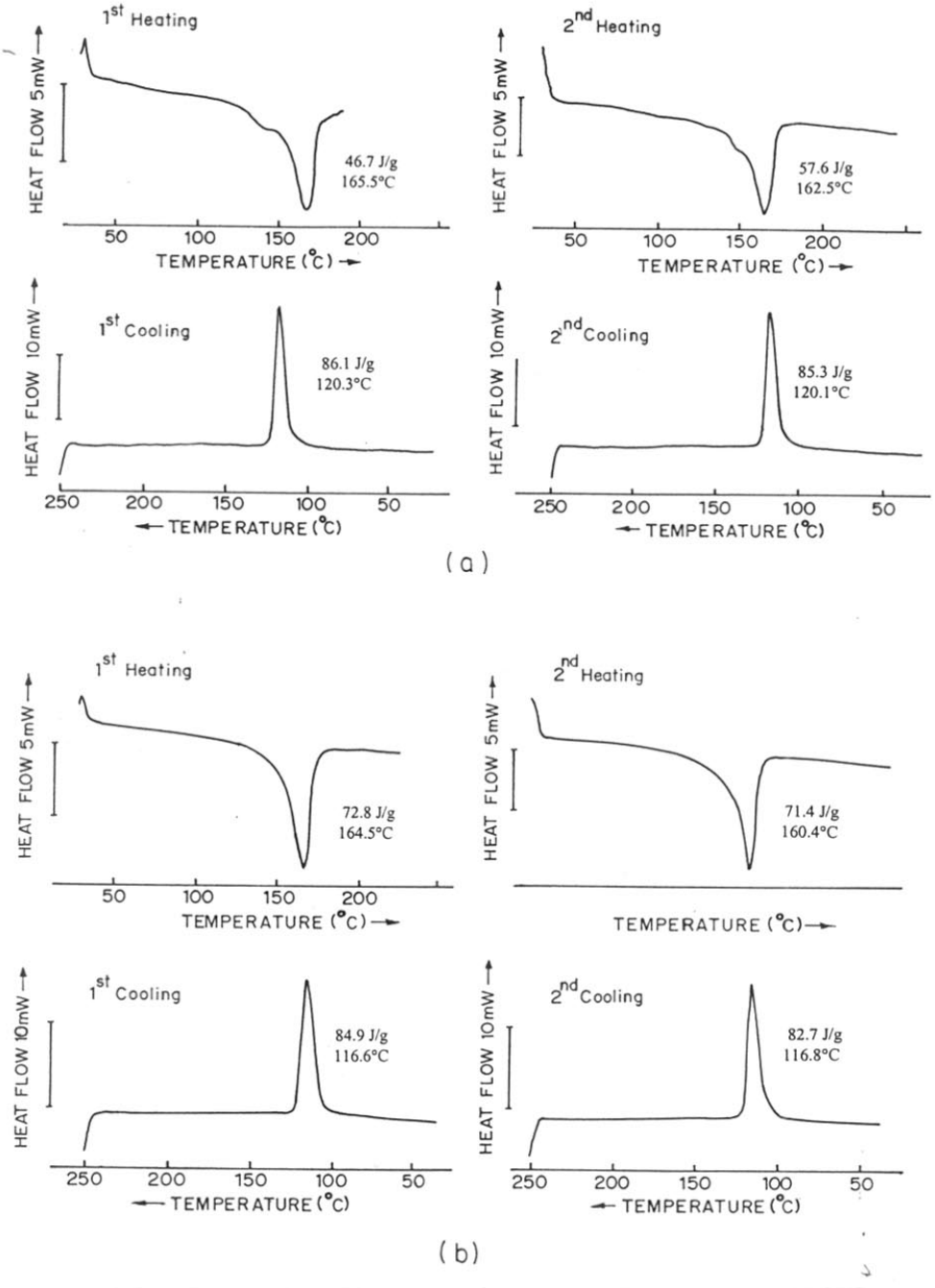

Figure 3.21 DSC curves of extruded pellets (a) PP-CaS(ISW) (b) PP-CaS(IS) containing 10% additive concentration.

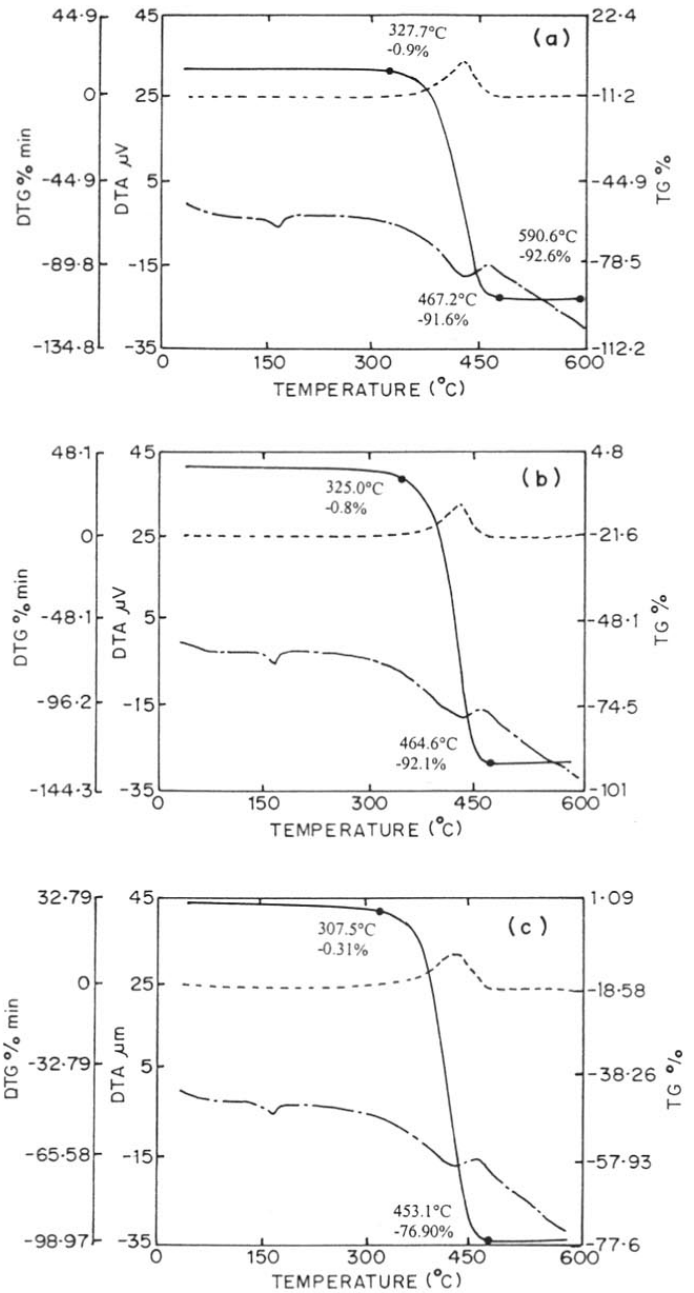

Figure 3.22 TGA curves for PP-CaS(ISW). Curves a, b and c represent the additive concentration of 9, 13 and 20 wt.% respectively

content can be derived from the residual weight. The DTA curve shows the melting of PP at 163°C and the sharp degradation transition of PP at 454°C. It can be seen from the figure that for composite with 9% $CaSO_4$ (ISW), the percentage loss of PP was found to be 91.6% with 8.4% quantity of $CaSO_4$ present in the sample while the expected value of $CaSO_4$ was 9%. The percentage loss of PP for composite with 15 and 25 wt.% $CaSO_4$ (IS) were 92.1% and 76.90% respectively with 8% and 23% amount of $CaSO_4$ remaining corresponding to their expected values of 13% and 20% respectively. Thus, these various results are in good agreement with the actual amount of $CaSO_4$ used. However, it should be pointed out that the $CaSO_4$ transition from monoclinic hydrated state to anhydrite state was not observed in these curves as the samples used for analysis were extruded pellets where the $CaSO_4$ gets transformed to the anhydrite state on the barrel itself rather than after extrusion.

As it is well known that $CaSO_4$ imparts flame retardancy when incorporated in polymers, the flame retardancy tests were carried out for pure PP, PP-CaS(IS), and PP-CaS(ISW) composites. Table 3.10 represents the percentage of O_2 index values for these composites. It is interesting to note that there is a significant increase in the oxygen index values with the increase of additive concentration for both PP-CaS(IS) and PP-CaS(ISW) composites as compared to pure PP. This rise in oxygen index values clearly indicates good dispersion of $CaSO_4$ crystallites in PP. This is because better the dispersion of $CaSO_4$ in PP, the more evenly the heat of combustion of resin is absorbed homogeneously by the endothermic decomposition of $CaSO_4$. Thus $CaSO_4$ quenches the flame and acts as an effective flame retardant for polypropylene.

3.3.3 Mechanical Properties of PP-$CaSO_4$ Composites

The mechanical properties viz. impact and tensile strength of these composites were evaluated and correlated with the structure and morphology of the composite. The mechanical properties such as tensile modulus, elongation etc. were measured by standard techniques. Figures 3.23a, b and c represent the plot of stress vs strain for PP-CaS(IS) and PP-CaS(ISW) both containing 10% additive concentration along with unfilled PP. The various values such as displacement at maximum load, stress at maximum load, stress at auto break, load at maximum load etc for the two cases of $CaSO_4$ (IS) and $CaSO_4$ (ISW) along with the unfilled PP are indicated in Table 3.11. It is seen from the comparison of these different values that there is a slight decrease in the elongation at break for high filler concentration but otherwise it

Table 3.10 Represents the % of O_2 index values for PP-CaS(ISJ) and PP-CaS(ISWJ) composites

Composition	Wt. %	O_2 index values
Pure PP	0	16.0
PP-CaS(ISJ) containing additive concentration	5 10 15 25	16.5 17.5 17.8 18.0
PP-CaS(ISWJ) containing additive concentration	5 10 15 25	16.2 17.2 17.9 18.2

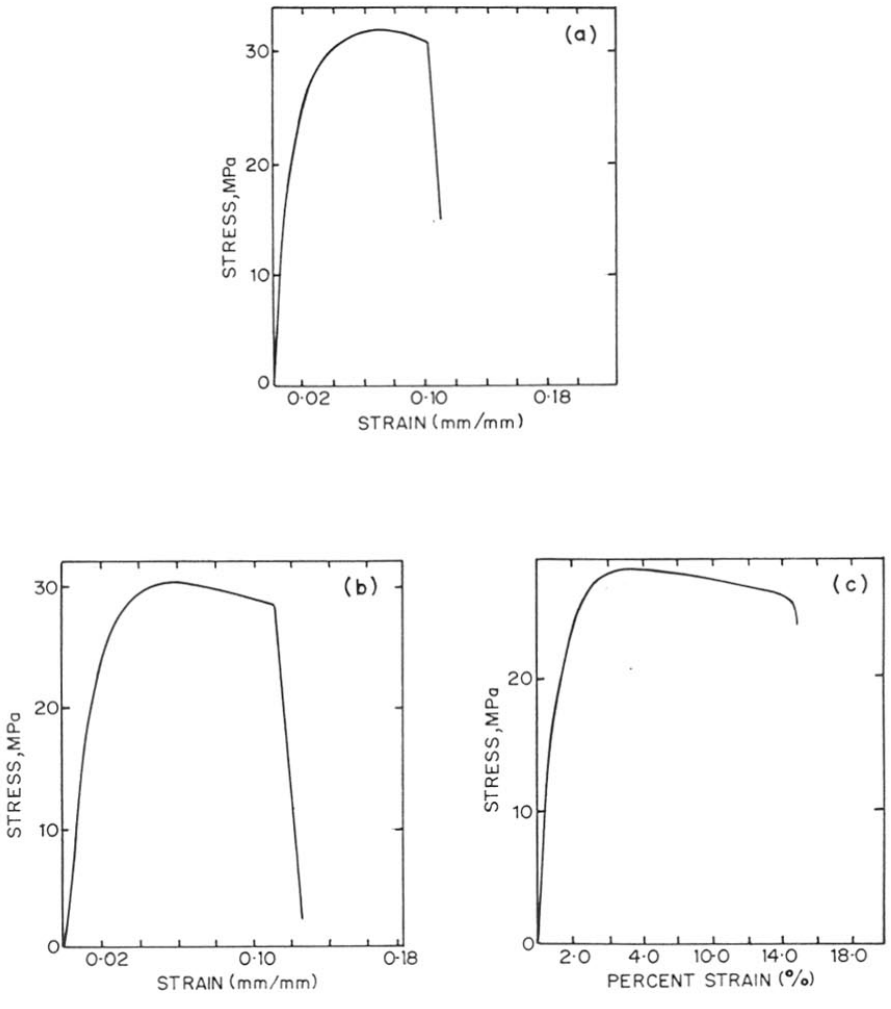

Figure 3.23 Plot of stress vs strain for PP (curve a); PP-CaS(IS) (b) and PP-CaS(ISW) (c). The additive concentration in both is 10%.

Table 3.11 Mechanical properties of PP- $CaSO_4$ composites

Composition	wt.%	Displacement at max load (mm)	% Strain at max. Load (%)	Load at max. Load (KN)	% Stress at max. load (MPa)	Strain at auto break (%)	Stress at auto break (MPa)	Tensile modulus (MPa)
Pure PP	0	4.04	8.10	1.25	31.86	13.20	1 3.89	1566
PP-CaS(IS) Additive concentration	5	3.04	6.13	1.22	31.10	10.32	29.41	1674
	10	2.96	5.93	1.18	30.12	12.74	27.57	1743
	15	2.78	5.56	1.13	29.08	11.21	26.74	1790
	25	0.14	4.61	1.07	27.40	8.14	25.88	1827
PP-CaS (ISW) Additive concentration	5	2.98	5.96	1.17	30.60	13.46	27.07	1925
	10	2.88	5.76	1.10	28.69	15.70	25.70	1986
	15	2.56	5.14	1.14	29.45	10.69	26.78	2212
	25	2.19	4.38	0.98	26.54	7.52	24.76	2158

remains more or less same. On the other hand, CaS(ISW) is effective in increasing the tensile strength of the composite which also exhibits a significant improvement in the impact strength up to a filler concentration of 10-15 wt.% which will be discussed later in the paper.

The variation of tensile modulus with composition of filler is shown in Fig.3. 24. Curve A corresponds to the tensile modulus of PP-CaS(IS) and curve B for PP- CaS(ISW) composites respectively. It is interesting to note that tensile modulus increased by almost 1.5 times for PP-CaS(ISW) as compared to pure PP. It increased with the increase of filler concentration upto 20 wt.% above which it showed a tendency to decrease slightly with the increase of filler loading. On the other hand, PP-CaS(IS) had only slight improvement in the tensile modulus as compared to unfilled PP. These various results can be explained on the basis of various factors such as crystalline phase, orientation, filler-matrix interaction and the aspect ratio of filler which govern the tensile strength in thermoplastic polymers.[41,42]

The increase in tensile modulus values for PP-CaS(ISW) may be associated to preferential growth of β phase of PP. This is because the type of crystalline phase has an influence on the tensile modulus of the composite. The α PP has a monoclinic structure with lattice parameters of a = 6.66 Å, b = 20.78 Å and c = 6.49 Å and β = 99.6° while the β phase of PP has a hexagonal structure with lattice parameters of a = 12.74 Å and c = 6.35 Å. In the latter case, the chains are packed in much closer configuration than the former, which are therefore difficult to displace with respect to each other. Moreover, the spherulites in the β phase are smaller and volume filling (see Fig.3.13a). These have more densely packed crystalline lamellae as compared to α phase, which have loose and widely spaced lamellae in their internal morphology. The latter can be discerned from the well-defined radial branches seen in the large α type spherulites. It is also reported that the β phase nucleated PP using quinacridone has much higher tensile strength than the normal PP.[43] Thus the presence of β phase in PP can lead to higher tensile modulus values than the normal PP.

The second factor governing the tensile strength is the orientation of crystallites. It is well known that tensile strength is more if the crystals are more aligned along the main axis as against the transverse direction of the tensile specimen.[44,45] This has been depicted in Fig.3.15 which reveals the needle shaped crystals of the additive are mostly oriented along the long axis for PP-CaS(ISW) type composites. These exhibited an increase of tensile modulus value as compared to PP.

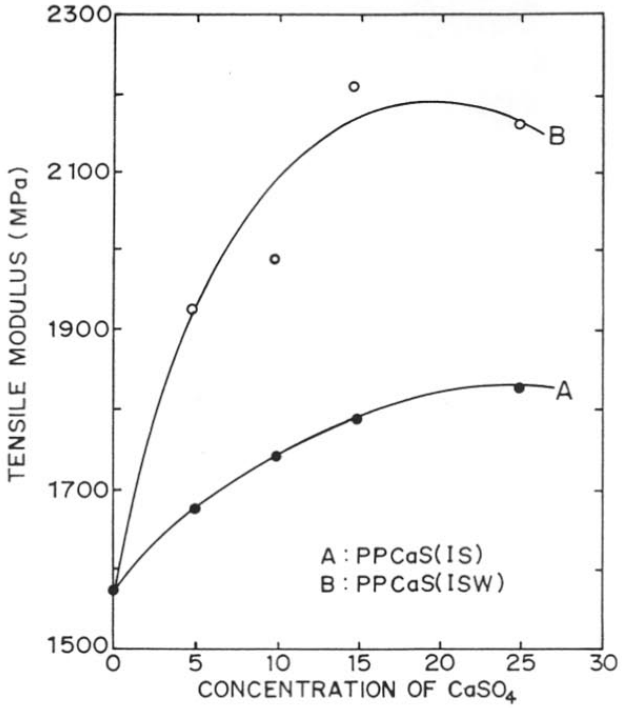

Figure 3.24 Variation of tensile modulus with composition of filler

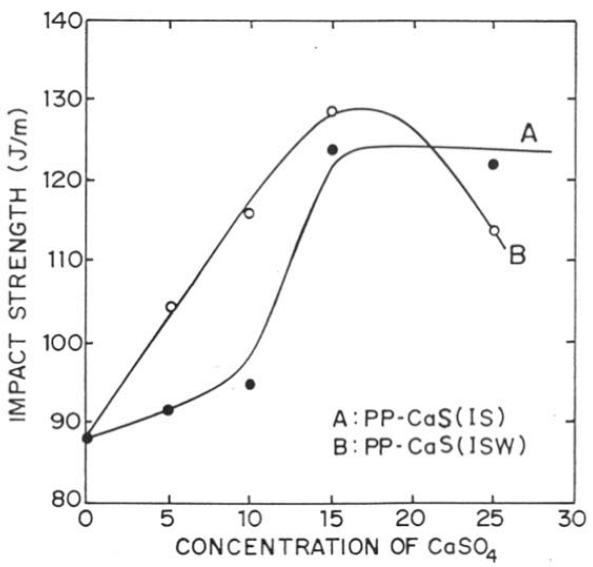

Figure 3.25 Variation of impact strength with the filler concentration

The third factor affecting the tensile strength is the interaction between the filler and the matrix. Greater the strength of bond between the filler and matrix, higher is the tensile strength of the composite. In case of PP-CaS(IS), the presence of PEO surrounding the crystallites undergoes deformation easily when the load is applied due to its low T_g and more flexibility than PP[46]. Therefore, it prevents the transfer of load from the matrix on to the filler thus making the filler-matrix bond weak and this results in a lowering of tensile strength values as compared to PP- CaS(ISW). On the other hand, in case of PP-CaS(ISW) there is good interfacial bonding due to the nucleated PP crystallites around the additive and the tensile load is transmitted from the matrix to crystallites giving rise to an increase of tensile strength values. However, with high filler loading above 25 wt.% the tensile strength has a tendency to decrease. This could be due to agglomeration of $CaSO_4$ crystals giving rise to weak points at which there is poor inter-crystallite adhesion.

Lastly, the aspect ratio of crystallites also affects the tensile strength of the composite. Higher aspect ratio of the additive gives good reinforcing effect and hence higher tensile strength as observed for all PP-$CaSO_4$ composite. Even in the case of PP-CaS(IS) the slight improvement in the tensile strength as compared to pure PP could be due to this factor. However, this improvement is quite small as compared to other factors mentioned above.

The impact properties of these composites (notched impact values) were measured by the Izod impact tester. Figure 3.25 shows the variation of impact strength with the filler concentration ranging from 0 to 25 wt.% for both the types of $CaSO_4$ added to PP. The impact strength increases with the filler content upto 15 wt.% for both the types of $CaSO_4$ in the composite (120 J/m) as compared to pure PP, which shows impact strength of 85 J/m. It can be seen that the impact strength is much higher for PP-CaS(ISW) than for PP-CaS(IS) at low filler concentration while at high filler concentration both the types have same value of impact strength. These results can be explained on the basis of different factors such as the crystallinity of the matrix, crystallite or spherulite size, bonding between the filler and the matrix and also the defects or stress points in the thermoplastic material, which affect its impact strength.

Generally in semicrystalline polymers, it has been observed that higher is the crystallinity , lower is the impact strength. However, we have been able to achieve high impact strength together with high crystallinity in PP-$CaSO_4$ composites. This is apparent from the Table 3.9 as explained earlier, which indicates that the β content and the crystallinity to be

higher for both the types of PP-$CaSO_4$ systems as compared to pure PP. This rather surprising result can be attributed to the size of the spherulites.

The spherulite size plays a significant role in governing the value of impact strength. Smaller is the size of spherulites, higher is the impact strength. In the case of PP-CaS(ISW) where the smaller β phase spherulites are mainly observed, the impact strength is higher while in case of PP-CaS(IS) the presence of PEO surrounding the crystallites inhibits the nucleation and generation of β phase and accordingly the spherulites are large and the impact strength is lower.

The presence of stress points or defects in the specimen also affects the impact strength and this can take place especially at high filler loading. As the notched specimens were used for impact strength measurements it may be noted that crack propagation rather than crack initiation will be the main deciding factor for impact strength. The presence of defects can give rise to an easy path for crack propagation. From the Fig. 3.25 it can be seen that the impact strength shows a tendency to decrease at high filler loading greater than 25 wt.% especially for PP-CaS(ISW). On the other hand, the impact strength for the PP-CaS(IS) composite may remain more or less constant even at high filler loading greater than 25 wt.%. This can be due to the presence of PEO surrounding the crystallites, which acts as an effective absorber of the impact force. The PEO content in the composite would be higher at high filler loading and hence, its effect is predominantly seen at concentrations >20 wt.%. Thus, although the impact strength in this case is lower than PP-CaS(ISW) due to the presence of large spherulites, the impact strength may remain sufficiently high even at high filler loading which could be advantageous for practical applications.

3.4 Conclusions

From these studies following important conclusions can be drawn:

(a) Polymer mediated growth is clearly observed in the case of synthesis of $CaSO_4$. PEO complexed with inorganic salt ($CaCl_2$), which is further, reacted so as to form $CaSO_4$.

(b) Orientation of matrix (PEO) induces orientation of $CaSO_4$ crystallites during shearing where the long axis is parallel to the direction of shearing of the polymer. Also, the extrusion of PP-CaS(IS) gives rise to appreciable changes in the intensities corresponding to reflections (100) and (111) from the $CaSO_4$ crystals of γ phase.

(c) The $CaSO_4$ made by *in situ* deposition when incorporated in PP nucleates preferentially the β form and the $CaSO_4$ itself gets transformed from dihydrate to γ form (anhydrite) of $CaSO_4$.

(d) The presence of PEO in PP-$CaSO_4$ composites gives α form of PP and prevents the preferential form of β form of PP.

Thus, polymer induced crystallization can be effectively used for controlling the crystal structure, morphology, particle size, etc. of a filler used in PP composite. Such modified fillers having high aspect ratio can yield better properties in PP composites.

3.5 References

1. W.C. Wake, Fillers for Plastics, The Plastic Institute: London (1971).
2. A. King , Plasticisers, Stabilizers and Filler Ritchie, P.D. et al., Eds., The Plastics Institute, London, England (1972).
3. R. Gachter,, H. Muller, Plastic Additives Handbook, Hanser: New York, NY, (1981)
4. J. Stepek , H. Daoust, Additives for Plastics, Springer-Verlag: New York, NY, (1983)
5. H. S. Katz, J.V. Milewski, Handbook of Fillers and Reinforcements for Plastics Van Nosrand Reinhold: New York, NY (1978).
6. J.V. Milewski, H.S. Katz, Handbook of Reinforcements for Plastics, Van Nostrand Reinhold: New York, NY (1987).
7. N.S. Enikolopyan, Filled Polymer I, Eds., Adv. In Polymer Sci., **96** (1990).
8. M. Fujiyama and T. Wakino, J. Apply. Polym. Sci. **43** (1991) 47.
9. Varga, Jozsef, Schulek-Toth, Ferenc, Magy. Kem. Poly. **95(9)** (1989) 363-72
10. F. Rybnikar, J. Macro. Mol. Sci. Phys., **B 19** (1981) 1.
11. Showa, High Polymer Co. Ltd., Jpn. Kokai Tokkyo Koho JP/5849, 653 (8349, 653) 16 Sept. 1981.
12. Von Haebler, Alexander (Von Haebler, Lena), S. African ZA, 8203, 802 28th May, 1982.
13. Hirai, Takayuki, Jpn. Kokai Tokkyo Koho, 82,67,066, 23 Apr. 1982.
14. M. Franciscus Hubertus Jacobus, P.Jacques Peter Laurentius, S.Paul., Eur. Pat. Appl. EP55,001, 30th June 1982.
15. Matsushita Electric Works, Jpn. Kokai Tokkyo Koho JP 8200,155, 05 Jan.(1982).
16. Winslow, Jerry G. (United States, Gypsum Co.), 3 Jul 1982, US Appl. 854774, 25 Nov. 1977.
17. N. Takeshi, I. Ikuo, S. Akihiro, O. Katsumi (Sekisky Chemical Co. Ltd., Jpn. Kokai Tokkyo Koho JP 60,186,552 (85,186,552) ,5th Mar 1984.
18. T.T. Pitts, J. Cell Plastics, **7(4)** (1971) 202.
19. W.K. Tank, and W.K. Neill,, J. Polymer Sci., **C6** (1964) 65.
20. H.W. Angell,, Proc. Forest Prod. Res. Soc., **5** (1951) 107.
21. R.M. Pruitt, J. Cell Plastics, **6** (1970) 262.
22. J. Di Pietro and H.J. Stepniczka , Fire and Flammability, **2** (1971) 36.
23. Plastic Technology, March (1995) 44.

24. S. Radhakrishnan, J. Cryst. Growth, **141** (1994) 437.
25. S. Radhakrishnan and V.M. Nadkarni, Int. J. Polym. Mater., **11** (1986)79.
26. S. Radhakrishnan and S.G. Joshi, Furo. Polym. J., **23** (1987) 819.
27. ASTM Diffraction Files, 1-0999, 2-0134, 2-0625, 6-0046, ASTM, Washington (1995).
28. E.C.S. Dickson and S.W. Binks, Phil. Mag., **2** (1952) 114.
29. G.C.H. Cheng and J. Zusman, Acta. Cryst., **16** (1963) 767.
30. R.W.G. Wyckoff, "Crystal Structures", Vol.3, John Wiley, New York, p.18 and 642 (1968).
31. S. Radhakrishnan and D.R. Saini, J of crystal growth, **129** (1993) 191.
32. J.M.G. Cowie and S.H. Cree, Ann. Rev. Phys. Chem., **40** (1989) 85.
33. C.A. Vincent, Prog. Solid State Chem., **17** (1987) 145.
34. A. Khare, A. Mitra and S. Radhakrishnan, J. Mater. Sci., **31** (1996) 5691-5695.
35. M.J. Folkes and D.A.M. Russell, Polymer, **21** (1980) 1252.
36. R. Bailey and B. Rzepka, Int. Polym. Process, **6** (1991) 35.
37. A.G. Walton in "Nucleation", edited by A.C. Zettelmoyer, Marcel Dekker, NewYork, (1969) Chpt.5.
38. K. Mauritz, E. Bauer and A. Hopinger, J. Macromol. Sci. Macromol. Rev., **8** (1978) 1.
39. S. Radhakrishnan and R. Joseph, Sp. Issue on Cryst. and Cryst. Growth, Ferroelectrics, **142** (1993)189.
40. S. Radhakrishnan, K. Kane, K. Kadu and H.P. Natu, J. Appl. Polym. Sci., **58** (1995) 571.
41. I.M. Ward, Mechanical Properties of Solid Polymers, J. Wiley & Sons Ltd. New York (1983).
42. F. Lisy, A. Hiltner, E. Baer, Polymer Prepr., **32(2)** (1991) 21.
43. S. Radhakrishnan, M. Tapale, E. Rairkar, V. Shirodkar and H.P. Natu, J. Appl. Polym. Sci., **64** (1997) 1247.
44. Y. Suetsugu, Int. Polym. Process, **5** (1990) 184.
45. D. Hull, Introduction to Composite Materials, Cambridge, Univ. Press, (1981).
46. F.C. Bailey and J.V. Koleske, Alkylene Oxides and their Polymers, Marcell Dekkar, NY (1991).

Chapter 4

In Situ Fibre Formation of PP/SBS Blend and the Structure and Properties of Hybrid Composites of PP/SBS/glass

4.1 Introduction

Polypropylene (PP), a widely used commodity polymer, is known to be highly crystalline and possesses good tensile strength. However, its impact properties fall short of desirable values. Hence, a number of efforts have been made in the past to improve impact properties using impact modifiers. These impact modifiers are in general flexible elastomeric polymers of primarily amorphous in nature and very low T_g. The various impact modifiers investigated in the past for PP are ethylene-propylene monomer (EPM)[1], ethylene-propylene-rubber (EPR)[2,3], ethylene-propylene-diene-monomer (EPDM)[4], acrylonitrile-butadiene-styrene (ABS)[5], polyisobutylene (PIB)[6,7], styrene-butadiene-styrene (SBS)[8], styrene-butadiene rubber (SBR)[9], polybutadiene (PBu)[10] etc. The macroscopic properties of blends with these impact modifers have been extensively investigated and reviewed. The effects of these high impact additives on the morphological characteristics of PP have also been studied to some extent.[8,11]

Greco et al.[2] report that the presence of EPR as an impact modifier in PP blends influences the structure and morphology of the blend. They showed that EPR acts as a nucleating agent for iPP spherulites. The composition of copolymer used, affected the state of dispersion of the EPR as well as the thermal and mechanical behaviour of the blends for the crystallization conditions studied. A thorough investigation of the effect of block EPR copolymers composition with different C_2/C_3 ratio on the morphology of iPP revealed that an increase of C_3 content in the copolymer induced higher compatibility and also affected the impact and tensile properties.

Choudhary et al.[4] studied the effect of EPDM rubber on crystallization behaviour, morphology and mechanical properties in PP/EPDM blends. They found that PP/EPDM blends were incompatible at all compositions. Addition of 10% wt. of EPDM to PP, resulted in an increase in spherulite size. Higher concentrations of EPDM resulted in a decrease in spherulite size. Optical micrographs showed that the rubber was distributed both in the intra and inter-spherulitic regions. The heat of fusion, as measured by DSC and percentage crystallinity as measured by WAXD, of these blends decreased on increasing EPDM content. SEM revealed a skin- core morphology in injection moulded specimens.

The influence of polyisobutylene (PIB) on the morphology, crystallization and mechanical properties of iPP was investigated by E.Martuscelli et al.[6]. In these studies PIB act as a nucleating agent for iPP spherulites. L. Biauchi et al.[7] carried out morphological

observations and mechanical tests on sheet specimens of iPP/PIB blends under different crystallization conditions. They found two kinds of morphologies particularly at high crystallization temperatures: a spherulitic one in the centre and a row- like structure on the edges. The size of the spherulites as well as the thickness of the row- like regions decreased with diminishing T_c and was found to be independent of the amount of rubber. The rubber particles seemed to be evenly dispersed into the iPP matrix for samples quenched at low T_c whereas for the isothermally crystallized (at high T_c) samples, the rubbery domains were concentrated at the edges of the spherulites as opposed to the centre. The overall crystallinity as measured by DSC decreased with increasing amount of PIB.

A simpler and less expensive elastomer viz. polybutadiene was also investigated by Gupta and Ratnam[10] in blends with PP. The XRD and DSC revealed a distinct influence of PBu content on the crystallization of PP.

Takashima et al.[12] disclosed a blend of PP, PIB and BR with significant improvements in impact properties over PP. Pocorny & Van Henten[13,14] have suggested the use of SBS-block copolymers as modification agent for PP.

The reports of various authors described above indicate that blends of PP with various elastomers have shown improvements in not only the impact resistance but also the melt flow behaviour that is related to processability and crystallization of PP. However, the tensile strength or modulus deteriorates. Thus, in order to achieve a suitable balance in tensile and impact properties , strategies such as composites with fibres formed *insitu* , ternary blends and hybrid composites can be conceived.

The formation of fibres *in situ* i.e during the actual melt processing of the components have drawn considerable interest among various authors. The *in situ* formation of fibre has been observed in polyolefin blends such as SBS/PS blends[15,16],SBS/HDPE blends[17,18] and in some thermotropic liquid crystalline polymer graft or block copolymers[19] etc as has already discussed in section 1.6.5.

Recently, a number of papers are being published on ternary blends and/or formation of hybrid composites are being investigated by several authors in order to overcome the drawbacks of toughening where there is improvement of impact strength but at the same time the tensile modulus deteriorates. The introduction of HDPE into the mixture of PP/SBS is a ternary blend investigated by several authors.[20] It gave rise to not only high ductility and impact strength (700 J/m) but also balanced mechanical properties. Zhang et al.[21] studied the

effect of processing on the properties and morphology of these ternary blends and found that the morphology of the SBS dispersed phase particle was closely related to the mechanical properties of the ternary blend and it was very much dependent upon the processing parameters used. Thus, the studies of such hybrid composites or ternary blends are still in progress.

Our survey of literature indicated the following shortcomings in the earlier data:

(a) A detailed investigations on the PP blends containing impact modifiers such as thermoplastic elastomers have not been carried out before especially in terms of structure, morphology, crystallization behaviour and its correlation with mechanical properties of the resulting composites.

(b) The *in situ* fibre formation, which is of specific importance for improving the properties, has not been tried so far for PP blends.

(c) The hybrid composites can give good balance of tensile strength together with improved impact resistance. Such studies are especially needed for PP blends which can lead to improved properties.

Therefore, we decided to undertake studies to examine the structure development and properties of PP/SBS blends and *in situ* fibre formation in the same and modify the structure and the properties by addition of glass fibres as the third component.

4.2 Experimental

(a) Preparation of the blends

Binary blends of iPP (Koylene M0030 grade) obtained from IPCL and SBS (Cariflex CTR 1102) from Shell Corporation were prepared by solution blending technique as described in section 2.7. The compositions contained 10 to 40 wt.% SBS. A few compositions were prepared by melt blending technique described in section 2.5 using precipitated powders. The crystallization behaviour of these samples prepared by different methods was studied using optical polarizing microscopy as before. The isothermal crystallization temperature was kept at 105°, 110° or 115°C for these studies.

In order to investigate the structure by wide angle X-ray diffraction, two sets of PP/ SBS blends with different concentrations of SBS ranging from 10 to 40 wt.% were pelletized as described earlier in section 2.5. One set of pellets were designated as solution grown samples; while the other set was allowed to undergo melt crystallization process under the conditions mentioned earlier. Some of the PP/ SBS blend samples were extruded at a mild

extrusion rate from a melt indexer and a thin section of these samples were observed under SEM in order to determine the dispersion state of the blend with respect to SBS concentration. The DSC studies were carried out for different concentrations of SBS with respect to PP to analyse the T_g and the crystallization temperature (T_c) of these blends. The morphological changes in the isothermal crystallization as well as orientation at a particular concentration of SBS were examined by taking the micrographs of the samples on an optical polarizing microscope. The skin and core layer of injection moulded PP/ SBS blends were studied by XRD after sectioning the samples along the machine direction. The complete details of the characterization techniques used have already been described in section 2.9.

(b) Preparation of the Composite

Composite was prepared by the addition of chopped glass fibres (FGP Limited, diameter 15 μm) to PP/SBS blends containing 0 to 40 wt.% SBS. The preparation of the composite by melt processing has been discussed in section 2.5. Two sets of glass fibre concentrations were made with respect to total blend (PP/SBS): in one set the glass fibre was varied from 5 to 15 wt.% for studying the crystallization behaviour and morphology and in another set it was varied from 20 to 40 wt. % for studying the mechanical properties.

(c) Measurement of Properties

Mechanical properties such as impact strength, tensile modulus and elongation were investigated for the injection moulded composites. Commercially available PP pellets along with SBS pellets and the glass fibres were simultaneously mixed in desired proportions and first compounded using Brabender plasticorder single screw extruder. The PP/SBS blends with 30 and 40 wt.% SBS was compounded with glass fibres so as to give composition with 20 to 40 wt. % glass with respect to total blend. The temperature conditions set in the single screw extruder were same as mentioned in section 2.5. The screw speed was controlled at 30 rpm for PP/ SBS containing glass fibres and 40 rpm for PP filled with glass fibres. These samples were pelletized and injection moulded as described before (section 2.5). The notched impact and tensile properties were determined for moulded specimens and compared with those of PP prepared in the similar manner.

4.3 Results and Discussion

4.3.1 Structure Development and Properties of Blends

Figure 4.1a shows the WAXD for PP/SBS blends melt crystallized at 115°C and Fig. 4.1b shows the WAXD of solution blended PP/SBS samples. The curves A,B,C and D in both figures correspond to concentrations of SBS ranging from 10, 20, 30 and 40 wt.% respectively.

In both melt crystallized and soution blended samples, the characteristic diffraction maxima of monoclinic α crystalline form of PP are present in the diffraction patterns over the complete range of compositions studied. In case of melt crystallized samples, (Fig.4.1a) amorphous scattering of SBS increases with increase of SBS content. Therefore, one would expect the overall intensity of XRD peaks to decrease with the addition of amorphous SBS. However, it is interesting to note that the relative intensities of these peaks vary with respect to SBS composition. The reflections corresponding to peakII (040) and peakIV (131) planes get affected by the presence of SBS in PP. In case of solution blended samples, (Fig.4.1b) the intensities of the peaks are much lower than those observed for melt crystallized samples. Further, there is no sharp distinction in the two reflections observed for (131) and (041) occurring at 2θ of about 21 to 22°. Also, the reflections are somewhat broader than those obtained for melt crystallized samples. This extent of broadening suggests that the crystallite size is lower in solution blended samples which can be associated with better molecular mixing and formation of smaller domains.

Figure 4.2a and b represents the variation in the intensities of the peaks with respect to first peak (2θ = 14°, 110 reflection of α phase of PP) for melt crystallized and solution blended samples. For melt crystallized samples (Fig.4.2a) at a certain composition the (040) reflection (peak II) has maximum intensity and is more affected than the other peaks in presence of SBS. However, only peak IV (131/041) reflection is enhanced in solution blended samples (Fig. 4.2b) while the other reflections are suppressed in presence of SBS. The variation in intensities of XRD peaks are usually observed when preferential orientation of crystallites along certain direction takes place. Since the above samples were made under normal conditions where no melt flow or orientation could take place, the variation in the intensities of different peaks would have to be associated with preferential growth mechanism rather than orientation. Since (040) and (041) reflections are mainly affected, it can be concluded that there is a preferential growth of PP crystallites along the b-axis during their nucleation.

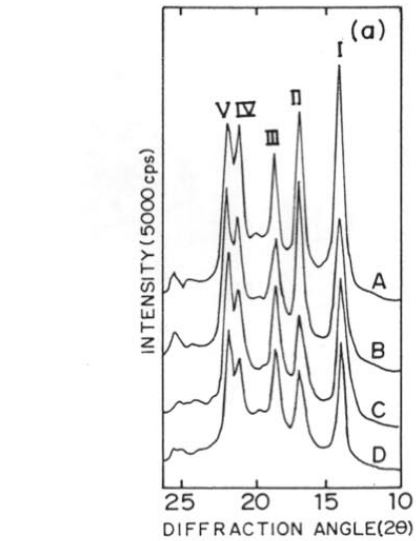

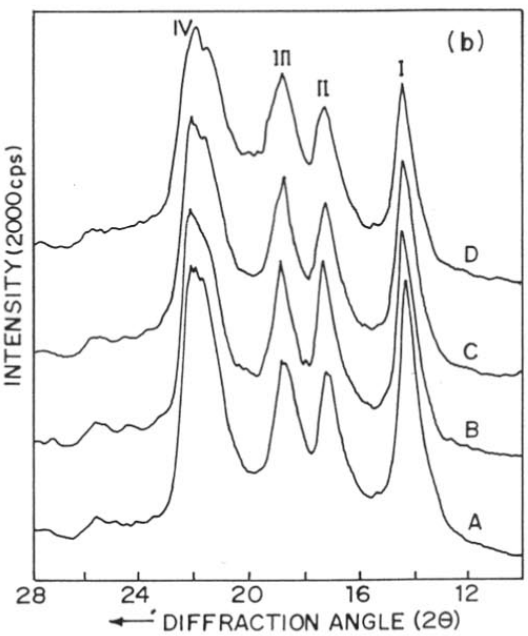

Figure 4.1 WAXD scans for PP/SBS blends: (a) melt crystallized at T_c = 115°C (b) solution blended PP/SBS samples
Curves A, B, C and D correspond to SBS concentrations of 10, 20, 30 and 40 wt.% respectively.

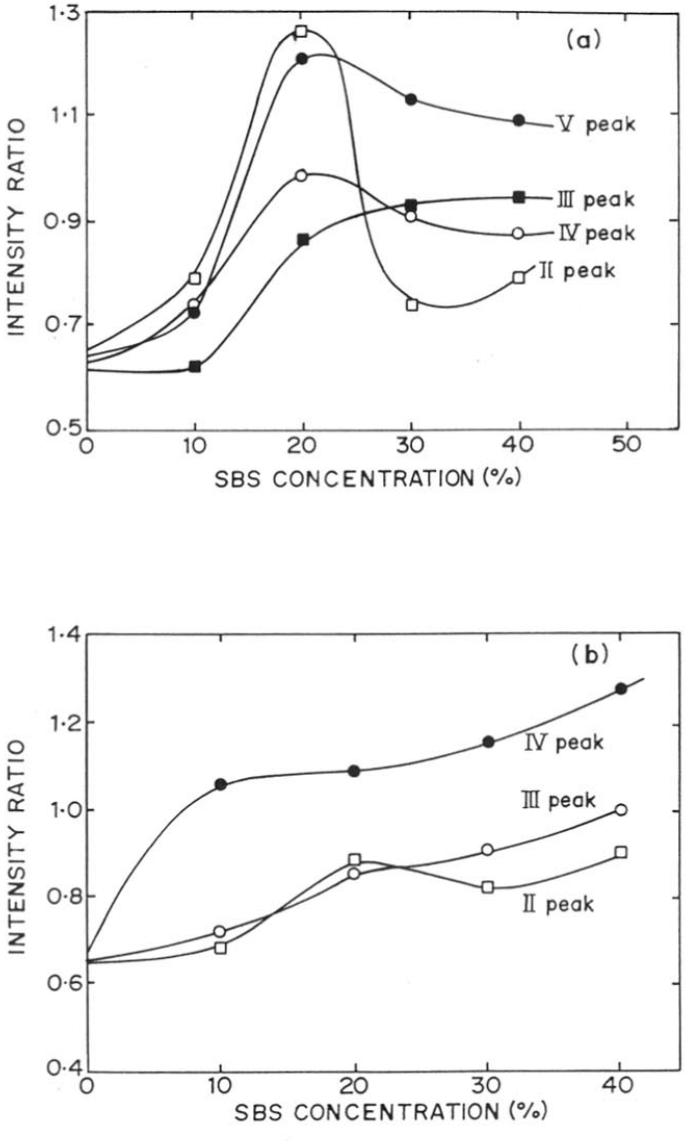

Figure 4.2 Variation in the intensities of the peaks with respect to first peak (a) For melt crystallized samples (b) Solution crystallized samples

The degree of crystallinity (C_i) of the blends calculated from the XRD data as a function of SBS concentration for solution blended and melt crystallized samples is shown in Fig. 4.3. It also shows a plot of expected crystallinity for a blend material containing different mass fractions of SBS (which is known to be amorphous) uniformly dispersed in it as calculated using the following simple rule of mixture as:

$$C_i \text{ (blend)} = m_1 C_{i\,1} / (m_1 + m_2) + m_2 C_{i\,2} / (m_1 + m_2) \qquad (4.1)$$

Where $C_{i\,2} = 0$ (for SBS) and $C_{i\,1} = 62\%$ (for PP), m_1 = mass fraction of PP and m_2 = mass fraction of SBS. For both melt as well as solution blended samples, the observed C_i values are higher than that expected from above relationship (eqn.4.1). The C_i decreases more rapidly with increasing concentration of SBS in solution blended samples than in melt crystallized blends which suggests that there is better mixing in the solution blended samples while large phase segregation occurs in melt crystallized samples. Both these observations suggests that although PP and SBS are not miscible, there appears considerable interaction between them since the SBS domains in PP/SBS blends affect the crystallization process of PP.

Figure 4.4 shows the crystallization behaviour of the blends plotted in terms of transmitted light intensity as a function of time. The isothermal melt crystallization was studied at three temperatures 105°, 110° and 115°C but Fig.4.4 shows typical plots at 115°C. It can be seen from this graph that as the induction period for nucleation decreases, the crystallization rate increases in presence of SBS especially for small spherulites as compared to normal large PP spherulites.

The crystallization half time ($t_{1/2}$) and crystallization rate (slope at $t_{1/2}$) were deduced from these graphs and plotted with respect to SBS composition which are indicated in Fig.4.5a and b respectively. It can be observed from the above figure that $t_{1/2}$ value varies considerably with SBS concentration. A minimum in $t_{1/2}$ value is seen for composition of 20 wt. % SBS. This trend is observed for all the three crystallization temperatures (105°, 110° and 115°C) studied but it is more pronounced at higher T_c of 115°C. The increase of $t_{1/2}$ value at higher concentration of SBS could be associated with the agglomeration of SBS domains due to which the effective nucleating surface area decreases. Nevertheless, the $t_{1/2}$ values observed here are much lower than that for PP indicating that the growth rate of spherulites in presence of SBS is quite high as compared to the growth rate in pure PP at all three temperatures. The

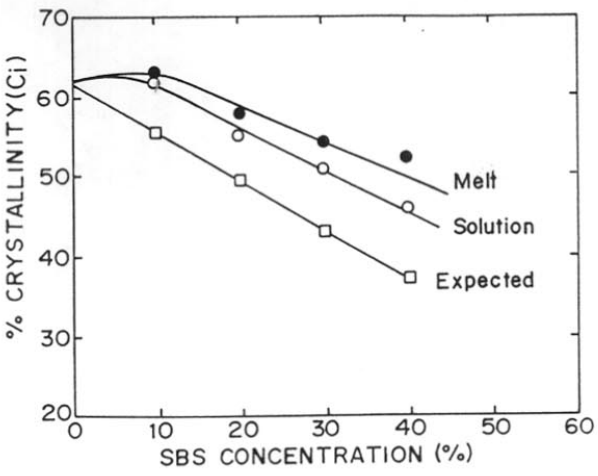

Figure 4.3 Percentage crystallinity (C_i) of the blends as a function of concentration of SBS for solution blended and melt crystallized samples

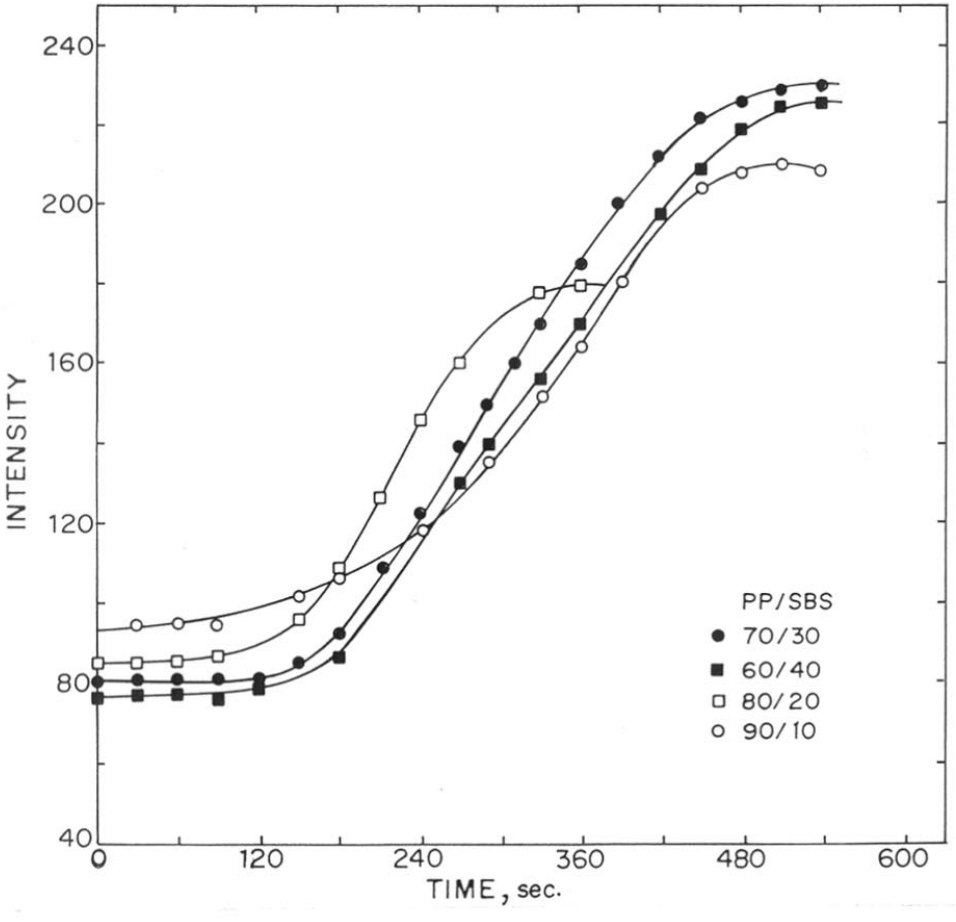

Figure 4.4 Graph of intensity as a function of time in seconds for PP/SBS blends at $T_c = 115^{\circ}C$.

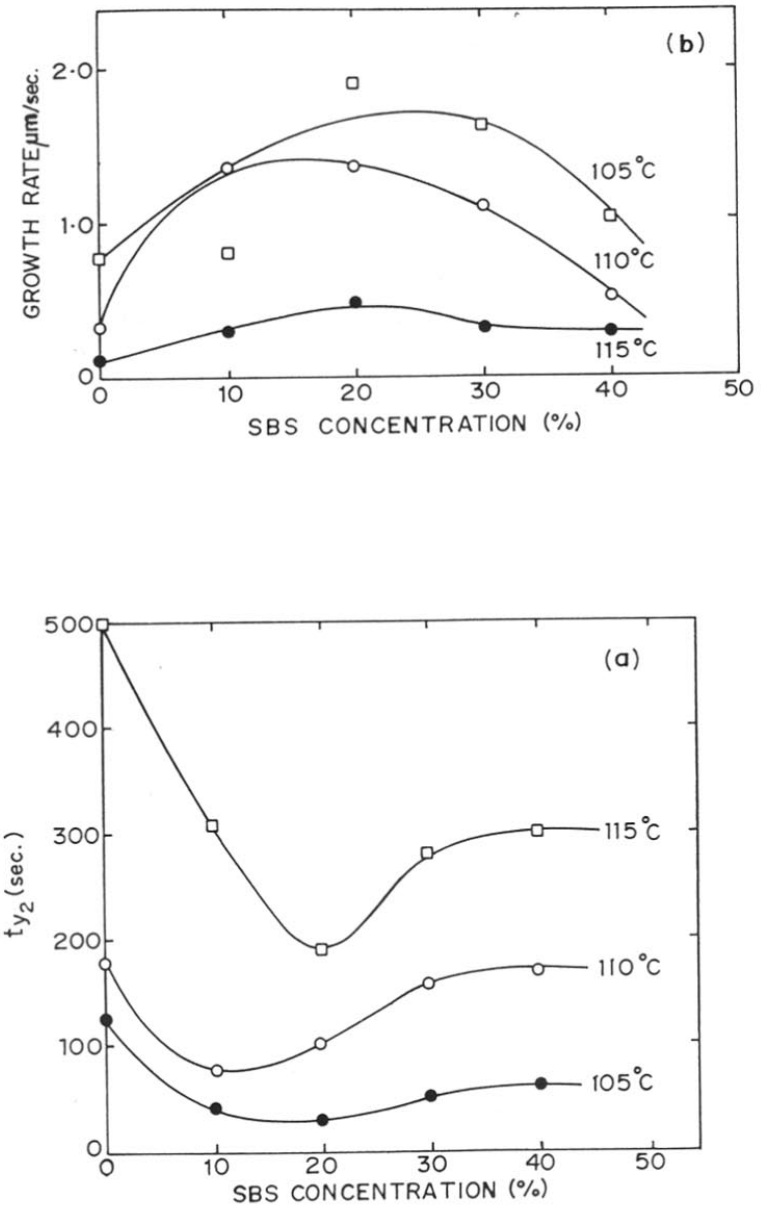

Figure 4.5 Crystallization half-time (a) and growth rate (b) with respect to SBS concentration at T_c=115°C

growth rate of spherulites reaches a maximum at a certain composition of SBS between 20% to 30% at which $t_{1/2}$ value is minimum, suggesting that SBS domains act as nucleating centres for PP spherulites.

Gupta and Ratnam[10] have reported the crystallization behaviour of PP/PBu blends. The XRD scans of these blends showed an increase in the ratio of intensity of (040) reflection to that of (110) reflection with increase of PBu content. This implies a preferential growth of crystallites in certain direction which has been observed in the present study also. They also observed a higher value of degree of crystallinity for PP/PBu blends (3 wt.%) than for virgin PP calculated from the diffraction pattern. These findings by them clearly show the interaction of PBu domains on the nucleation of PP. On the other hand, studies on PP/ PS blends[22] showed no effective influence of PS domains on the nucleation of PP. The spherulitic growth rate in the blends were found to be independent of concentration of PS. Hence, it is quite likely that the polybutadiene domains rather than the styrene blocks in the SBS take part in the nucleation of PP.

Figure 4.6a and b show the optical micrographs for blends containing 0%SBS (pure PP) and (80/20) PP/SBS respectively. Pure PP has large well developed spherulites associated with its α phase. The PP/SBS blends contain two types of spherulites: one having similar morphology as that of pure PP and the other much smaller in size having diferent internal morphological features than that of pure PP. These small spherulites are seen to cluster around the SBS domains. By comparing these micrographs, we can conclude that the SBS domains have definite tendency to nucleate small spherulites having different internal morphological features than normal PP spherulites.

In a non-miscible, non interactive two phase system without any compatibilizer, the crystallization behaviour would be independent of either of the phases and the overall total crystallinity would decrease with the increase of amorphous component in the blend composition. In the present case of PP/SBS blend, not only are the crystallization half times, growth rates and the spherulite sizes affected by the concentration of amorphous component but also the crystallinity and variation in intensity of certain reflections in the XRD are altered. All these observations are complementary to each other and support the above hypothesis that SBS domains nucleate small spherulites having different morphological features in PP.

The DSC thermograms for the melt blended samples with different concentrations of SBS and PP are shown in Fig. 4.7. The heating curve shows a low glass transition temperature

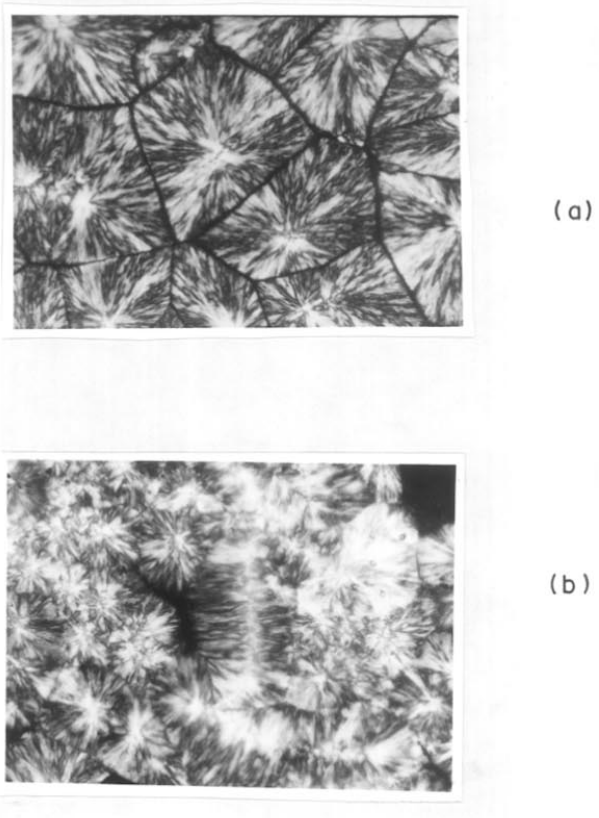

Figure 4.6 Optical micrographs of (a) pure PP (b) (80/20) PP/SBS (net magnification 450 x)

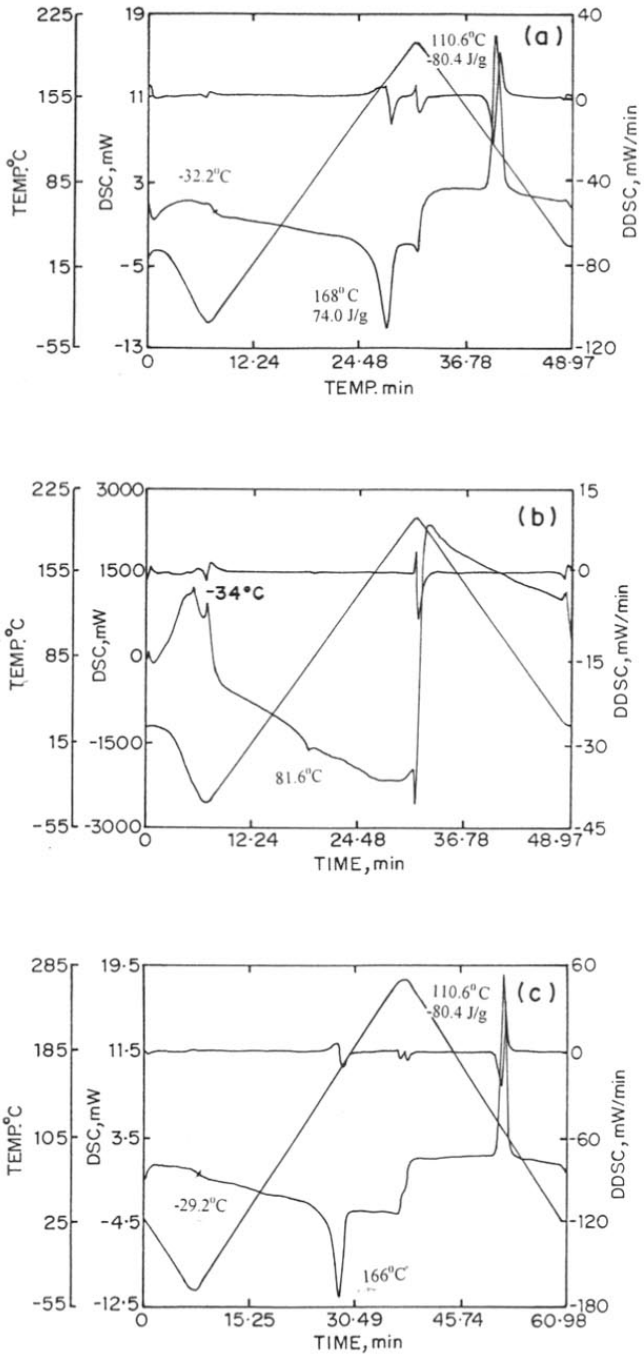

Figure 4.7 DSC curves (a) pure PP (b) pure SBS (c) (90/10) PP/SBS

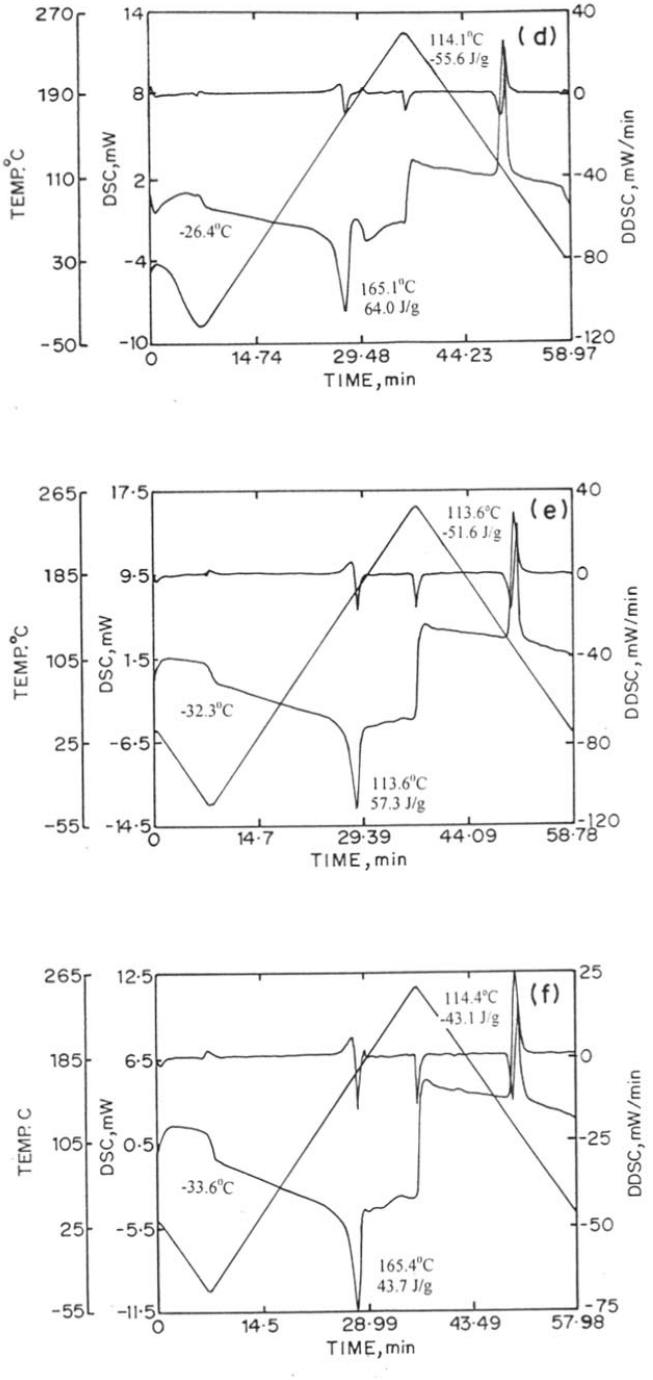

Figure 4.7 DSC curves (d) (80/20) PP/SBS (e) (70/30) PP/SBS and (f) (60/40) PP/SBS

(T_g) and a sharp melting endotherm, which is due to melting point of PP. In the cooling curves, there is only one sharp exotherm observed in the region 110°C to 115°C associated with the crystallization of PP. The effect of SBS on the various transition temperature i.e. T_g, T_m and T_c is depicted in Fig.4.8. The crystallization temperature T_c increases (by about 5°C) as compared to pure PP and then remain steady with the increase of SBS concentration from 0 to 40%. The small increase in the crystallization temperature is due to the nucleation of PP spherulites by the SBS domains. T_g also varies with the addition of SBS in PP as shown in Fig. 4.8a. The small increase in T_g could be due to the interpenetration of butadiene domains in the amorphous region of PP, leading to a reduction of the total free volume. It is interesting that the T_g for pure SBS due to the polystyrene domains expected at 81°C is not clearly seen in the DSC of PP/ SBS blend. Further, the T_g of polybutadiene domains of SBS lie in the low temperature region (-34°C). The ΔH value (J/g) determined from the melting endotherms have been plotted as a function of SBS composition in Fig.4.8 b. The values of ΔH estimated from simple rule of mixture assuming SBS as amorphous and non interactive with PP have also been shown for different compositions for comparison. The observed ΔH values are higher than the expected ΔH for the blends upto SBS concentration of 30%. This suggests that there is higher crystallinity in the blend than that expected for simple mixture which can be due to nucleation of PP by SBS domains as mentioned earlier.

The new outstanding feature of the present experiment was observed in melt crystallized PP/ SBS samples subjected to shear stress in molten state. Figure 4.9 shows the optical micrograph of PP/SBS sample containing 20% SBS. Extensive fibre formation and orientation in the direction of the shear stress is seen in the micrograph. The fibres appear as black streaks (being amorphous these appear black under crosspolar condition of microscope). It is hence, not surprising to find the fibrous morphology in injection moulded samples where the melt is subjected to much higher shear stress. This was confirmed by the SEM studies on fractured surfaces of injection moulded specimens. Figure 4.10 depicts the SEM micrographs of melt extruded samples. It reveals a two Phase morphology consisting of spherically shaped SBS particles distributed in the continuous PP matrix. The spherical domains which are seen at low concentration of SBS get elongated at high concentrations (≥30%) and ultimately give rise to extensive fibrous morphology at or above 40 wt.% of SBS. The generation of fibres *'in situ'* i.e. during the melt processing of components was observed only recently in certain polyolefin blends.[15-18]The exact mechamism of such fibre formation is not yet fully

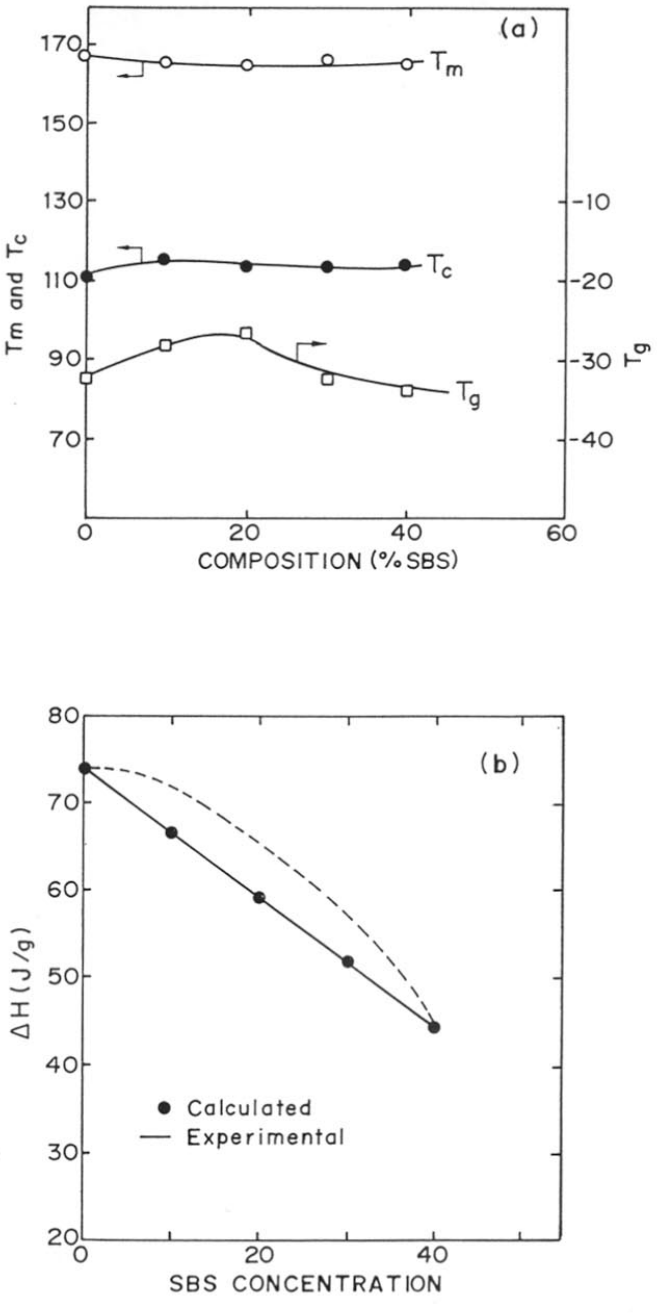

Figure 4.8 (a) Plot of T_g, T_c and T_m vs concentration of SBS
(b) Plot of J/g vs SBS concentration

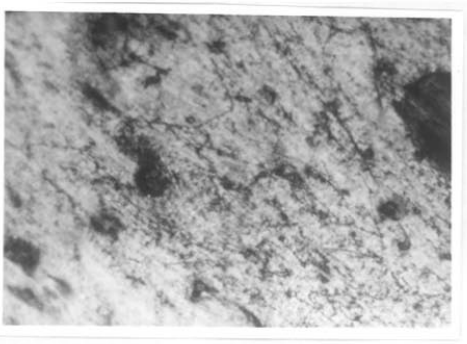

Figure 4.9 Optical micrograph of (80/20) PP/SBS sheared sample (700 x net magnification)

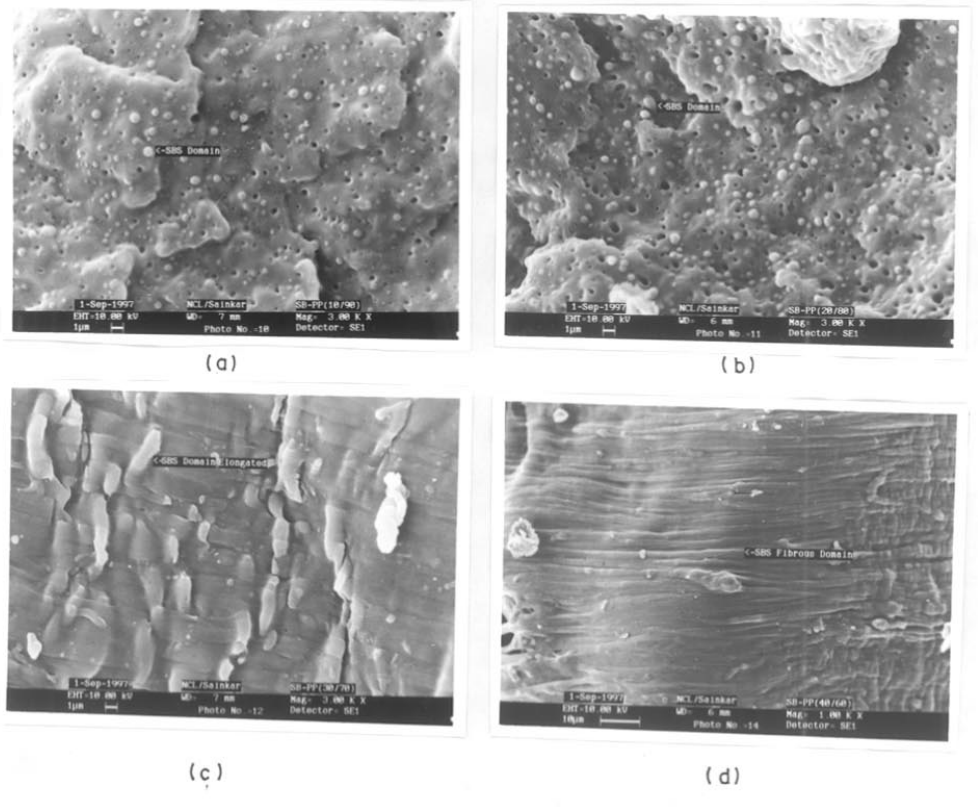

Figure 4.10 SEM micrographs of fracture morphology of melt extruded samples (a) (90/10) PP/SBS (b) (80/20) PP/SBS (c) (70/30) PP/SBS (d) (60/40) PP/SBS

understood. In the present study, we observed that the *in situ* fibre formation takes place at an appropriate composition (above 30%) and under shear stress. These features were clearly seen in the injection moulded specimens. These observations clearly bring out that both SBS as well as oriented domains of PP exhibit complete fibrous morphology at a certain concentration of the blend i.e. above 30% SBS. Thus, *in situ* fibre formation originates from the elongated domains of SBS, which preferentially nucleate PP with b-axis orientation as explained above.

The injection moulded specimens were used for characterization of mechanical properties. Figure 4.11 shows the stress-strain behaviour of PP/ SBS blends containing 10, 20,30 and 40 wt.% SBS respectively. PP exhibits a yield strain of 13-14% and yield stress (i.e. the highest stress reached just before yielding) of 32 Mpa (see Fig.3.23). On addition of SBS the yielding process seems to undergo changes such that the percentage strain increases with increase of SBS concentration while its corresponding yield stress decreases. The value of percentage strain, stress and maximum load, Young's modulus, elongation at break, etc. related to tensile properties are given in Table 4.1. It can be concluded from these values that while elongation increases with increase of SBS content, the Young's modulus decreases. The PP/SBS blend containing 10% SBS shows strain at break of 215% compared to 13% for pure PP. Blends containing 20%, 30% and 40% SBS show strain at break of 268%, 226% and 419% respectively. These various findings can be explained on similar lines discussed earlier in section 3.3.3. The crystallinity of these blends decreases at high concentration of SBS (see Fig.4.3) which gives rise to lower tensile modulus at high SBS content. Pure PP has a tensile modulus of 1372 MPa while that for SBS is 17 MPa.[23] From these values, one can estimate the tensile modulus of PP/SBS blends of diifferent compositions using the simple rule of mixtures. Given two materials of elastic moduli E_1 and E_2, which may be arranged in parallel, or in series combination separately, the modulus of the blend can be given as:

$$E_c = \phi_1 E_1 + \phi_2 E_2 \qquad \text{for series} \qquad (4.2)$$

$$1/E_c = \phi_1/E_1 + \phi_2/E_2 \qquad \text{for parallel} \qquad (4.3)$$

where ϕ_1 and ϕ_2 are the volume fractions of the two materials.

An alternative model attributed to Takayanagi [24] proposed a combination of both series and parallel given by the relation

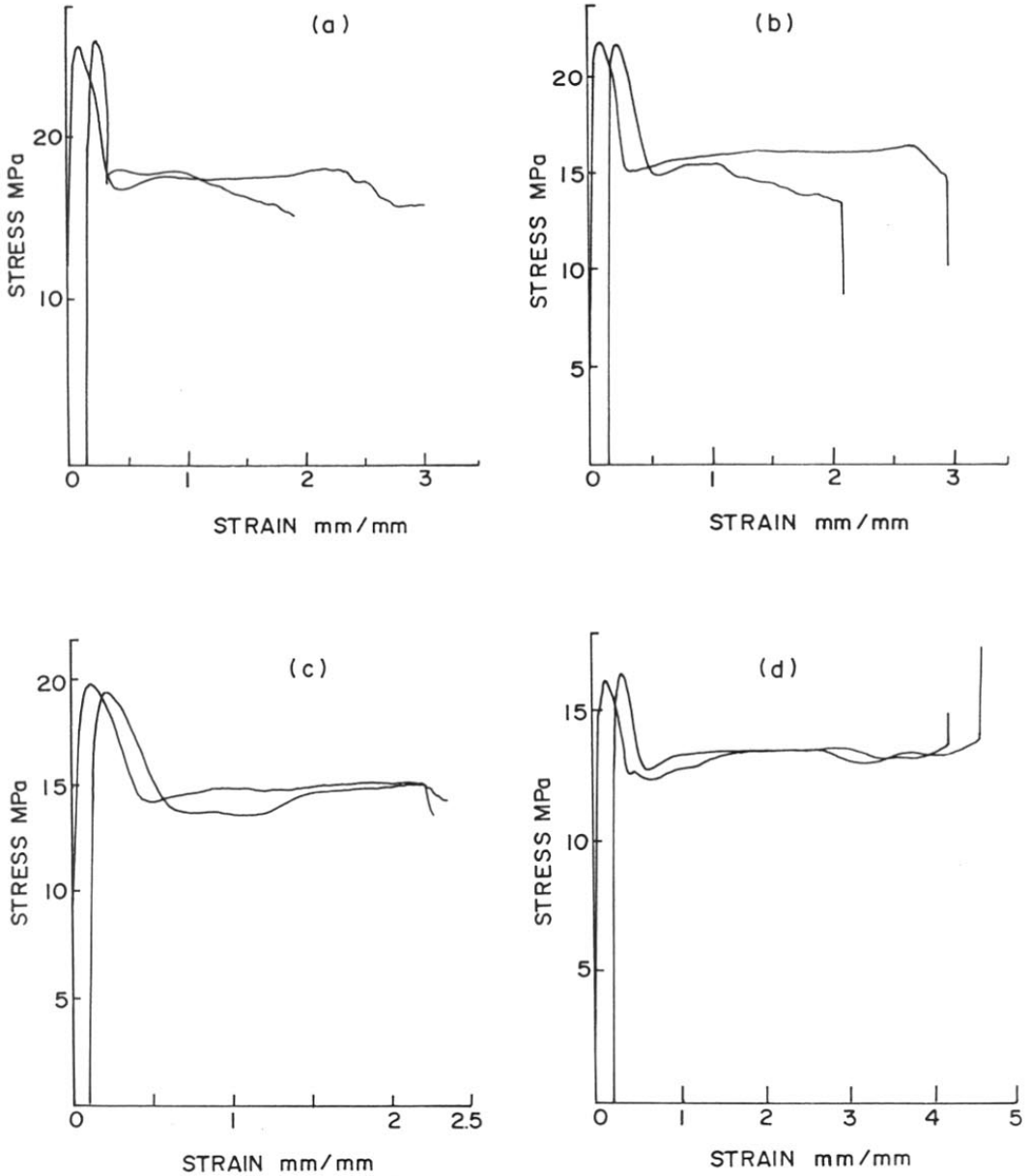

Figure 4.11 Stress vs strain behaviour of PP/SBS blends.
Concentration of SBS ranging from (a)10 (b)20 (c)30 and (d) 40 wt.%

$$E_{ca} = [(h / \phi_1 E_1 + \phi_2 E_2) + (1\text{-}h / E_2)]^{-1} \quad (4.4)$$

$$E_{cb} = [\phi_1 (h / E_1 + 1\text{-}h / E_2)^{-1} + \phi_2 E_2] \quad (4.5)$$

where h is the fraction of fibres parallel to the direction of measurement.

From the above equations, we assume that the SBS domains at any composition are arranged in both series and parallel mode in fractional amounts.

The tensile modulus calculated from equations 4.2 to 4.5 and those actually observed are shown in Fig. 4.12 for varying SBS concentration. According to Takayanagi model of series and parallel combination, the major fraction of SBS domains arranged in parallel was taken to be h = 0.85 and a minor fraction arranged in series as 0.15 with respect to specimen axis. It is interesting to note that the expected tensile modulus values for 30 and 40 wt.% SBS in PP are 780 Mpa and 670 MPa respectively according to parallel and series combination whereas the actual values are 907 MPa and 787 MPa corresponding to these compositions. If the morphology had remained just spherical (as observed at low concentration of SBS i.e 10 or 20%) at these concentrations of SBS, there would not have been any improvement in the tensile strength which in fact would have considerably reduced. Thus, *in situ* fibre formation gives higher tensile modulus due to high aspect ratio than that which would have been obtained from simple PP/ SBS blend having spherical domain morphology.

It is also interesting to note that these blends show a synergistic behaviour in terms of elongation as compared to pure PP (13) and pure SBS (880).[23] This enormous increase of elongation as seen in the blends (see Table 4.1) is due to good interfacial bonding or interaction between the SBS and PP because of partial miscibility as observed in the variation of T_g by addition of SBS in PP (see Fig. 4.8a). Due to this partial miscibility, incorporation of SBS in the amorphous region of PP occurs which gives rise to high elongations of 419% at (60/40) PP/SBS blend. Also, the other important factor causing an enormous increase of elongation is the *in situ* fibre formation occurring at 40% concentration of the blend. The *in situ* fibre formed tend to get oriented during the tensile testing thus resulting in higher elongation at break.

Figure 4.13 shows the variation of notched impact strength with SBS composition. The impact strength increases dramatically with increase in SBS concentration up to a maximum of

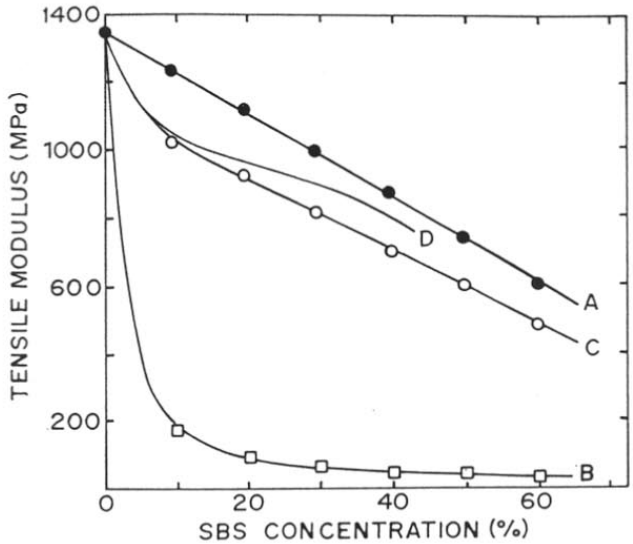

Figure 4.12 Variation of tensile modulus with respect to SBS composition:
Curve A: Expected modulus arranged in series
Curve B: Expected modulus arranged in parallel
Curve C: Combination of both series and parallel (Takayanagi model)
Curve D: Experimentally obtained values

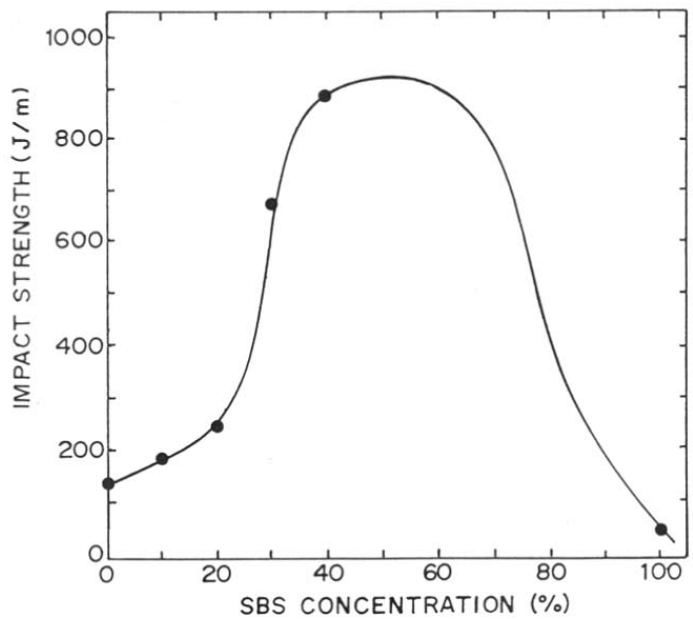

Figure 4.13 Variation of notched impact strength with respect to SBS composition

Table 4.1. Mechanical properties of PP/SBS blends

Properties	Pure PP	SBS concentration			
		10%	20%	30%	40%
Stress at auto break (MPa)	13.89	15.23	14.24	14.01	15.71
% strain at auto break (%)	13.20	215.50	268.10	226.50	419.30
Displacement at max. load (mm)	4.05	4.59	5.30	6.05	6.85
Load at Max. Load (KN)	1.25	0.98	0.86	0.76	0.67
Stress at Max. Load (MPa)	31.86	25.68	22.02	19.65	17.22
Strain at Max. Load (mm/mm)	0.08	0.09	0.10	0.12	0.13
% Strain at max. Load (%)	8.1	9.2	10.6	12.1	13.7
Displacement at auto break (mm)	8.2	107.5	134.0	113.2	10.6
Load at auto break (KN)	0.35	90.58	0.55	0.78	0.59
Modulus (Aut Young) (Mpa)	1372	1046	965.0	907.3	787.2
Izod Impact (notched) (J/m)	85	181	245	675	897

900J/m at 50%SBS and then drops with further increase of SBS concentration. The 0% SBS (pure PP) shows an impact strength of 85 J/m while 100% SBS shows that of 59.7 J/m. Another important observation was that the specimens having high concentration of SBS (> 30%) did not break completely suggesting that ductile fracture was occurring. This is evident from the SEM photographs of fracture morphology of the melt extruded samples (see Fig.4.10). This increase in impact behaviour as illustrated above, can be explained on the basis of various factors such as spherulite size, crystallinity, interfacial adhesion etc which affect the impact strength as has already been discussed in section 3.3.3. Although SBS domains nucleate spherulites which are much smaller in size than those in pure PP(see Fig.4.6) and also the crystallinity changes slightly due to the presence of SBS in PP, the interfacial bonding due to interaction between butadiene and PP matrix appears to be much more effective in improving the impact values.

The presence of stress points or defects in the specimen also affects the impact strength. As the notched specimens were used for measurements of impact strength, it may be noted that crack propagation rather than crack initiation will be the main deciding factor for impact strength. The dramatic improvement in the impact strength is due to SBS (rubbery phase) which acts as an effective absorber of impact force. It prevents the crack propagation without cavitation and thus, increases the impact strength. It should be noted that the dramatic improvement in the impact strength of the blend at high concentration of SBS i.e. 40% is almost 8 times that of pure PP which is much more than that expected for such blends. This could also be due to *in situ* fibre formation as discussed earlier in addition to nucleation of PP by SBS. Thus these various findings are in agreement with the crystallization behaviour and morphological features observed in these blends.

4.3.2 Structure Development and Properties of Hybrid Composites

From the studies on the structure development and properties of PP/SBS blends, it can be surmised that although there is a tremendous improvement of impact strength of these blends, on the whole the tensile modulus decreases in the presence of SBS. In order to improve the Young's modulus together with enhancement of impact strength or obtain a synergistic behaviour it was proposed to make a hybrid composite of glass fibres and PP/SBS blend as the presence of one may affect the interaction between two other components. The studies on the effect of glass fibres on structure development and the properties of these

composites were undertaken. The results of this exercise are described in this section. The interactions between the components taken individually have been studied first. The PP/SBS system has already been described in section 4.3.1. The PP-glass fibre system is described below.

Figure 4.14 shows the WAXD patterns for isothermally (T_c = 115°C) melt crystallized PP containing 5,10 and 15 wt.%glass fibre. It can be seen from this figure that the various reflections conform to the α crystalline form of PP having monoclinic structure. The peak positions remain same in all cases but their intensities change considerably with the increase in the concentration of glass fibres. The relative intensities of peaks at 2θ of 16.8° and 21.6° corresponding to reflections (040) and (041) increase while that for peaks at 2θ of 14.2° and 18.4° corresponding to reflections (110) and (130) decrease with increase in the concentration of glass fibres.

The various factors, which give rise to changes in relative intensities of the peaks in the WAXD scans have been discussed in section 4.3.1. of this chapter. It is mainly the preferential growth and/or orientation of crystallites with respect to sample surface which accounts for such changes. In the present case, the b-axis appears to be preferentially oriented perpendicular to the sample surface due to the nucleated growth of PP in presence of glass fibres. This is rather surprising since, our earlier discussions indicate that new nucleation of PP/change of phase.

Similar studies were carried out on hybrid composites of 10, 20 and 30% SBS in PP containing various concentrations of glass fibre with respect to the total blend. Fig.4.15 shows the typical WAXD scans for (70/30) PP/SBS blend with different glass concentrations ranging from 5 to 40 wt.%. It is evident from this figure too that there is no change in the crystalline phase of PP i.e. α crystalline configuration of PP is obtained. The presence of SBS and glass which are both amorphous in nature causes a reduction in the total crystallinity at high concentration of additive (i.e. 30% SBS). Also, it can be observed that the effect of glass on the orientation of crystallites is not as prominent as that noted for pure PP with glass. The relative intensities of the peaks decrease monotonically as against large changes observed for the latter case.

The percentage crystallinity (C_i) of PP containing only glass (0%, SBS), 10% SBS, 20% SBS and 30% SBS were determined from the XRD data. Figure 4.16 shows the variations of crystallinity with respect to glass fibre concentration for melt crystallized samples (curve represented by symbol B). It also shows a graph of crystallinity expected for

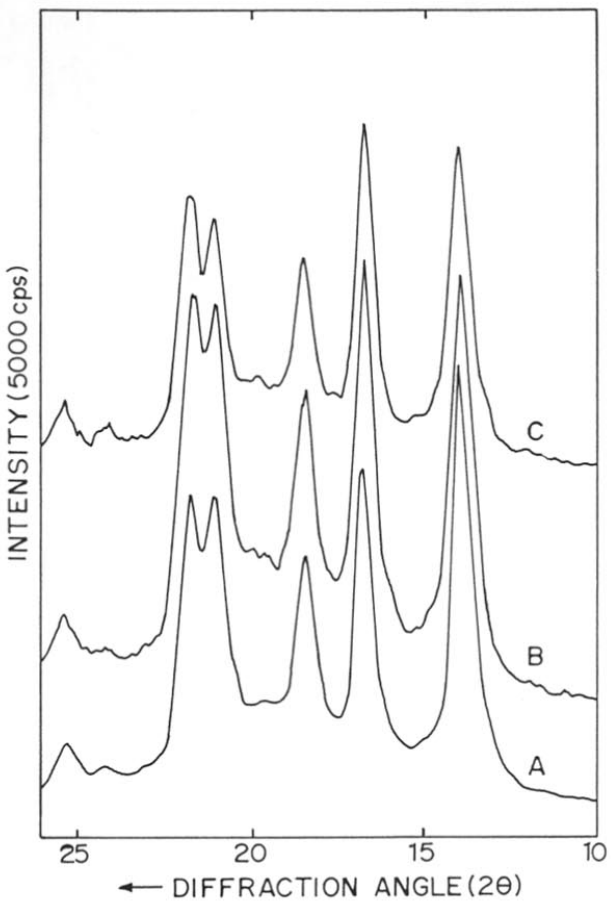

Figure 4.14 WAXD for PP filled with glass fibres isothermally melt crystallized at $T_c = 115°C$. Curves A, B and C correspond to glass concentrations of 5, 10 and 15 wt.% respectively.

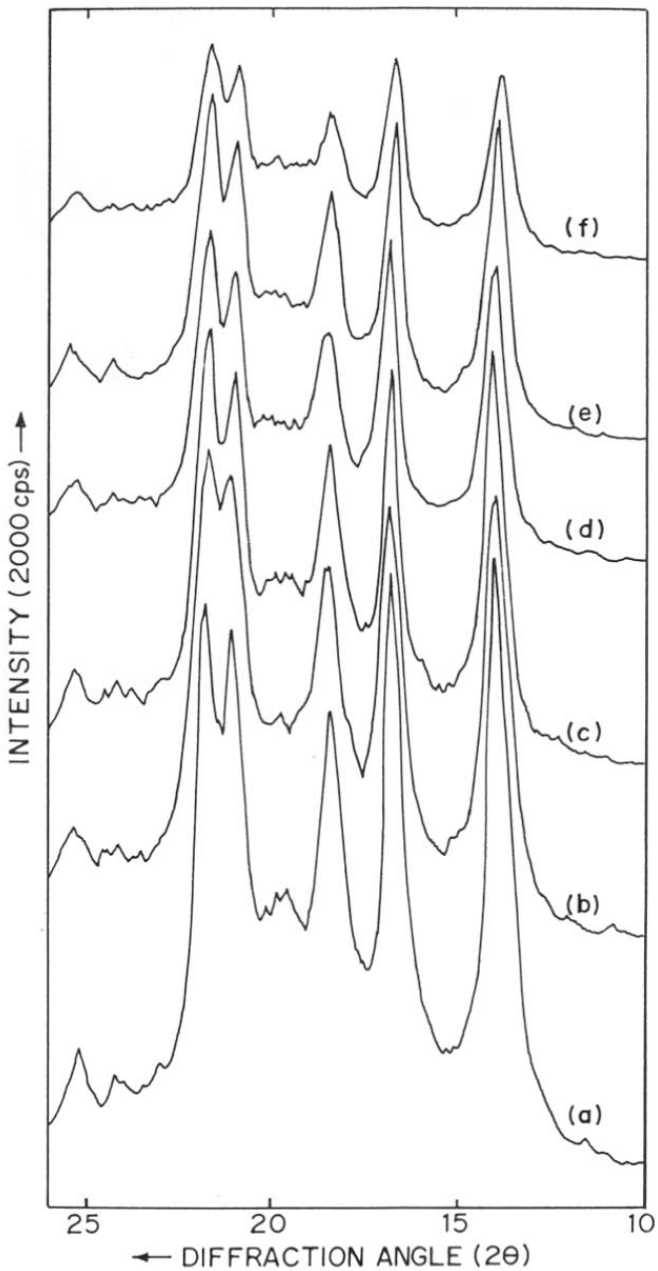

Figure 4.15 WAXD for (70/30) PP/SBS filled with glass fibres. Curves (a) to(f) correspond to glass fibre concentrations of 5, 10, 15, 20, 30 and 40 wt.% respectively

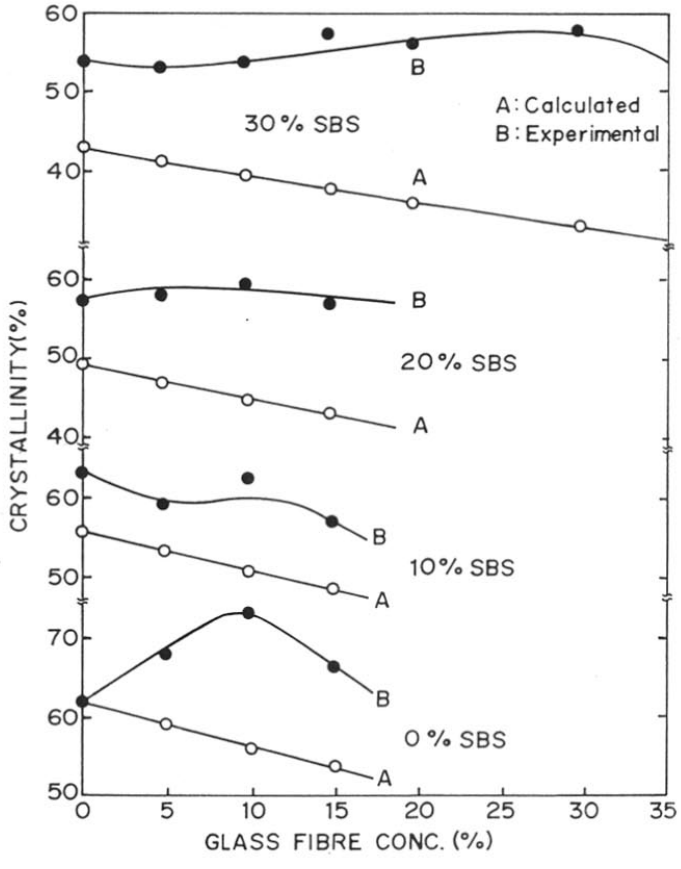

Figure 4.16 Percentage crystallinity (C_i) of PP/SBS/glass with respect to glass fibre concentration at T_c = 115°C.

homogeneous material containing different mass fractions of both SBS and glass (both amorphous)(curve represented by symbol A). It is interesting to note from the figure that the observed C_i values are much higher than the expected values for all compositions. In the case of 0% SBS i.e. PP containing only glass fibres, the C_i value increases with the increase in the glass fibre concentration as compared to pure PP (62%). It reaches a maximum at 10% glass concentration and then drops with further increase of glass concentration to 15%. On the other hand, in the case of (90/10) and (80/20) PP/SBS blend, the C_i values remain more or less constant irrespective of addition of glass fibre upto 15% . While in the case of (70/30) PP/SBS blend , it drops at 40% glass fibre concentration . These various observations suggest that at 0% SBS there is nucleation by glass fibres whereas at 10, 20 and 30% SBS in PP, the nucleating effect of glass is reduced due to the presence of SBS which prevents or does not allow complete nucleation of PP by glass fibres.

The crystallization behaviour was simultaneously monitored for these composites at isothermal crystallization temperature of 115°C by continuously recording images and measuring the transmitted light intensity. Figure 4.17 shows the plot of intensity recorded as a function of time in seconds for 0% SBS (curve A) and (90/10) PP/SBS blend containing glass (curve B) . The crystallization half time ($t_{1/2}$) and the crystallization rate were determined from these curves. The crystallization rate is higher and the induction period for nucleation lower for 0% SBS compared to PP/SBS blend containing glass.

Figure 4.18a shows the plot of $t_{1/2}$ as a function of glass fibre concentration. It is evident that $t_{1/2}$ value decreases considerably after incorporating glass fibres in PP. For low concentration of SBS (10%) the $t_{1/2}$ value decreases in presence of glass fibre as compared to PP/SBS without glass fibres while for higher SBS content (20% and 30%) the $t_{1/2}$ value remains low and more or less constant irrespective of the presence of glass fibres. Figure 4.18 b gives the plot of growth rate as a function of glass fibre concentration. In the figure a higher growth rate is observed for compositions containing glass fibres compared to those without glass fibre. Figure 4.19a and b shows the optical micrographs for 0% SBS i.e. PP containing 10%glass fibre and (80/20) PP/SBS blend containing 10%glass. In the case of 0% SBS (PP containing only glass) some spherulites can be seen to cluster around the glass fibre but no distinct transcrystalline morphology is observed. This has also been reported by Martuscelli et al. and other auhors[25,26] who concluded that the nucleation density increases in presence of glass fibres and the average dimensions of iPP spherulites become smaller but no

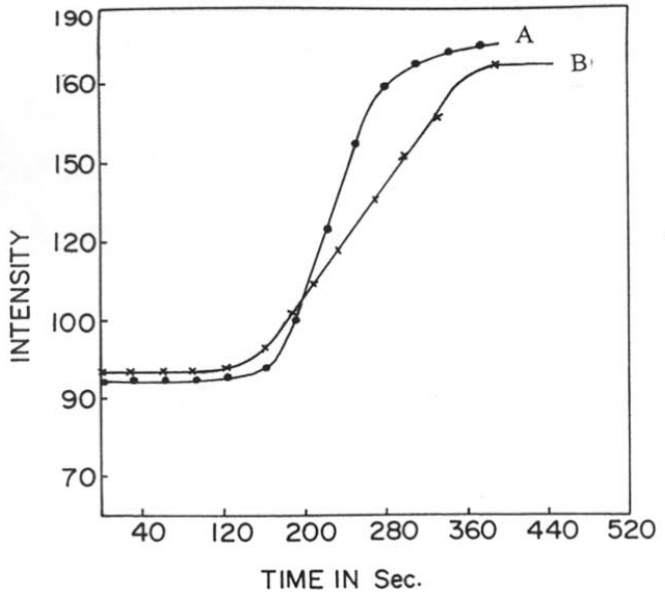

Figure 4.17 Graph of intensity as a function of time in seconds
(A) PP with 10% glass (B) (90/10) PP/SBS containing 10% glass

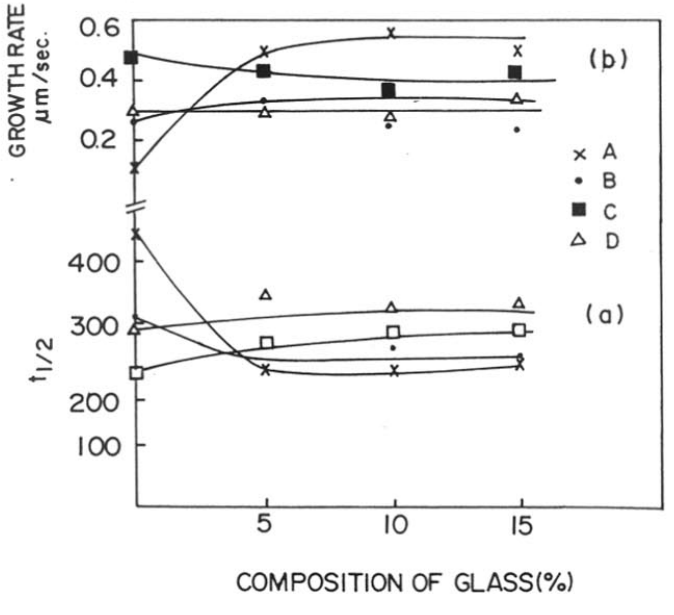

Figure 4.18 Crystallization half time (a) and growth rate (b) of PP/SBS with respect to glass fibre concentration. A= PP filled with glass (0% SBS), B= (90/10) PP/SBS , C= (80/20) PP/SBS , D= (70/30) PP SBS

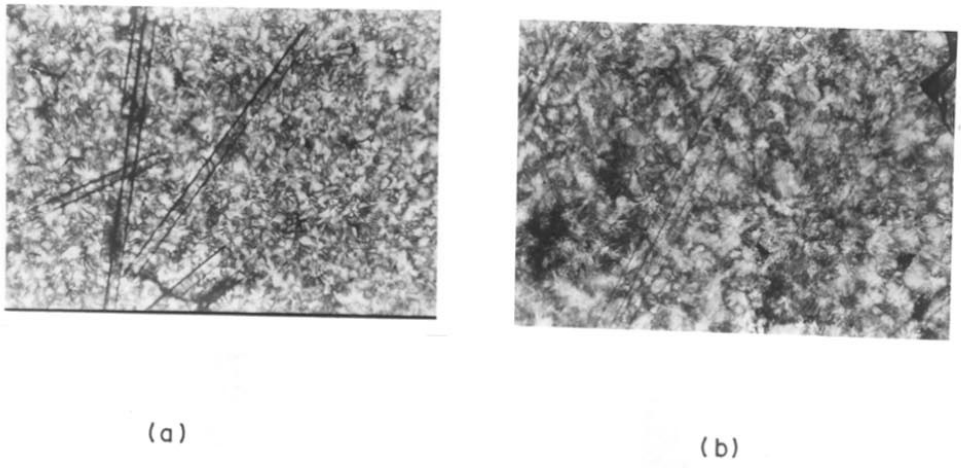

Figure 4.19 Optical micrographs of (a) PP with 10% glass (0%SBS)
(b) (80/20) PP/SBS containing 10% glass (450 x net magnification)

transcrystalline region between glass fibres and matrix interface was observed by them. On the other hand, the photomicrograph of PP/SBS containing glass in this study shows the presence of glass surrounded by SBS domains in the PP matrix.

These various findings clearly suggest that both SBS and glass could be nucleating PP crystallites. However, the relative nucleation efficiency of these two components decides what component will affect the crystallization behaviour. At low concentration of SBS, the glass fibres affect the crystallization rate and $t_{1/2}$ much more than that at high concentration of SBS. Further, the nucleating efficiency of glass fibre is seen to decrease at high concentration of SBS since the latter surrounds and adheres preferentially to glass fibre than the PP matrix thus creating an intermediate layer between PP and glass fibre. This reduces the nucleation effect of glass fibres but can lead to better bonding between glass fibre and surrounding matrix.

The injection moulded specimens of these composites were investigated for structure and morphology in different directions with respect to machine direction/melt flow.

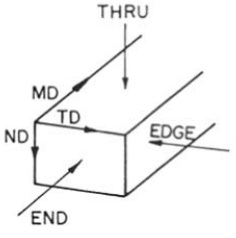

Figure 4.20 Shows the schematic diagram of specimen cut along the machine direction where MD = machine direction

TD = transverse direction

ND = normal direction

The studies on the structure of skin and core layers of injection moulded PP have already been reported by various authors.[27,28] The explanation for higher molecular orientation in the skin region than the core has been discussed in section 3.3.2. Figure 4.21 shows the WAXD scans of specimens along the machine direction of skin and core layers of injection moulded specimens of (a) 40%glass in PP (b) (60/40) PP/SBS blend and (C) (60/40) PP/SBS blend with 20% glass respectively. As explained earlier, the skin layer of pure PP shows a small β content and higher orientation of b-axis compared to the core region. This orientation

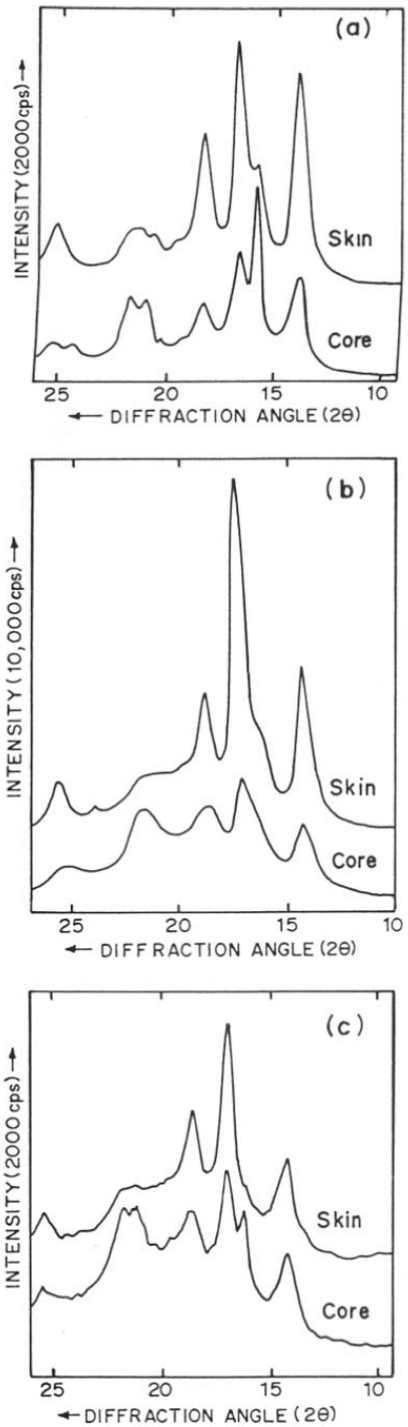

Figure 4.21 WAXD scans of skin and core layers of injection moulded specimens cut along machine direction (a) PP with 40% glass (b) (60/40) PP/SBS (c) (60/40) PP/SBS with 20% glass

of b -axis in the skin layer with some β phase could be due to a combination of high shear and elongational flow rates developed during melt flow as already explained in section 3.3.2.

On the other hand, the core layer of these specimens show interesting behaviour. In case of PP filled with 40% glass, a high intense peak is observed at 2θ of 16.1° which corresponds to the 300 reflection of β phase of PP. This β peak occurs even in (60/40) PP/SBS blend with 20% glass while in case of (60/40) PP/SBS blend without glass, no such β peak is observed. Thus, from the comparison of core layers of these composites, one can conclude that the enhancement of β phase in the core layer occurs only if there is a presence of a fibrous component (glass fibre as in our present case).

The effect of glass fibres on the structure development in the skin and core layers of PP/SBS injection moulded specimens were studied in detail. Figure 4.22 shows the WAXD of PP/SBS (70/30) blend containing 20,30 and 40% glass fibres represented by symbols a, b and c. Similarly (60/40) PP/SBS blend containing 20,30 and 40% glass fibres were studied. It was observed that at low SBS and glass fibre content the intensity of the (040) peak increases especially in the skin layer. Further , the overall crystallinity depends on the presence of glass fibres.

The crystallinity values (C_i) were determined from the WAXD scans for skin and core layers of these composites and these are shown in Fig. 4.23 as a function of concentration of glass fibre for different concentrations of SBS viz. 0 (a), 30 (b) and 40 wt.%(c) with respect to the PP matrix respectively. It may be noted that glass fibres are amorphous and do not contribute to overall crystallinity. The C_i value is seen to be more for the skin region than the core region for these samples especially for low fibre content. The overall crystallinity decreases with the increase in concentration of glass fibres. However, the decrease is more rapid when the concentration of SBS is higher. These findings can be explained on the basis of melt flow and shearing during injection molding process. The skin layer is subjected to much higher stress than the core region due to which molecular orientation is induced. Thus, the crystallization in the skin occurs under shear stress leading to higher C_i values than those at the core.

In order to explain the variation of C_i with respect to the glass fibre concentration, one has to look into different processes involved during crystallization of injection moulded samples. The mould surface cools faster than the core since the mould walls are water cooled. Also, the melt near the surface is subjected to shear stresses. The glass fibres have higher

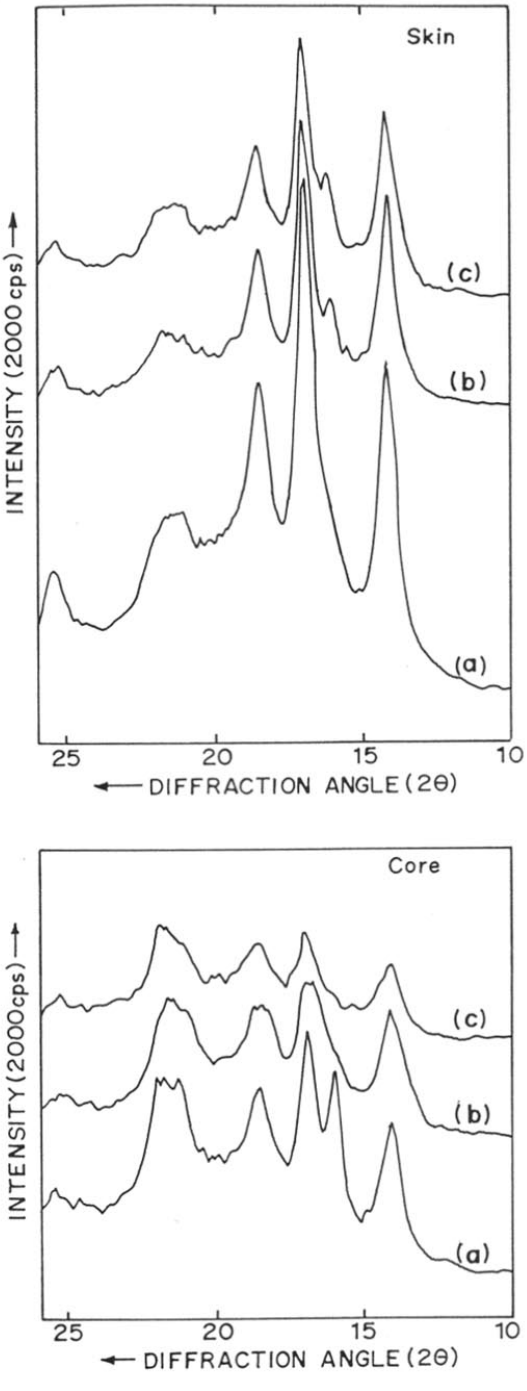

Figure 4.22 WAXD scans of skin and core layers of (70/30) PP/SBS containing glass fibres. Curves (a), (b) and (c) correspond to glass fibre concentration of 20, 30 and 40 wt.% respectively

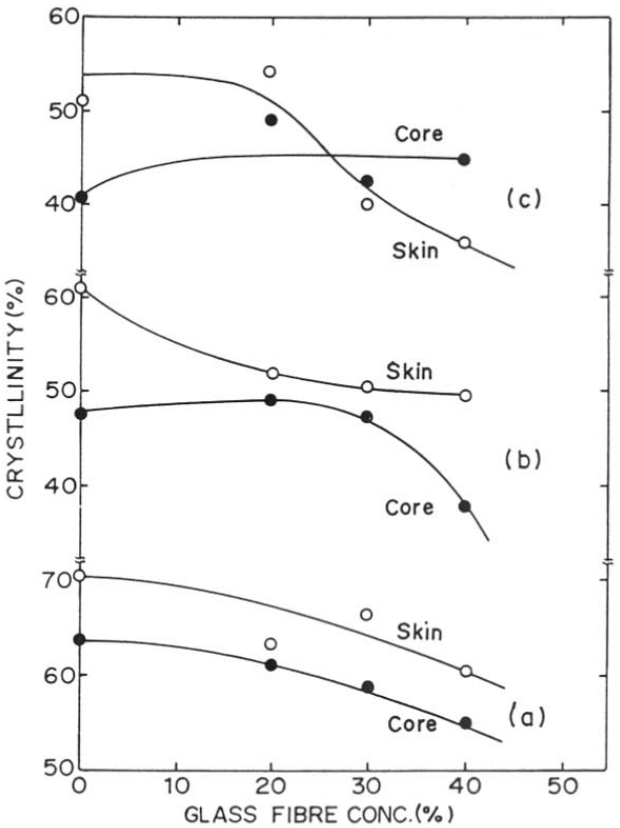

Figure 4.23 Percentage crystallinity for skin and core layers as a function of glass fibre concentration
(a) PP/glass (0% SBS) (b) (70/30) PP/SBS (c) (60/40) PP/SBS.

thermal conductivity than the polymers. Increase in the glass fibre content leads to better heat transfer and rapid cooling. It also disrupts the flow of the melt leading to more random orientation of crystallites. Hence, the overall C_i decreases with the increase of glass fibre content. This effect is more pronounced in composites having high glass fibre concentration (> 40%). Further, the presence of SBS prevents any nucleating effects (as discussed earlier) that may occur on the glass surface/ or tips of fibres. Hence there is rapid reduction of C_i value for PP composites containing high concentration of SBS as well as glass fibres.

The DSC studies (Fig. 4.24a & b) on these composites confirmed the above observation regarding the nucleation efficiency of glass fibres. Composites of pure PP and glass fibre gave rise to slightly higher crystallization temperature than pure PP. In presence of SBS, however, the T_c does not increase significantly thus clearly suggesting that nucleation of PP crystallites by the glass fibres was prevented by the SBS domains surrounding them.

Figure 4.25 shows the SEM micrograph of a fractured surface of injection moulded specimens . Figure 4.25a represents the micrograph of PP filled with 30% glass fibres and Fig. 4.25b of (70/30) PP/SBS with 20% glass fibres. On comparing these two micrographs it is interesting to note that PP filled with glass fibre show a brittle behaviour while that in the presence of SBS, a transition from brittle behaviour to ductile nature is observed. Figure 4.25c represents the micrograph of PP filled with 20% glass fibres while figure 4.25d that of (70/30) PP/SBS containing 20% glass fibres. On comparing these two figures, it is obvious that in the former case, there is a poor fibre matrix bonding and due to which the fracture surface exhibits fibre pull out in many regions. Darlington and Smith[29] have reported the SEM of glass fibre reinforced PP injection moulded disc where they observed the similar voids as in the present case. However, in the PP/SBS/glass (Fig. 4.25d) good adhesion and a better bonding between glass and the surrounding matrix is observed with the fracture surface being relatively smooth. This clearly shows that SBS adheres better to glass fibres than the PP matrix and thus forms a interlayer between the glass and the PP matrix. Figure 4.25e represents the micrograph of high concentration of SBS with high glass content i.e (70/30) PP/SBS with 40% glass fibres. It is very clear that there is large orientation of glass fibres present in these samples. This type of fibre orientation or alignment of injection moulded specimens has been studied earlier by Ramsteiner et al.[30] They also observed similar type of fibre orientation for fractured surfaces of glass fibre reinforced nylon 6. They have attributed this to the flow field in the melt extrusion/injection moulding process.

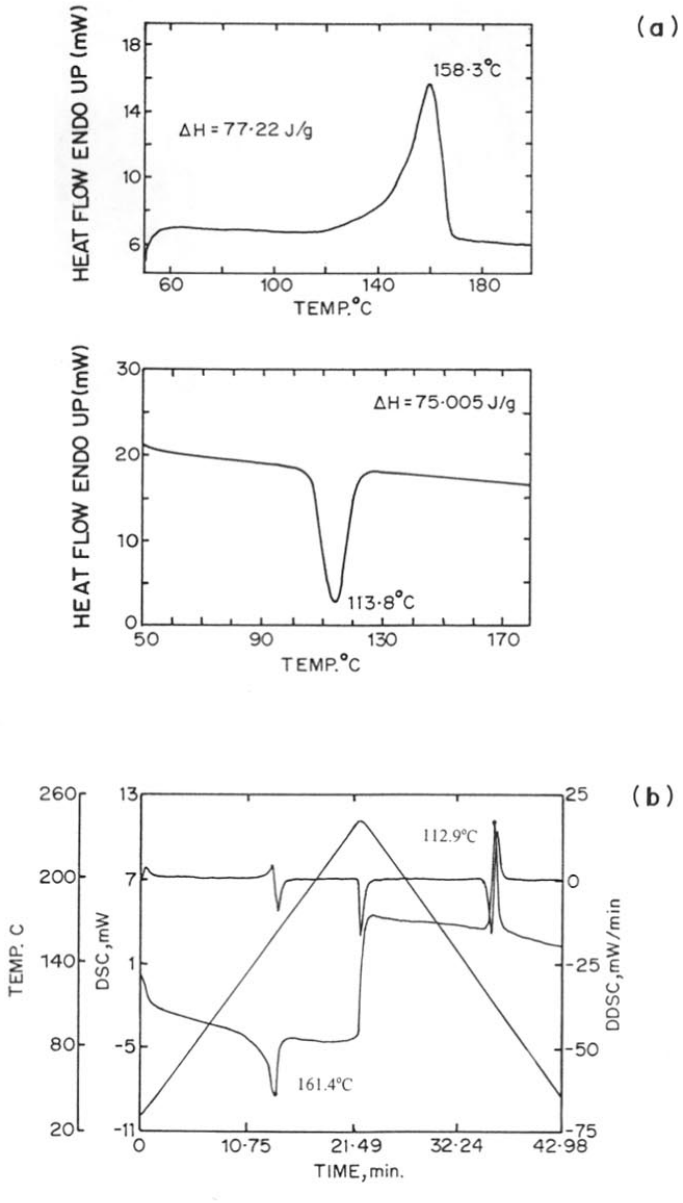

Figure 4.24 DSC curves for (a) PP with 15% glass fibres (b) (70/30) PP/SBS containing 15% glass

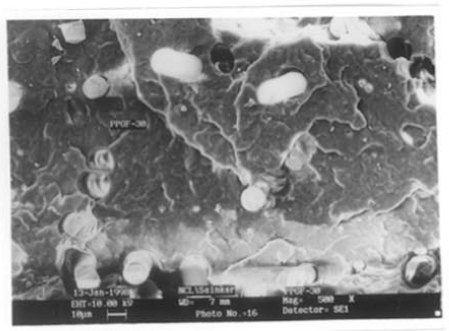

(a)

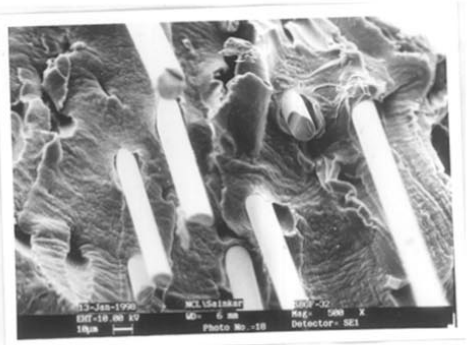

(b)

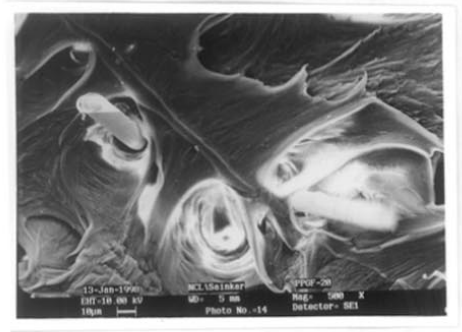

(c)

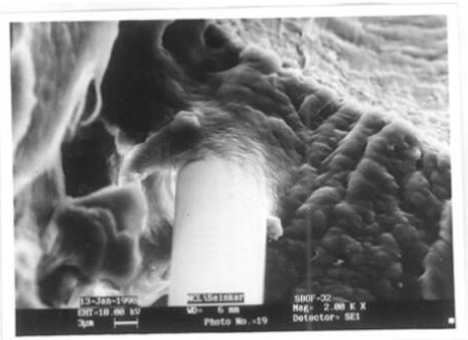

(d)

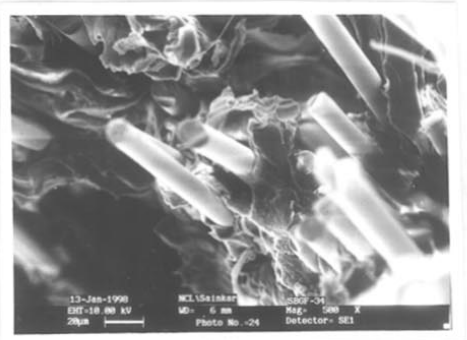

(e)

Figure 4.25 SEM micrographs of fractured surface of injection moulded specimens
(a) PP with 30% glass (b) (70/30) PP/SBS with 20% glass
(c) PP with 20% glass (d) (70/30) PP/SBS with 20% glass
(e) (70/30) PP/SBS with 40% glass fibres

The mechanical properties viz. impact strength and tensile modulus of these composites were measured in the same manner as described before and correlated with the structure and morphology of the composite.

Figure 4.26 shows the stress-strain curves for PP/glass and (60/40)PP/SBS blend containing glass fibre in the concentration ranging from 20 to 40 % respectively. The various properties such as tensile modulus, toughness, stress at break, elongation etc. derived from these curves are represented in Table 4.2. From the comparison of the curves and the different values in table, it can be seen that the PP/glass fibre composites exhibit a sharp break point whereas those containing both SBS and glass fibre show a definite yield point as well as high elongation before break.

Figure 4.27 represents the plot of tensile modulus and impact strength as a function of concentration of glass fibres. It can be seen that the tensile modulus of PP/ glass increases with increase in the addition of glass fibres. At 40 % glass, the tensile modulus shows improvement by a factor of 3.5 times as compared to pure PP. For PP with 30 and 40% SBS containing glass fibres also show corresponding increase in tensile modulus with increase in the addition of glass fibres but this increase is not as high as observed for PP/glass.

The impact strength of PP/glass remains unaffected irrespective of glass fibre concentration. For PP with 30 and 40% SBS containing glass the impact strength decreases with increase of glass fibre concentration but is remarkably high as compared PP/glass .

These various results obtained can be explained on the basis of structure and morphology developed which affects the impact and tensile modulus. In case of PP/glass without SBS, the increase in tensile modulus may be attributed to high crystallinity induced by the glass fibre (see figure 4.16) as well as its reinforcing effect. Higher the crystallinity, higher is the tensile modulus. This in turn implies the high nucleation efficiency of glass for PP spherulites. The other factor, which could have caused this improvement, is the orientation of glass fibres. It is well known that the tensile modulus is higher if the fibres are better aligned along the main axis as against the transverse direction of the tensile specimen. This has been depicted in Fig. 4.28 Which shows the optical micrograph of injection moulded PP-glass taken in the reflection mode. The fibres are mostly oriented along the long axis for PP/glass composites. This gives rise to the high tensile modulus. Lastly, the aspect ratio of the fibres also affects the tensile modulus of the composite. Higher aspect ratio of the fibres gives good reinforcing effect and hence higher tensile modulus. The tensile modulus of glass filled PP has

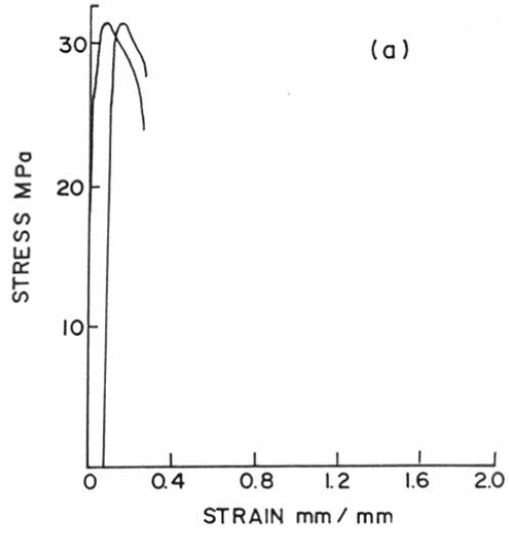

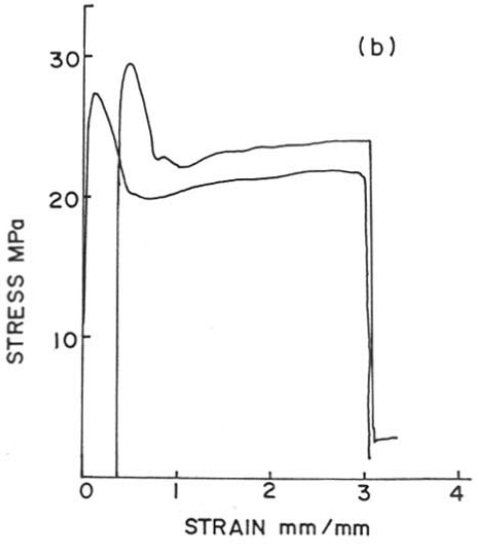

Figure 4.26 Stress vs strain curves for (a) PP with 20% glass (b) (70/30) PP/SBS containing 20% glass

Table 4.2. Mechanical properties of PP/SBS/glass hybrid composites

Composition	Displacement at max. load (mm)	% Strain at max load	Load at max load (KN)	Stress at max load (MPa)	% Strain at auto break (%)	Stress at auto break (MPa)	Modulus (Aut Young) (MPa)	Toughness (MPa)	Izod Impact (notched) (J/m)
Pure PP	4.04	8.10	1.25	31.8	13.2	13.89	1372	6.84	85.0
20% PG	3.59	7.18	1.19	31.2	18.1	26.31	2557	5.63	95.2
30% PG	2.93	5.87	1.29	33.5	11.1	30.06	3821	3.35	82.3
40% PG	1.92	3.89	1.29	33.7	4.3	33.06	4833	1.22	72.2
PSG 32	5.28	10.60	0.80	21.3	304.5	16.73	2317	45.72	279.3
PSG 33	4.27	8.54	0.75	19.8	231.4	13.44	3179	9.56	240.9
PSG 34	3.16	6.39	0.76	20.4	23.6	13.34	3834	4.50	192.5
PSG 42	6.49	13.04	0.74	19.3	423.9	17.36	2022	57.88	468.8
PSG 43	4.61	9.23	0.65	17.2	271.9	10.83	2799	40.97	357.3
PSG 44	3.12	6.26	0.56	15.1	72.9	9.75	3055	8.40	272.0

20% PG = PP with 20% glass
30% PG = PP with 30% glass
40% PG = PP with 40% glass

PSG 32 = (70/30) PP/SBS with 20% glass
PSG 33 = (70/30) PP/SBS with 30% glass
PSG 34 = (70/30) PP/SBS with 40% glass

PSG 42 = (60/40) PP/SBS with 20% glass
PSG 43 = (60/40) PP/SBS with 30% glass
PSG 44 = (60/40) PP/SBS with 40% glass

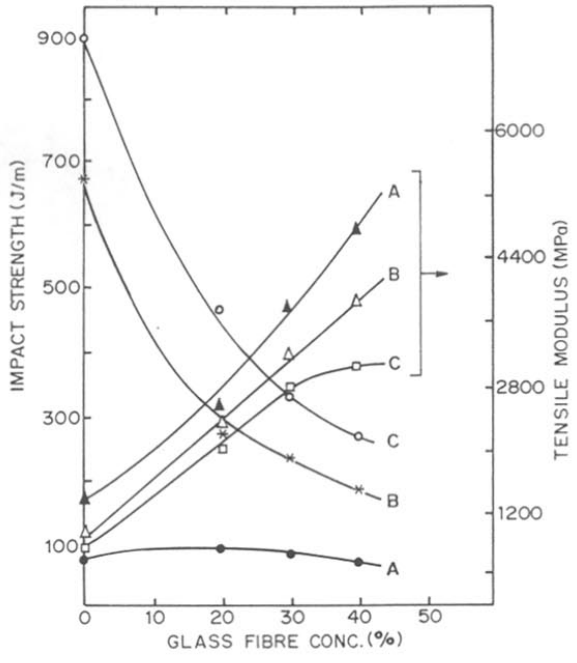

Figure 4.27 Plot of tensile modulus and impact strength as a function of glass fibre concentration. A = PP filled with glass, B = (70/30) PP/SBS containing glass, C = (60/40) PP/SBS containing glass

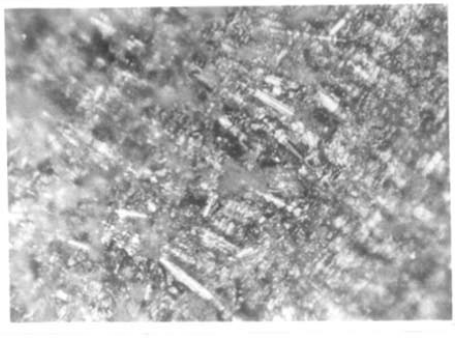

Figure 4.28 Optical micrograph of injection moulded PP filled with 10%glass fibres in the reflection mode (100x net magnification)

been studied by various authors.[31-34] It is interesting to note that the tensile modulus increased by a factor of 3.5 times for 30% glass fibres as compared to 1.5 times increase as reported earlier by other authors.[35] This clearly shows that the rise in tensile modulus as observed by us could be associated mainly with the structure development in the PP/glass as explained above. One must also remember that only certain type of glass fibres can give nucleation effects which depends on the surface modification, sizing, etc. used during their preparation.

For the PP/SBS blends with 30% and 40% SBS containing glass fibres, the tensile modulus showed a corresponding increase with the increase of glass fibre concentration. However, the tensile modulus obtained is considerably lower than the PP/glass system. The increase in modulus can again be associated, apart from reinforcing effect, with the crystallinity induced by glass fibres. The presence of rubbery matrix causes a decrease in modulus. However, at high concentration of SBS, the nucleation efficiency of glass fibres is seen to decrease as explained earlier. Hence, lower modulus is obtained in these as compared to PP/glass. A better bonding or good adhesion between the fibre and the surrounding matrix is seen in SEM micrograph (see Fig.4.25d) with enormous elongation seen where the glass is surrounded by SBS forming an intermediate layer between the fibre and the PPmatrix. Thus, one obtains higher toughness values in PP/glass fibre composites due the presence of SBS.

The impact strength for the PP/glass system almost remained unaffected or showed a tendency to decrease with an increase in the glass fibre concentration. This could be associated with high crystallinity induced by the glass fibres since the impact strength is lower at higher values of crystallinity . Secondly, the presence of stress points or defects in the specimen also affects the impact strength of these composites i.e. the bonding between intergranular fibres plays an important role. On the other hand, the number of stress points increase when the composite is loaded with high fibre concentration, the crack propagation became easy. These two factors result in an improvement in impact strength. Thirdly, the hammer in the Izod impact test strikes the specimen normal to the fibre length, which is along the specimen length. It should be noted that the strength perpendicular to the glass fibre is poor than that observed along the glass fibre. This also leads to lower impact values. On the other hand, in case of PP with 30 and 40% SBS containing glass the impact strength improved considerably as compared to the PP/glass system. This increase can be attributed to the presence of SBS surrounded by glass which acts as an effective absorber of impact force and also due to good adhesion existing between the SBS and glass (see Fig.4.25d), enhancement of impact strength

values are observed. Secondly, due to the presence of rubbery matrix the number of stress points or defects are reduced and thus causes a rise in impact strength. However, the impact strength decreased with the increase of glass fibre concentration which could be due to the brittle nature of glass which makes crack propagation easy by forming defects and hence leads to a decrease in impact strength values.

Figure 4.29 shows the graph of impact strength and percentage elongation at break as a function of glass fibres. It is interesting to note that in the case of PP/glass system, the percentage elongation at break decreases with increase in the concentration of glass fibres. Also, the elongation at break values are very low compared to PP/SBS containing glass. The considerably low elongation at break values for PP/glass is due to brittle nature of the glass and also due to high crystallinity induced by glass fibres. On the other hand PP with 30 and 40% SBS containing glass shows an initial increase of elongation at break at low concentration of glass fibres (20%) compared to (70/30) and (60/40) PP/SBS blends without glass and with further increase of glass fibre concentration the elongation at break values also decrease. Thus, enormous elongation is observed for PP/SBS blend at 20% glass concentration. This synergistic behaviour observed at a particular concentration of glass fibres (20 %) could be due to strong interaction between the SBS and glass as well as the spherulite size obtained in such composites (see Table 4.3).

Table 4.3 Gives the average spherulite size dimensions for PP/SBS blend and PP/SBS/glass hybrid composite

Composition	Crystallization condition	Average spherulite size in μm
Pure PP	115°C, T_c = 20 mins.	50-60
(80/20) PP/SBS	115°C, T_c = 20mins.	23-25
PP with 10% glass	115°C, T_c= 20 mins.	12-15
(80/20) PP/SBS with 10% glass	115°C, T_c= 20mins.	18-20

The Takayanagi model of series and parallel combination was used to study the effect of glass on PP/SBS blend. The modulus values were calculated according to simple rule of mixture by first calculating the modulus for series and parallel separately according to the relation as explained earlier. Then the total tensile modulus of combination of both series and parallel was calculated according to Takayanagi model as given earlier. Figure 4.30 shows the

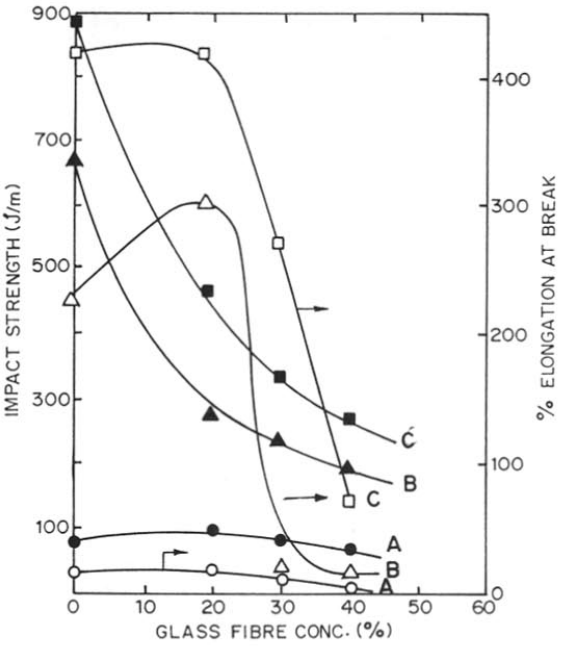

Figure 4.29 Plot of impact strength and percentage elongation at break as a function of glass fibre concentration. A= PP filled with glass fibre (0% SBS) , B = (70/30) PP/SBS containing glass, C= (60/40) PP/SBS containing glass

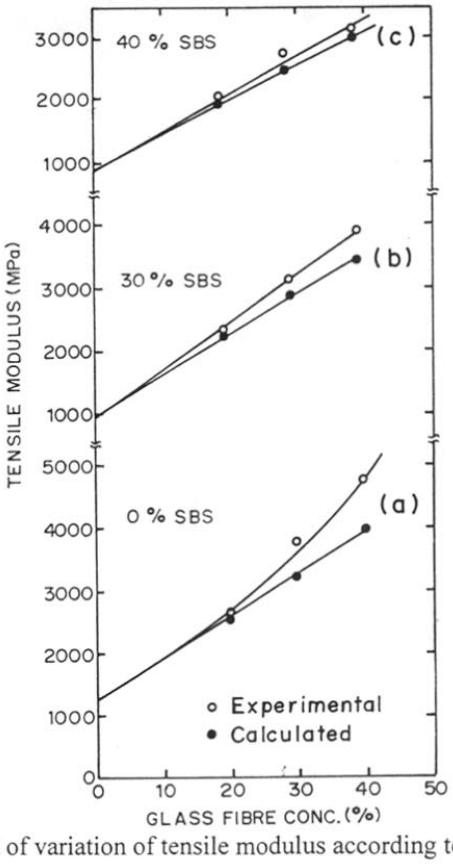

Figure 4.30 Plot of variation of tensile modulus according to Takayanagi model as a function of glass fibre concentration.
(a) PP/glass (0% SBS) (b) (70/30) PP/SBS containing glass
(c) (60/40) PP/SBS containing glass.

plot of tensile modulus as a function of glass fibre concentration for PP/ glass without SBS (0% SBS), (70/30) PP/SBS and (60/40) PP/SBS. The tensile modulus of PP and glass fibre were taken as 1372 and 72400 MPa[36] respectively. The fractional amount for PP/glass system for series and parallel was taken as 0.28 and 0.72 respectively. A large deviation is observed from the expected value as the glass fibre concentration increases. The expected modulus values were calculated in the same manner as explained above for the blends. For (70/30) and (60/40) PP/SBS blends,the observed modulus values were 907.3 MPa and 787.2 MPa respectively. The fractional amounts taken for (70/30) and (60/40) PP/SBS blends containing glass fibres for series were 0.28 and 0.24 and for parallel were 0.72 and 0.76 respectively. It is apparent from the figure that for both (70/30) and (60/40) blends with glass the presence of SBS gives less deviation from the expected values. On the basis of nucleation phenomena as already explained before, we can say that PP/glass composites which show high crystallinity values is due to strong nucleation efficiency of glass fibres on PP spherulites. Due to this high C_i values, large deviation from the expected value has been observed. On the other hand, at high concentrations of SBS (30 and 40%), the presence of SBS inhibits the nucleation efficiency of glass fibres on PP spherulites as seen earlier which shows a decrease in the C_i values and thus, shows less deviation from the expected values.

4.4 Conclusions

In this chapter we have illustrated that although PP and SBS are not miscible, good mutual interaction between PP and SBS especially between the butadiene groups of SBS and the amorphous phase of PP definitely causes significant changes in the crystallization behaviour of PP in these blends. The SBS domains change from spherical to fibrous morphology under stress and also induce nucleation in PP. The fibrous morphology results in enhanced mechanical properties. The glass fibres present, having high aspect ratio (16to 20) act as stronger nucleating agent for PP than SBS and also reinforce the composite. Synergistic effects are seen in the value of elongation/toughness of such composites. Thus,hybrid composites can be formed having higher tensile modulus (due to glass) but at the same time improved toughness properties (due to SBS). Thus, polymer mediated growth plays an important role in the type of structure that is developed leading to improvement in properties in such materials.

4.5 References

1. H.L. Morris, Hand book of Thermoplastic Elastomers, Van Nostrand Reinhold, New York (1979) Chapt. 2.
2. F. Coppola, R. Greco and E. Martuscelli and H.W. Kammer and C. Kummerlowe, Polymer, **28** (1984) 47.
3. D.R.Paul and S.Newman, Polumer Blends, Academic, New York, **2** (1978).
4. V. Choudhary, H.S. Varma, I.K. Varma, Indian Inst. Tech., New Delhi, Polymer, **32** (1991) 2354.
5. C. Markin and H.L. William , J. of Appl. Polm. Sci. **25** (1980) 2451.
6. E. Martuscelli, C. Silvestre and G. Abate, Polymer, **23** (1982) 229.
7. L. Bianchi, S. Cimmino, A. Forte, R. Greco, E. Martuscelli, F. Riva, C. Silvestre, J. of Mater. Sci., **20** (1985) 895.
8. Th. Laus, Angew.Makromol. Chem., **60/61** (1977) 87.
9. G.A.Bohn, G.R. Hamed and L.E. Yescelius, Ger. offen., **2** (1978) 697, 825.
10. A.K. Gupta and B.K. Ratnam, J. of Appl. Polym. Sci., **42** (1991) 297.
11. R.C.Thomon, Rubb. Chem. Tech., **50** (1977) 24.
12. N. Takashima ,Mitsubishi Petrochemical Co., Inv., Jap. Pat. 6254 (67) (1963).
13. Paper of firm Shell AG.
14. K. Van Henten, Rubber, Asbestos, Plastic, **26** (1973) 387.
15. M.J. Folkes and P.W. Reip, Polymer, **27** (1986) 377.
16. F.Ehtaiatkar, M.J.Folkes and S.C.Steadman , J.of Mater. Sci., **24** (1989) 2808.
17. S.C.Steadman , The *insitu* production of PE fibres from polymer blends, PhD Thesis, Brunel University.
18. J.A. Odell, D.T.Grubb and A.Keller, Polymer, **19** (1978) 617.
19. G.W.Calundann, M. Jaffe ,Proc. Robert A. Welsh Conferences on chemical Reasearch xxvi , Synthetic Polymers, 247 (1982).
20. D.S. Chiu, Z. Zhang, G.G. Siu, J. Reinf. Plast. Compos., **15(1)** (1996) 74.
21. Z. Zhang, D.S. Chiu, G.G. Siu, J. Reinf. Plast. Compos., **15(5)** (1996) 452.
22. Z. Bartczak, A. Galeski and N.P. Krasnikova, Polymer, **28** (1987) 1627.
23. A.K.Bhowmick , H.L. Stephens, Handbook of Elastomers, Marcel Dekker, Inc. (1988) 318.

24. M.J. Folkes and P.S. Hope, Polymer Blends and Alloys,Chapman and Hall, London (1993) Chapt. 6.

25. E. Devaux and B.Chabert, Polymer Communications, **31** (1990) 391.

26. M. Avella, E. Martuscelli, C.Sellitti, J. Mater. Sci., **22** (1987) 3185.

27. J.P. Trotignon and J. Verdu, J. of Appl. Polym. Sci., **34** (1987) 1.

28. M. Fujiyama, T. Wakino and Y. Kawasaki, J. of Appl. Polym. Sci., **35** (1988) 29.

29. M.W. Darlington and G.R. Smith, Polymer, **16** (1975) 459.

30. Ramsteiner and R. Theysohn, Polymer Composites, **111-119** (1979)

31. W.B. Titow and B.J. Lanham, Reinforced Thermoplastics, Applied Publishers Ltd., London, Chapt. 2 (1975) p.18.

32. M.J.Folkes, Short Fibre Reinforced Thermoplastics, Wiley. Letchworth. England (1982).

33. A.Whelan and J.L.Craft, Developments in Plastic Tech., **2** Chapt.4 (1985) p.211.

34. H.F.Mark, N.M.Bikales, C.G.Overberger , Encyclopedia of Polm. Sci.& Engg., **13**(1985) 487.

35. E.Moore , Polypropylene Handbook, Hanser Publishers, New York (1996).

36. A.Whelan and J.L.Craft, Dvelopments in Plastic Tech., **3**, Elsevier Appl. Sci. Publishers Ltd. (1986) p.14.

Chapter 5

Structure Development at PP/PET Interface and Modification of Properties in PET Fibre Filled PP Composites

5.1 Introduction

Fibres have been used extensively to improve the strength and rigidity of polymers. Numerous studies have been reported concerning the reinforcement of PP and other thermoplastic polymers using different fibres in order to achieve improvement in the tensile modulus.[1-3] Amongst the various fibres that have been used, the studies on reinforcement using glass fibres are most common.[4,5]

In addition to the improvement in the modulus, the fibres induce transcrystalline morphology in polymers as has been recently reported to occur in PP crystallized in contact with carbon fibres and aramid fibres[6,7] and some polymeric fibres.[8-12] Transcrystallinity has also been observed in many other semi-crystalline polymers including PPS[13], PEK[13], Ny 6,[14] Ny 66[3], PET[15,16] and PEEK.[17]

Hobbs was the first to observe row nucleation at the fibre surface during the crystallization of iPP against type I (high modulus) and type II (high strength) carbon fibres.[18] A marked difference in the nucleating ability between the two fibre types was observed. The type II fibres were highly disoriented and proved to be poor nucleants as the spherulites nucleated in the bulk polymer with the same density as on the fibre surface. By contrast, the type I fibres showed a strong tendency to nucleate spherulites in the PP matrix that was evenly distributed along the fibre. This difference in the microstructure observed was associated with the epitaxial growth of the PP on the exposed graphite planes. Studies have also been carried out with PEEK, PEKK and PPS and fibres such as PAN based Au-4 (untreated AS-4) carbon, pitch based carbon, poly(p-phenylene terephthalamide) (PPDT) aramid and E-glass.[19] The PPDT aramid and pitch based carbon fibres were found to induce a transcrystalline interface in all the three polymers because of an epitaxial effect. Under certain conditions, transcrystallization was also observed in PAN based carbon and E-glass fibres which was partially attributed to the thermal conductivity mismatch between the fibre and the matrix. Transcrystalline morphology has also been seen at the interface of iPP-nylon 6 in a melt blend of iPP-nylon 6.[20]

Thomason and Van Rooyen[21] studied the dependence of transcrystallinity upon the crystallization temperature. With increase of crystallization temperature, the surface morphology changed from transcrystalline to spherulitic morphology. Both aramid and high modulus carbon fibres induced transcrystallization in PP at T_c below 138°C. However, above 138°C no tanscrystallization was observed in quiesently crystallized PP. The investigation of

transcrystallization of PP around different aramid fibres i.e. Kevlar 49 (Du Pont) and Twason D1056 (Inka) aramid fibre revealed higher nucleation density at the fibre surface at the crystallization temperature of 130°C than at 135°C. The absence of transcrystallinity at higher temperature was attributed to the reduced density of nucleation sites due to lower supercooling on the substrate surface. For iPP the convenient range of crystallization temperature for generating transcrystallinity has been reported to be between 120 and 130°C. Martuscelli et al.[22,23] showed that during the isothermal crystallization of iPP, the presence of glass fibres increased the overall nucleation density of spherulites without any transcrystallinity. This was also observed by us in the previous chapter. In case of iPP/kevlar fibre composite[24,25] the nucleation efficiency of fibre was even higher. The transcrystalline region was found to occur at isothermal crystallization temperature range from 121° to 135°C. The radial growth rate of spherulites was found to be the same for spherulites nucleated on the fibre surface and in the bulk. The authors also analysed the isothermal crystallization kinetics using the Avrami equation.[26] The values of exponent n for plain iPP was around 2 while for PP reinforced with carbon or Kevlar fibres were around 3. The reinforced iPP samples showed values of $t_{1/2}$ five times lower than the plain iPP. Such a finding suggested that a heterogeneously nucleated three-dimensional growth of crystals was induced by the presence of fibres. Even in the case of crystallization of iPP/carbon fibre[27] similar behaviour was observed i.e. the nucleation density was very much greater along the fibre surface than in the bulk at T_c of 135°C. The transcrystalline region extended approximately to a distance of 130 μm from the fibre surface. For other polymer resins such as nylon 66, enhanced rate of crystallization was observed in presence of aramid and carbon fibres.[28] In case of iPP-nylon 6[20] heterogeneous nucleation of one phase over the other and formation of co- crystallite was studied by DSC.

M.J. Folkes et al.[29]explored the development of transcrystallinity at the PP/glass interface and showed its dependence on the MFI and hence molecular weight of polypropylene. The frequency of nucleation along the fibre was found to be high for the low molecular weight PP, with the lateral extent of layer being of the order of 10 fibre diameter or 150μm. With increasing molecular weight of PP, the layer of transcrystallinity became less uniform with some parts of the fibre incapable of nucleating the polymer.

Chatterjee et al.[9] studied the effect of role of the structure of fibre in the generation of transcrystalline morphology in different polymers. Fibres of PET, Penton, Ny 6, Ny 66, Ny 610 in iPP were studied. The crystallographic unit cell at the fibre surface was found to be

different from that of the crystallizing polymer. In the case of iPP/cellulose[8] the crystalline form of cellulose depended on geometric properties of the surface such as roughness or fibrillation which inturn controlled the transcrystallization adjacent to the fibre. Thus, it can be seen that all the substrates, which have been reported to induce transcrystallinity, are crystalline. On the other hand, there exist crystalline substrates that are either moderately active or completely inactive as nucleants. This implies that crystallinity is a necessary but not a sufficient condition for a substrate to be a strong nucleating agent in the amorphous to crystalline phase transformation under study.

Thomason et al.[30] studied the effect of sizing on the growth of the transcrystallzation region. They found that the sized version (Apo1104ms) of HM carbon fibres nucleated the PP, but very few nucleation sites were observed whereas, the unsized fibre nucleated a high density of transcrystallization. They attributed the fewer nucleation sites for the sized fibre to the coating, which when mixed with PP near the fibre surface changes its crystallization behaviour. In the case of high strength carbon and glass fibres, no transcrystallinity was observed in the absence of sizing while the silane coated glass fibres showed transcrystallization to some extent in PP.[31]

Misra et al.[32] reported the influence of mechanical stress during the melt on the development of transcrystallinity. They found that PP/glass fibre composite showed pronounced transcrystallinity when the fibres were pulled through the matrix immediately after the specimen was transferred from one hot stage of 220°C to another maintained at 136°C.

Studies of the influence of the transcrystalline interface on the mechanical properties of some fibre reinforced polymer systems were also investigated. Barlow et al.[17,33,34]showed that carbon fibre reinforced PEEK gave higher interfacial bond strength and high transverse tensile strength when transcrystallinity is formed. Kantz and Corneliussen[35] showed that reinforcement by PA 6,6 and PET fibres increased the yield strength and elongation at break of the PP. Campbell and Qayyum[7] reported a similar result for the same fibre-matrix combination. They also found the elongation to break of the PP increased with volume fraction of the fibres. They attributed their findings to two factors. Firstly, increased ductility of the matrix as a result of a decrease in spherulite size and secondly, the transcrystalline morphology at the fibre surface restrained local necking and distributed strain more uniformly over the fibres.

Our survey of literature indicated the following shortcomings in the earlier data:

(a) The various authors have not investigated in detail the crystallization behaviour and kinetics of transcrystalline phase.

(b) The correlation of growth and morphology on the mechanical properties of the fibre - matrix composites was not studied in depth.

(c) The fibres, which were investigated, were quite expensive and were not easily processable.

Hence, in the present studies, we decided to work on PET fibre filled PP based composites. We selected PET fibre for our studies because it offers the following advantages over other fibres.

(a) It is a cheap material

(b) Its density is low as compared to glass and has a high modulus of 2758 Mpa.[36] Therefore lighter composites with high moduli can be obtained.

(c) The fibre can be made as thin as possible.

(d) Fibrous morphology of PET will show reinforcement effect due to high aspect ratio.

(e) PET fibres create a region of transcrystalline morphology in PP, which enhances mechanical properties.

(f) It can be easily processed.

In this chapter, we have investigated the structure development at PP/PET interface by studying the crystallization behaviour, transcrystalline morphology, and kinetics of crystallization. We have also carried out studies on the effect of compatibilizers i.e. maleic anhydride on the PP/PET composite system.

5.2 Experimental

(a) Preparation of composite

Polypropylene powder (Isotactic PP, Koylene SM030, IPCL, Baroda, MFI 8-10) was prepared in the same manner as described in section 2.2 for the crystallization studies. Polyethylene terephthalate fibres (PET fibres,Garware POY, Strength 120 g/denier, 15 μm diameter) chopped to 4 to 5 mm length were added to PP powder in the desired proportions ranging from 2 to 16.6 wt.% and mixed thoroughly in an agate mortar. A small quantity of each composition was melted on a glass slide at 200°C and kept for 1 to 2 minutes to allow wetting of the fibres. Since the melting point of PET is higher than 200°C the fibres remain in tact.

The isothermal crystallization behaviour was studied at crystallization temperatures of 100°C, 105°C, 110°C and 115°C respectively. The details of preparation of the melt crystallized samples have already been discussed in section 2.5. The spherulitic growth rate was monitored with respect to time at a constant crystallization temperature by continuously recording images using a video camera attached to a microscope. These were subsequently analysed in the selected area close to the PP/fibre interface for changes in the intensity (or grey scale) using an image analyser sytem. In order to investigate the structure by WAXD, the powder containing different concentration of PET fibre ranging from 2 to 16.6 wt.% were first pelletised in a single ended compaction die. These pellets were then melted and isothermally crystallized in the hot stage of the optical polarising microscope (as described in section 2.6) for 20 minutes and then quenched in methanol. The samples were scanned for structure development using an X-ray Philips defractometer.

In another set of experiments, the polypropylene was mixed with a compatibilizer i.e. maleic anhydride (MA) in different concentrations of 5, 10 and 15wt.%. The samples were heated to the melting point of PP so as to obtain MA grafted PP. In some cases, the PET fibres were added in desired quantity to the samples during the process. The crystallization behaviour of all these samples were studied in the same manner as described earlier. Some of the PP/PET composites (with and without MA) were extruded at a mild extrusion rate of 2g/minute from a melt indexer at a temperature of 190°C. A thin section of these samples were observed under SEM in order to determine the morphological changes in the melt processing. The complete details of the characterisation techniques by XRD, DSC, SEM and optical microscopy have already been described in section 2.9.

(b) Measurement of properties

Mechanical properties such as impact strength and tensile modulus were investigated for these composites which were melt compounded and injection moulded in the manner described in section 2.5. The commercially available polypropylene pellets were mixed with PET fibres chopped to 3 cm length in the desired proportions and compounded using single screw extruder. Another set was made where the maleic anhydride was first added to PP at 10% concentration and then PET fibres were mixed and compounded as described before. The temperature conditions set were same as described in section 2.5. The screw speed was maintained at 14-16 rpm for PP/PET and 20 rpm for PP/PET containing MA. These samples were pelletized, dried and injection moulded in the same manner as described before. The

notched impact and tensile properties were estimated for these moulded specimens and correlated with the structure and morphology of the composite.

5.3 Results and Discussion

5.3.1 Structure Development in PP/PET Composite

Figure5.1 shows the wide angle X-ray diffraction for PP containing different concentrations of PET fibres. The crystallization behaviour was studied at crystallization temperatures of 100°C, 105°C, 110°C and 115°C but, here we have shown only the results at 110°Cand 115°C. In these figures, curves A, B, C, D and E correspond to PET concentrations of 2, 4, 7 and 11wt% respectively. These XRD scans reveal identical reflections corresponding to monoclinic α crystalline phase of PP (as noted in earlier chapter) at all concentrations of PET. However, the intensities of the peaks change considerably depending on the concentration of PET fibres. In case of pure unoriented PP having α phase, the intensity of (110) reflection at 2θ of 14.2° (peak 1) is usually the highest. On the other hand, with increase in concentration of PET fibres, the intensity of (040) reflection occurring at 2θ of 16.7° (peak 2) becomes higher than the rest. The peak at 2θ of 21.7° corresponding to (041) reflection (peak 4) is also affected by the presence of PET fibres.

The variations of intensities of 2nd and 4th peak in relation to peak 1 as a function of the concentration of PET fibres are shown in Fig.5.2. Curves A, B, C and D correspond to samples crystallized at T_c of 100°C, 105°C, 110°C and 115°C respectively. It is clear from this figure that the intensity of (040) reflection (peak 2) increases appreciably with the increase of PET concentration and shows a maximum intensity at about 7% of PET. The intensity of (041) reflection (peak 4) also shows similar behaviour. Since the intensity of (040) and (041) reflections are mainly affected by the presence of PET, it can be concluded that the growth of crystallites along the b-axis is considerably affected by the presence of PET.

Figure 5.3 shows the optical micrographs of PP samples containing 10wt.% PET fibres at various stages of T_c = 115°C. It is evident from these micrographs that extensive nucleation is observed first at the fibre surface, giving rise to columnar growth or transcrystalline phase of PP at the PET fibre surface. The normal PP spherulites are seen to appear at a region away from the interface much later than the nucleation period of the transcrystalline phase.

The kinetics of crystallization in the transcrystalline zone was monitored by the spot intensity measurements (at the selected area on the images recorded by video camera attached

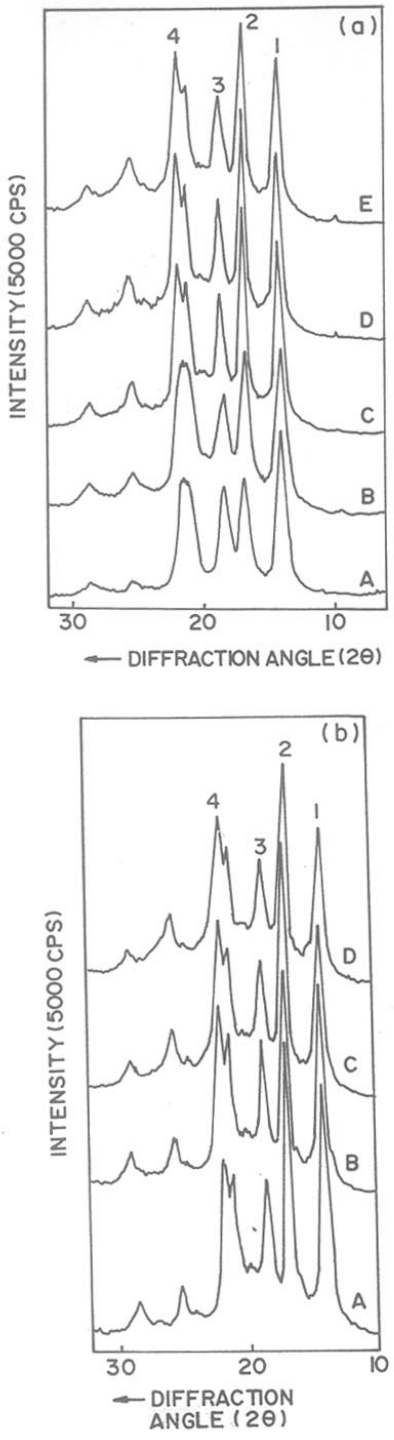

Figure 5.1 WAXD scans for PP/PET isothermally melt crystallized at (a) T_c= 110°C and (b) T_c=115°C. Curves A, B, C and D correspond to PET concentration of 2,4,7 and 11wt.% respectively

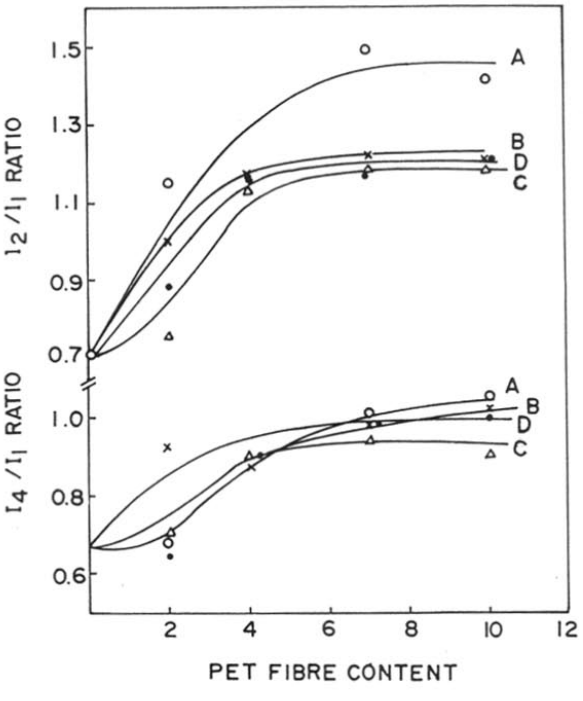

Figure 5.2 Plot of variation of intensities of 2nd and 4th peak in relation to the peak 1 as a function of PET fibre content. Curves A, B, C and D correspond to samples crystallized at T_c of 115°, 110°, 105° and 100°C respectively.

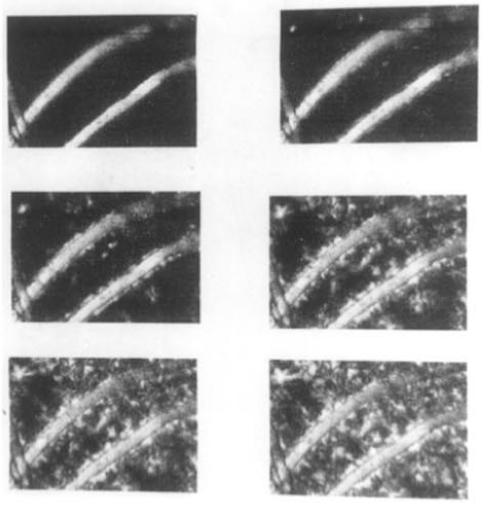

Figure 5.3 Optical micrograph of PP containing 10wt.% PET fibre at various stages of crystallization at T_c= 115°C (net magn. 1000x)

to the microscope). Figure 5.4 shows the crystallization of PP by a plot of intensity as a function of time at T_c =115°C. The curves A, B, C, and D correspond to crystallization of PP near the fibre interface with PET concentration of 2, 4, 7, and 11 wt.% respectively while the curve E correspond to crystallization of PP away from the fibre (in the normal bulk). From the comparison of the curves, it is evident that the crystallization process at the fibre interface or transcrystalline zone is much faster than that in the bulk. The induction period is much smaller than that in the bulk (curve E). The crystallization half time $t_{1/2}$ and crystallization rate were determined from these curves for the various crystallization temperatures of 105°C, 110° C and 115°C which are shown in Figure 5.5a and b. There is a remarkable decrease in the $t_{1/2}$ values as compared to pure PP which is clearly observed at T_c = 115°C. The $t_{1/2}$ value initially decreases and then attains a limiting value of 160 seconds, 100 seconds and 40 seconds for T_c of 115°C 110°Cand 105°C respectively with increase in fibre concentration upto 16.6 wt.%. The growth rate is also quite high for the crystals growing near the PP/PET interface as compared to PP crystals growing at places away from the interface (see Fig. 5b). The growth rate increases with increase of PET concentration upto 7 to 10 wt.% and then attains a limiting value above this concentration.

These findings clearly suggest that the PET fibre initiates heterogeneous nucleation in the PP matrix giving rise to first transcrystalline morphology at the fibre interface followed by subsequent growth of crystallization in bulk.

Figure 5.6 shows the variation of crystallinity as a function of PET fibre content determined from the XRD scans. It can be seen that the crystallinity is much higher in presence of PET fibres, which increases from 62% in virgin unoriented PP to 75% in PP/PET. This enhancement of crystallinity value clearly suggests preferential nucleation of PP on the surface of PET fibres giving rise to transcrystalline morphology. Thus, from the crystallization half time, growth rate and also crystallinity and intensities of certain reflections in XRD it can be concluded that there is a considerable interaction between the PET fibre and the PP matrix.

The crystallization kinetics for both for normal PP spherulites as well as those in the transcrystalline phase were analysed according to the Avrami equation.[26]

$$\log (I_m - I_t / I_m - I_o) = A_v t^n T \qquad (5.1)$$

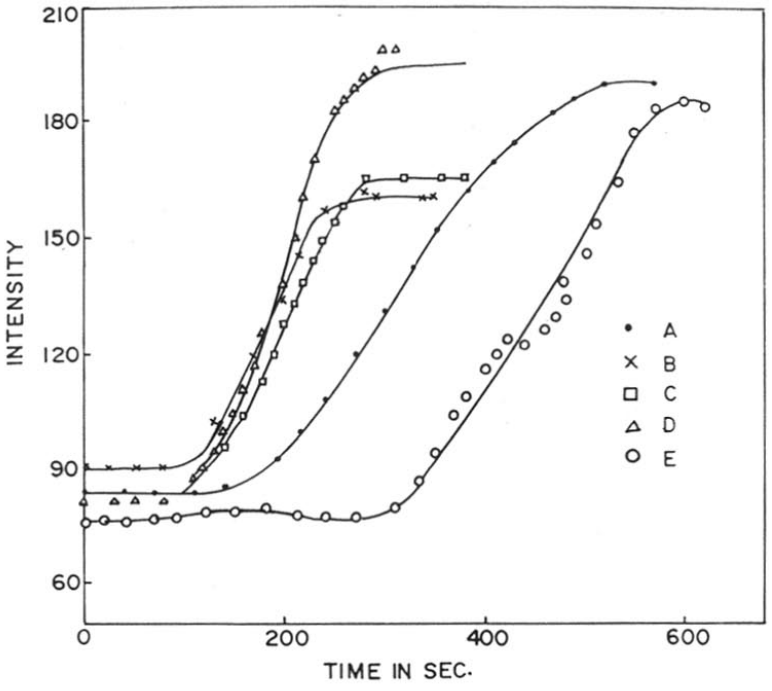

Figure 5.4 Plot of intensity as a function of time for PP/PET isothermally melt crystallized at 115°C. Curves A, B, C and D correspond to PET fibre concentration of 2, 4, 7 and 11wt.%. Curve E corresponds to that of Pure PP.

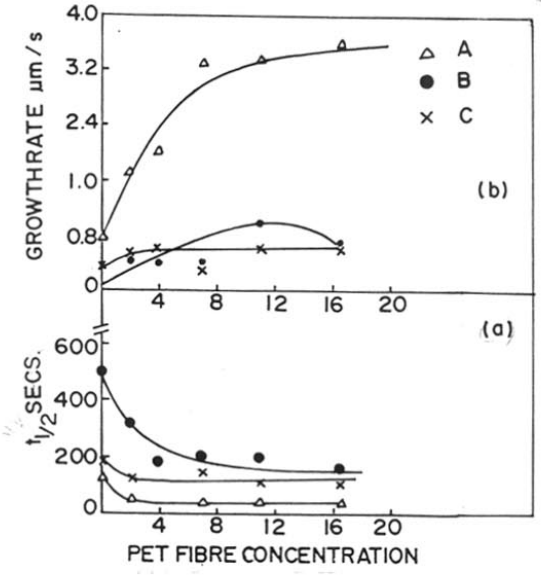

Figure 5.5 Plot of crystallization half time $t_{1/2}$ (a) and growth rate (b) of PP as a function of PET fibre content. Curves A, B and C correspond to T_c at 105°, 110°C and 115°C.

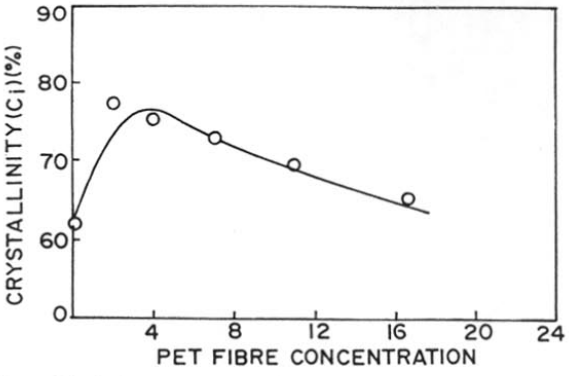

Figure 5.6 Variation of crystallinity C_i (%) as a function of PET fibre content at T_c =115°C

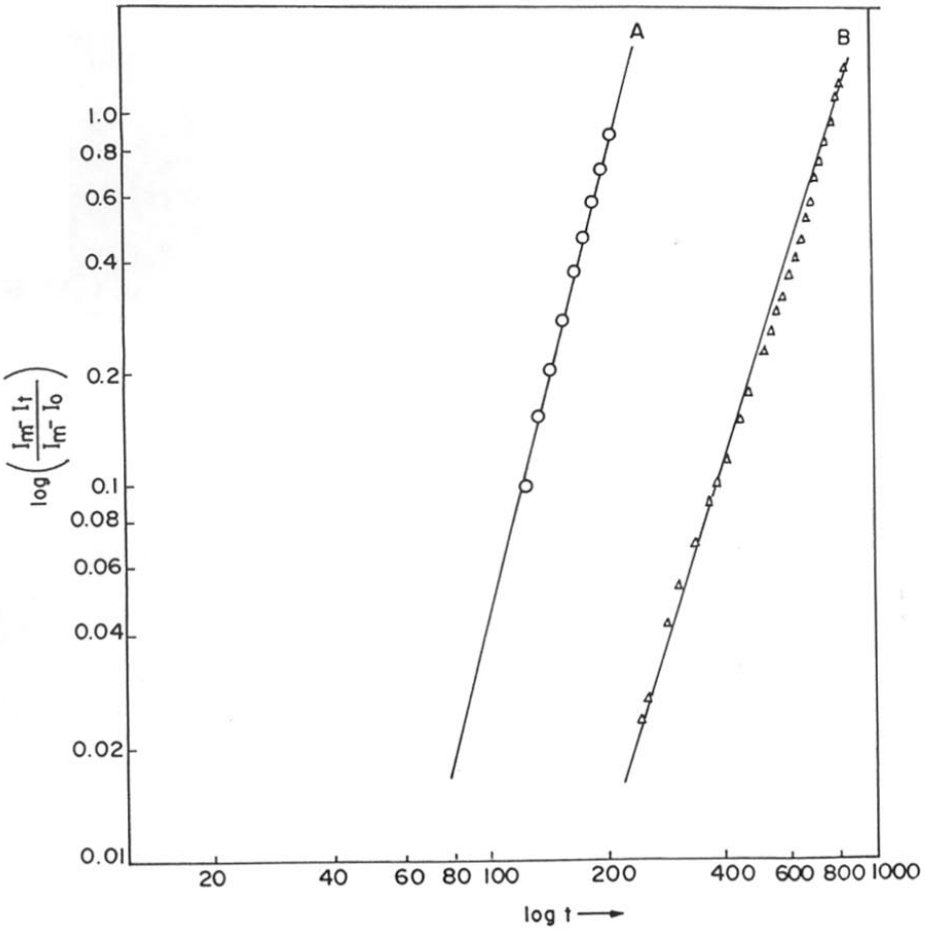

Figure 5.7 Avrami plot of log (fractional conversion) Vs time on log-log scale. Curve A = PP/PET at T_c= 115°C and curve B = Pure PP.

where I is the intensity value through the cross-polar due to the formation of crystallites, A_v is a constant, n is the Avrami exponent and T is the temperature. The subscripts t, m and o denote the corresponding values of I at time t, t= m and t = o respectively. Figure 5.7 shows the Avrami plot of log (fractional conversion) vs time on log-log scale. Curve A and curve B are the Avrami plot of PP/PET and pure PP at 115°C respectively. The values of n were found to be about 3 for normal PP and 4 to 4.5 for the transcrystalline phase of PP grown at PET interface. The higher value of n for the transcrystalline phase clearly indicates the heterogeneous nucleation and linear growth of crystallites. Turnbull and Vonnegut[37] have attributed the presence of transcrystalline phase to the closeness of match between the lattice parameters of substrate and polymer matrix crystals. Thus, the development of transcrystallinity may be associated with the oriented overgrowth of PP crystallites on PET fibres. According to lattice mismatch theory, if the mismatch parameter (δ_l) defined as

$$\delta_l = |pl_s - ql_g| / |l_s| \times 100 \qquad (5.2)$$

where l is the lattice parameter along any axis; p and q are integers. The subscripts s and g represent substrate and growing media, is less than 10% then there is a preferential growth or even epitaxial growth of one phase over the other.

If one considers the lattice parameters of the α phase of PP a = 6.5 Å, b = 20.9 Å, c = 6.5 Å and β = 99.3° with those of PET (a = 4.56 Å, b = 5.94 Å, c = 10.75 Å and α = 98.5°, β = 118°, γ = 112°. The lattice mismatch between b-axis of PP and 2 × c-axis of PET is less than 3% while that between c-axis of PP and b-axis of PET is less than 8.5%. Hence, it is quite likely that the {bc} planes of the PP crystals get aligned initially along the fibre axis of PET fibres and subsequently these crystals grow with preferential b-axis orientation. The alignment of b-axis of crystallites gives rise to a change in the intensity of (040) reflection as observed in this case. These observations clearly indicate that since there is preferential orientation of b-axis and/or {bc} planes of PP crystallites along the c-axis of PET fibre, the crystal structure of fibre material could be important for the development of this transcrystalline phase.

5.3.2 Structure Development in PP-g-MA/PET Composite

(a) Crystallization behaviour of PP-g-MA

The crystallization behaviour of PP-g-MA was monitored by recording the growth of spherulites as a function of time in the same manner as described earlier at T_c of 115°C. Figure 5.8 shows the plot of intensity as a function of time for PP-g-MA. Curves A, B and C correspond to MA concentration of 5, 10 and 15 wt.% respectively with respect to the PP matrix. In presence of MA, the induction period is much smaller as compared to pure PP. The crystallization half time and the crystallization rates were determined from these curves. These are plotted with respect to concentration of maleic anhydride which is shown in Fig.5.9a and b. It is evident from the figure 5.9a that the $t_{1/2}$ value shows a considerable decrease in presence of MA as compared to pure PP. Also with increase in conc. of MA from 5 to 15 wt.% the $t_{1/2}$ value remains practically constant. The crystallization or growth rate values are also quite high for PP-g-MA as compared to pure PP (see Fig.5.9b). L. Popisil et al.[38] observed similar decrease of $t_{1/2}$ values and increase of crystallization rates for PP-g-MA at T_c of 135°C and 139°C respectively. Such studies were also carried out by Jingjiang et al.[39]

The considerably low $t_{1/2}$ values and substantially high growth rates in maleated PP can be explained as follows. The grafting of MA on to PP[40,41] chains can be represented schematically as

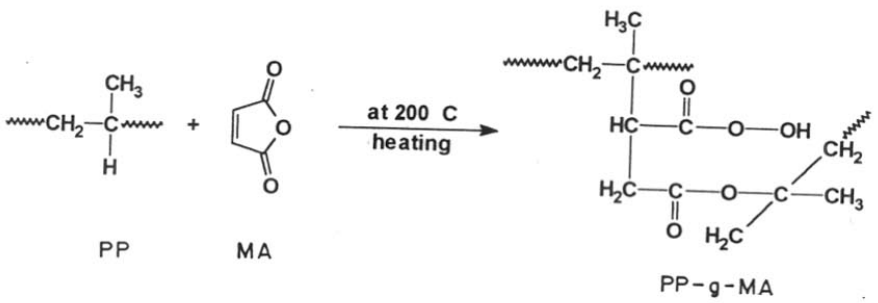

According to this scheme , for 10wt.% of MA on to PP, the MA monomer/molar ratio is 1: 24 i.e for every 24 units of propylene ,there is one unit of MA grafted. During crystallization , the linear chains segments without grafts participate in the crystals while the grafts are excluded from the crystals. Therefore, as the MA concentration increases, the length of the linear chain segments decreases. This reduces the lamellar thickness which due to

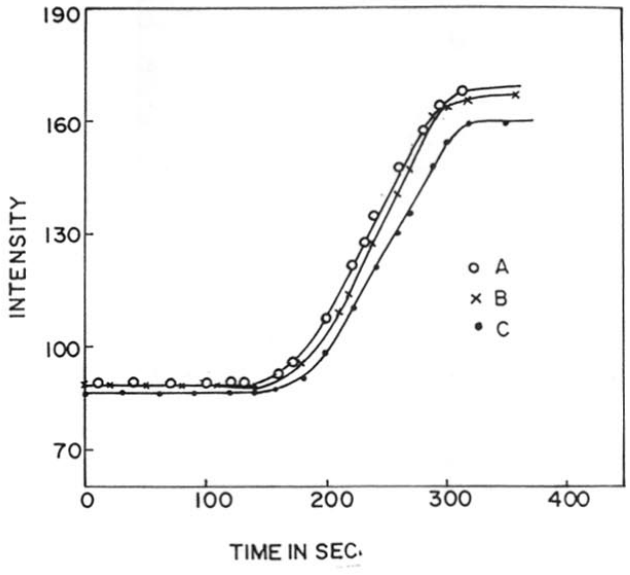

Figure 5.8 Plot of intensity as a function of time for PP-g-MA . Curves A, B and C correspond to MA concentration of 5, 10 and 15wt.% .

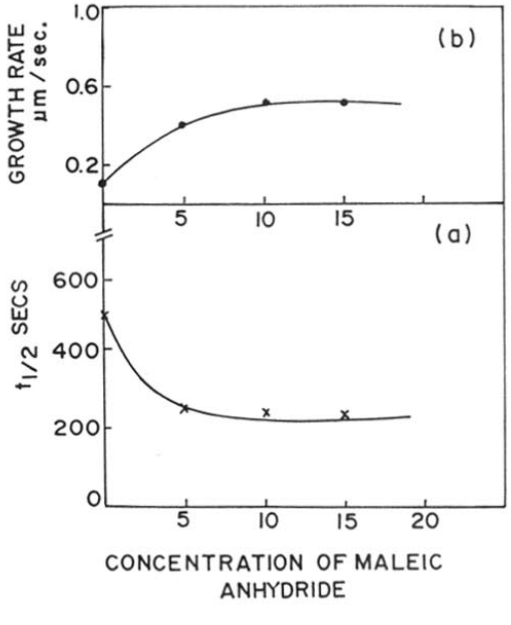

Figure 5.9 Crystallization half time, $t_{1/2}$ (a) and growth rate (b) of PP as a function of MA concentration.

closed packing of PP crystallites, crystallizes with a fair decrease in spherulite dimensions (average size of 15-20μm).

(b) Crystallization behaviour of PP/PET compatibilized with MA

Figure 5.10 I, II and III shows the WAXD scans for the PP-g-MA/PET with concentration of MA ranging from 5 to 15wt.% isothermally crystallized from melt at T_c of 115°C as a function of PET concentration. Curves A, B and C correspond to PET concentrations of 4, 7 and 11 wt.% respectively. In all the cases, characteristic diffraction maxima of monoclinic α crystalline form of PP are obtained. However, the intensity of peak at 2θ of 16.7° due to (040) reflection remains almost unaffected in presence of MA with varying PET fiber content. Figure 5.11 shows the of variation of intensity of 2nd peak in relation to the peak 1 (2θ = 14°, 110 reflection) as a function of PET fibre content at 115°C. Curve I shows the PP/PET without MA while curves II, III and IV correspond to PP/PET with 5, 10 and 15 wt.% concentration of MA. The peak intensity (peak 2) corresponding to (040) reflection is suppressed for the curves II, III and IV containing MA while in the absence of MA (curve I), the peak intensity of (040) reflection is appreciably high and it increases with increase of PET fibre content as explained earlier. The decrease in the intensity of peak 2 for PP/PET with MA compared to PP/PET without MA shows that there is no preferential orientation of b-axis in presence of maleic anhydride. The suppression of b-axis (040 peak intensity) can be associated with the absence of transcrystalline phase. We confirm this result in a later section using the crystallization behaviour and morphological studies of this system.

Figure 5.12 shows the optical micrograph of PP with 7% PET containing 10% MA isothermally crystallized at T_c = 115°C. Extensive nucleation is observed both at the fibre surface and as well as in the bulk at the same time (away from fibre interface). The spherulites are considerably smaller than 15μm. Also it is interesting to note that no transcrystalline morphology is observed at the fibre surface.

Figure 5.13 shows the WAXD scans for 7% PET fibre in PP with varying concentration of MA from 5 to 15 wt.% at T_c = 115°C. With the increase in concentrations of MA the intensity of peak 2 at 2θ of 16.7° due to (040) reflection of α phase of PP remains practically constant with respect to peak 1 (2θ = 14°, 110 reflection). This shows that the intensity of (040) reflection of peak 2 is unaffected with increase of MA concentration.

The isothermal crystallization behaviour was monitored by a plot of intensity as a function of time for PP/PET fibre containing 10% concentration of MA, which is shown in

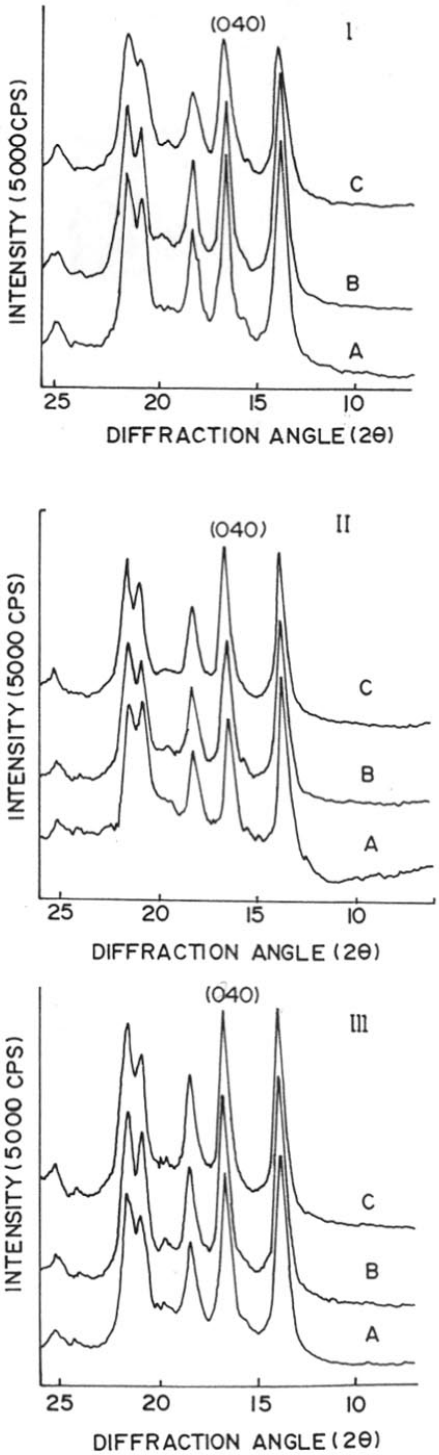

Figure 5.10 WAXD scans for PP-g-MA/PET. Symbols I , II and III correspond to MA concentration of 5, 10 and 15wt.% Curves A, B and C correspond to PET fibre concentration of 4, 7 and 11wt.%.

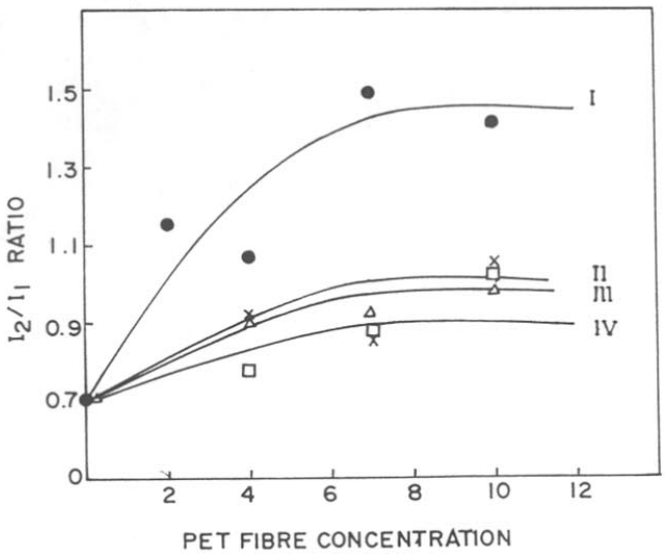

Figure 5.11 Plot of variation of intensity of 2nd peak in relation to 1st peak as a function of PET fibre content. Curve I is without MA and curves II, III and IV contains MA concentration of 5, 10 and 15%.

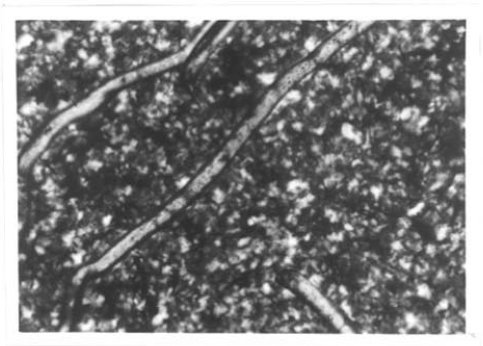

Figure 5.12 Optical micrograph of PP with 7% PET containing 10% MA at T_c= 115°C (net magn. 450x)

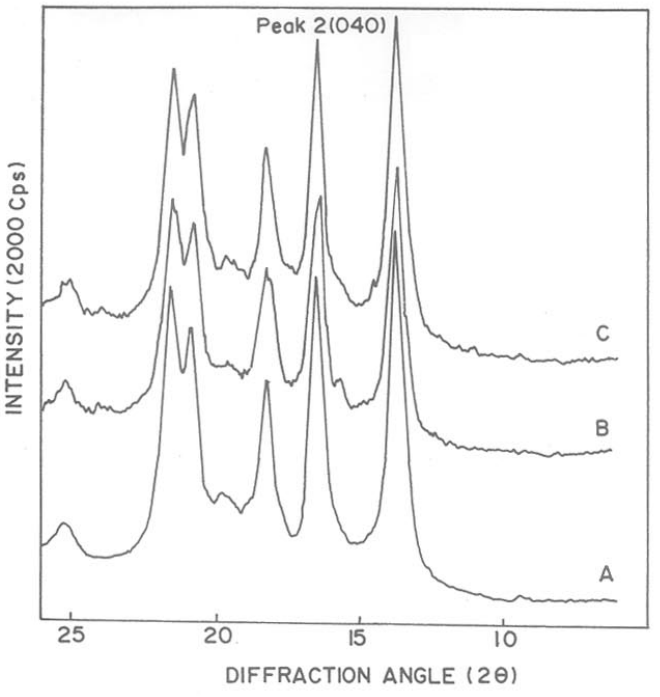

Figure 5.13 WAXD scans for PP-g-MA/PET (7% PET fibre). Curves A, B and C correspond to MA concentration of 5, 10 and 15 wt.%.

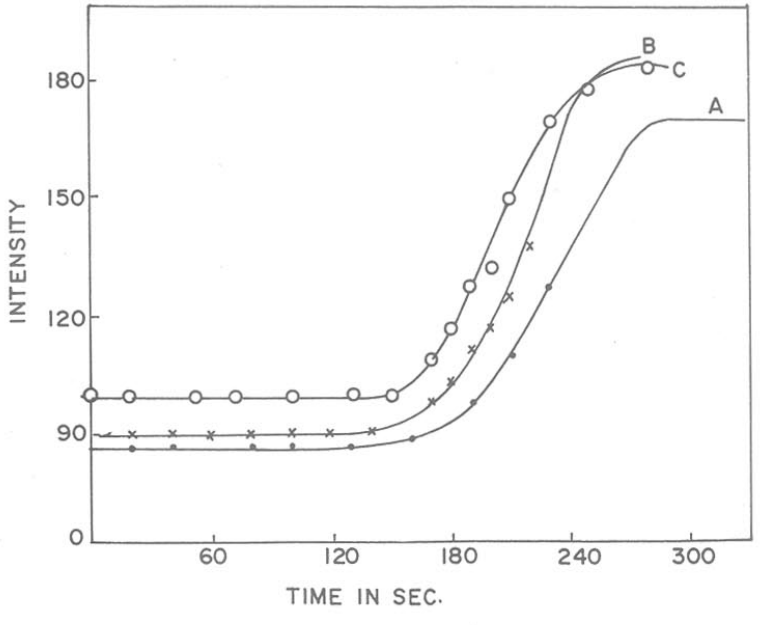

Figure 5.14 Plot of intensity as a function of time for PP-g-MA/PET (10% MA). Curves A , B and C correspond to PET fibre concentration of 4, 7 and 11wt.%.

Fig. 5.14. The curves A, B and C correspond to PET fibre concentrations of 4, 7 and 11 wt.% with respect to PP. .It is evident that the crystallization processes in the bulk as well as along the fibre surface are similar with no transcrystalline zone. The induction period is much smaller than that of pure PP. The crystallization half time and the crystallization growth rates were determined from these curves which are shown in Fig. 5.15a and b. The curve A and curve B show the $t_{1/2}$ and growth rate values for PP/PET without MA and PP/PET containing 10% MA respectively. Considerably lower $t_{1/2}$ values and higher growth rates were observed for PP/PET (curve A) as compared to PP-g-MA/PET (curve B) (containing 10 wt.% MA). Although, the $t_{1/2}$ values for latter case decrease as compared to pure PP, it is practically constant with the increase in PET fibre concentration upto 11 wt.%.

Figure 5.16 shows the variation of crystallinity for PP-g-MA/PET as a function of PET fibre content determined from XRD curves. Curve A and B shows the crystallinity of PP/PET and PP-g-MA/PET respectively. Higher C_I values of the order of 75% are observed for PP/PET compared to 62% for PP-g-MA/PET.

These findings can be explained as follows. The maleic anhydride is a well known compatibilizer for PP/PET system. During the melting process, One end of MA grafts to PP and the other end of carboxylic group allows hydrogen bonding with the PET fibre. The presence of both PET fibre and MA reduce the segmental motion of PP due to which the growth of crystallites is restricted giving rise to small crystallite or spherulite size (see Fig. 5.12). Also, the MA does not allow the PET fibre to actively initiate nucleation of PP. So no transcrystalline morphology is observed. These factors together contribute to lower C_i values as observed above.

The DSC thermograms of these samples were investigated in order to study the difference between the transcrystalline layer of PP/PET and that of PP-g-MA/PET which are shown in the Fig.5.17a and b. It can be seen from the figures that PP/PET exhibits an exothermic peak at 121° C while PP-g-MA/PET exhibits an endothermic peak at 118°C respectively. The increase in crystallization temperature in the former case as compared to latter can be attributed to PET acting as a strong nucleating agent for PP giving rise to transcrystalline morphology. The presence of transcrystallinity can be clearly observed in the endotherm of PP/PET, which shows a broad peak having a total ΔH value of 145.38 J/g. This broad peak is divided into two peaks, the lower peak has a ΔH of 58.8 J/g which corresponds to transcrystalline zone (fast crystallization process) giving rise to small spherulites along the

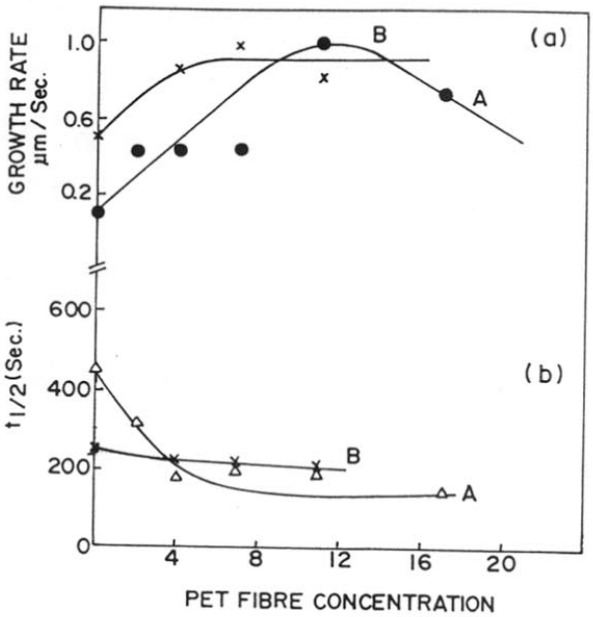

Figure 5.15 Crystallization half time , $t_{1/2}$ (a) and growth rate (b) of PP as a function of PET fibre content. Curve A= PP/PET and curve B = PP/PET containing 10%MA.

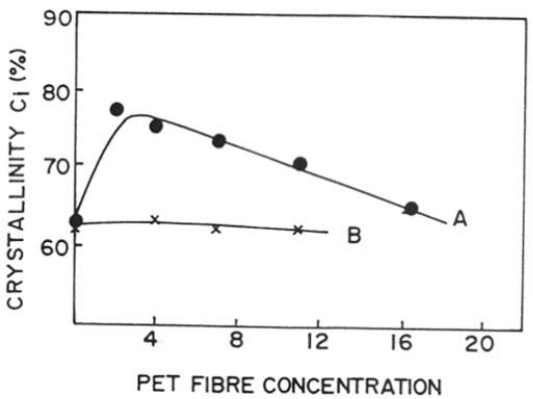

Figure 5.16 Variation of crystallinty C_I (%) for PP-g-MA/PET as a function of PET fibre content. Curve A= PP/PET and curve B = PP/PET containing 10% MA.

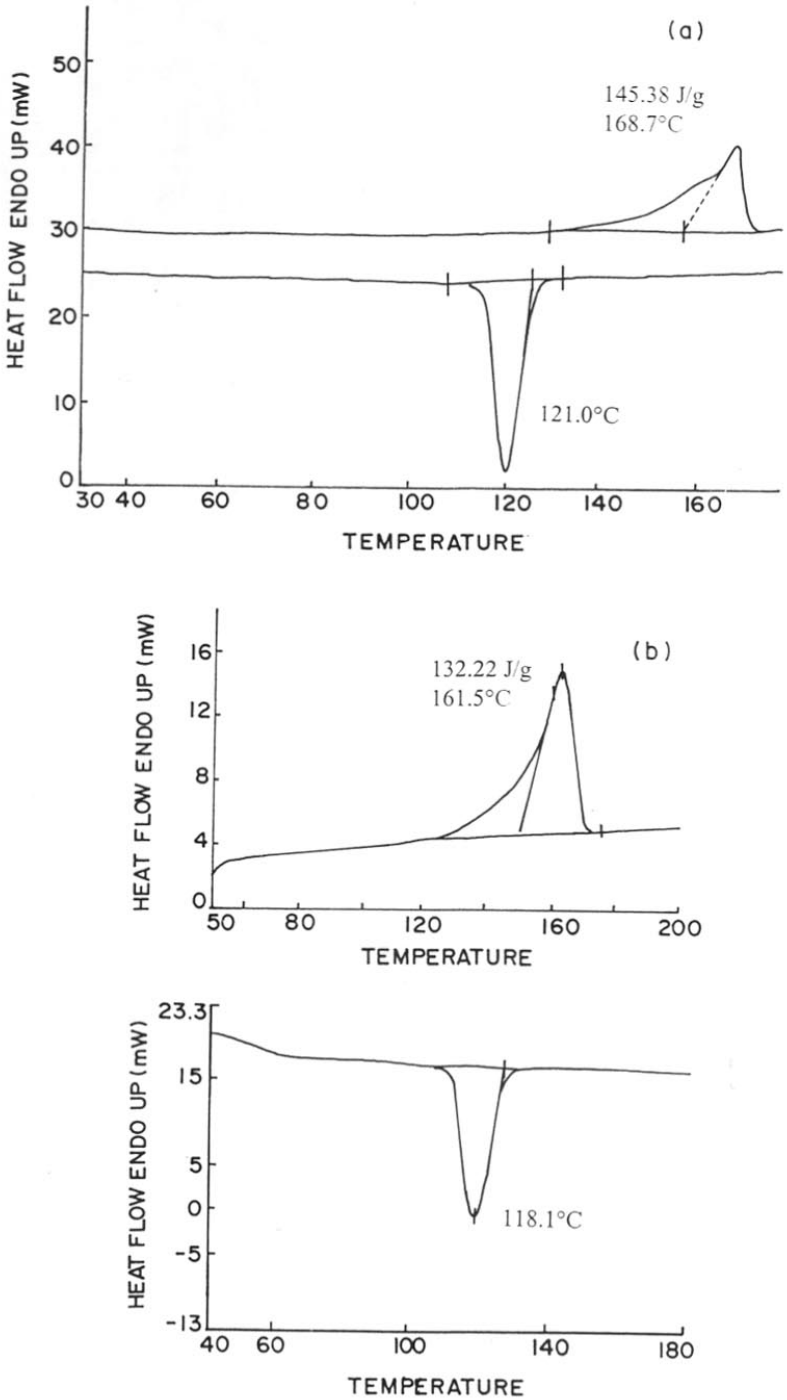

Figure 5.17 DSC curves for (a) PP with 7% PET (b) PP with 7% PET containing 10% MA.

fibre surface while the ΔH of 86.5 J/g corresponds to big spherulites away from fibre surface. Thus a total of 145.38 J/g contributes to high crystallinity in iPP. On the other hand, a single endothermic peak is observed for PP-g-/MA/PET having a ΔH of 132.22 J/g. This clearly indicates that the presence of MA prevents the formation of transcrystalline growth of PP spherulites on the surface of PET.

In order to investigate the fibre-matrix interaction, the melt extruded PP-PET composites were examined for SEM after sectioning along the transverse direction. Figure 5.18 shows the SEM micrographs for PP/PET (Fig. 5.18a, b and c) and PP-g-MA/PET (Fig.5.18c and d). The fibre pull out is clearly seen in PP/PET sample (Fig.5.18a and b) suggesting a weak adhesion between the PET fibres and PP matrix. Also (Fig.5.18c) the PET fibres are seen to be surrounded by a thin region near the fibre matrix interface. This thin layer can be attributed to transcrystalline phase of PP occurring at the interface. On the other hand, the micrograph of PP-g-MA/PET shows strong fibre matrix adhesion with very little fibre pull out. Thus, we can say that the maleic anhydride acts as a good compatibilizer or wetting agent.[42-46] It wets PET fibre and grafts PP matrix to it. There is no transcrystalline zone observed in the presence of MA.

5.3.3 Mechanical Properties of PP/PET Composites

The impact and tensile modulus were evaluated for injeciton moulded samples and correlated with structure and morphology. Figure 5.19a and b shows the typical stress-strain curves for PP containing 10% PET without and with 10%MA respectively. The various properties such as stress at autobreak, load at max. load, strain at break. tensile modulus etc are indicated in the Table 5.1 for these composites. (About 8-10 samples were analysed but only their average values are indicated in the table). From the stress-strain curves, it can be seen that pure PP(see section 3.23a) exhibits a well defined yield point while PP/PET with and without MA breaks suddenly with no well defined yield point. Also in case of PP-g-MA/PET the strain at break is considerably high as compared to PP/PET composite.

Figure 5.20 shows the variation of tensile modulus with PET fibre concentration. The experimental values have been compared with those expected for a blend PP/PET with and without MA. The expected values were evaluated assuming a non-interactive PP/PET blend having uniform spherical domains of PET dispersed in PP and using a simple rule of mixtures as[47]

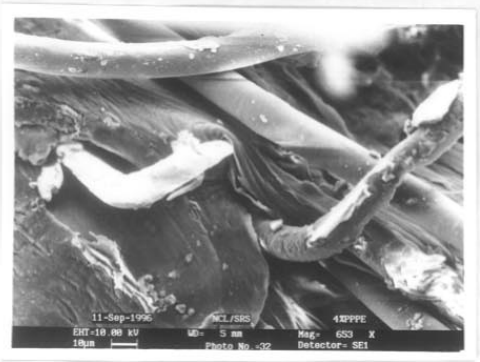

(a)

(b)

(c)

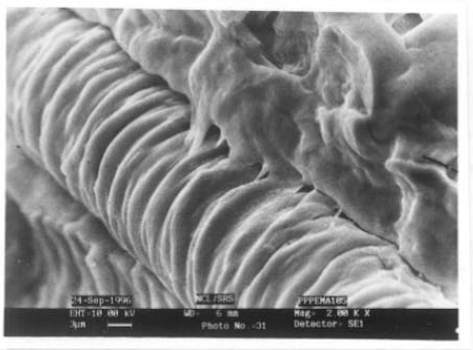

(d)

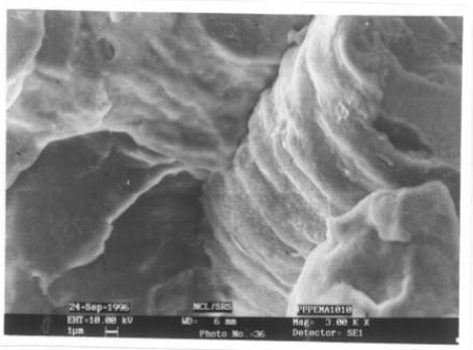

(e)

Figure 5.18 SEM micrographs of melt extruded samples sectioned along tranverse direction. (a) PP with 4% PET (b) PP with 10% PET (c) PP with 7% PET (d) PP with 10% PET containing 5% MA (e) PP with 10% PET containing 10% MA.

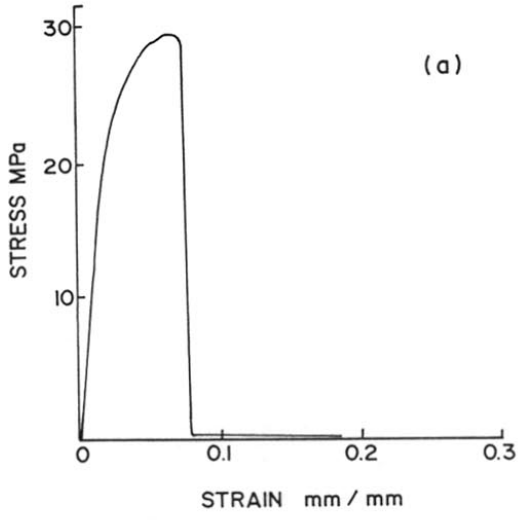

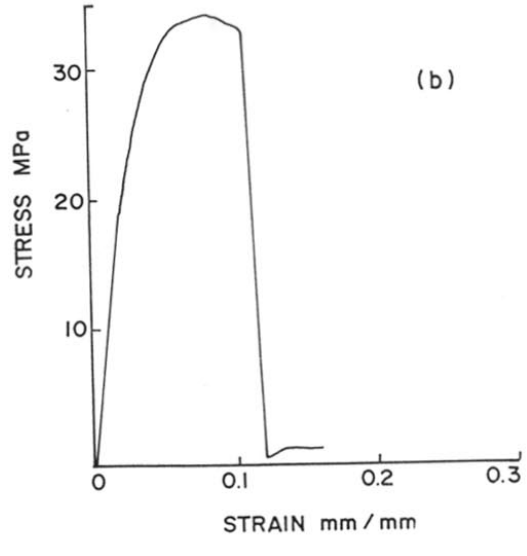

Figure 5.19 Plot of stress Vs strain for (a) PP with 10% PET (b) PP with 10% PET containing 10% MA.

Table 5.1 Tensile Properties of PP/ PET and PP-g-MA/PET composites.

Composition	Stress at auto break (Mpa)	% strain at auto break (%)	Stress at max. Load (MPa)	% strain at max. load (%)	Displacement at max. load (mm)	Load at max. load (KN)	Strain at max. load (mm/mm)	Load at auto break (KN)	Displacement at auto break (mm)	Modulus (Mpa)
PP	9.17	123.70	30.16	9.81	4.89	1.70	0.09	0.35	61.85	1372.0
PPPE 2%	22.91	3.02	22.98	3.16	1.17	0.08	0.03	0.08	1.21	1420.7
PPPE 3%	21.04	2.43	24.02	2.85	1.09	0.07	0.02	0.06	0.92	1601.2
PPPE 7%	0.77	0.33	21.54	1.98	0.72	0.08	0.01	0.00	0.07	1768.8
PPPE 8%	26.12	4.15	29.28	4.19	1.59	0.11	0.04	0.10	1.57	1634.3
PPPE 10%	24.68	5.58	25.07	4.83	1.88	0.09	0.04	0.09	2.18	1570.5
PEM 4%	29.37	29.61	31.18	31.91	36.70	1.22	0.31	1.15	34.06	1542.0
PEM 9%	28.08	36.31	29.03	37.16	42.74	1.12	0.37	1.09	41.76	1566.0
PEM 14%	25.10	40.06	25.52	40.50	46.57	1.02	0.40	1.01	46.08	1601.0
PM 10%	21.78	23.58	27.62	31.74	36.50	1.05	0.31	0.82	27.12	1288.0

PPPE 2% - PP containing 2% PET
PPPE 3% - PP containing 3% PET
PPPE 7% - PP containing 7% PET
PPPE 8% - PP containing 8% PET
PPPE 10%- PP containing 10%PET

PEM 4% - PP with 4% PET containing 10% MA
PEM 9% - PP with 9% PET containing 10% MA
PEM 14% - PP with 14%PET containing 10% MA
PM 10% - PP containing 10% MA.

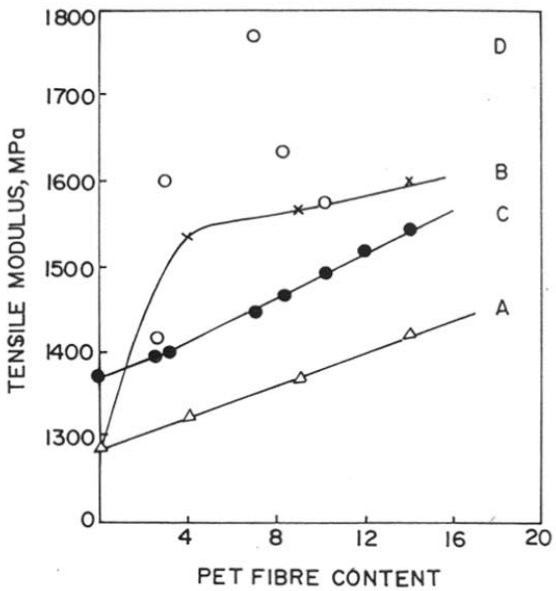

Figure 5.20 Variation of tensile modulus with PET as a function of PET fibre content according to simple rule of mixture.

$$E_c = \phi_A E_A + \phi_B E_B \quad (5.3)$$

where E_c is the combined modulus of both PET (globular form) and PP, E_A and E_B are the tensile modulus of PET (globular) as 2758 Mpa[36] and PP as 1372 MPa respectively. The ϕ_A and ϕ_B are the volume fractions of corresponding to PET and PP respectively. In case of PP-g-MA/PET, the value of E_B was taken for maleated PP is (1288 Mpa) rather than pure PP. In the figure, curve A and C correspond to expected modulus values for PP/PET with MA and PP/PET without MA. The curve B corresponds to experimental modulus values for PP/PET with MA and the symbols 'o' correspond to experimental modulus values for PP/PET without MA. There is a considerable increase of tensile modulus in presence of PET fibres in PP with and without MA as compared to matrix alone (pure PP or PP/MA).

The increase of tensile modulus in PP/PET fibre composites can be due to:

(a) Reinforcing effect of PET fibres (b) Higher crystallinity and (c) Transcrystallinity.

It is seen that although PET by itself has higher modulus than PP, its blend as a simple dispersed system does not show much improvement as noted in the present case. The fibrous nature with high aspect ratio certainly plays an important role. Further, PP/PET has higher crystallinity (75%) as compared to PP homopolymers (62%). Finally the increase of modulus value can originate from the transcrystalline morphology which tends to be columnar crystalline structure at the fibre-matrix interface leading to better interaction between the matrix and the fibres.

Increase of modulus values for PP-g-MA/PET as compared to their expected values can be attributed to:

(a) Good interfacial adhesion between fibre and matrix and (b) Reinforcement effect of PET fibre. It is well known that maleic anhydride grafted on a polymer acts as a good wetting agent and has been used as a compatibilizer for many polymers. As observed earlier in the presence of maleic anhydride the strong interfacial adhesion between the PET fibre and the matrix is achieved. Secondly, as explained earlier the high aspect ratio of PET fibre contributes to an increase of modulus values compared to expected modulus values which are calculated for globular PET.

It is also interesting to note that the modulus value is higher for PP/PET compared to PP-g-MA/PET at the same PET fibre concentration. This is due to transcrystalline morphology observed in the former case and its absence in the latter.

Table 5.2 Izod impact strength of PP/PET and PP-g-MA/PET composites.

Composition	Izod impact strength (notched) J/m
Pure PP	85.0
PP with 4% PET	108.1
PP with 9% PET	117.4
PP with 14% PET	123.3
PP with 10% MA	152.5
PP with 4% PET containing 10% MA	115.7
PP with 6% PET containing 10% MA	120.2
PP with 9% PET containing 10% MA	96.0
PP with 14% PET containing 10% MA	90.6

From the various reports on the effect of transcrystallinity on the interfacial adhesion in composite materials, it has been found that different views exist with different groups. Some authors[48-50] showed that the fibre-matrix bond strength reduced after the generation of transcrystallinity around the fibres giving rise to poor composite properties while the others[51] have found that it makes little difference to adhesion. However, Schornhorn et al.[52] have shown that if transcrystalline layers are strong it may be advantageous in achieving good adhesion. Our results are in good agreement with their observations.

The impact properties of these composites (notched impact values) are shown in Table 5.2. It can be observed from the table that both PP/PET and PP-g-MA/PET show increase of impact strength as compared to pure PP (85 J/m). The increase is almost 1.4 times than that of pure PP. In case of PP/PET, the impact strength increases with the increase of fibre concentration up to 14% while that for PP-g-MA/PET, it increases up to PET content of 6% and tends to decrease slightly with the further increase in fibre concentration. These results can be explained on the basis of spherulite size, bonding between the fibre and matrix and the defects or stress points in the thermoplastic material containing excess fibres. For PP/PET although α form of spherulites are observed, the size of spherulites are considerably small as compared to those in pure PP. Due to the smaller size of spherulites, the impact strength is higher. Hence, high impact strength values are observed in PP/PET as well as in PP-g-MA/PET as compared to pure PP.

5.4 Conclusions

In these studies, we have established that polymer mediated growth is observed in the case of PP/PET composite at an interface where the PET fibres influence the crystallization of PP through crystal - crystal interaction. PET acts as a strong nucleating agent for PP spherulites giving rise to transcrystalline growth. On the other hand, the presence of MA prevents the formation of transcrystalline growth of PP on the surface of PET fibres but at the same time gives strong fibre - matrix bonding which affects the mechanical properties of the composites as well. Thus, the influence of fibre on PP matrix and vice versa is seen giving an improvement in the mechanical properties of the PP composites.

5.5 References

1. D.W. Clegg and A.A. Collyer ed. "Mechanical Properties of Reinforced Thermoplastics" Elsevier, London, (1986) p. 2.
2. F.G. Krautz, J. of Society of Plastic Eng., **27** (1971) 74.
3. R.H. Burton and M.J. Folkes, Plast. Rubber Processing Appl., **3** (1983) 29.
4. W.B. Titow and B.J. Lanham in Reinforced Thermoplastics, Applied Sci. Publishers Ltd. London, Chapt. 2 (1975) p.18
5. N. J. Morristown, Reinforced Capron. Nylon for Injection Moulding, CL-300-884, Allied Corp.
6. J.L. Thomason and A.A. Van Rooyen, J. Mater. Sci., **27** (1992) 5.
7. D. Campbell and M.M. Qayyum, J. Polym. Sci. Poly. Phys. Edn., **18** (1980) 83.
8. A.L. Disalvo, J. Polym. Sci. Polym. Lett. Edn., **12** (1974) 509.
9. A.M. Chatterjee, F.P. Price and S. Newman, J. Polym. Sci. Polym. Phys. Edn., **13** (1975) 2369.
10 Idem, J.of Polym. Sci. Polym. Phys. Edn., **13** (1975) 2385.
11. Idem, J.of Polym. Sci. Polym. Phys. Edn., **13** (1975) 2391
12. M.R. Kantz and R.D. Cornelliussen, J. Polym. Sci., Polym. Lett. Edn., **11** (1973) 285.
13. B.S. Hsiao and E.J.H. Chen, in "Controlled Interphases in Composite Materials" edited by H. Ishida, Elsevier, New York, (1990) p. 613.
14. T. Bessel and J.B. Shortall, J. Mater. Sci., **10** (1975) 2035.
15. P. Bussi and H. Ishida, in "Controlled in Composite Materials" edited by H. Ishida Elsevier, New York, (1990) p. 391.
16. T. He and R.S. Porter, J. Appl. Polym. Sci. **35** (1988) 1945.
17. J.A. Peacock, B. Fiffe, S.E. Nield and C.Y. Barow, in "Composite Interfaces" edited by H. Ishida and J.L. Koenig ,Elsevier, New York ,(1986) p. 143
18. S.Y.Hobbs, Nature (London) Phys. Sci. **234** (1971)12.
19. E.J.H. Chen and S.H. Benjamin, Polym. Eng. Sci. **32** (1992) 280.
20. P.K. Sengupta and D. Mukhopadhyay, Polym. Sci. (Symp. Proc. Polym.'91) edited by S. Sivaram, **2** (1991) 855.
21. J.L. Thomason and A.A. Van Rooyen, J. Mater. Sci., **27** (1992) 897.
22. E. Devaux and B. Chabert, Polymer Comunications , **31** (1990) 391.
23. A. Avella , E. Martuscelli , C. Sellitti , J. of Mater. Sci. **22** (1987) 3185.

24. M. Avella, G.D. Volpe, E. Martuscelli and M. Raimo, Polym. Engg. & Sci., **32** (1992) 377.
25. M. Avella, E. Martuscelli, B. Parcucci and M. Raimo, Polym. Engg. & Sci., **32** (1992) 383.
26. L. Madelkern, Crystallization in Polymers, McGraw Hill, New York (1964).
27. J.L. Thomason and A.A. Van Rooyen, J. Mater. Sci., **27** (1992) 889.
28. M. Klein and G. Marom, Composites, **25 (7)** (1994) 706.
29. M.J. Folkes and S.T. Hardwick, J. Mater. Sci. Letters, **3** (1984) 1071
30. J.L.Thomason in "Interfacial Phonomena in Composite Materials" edited by F.R.Jones Butter worms Scientific, London (1989) 171.
31. L.W. Chen and P.H. Lin in "Advanced Composite Materials and Structures" edited by G.C. Sih and S.E. Hsu (VNU Science Press, Utrecht, 1987) p. 659.
32. A. Misra, B.L. Deopura, S.F. Xavier, F.D. Hartley and R.H. Peters, Angew. Makromol. Chem., **113** (1983) 113.
33. J.T. Hartness, SAMPEJ, **20** (1984) 266.
34. Y. Lee and R.S. Porter, Polym. Engg. & Sci., **26** (1986) 633.
35. M.R. Kantz and R.D. Corneliussen, J. Polym. Sci. Polym. Letts. Edn., **11** (1973) 279.
36. F.W. Billmeyer ,Textbook of Polymer Sci., John Wiley & Sons, New York, (1984)
37. D. Turnbull and B. Vonnegut, Industrial and Engineering Chem., **44** (1952) 1292.
38. L. Popisil and J. Jancar, J. Mater. Sci. Lett., **9** (1990) 495.
39. Liu, Jingjiang (Changchun Inst. Appl. Chem. Acad. Sin. Changchun, Peop. Rep. China, Yingyong Huaxue **10(1)** (1993) 25.
40. S.B.Joshi and S.Radhakrishnan Polym. Sci. & Engg. group , Chemical Engg. Div., N.C.L, Pune-8
41. B.Schulz and M.Hartman , Acta Polym. **36 (7)** (1988) 361.
42. S.J. Park, B.K. Kim and H.M. Jeong, Eur. Polym. J., **26** (1990) 131
43. C. Chen, E. Fontan, K. Min and F.L. White, Polym. Engg. Sci., **28** (1988) 69.
44. F. Ide and A. Hasegawa, J. Apply. Polym. Sci., **18** (1974) 963.
45. B.K. Kim, S.Y. Park and S.J. Park, Eur. Polym. J., **27** (1991)349.
46. J. Duvall, C. Sellitti, C. Meyers, A. Hiltner and E. Baer, J. Appl. Polym. Sci.,**52** (1994) 195.

47. M.J. Folkes and P.S. Hope, Polymer Blends and Alloys, Chapman and Hall, London , (1993) Chapt.6.

48. M. J. Folkes, S.T.Hardwick and W.K.Wong "Polymer Composites ", Proceedings of the 28th Microsymposium on Macromolecules, Prague, July 1985 (Walter de Gruyter , Berlin) P.33.

49. M. J. Huson and W.J. McGill, Polym. Sci. Polym.Phys. Edn.,**22** (1985) 121.

50. M. J. Folkes amd W.K. Wong, Polymer (1986) submitted.

51. M. Masouka , Int. J. Adhesion and Adhesives, **1** (1981) 256.

52. T.K.Kwei , H.Schonhorn and H.L.Frish , J.of Appl. Phys., **38** (1967) 2512.

Chapter 6

Structure, Growth and Morphology of NLO Crystals Dispersed Micro Composites

6.1 Introduction

In the earlier chapters, composites of conventional polymer such as polypropylene were investigated in detail for the structure development and mechanical properties by incorporating various types of additives, fillers, fibres, etc. The present chapter deals with novel polymeric composites exhibiting nonlinear optical (NLO) properties that are important in the development of optoelectronic and photonic devices. Nonlinear optical properties are responsible for key functions in photonic technology. The ability of (NLO) active media in changing properties of light such as its frequency, phase, amplitude or transmission characteristics when the light passes through it is useful in photonics. For example, in the case of second harmonic NLO property, the incident beam having a NLO active media is of frequency ω whereas the emergent beam is found to be of frequency 2ω and emerges from crystal media at an angle different from that of primary beam. The application for the second order NLO materials include optical switching, frequency conversion and electro-optic modulation (EO).[1-3]

There are various types of NLO materials, which show second order NLO properties. These can be classified as inorganic crystals, organic materials, liquid crystalline polymers, guest-host systems, etc.[4-7] The nomenclatures for the various materials referred to are given in Table 6.1.

Various inorganic crystals have been used for second order NLO applications.[8-10] For example $LiNbO_3$ (lithim niobate) has been used for integrated optical devices while potassium titanyl phosphate and potassium dihydrogen phosphate have been used for laser frequency conversion. However, such crystals have low efficiency because of their small dipole moment and second order coefficient as compared to organic materials.

The organic materials have been currently identified as materials of choice because of their diverse molecular structures. There are a number of organic single crystals and polymers that have been reported to surpass both simple harmonic and linear first order coefficients.[11,12] These organic materials especially azo benzene derivatives have higher harmonic coefficients because the origin of the nonlinearity is primarily electronic. A fairly comprehensive list of such materials is available in the literature.[13-15] Materials such as mNA, COANP, DANS, etc. have shown large nonlinearities with potential applications for second harmonic generation (SHG) and EO modulation. However, there has not been much success so far in the implementation of these materials in devices due to difficulties in crystal growth processing

and lack of mechanical integrity and long term stability. Recently, ferroelectric liquid crystals have been developed which exhibit second order NLO responses.[16,17] However, the optical nonlinearities of these materials are relatively small.

Table 6.1 Nomenclature for the various materials

CO ANP	2-N-cyclooctylamino-5nitropyridine
CR	diethylene glycol bis-(allyl polycarbonate)
DAN	4-N-N-dimethylamino-3-acetamidonitrobenzene
DANS	4-dimethyl amino-4-nitrostilbene
DEANS	4-diethyl amino-4-nitrostilbene
DO 25	disperse orange dye
DR-1	disperse red dye
KDP	potassium dihydrogen phthalate
MBA-NP	2α-methyl benzyl amino-5-nitropyridine
MNA	meta nitroaniline
mNA	2-methyl-4 nitroaniline
NMBA	4-nitro-4'-methyl benzylidene aniline
PNA	para nitroaniline
PCHMA	poly(cyclohexyl methacrylate)
PEO	polyethylene oxide
PMMA	polymethyl methacrylate
PVAc	polyvinyl acetate
PVA	polyvinyl alcohol
PVDF	polyvinylidiene fluoride
P_4VP	poly (4-vinyl pyridine)
SAN	styrene-acrylonitrile copolymer
TCNQ	tetra cyanoquinodimethane
TTF	tetra thiofulvalene
TrFE	trifloro ethylene

Polymers offer several advantages over all the above materials. Polymeric films incorporating NLO moieties or guest-host systems have attracted a great deal of attention and are being seriously investigated for practical applications, especially for EO modulation. The

simplest means of achieving this is to form solid solutions or alloys by dissolving a low molecular weight guest in a suitable polymeric host. The main advantages of a polymeric host are high transparency, a reasonable T_g to minimise diffusion and relaxation from poling, high solubility of the guest and processability at low temperature without degrading the guest. Extensive studies have been carried out on various guest-host polymer systems.[18-23]

The first guest-host system was prepared in a mixture of liquid crystalline polymer by Meredith et al.[18]The researchers obtained a large second order nonlinear optical coefficient when molecules with large molecular hyperpolarizability such as DAN was doped into a thermotropic nematic liquid crystalline polymer host. The SHG obtained was considerably larger (100 fold) than could be obtained with a 2% DAN doped PMMA sample.

Singer et al.[19] reported the SHG in an azo dye disperse red/PMMA guest-host matrix. The measured SHG coefficient was approximately five times that of KDP. These results obtained were consistent with a thermodynamic model based on non-interacting molecular depoles. This dye (Disperse Red I) was also used by Kuzyk et al.[20] who studied the relative degree of binding of the guest to the host.

Karakus et al.[21]investigated the decay characteristics of poled polycarbonate films doped with NMBA and DAN. The alignment stability was higher for DAN doped Pc, which was attributed to hydrogen bonding in this system. Also they found that Pc served as a better solvent for nonlinear dopants than PMMA due to the ability of carbonyl group of the polymer chain to form hydrogen bonds with hydrogen atoms on the dopant.

Hill et al.[22] demonstrated for the first time that SHG from a poled composite of a nonlinear guest dissolved in a PVDF copolymer, was high. In addition they also showed that this material could be formed into waveguiding structures with an acceptable optical loss (~5 dB/cm) as is required in many signal processing systems. Studies on MNA have been investigated extensively in several host: PMMA[23,24] P_4VP, CR[19,24], PCHMA[24] and a novolac resin[24] (a low molecular weight cresol formaldehyde copolymer used in photo resists). In addition to these amorphous hosts, piezoelectric (PVDF/TrFE has also been used.[25] These showed advantages in the poling process as a result of their internal fields thus allowing room temperature poling and long term stability.

Related single ring nitroaniline and nitropyridines have also been loaded into hosts like PMMA, PCHMA, Pc, etc. Exceptionally high concentrations of up to 60 wt.% of single ring compounds such as MBA-NP have been achieved in Pc but above this value crystallization

occurred. Thus limiting values of the order of 10-20% were more common. Double ring compounds with higher β_e's (second order nonlinear electronic susceptibility) such as nitro amino stilbenes (DANs, DEANs), azodyes[26,27] and pyrazolines[28] have also been loaded in similar hosts but at lower concentrations.

Calvert et al.[29] developed a novel high efficiency crystal/polymer composite material for nonlinear optics based on the temperature gradient zone melting technique. After examination of crystal growth in such composites they indicated that the desirable qualities of the guest species could be strongly enhanced if the guest micro crystals were aligned within the polymeric host. Such composites could then be used as a waveguide. They also developed a new group of materials that combined optical property with mechanical ones such as strength and rigidity by growing 3-nitroanilines in a transparent polymer matrix.

Studies on SHG response and stability of corona poled guest-host carbonate thin films were carried out by Wan et al.[30] Poling conditions were achieved at temperatures less than glass transition temperature. Hydrogen bonding between the guest and Pc was proposed as the reasons for the high second order coefficient and long term stability of the films.

Matsuoka et al.[31] reported the effect of the substrate on the poling process of NLO guest-host systems. It was found that the nonlinear susceptibility of the electric poled polymer films on soda lime glass was much larger than those on fused quartz. The results were explained by considering the volume resistivity of the substrate.

The authors Toshiyuki, Watanabe, Kazuo, Yoshinaga et al.[32]reported the molecular doping of polyethylene oxide by PNA followed by a polarising freezing process which yielded a material having large SHG intensity 20-30 times that of urea. They have presented the results for 1:8 and 1:16 compositions of PNA/PEO films.

Miyata et al.[33] studied the nonlinear behaviour in a host-guest material consisting of a dispersion of highly oriented dye crystallites (PNA) in a polymer matrix (L caprolactum). The solution was prepared and allowed to spread on a substrate to form a thin film. Then they made straight streaks on the surface before the nucleation could take place so that the crystal grew perpendicular to the streaks. In another patent[34], the same inventors disclosed the orientation of an NLO material by an electric field for use as a waveguide. The material used was P-C_6H_4 Q(R) in poly oxyarylene matrix. The method comprised heating the material above the melting point followed by cooling it below melting point while applying a dc electric field.

Mandal et al.[35] have studied the nature of interaction between the guest and the host molecules, especially the compatibility and relaxation behaviour of corona poled guest host system. The guest molecules studied were mNA and DR-1 in different hosts such as PMMA, PS and SAN. Amongst these SAN was found to be the ideal matrix since the polymer itself relaxed slowly subsequent to poling and it accommodated a wide range of nonlinear optical molecules differing in molecular structure and polarity. Between PMMA and PS, PS proved to be a poor host material because of its incompatibility with polar active compounds. The high levels of loading could not be achieved in PS. In addition, they found that the poled complexes themselves were unstable except in case of mNA in PS, which was more stable than mNA in PMMA. Cheng et al.[36] have investigated the relaxation behaviour in PMMA films doped with aniline derivatives. The SHG intensity measured in poled films of PMMA doped with aniline derivatives indicated that dipole moment of the dopant molecules and doping level have a significant effect on the stability of SHG of the poled polymers. A mechanism based on free volume theory was proposed which interpreted the experimental observation satisfactorily. Hampsch et al.[37] also investigated the relaxation behaviour of 4 dopant molecules that is mNA(I), DANS(II), DR-1(III) and DO 25 (IV) in PMMA host. The trend in the relaxation properties was of the order of IV > III > II > I which reflected the influence of physical size on the ease of reorientation.

Kryszewski et al.[38,39] have extensively studied the dispersion of charge transfer complex salts such as (TTF-TCNQ, TTT-TCNQ), etc. in different polymers such as PVDF, PP, etc. In a few cases, they reported the morphology of such systems as comprising of tiny filamentary type crystals dispersed in the polymer matrix. They also observed spherulitic morphology when these charge transfer salts were dispersed in PVDF and long needle shaped oriented crystallites when grown in PP. However, they neither discussed the relevance of these features any further nor reported X-ray diffraction scans for the system.

Our survey of the literature indicated the following shortcomings in the earlier data:

(a) The various authors have investigated only the electro-optical properties of guest-systems without studying in detail the structural or morphological aspects.

(b) The authors have mainly used amorphous polymers and not crystalline ones. These amorphous polymers have free volume that allows greater chain mobility fast relaxation rendering these materials less stable.

(c) The NLO properties were measured for only low concentrations (10-20%) of NLO material

in polymer matrix.

Therefore, in the present case, we decided to study in detail the structure and growth behaviour or morphological aspects of optically active NLO crystals like PNA and MNA in various polymer matrices i.e. amorphous PMMA, semicrystalline PEO, PVA, PVAc and Pc, etc. We used high levels of additive concentration and investigated the various growth patterns. This chapter presents the interesting results obtained in these studies.

6.2 Experimental

The polymers dispersed PNA or MNA containing composite films were grown by different techniques and under different conditions. The various polymers and organic crystals such as PNA and MNA were procured from sources indicated in Table 6.2A.

Table 6.2A The list of materials used and their source.

Material	Source
PNA	BDH, England
MNA	BDH, England
PEO	Polyox WSR, BDH, England, MW= 3×10^5
PMMA	Gujpol, 932HR, GSFC, India
PVA	Lobachemie, MW= 75,000, India
PVAc	Polyvac, polychem , MW=60,000, India
Pc	Lexan 101, GE plastics

. The complete details of preparation of sample by different techniques have already been described in section 2.8. A brief summary of growth conditions used is given in Table 6.2B.

The structure, growth and morphology of these composite films were investigated by WAXD and optical polarising microscope. In order to investigate the amount of complex formation if any or the interactions between PNA or MNA and the polymer matrix, these films were characterised by different techniques such as IR, DSC and TGA. For some composite films, TEM (JEOL, JEM-1200 Ex, electron beam=100KV) was used in order to determine the size of PNA or MNA crystal dispersed in the polymer matrix.

Table 6.2B The type of polymers used and the various conditions of preparation of sample.

Composite	Solvent	Type of films grown	Growth conditions	Composition
PEO-PNA	Methanol	Solution cast (SC)	RT, evaporation and drying.	Concentrations of PNA varied from 10 - 50 wt.%
		Melt crystallization (MC)	Melted at 150°C, crystallized at 40° cooled at RT.	Concentrations of PNA varied from 10 - 50 wt.%.
		Powder blend composite (PC)	Compression moulded under a Pressure of 3000kg/cm^2 and melt Crystallized between teflon sheets.	Concentrations of PNA varied from 10 - 50 wt.%.
PMMA-PNA	Acetone	Solution cast (SC)	RT, evaporation and drying	Concentrations of PNA varied from 10 - 50 wt%.
		Melt crystallization (MC)	Melted at 200°C, crystallized at 60°C Cooled at RT.	Concentrations of PNA varied from 10 - 50 wt.%
		Crystallization under electric field (EC)	ITO/film/ITO on hot plate at 150°C, Electric field applied (12V) for 1 Hour and cooled for 1 hour.	PNA concentration of 30 wt.%.
PMMA-MNA	Acetone	Solution cast (SC)	RT evaporation and drying.	Concentrations of MNA varied from 30 - 50 wt %
		Melt crystallization (MC)	Melted at 180°C and crystallized at RT.	Concentrations of MNA Varied from 30 - 50 wt.%

6.3 Results and Discussion

6.3.1 Structure, Growth and Morphology of PEO-PNA Composite System

The crystallization behaviour of PEO dispersed with PNA was investigated for films prepared by different methods. Fig. 6.1 shows the WAXD scans of solution cast (SC) samples with different concentration of PNA; curves A to E corresponding to PNA concentrations of 10, 15, 35, 45 and 50wt.% respectively. Comparing these with the WAXD scans of pure PNA and PEO (Fig. 6.2a and b respectively), very large increase or decrease in intensities for some of the peaks are observed in PEO-PNA. The d-values and the relative intensities derived from these data are shown in Table 6.3 and Table 6.4. These various d-values indicate that the crystalline phases of PNA and PEO in these (SC) samples are the same as those of the original components. However, the relative intensities of the peaks, especially those corresponding to (101) and (012) reflections of PNA are distinctly different in the (SC) samples. PEO itself has only two major peaks in its WAXD scans designated as peak I and peak II (see Fig. 6.2b) in which peak I has much higher intensity than peak II. The WAXD scans of PEO-PNA samples with low concentration of PNA are similar to this. On the other hand, when PNA concentration is increased beyond 20%, there is a large change in the relative intensities of these peaks and peak II becomes more intense compared to peak I. The intensity of major reflections from PNA crystallites in the PEO-PNA composite films are also distinctly different from those in pure PNA. In the case of pure PNA, there are a number of sharp and intense peaks in the WAXD pattern. The peak 1 corresponding to 012 reflection ($2\theta \approx 25^{\circ}$) has the strongest intensity and peak 3 ($2\theta \approx 12^{\circ}$, (101) reflection) is of a medium intensity (see Fig. 6.2a). On the other hand, in PEO-PNA (SC) samples peak 1 of PNA has quite low intensity while peak 3 has the highest thus suggesting distinctly different type of growth pattern and/or orientation of crystallites with respect to film surface in these samples.

The variation of intensities of the different peaks in the WAXD scans PEO-PNA (SC) films with respect to composition is shown in Fig. 6.3. Some of the peaks show a maximum at a particular concentration of about 35% PNA. If PEO-PNA had contained the two phases with no interaction between them, just as in a mixture of the two components existing independently, then there would not have been any change in the relative intensities of WAXD peaks in this system. Further, a decrease or increase of the concentration of one component would have caused a corresponding decrease or increase in intensity of WAXD peaks

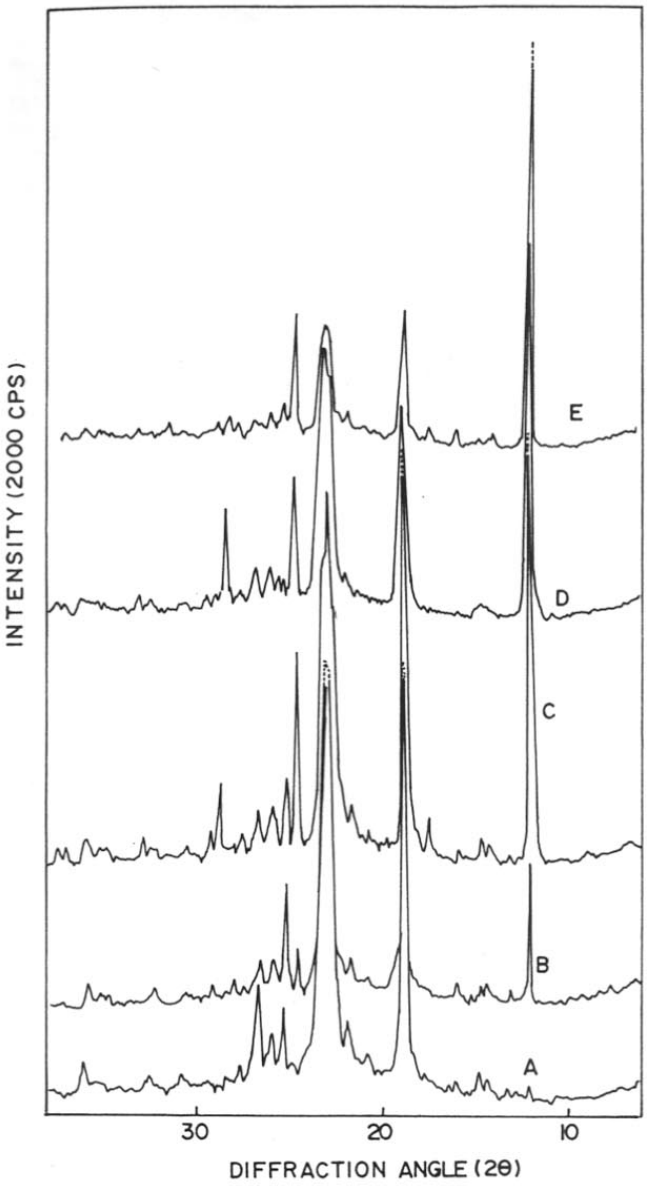

Figure 6.1 WAXD scans for PEO-PNA (SC) samples with different concentrations of PNA. Curves A-E correspond to PNA concentrations of 10, 15, 35, 45 and 50 wt.% respectively.

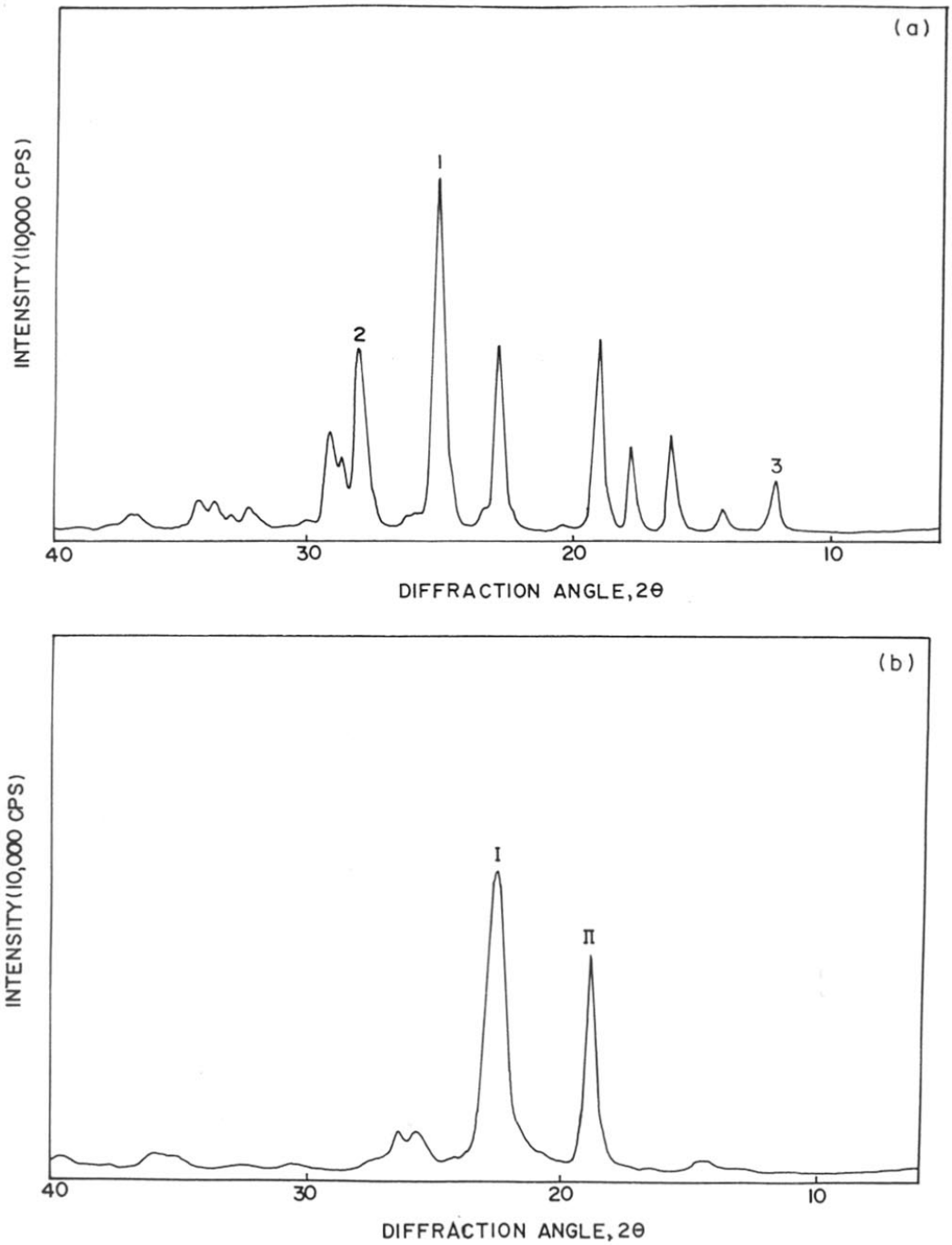

Figure 6.2 (a) WAXD scan for pure PNA (b) WAXD scan for pure PEO.

Table 6.3 X-ray diffraction in PEO-PNA grown by solution cast technique

Compositions of PNA in PEO										Remarks	
10%		15%		35%		45%		50%		PNA	PEO
d(obs)	I/I_o	d(obs)	I/I_o	d(obs)	I/I_o	d(obs)	I/I_o	d(obs)	I/I_o	hkl	hkl
7.20	3	7.20	43	7.20	100	7.20	100	7.20	100	101	
6.61	2	6.61	4								
								6.19	3		021
6.11	4	6.11	6	6.07	2					010	
5.91	5	5.91	5	5.91	3	5.95	4	5.91	2		110
5.47	4	5.47	7	5.47	1			5.51	4	110	
4.98	5			4.98	5			5.04	3	011	
4.67	88	4.67	80	4.67	58	4.65	54	4.67	31	111	120/111
4.23	9	4.23	9	4.23	4					002	
4.04	14			4.06	7	4.02	11	4.06	7	102	
				3.85	45	3.85	64	3.85	25	211	
3.81	100	3.81	100	3.80	35	3.81	73	3.82	24		112
3.58	7	3.59	16	3.59	26	3.59	37	3.60	29	202	
3.51	17	3.51	36	3.51	10	3.50	11	3.52	9	012	
3.41	13	3.41	14	3.41	7	3.41	13	3.43	7	310	033
3.32	21	3.32	14	3.31	7	3.31	14	3.33	5	112	131
3.22	6	3.22	7	3.21	4	3.22	7	3.22	4	311	200
				3.08	10	3.13	28	3.07	4	400/212	
		3.03	6	3.04	4	3.03	7			020	
2.90	4			2.90	2	2.90	5			401/120	
								2.84	5	021	
2.75	4	2.76	5			2.74	5			121	211
				2.71	3	2.70	6			220	

as per monoclinic structure of PNA
a = 12.33 Å, b = 6.07 Å and c = 8.59 Å, β = 91.45°
and monoclinic structure of PEO
a = 8.02 Å, b = 13.4 Å, c = 19.2 Å, β = 126°, obs: observed.

Table 6.4 X-ray diffraction of pure PNA and PEO

PNA 100%			PEO 100%		
d(cal)	I/I_o	hkl	d(cal)	I/I_o	hkl
7.12	15	101			
			6.18	5	021
			5.83	5	110
5.44	28	110			
4.96	25	011			
4.61	54	111	4.60	70	120/111
4.32	3	210			
3.88	54	211			
			3.82	100	112
3.74	8	301			
3.51	100	012			
3.40	6	310	3.40	14	033
3.38	6	112	3.34	14	131
3.18	52	311	3.24	5	200
3.07	21	212			
3.04	29	020			
2.95	4	120			
2.79	8	121	2.79	3	211
2.72	6	220			
2.63	9	411			
2.61	10	203			
2.44	6	320			

as per the monoclinic structure of PNA
$a = 12.33$ Å, $b = 6.07$ Å, $c = 8.59$ Å and $\beta = 91.45°$
and the monoclinic structure of PEO
$a = 8.02$ Å, $b = 13.4$ Å, $c = 8.59$ Å and $\beta = 126°$

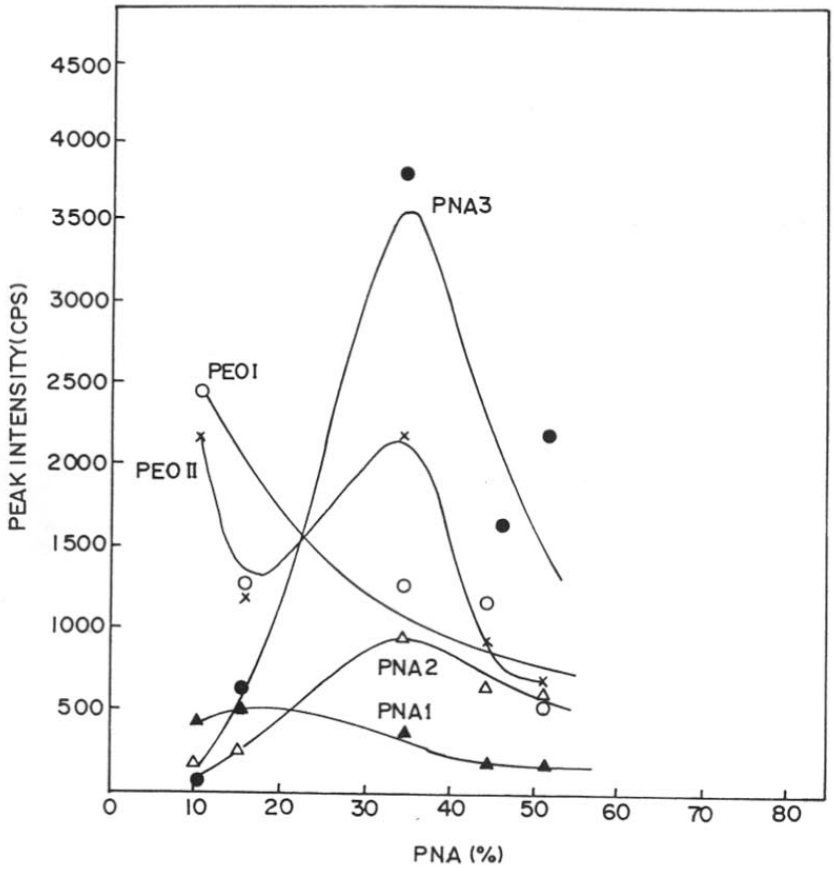

Figure 6.3 The variation of intensities of the different WAXD peaks in PEO-PNA (SC) films with respect to composition.

attributed to that component. For example, one would have then expected the PEO peaks I and II to decrease in intensity monotonically with the increase of PNA concentration. Similarly, the peaks 1, 2 and 3 of PNA would have increased in intensity without any change in the ratios of their relative intensities. However, the present observations show a distinctly different behaviour. The intensity of peak I of PEO show a continuous decrease in intensity but that of peak II does not. Even the major intense peak of PNA decreases drastically, while a minor (101) reflection (peak 3) exhibits a maximum intensity in PEO-PNA (SC) samples. These peculiar finding can be understood in terms of preferential growth and nucleation of crystallites along certain directions or their orientation which are discussed in greater detail later in this chapter.

The PEO-PNA (MC) samples show a different trend in the variation of the WAXD reflections than that noted in (SC) samples. Figure 6.4 depicts the WAXD scans for these samples and Fig. 6.5 shows the variation of intensities of corresponding peaks with respect to PNA concentration. The intensities of PEO peak I decrease monotonically while PEO peak II shows a maximum in intensity (at 25%) with the increase in concentration of PNA. The PNA peaks on the other hand show little variation up to a concentration of 40% of PNA, above which there is sudden increase in their intensities. The peak 3 of PNA in these (MC) samples are weak (compare Figs. 6.1 and 6.4, at $2\theta \approx 12^{\circ}$). The detailed analysis of intensities of various peaks have been presented in Table 6.5.

The powder blended compression moulded samples (PC) exhibit a mixed trend (see Fig. 6.6). The variation of intensities of peaks I and II of PEO are similar to PEO-PNA (MC) samples but the PNA peak 3 which was weak in (MC) samples appears quite prominent at all compositions studied (10 to 50% of PNA).

The morphology of these films were investigated using optical microscopy. PEO has large spherulitic morphology (Fig. 6.7a) while PNA consists of small globular type crystals (Fig. 6.7b). Further, PNA shows only weak birefringence (these crystals are not completely visible under cross polarised conditions). On the other hand, the PEO-PNA composite films exhibit bright shiny crystals which are placed in a spherulitic-like morphology. Figures 6.7c and 6.7d show the morphology of PEO-PNA (SC) films containing 10% to 30% PNA. It can be seen that the morphologies are PEO like but the internal structure of the spherulite is quite different. It contains intensely bright fibrils which in higher magnification appear similar to the transcrystallinity observed in polymers nucleating and crystallizing on fibres.[40,41] The

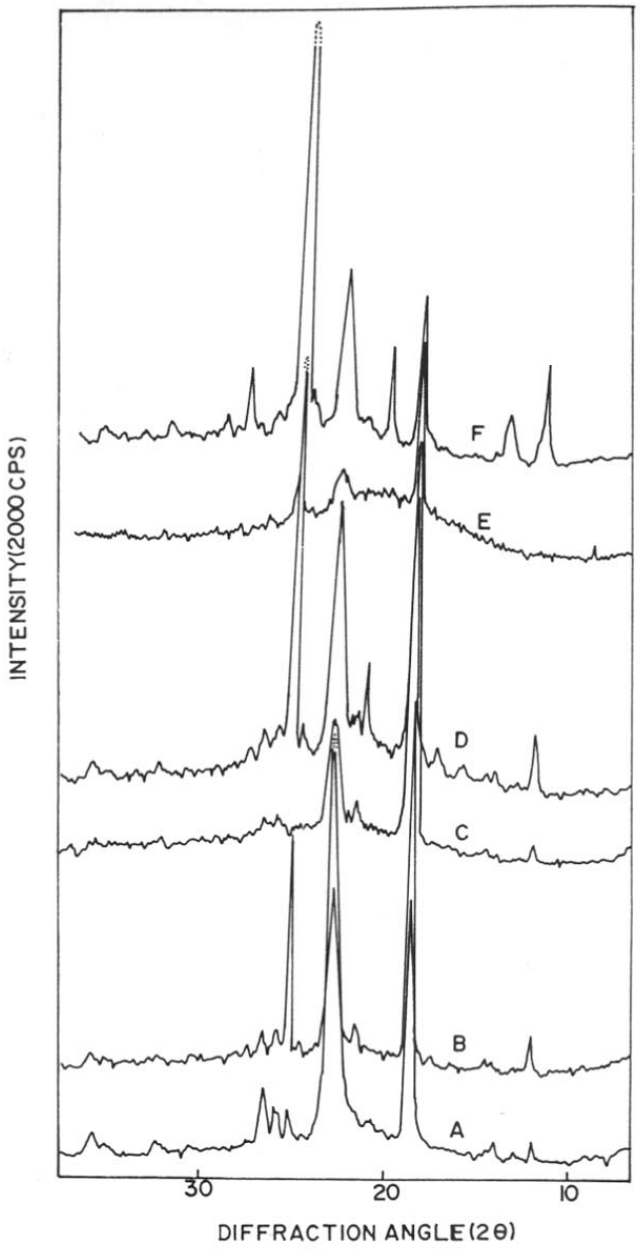

Figure 6.4 WAXD scans for PEO-PNA (MC) samples with different concentrations of PNA. Curves A-F correspond to PNA concentrations of 10, 15, 25, 35, 45 and 50 wt.% respectively.

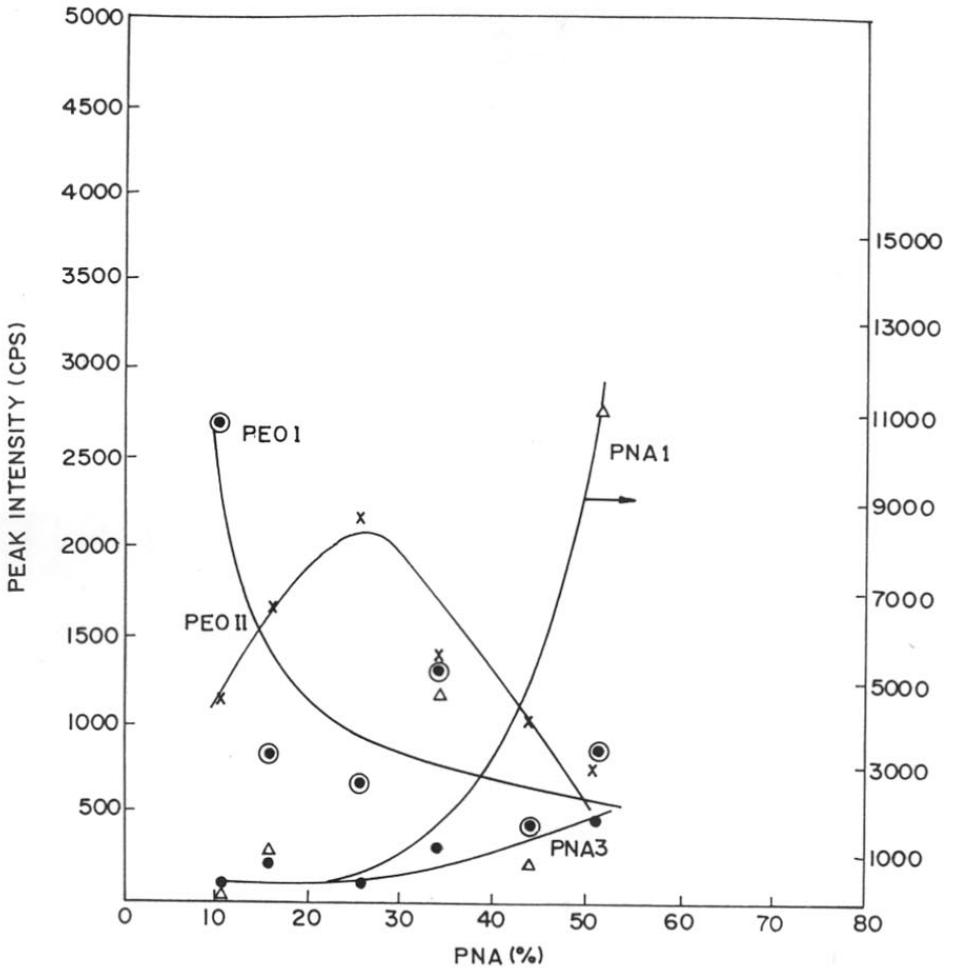

Figure 6.5 The variation of intensities of the different WAXD peaks in PEO-PNA (MC) films with respect to composition.

Table 6.5 X-ray diffraction in PEO-PNA grown by melt

Compositions of PNA in PEO												Remarks	
10%		15%		25%		35%		45%		50%		PNA	PEO
d(obs)	I/I_o	d(obs)	I/I_o	d(obs)	I/I_o	d(obs)	I/I_o	d(obs)	I/I_o	d(obs)	I/I_o	hkl	hkl
								9.40	10				
7.14	4	7.20	12	7.20	5	7.20	6			7.20	4	101	
6.11	4	6.11	4			6.11	3			6.15	2	010	
		5.95	5			5.95	2						
						5.51	3			5.44	1	110	
						5.06	5					011	
4.65	43	4.70	100	4.65	100	4.67	29	4.65	100	4.65	7	111	120/111
				4.21	10					4.27	5	002	
		4.15	9			4.15	12					300	
		4.06	13	4.04	13	4.08	8			4.04	2	102	
				3.96	12	4.00	7						
				3.85	29			3.88	38			211	
3.82	100	3.85	49	3.82	31	3.85	28	3.83	40	3.82	8		112
								3.72	26			301	
		3.59	9			3.59	7			3.56	3	202	
3.49	9	3.51	64			3.51	100	3.49	81	3.51	100	012	
3.40	9	3.43	12	3.41	10	3.43	6					310	033
3.33	12	3.34	11	3.31	9	3.31	6	3.31	19	3.31	2	112	131
		3.23	8			3.24	4	3.13	14	3.14	4	311	200
										3.08	1	400/212	
										3.03	2	020	

as per monoclinic structure of PNA

a = 12.33 Å, b = 6.07 Å and c = 8.59 Å, $\beta = 91.45^{\circ}$

and monoclinic structure of PEO

a = 8.02 Å, b = 13.4 Å, c = 19.2 Å, $\beta = 126^{\circ}$, obs: observed.

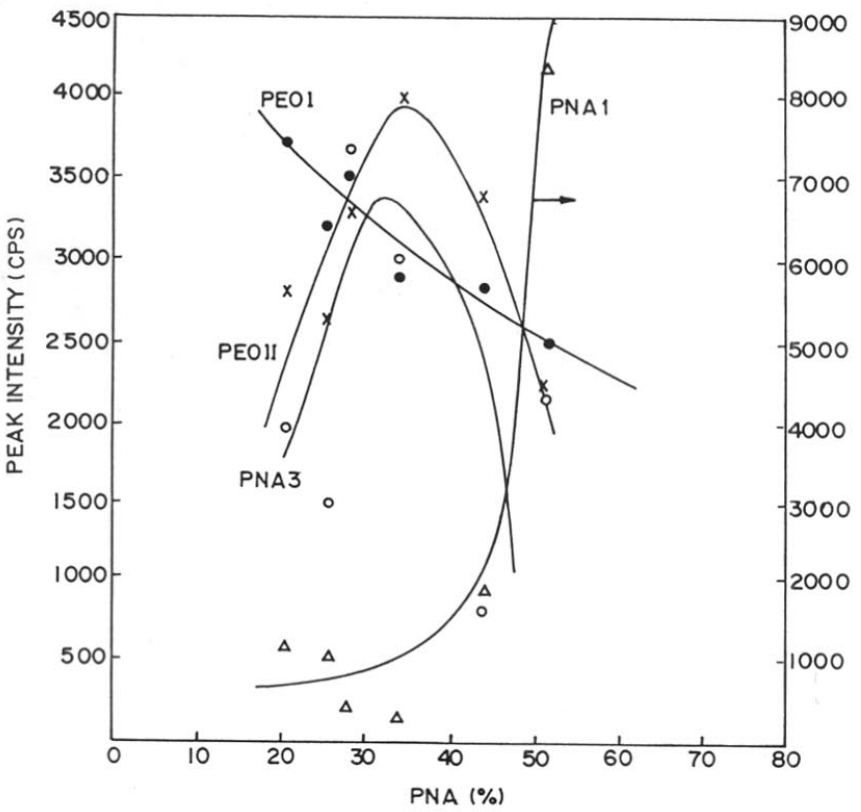

Figure 6.6 The variation of intensities of the different WAXD peaks in PEO-PNA (PC) samples with respect to PNA concentration.

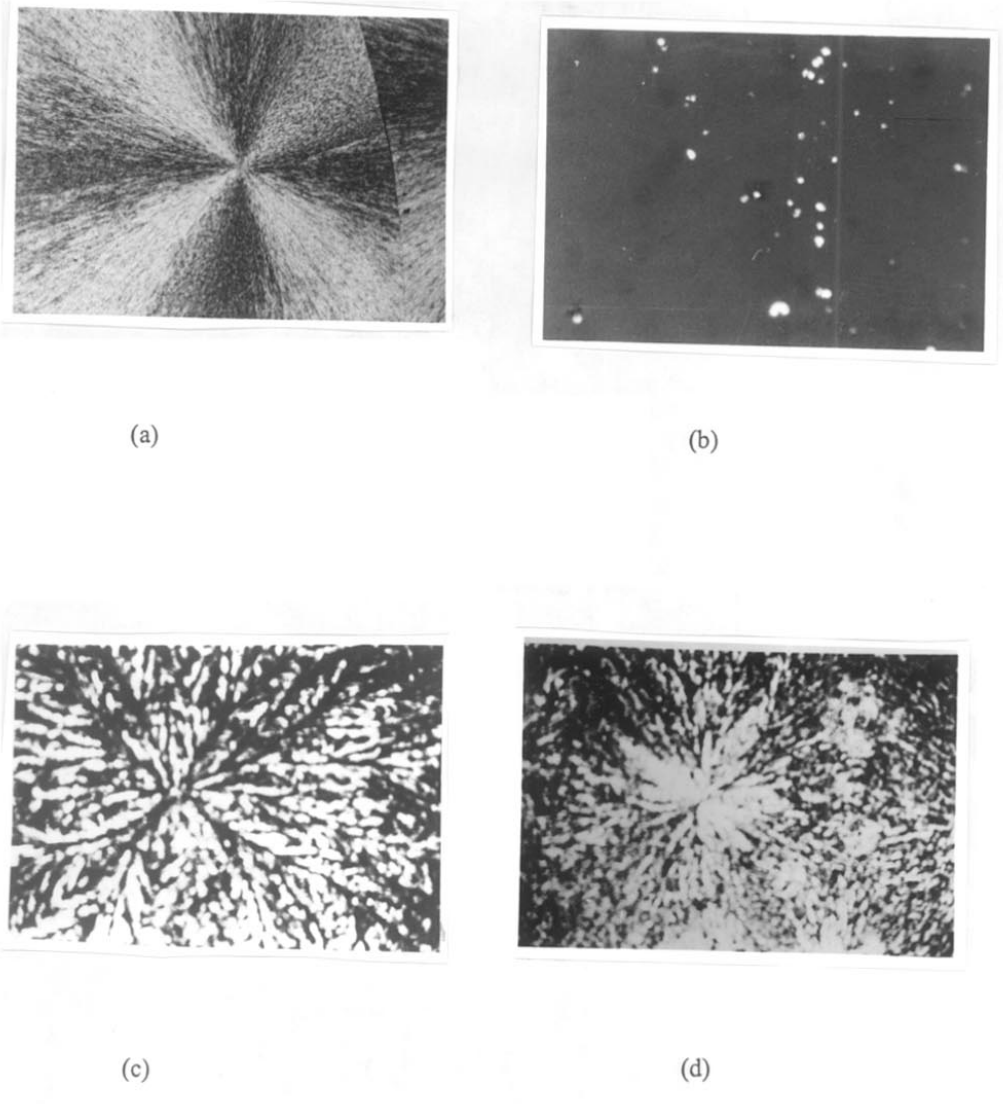

Figure 6.7 Optical micrographs for (a) pure PEO (b) pure PNA (c) PEO-PNA (SC) films of 10% and (d) 30% PNA respectively. (net magnification = 450x).

crystalline branches in these spherulities are widely spaced than those in PEO. When the PNA concentration is increased beyond 40%, the morphology changes to a distinctly two phased type as shown in Fig. 6.8b. It is evident from these micrographs that the samples contain both spherulitic type as well as tiny needle shaped crystals. At even higher concentration of PNA, that is beyond 70% the morphology consists of large sheaf like crystals emerging from a nucleating centre (see Fig. 6.8c). It is interesting to note that these are highly birefringent (very bright under cross polarised condition and contain thick crystalline arms with a large number of polymer- like crystallites nucleating along their edges which are distinctly seen at higher magnification (Fig. 6.8d). These features render them to be quite bright but with non-sharp boundaries at lower magnification; hence, it is difficult to record their micrographs.

In order to confirm the type of interaction between PEO and PNA and to check the possibility of the formation of a complex, the melting points were determined by an optical microscope with hot stage as well as by a differential scanning calorimeter. Figure 6.9 presents the results of melting point determination for different compositions of PEO-PNA. It is seen that a single melting point is observed at the extreme compositions (< 35% or > 70% PNA). For the mid range of compositions (40-70% PNA) there are two melting points of which the lower melting point is close to that of PEO while the higher one is likely to be due to the PNA crystals. However, there is significant lowering of melting points for both components. This can be attributed to dilution effect, which of course, presumes large interaction and good miscibility of components. A single melting point at the extreme compositions strongly suggests this possibility. The two melting points at the intermediate compositions can be due to the formation of two types of crystals/two phase morphology (see Fig. 6.8). The melting behaviour for a number of PEO complexes with inorganic salts as well as urea has been reported in the literature. In those cases, the new melting peaks in the DSC were observed at certain compositions with corresponding new WAXD patterns, suggesting new crystal structure and complex formation. The results presented here do not show any evidence for the development of new crystal structure but indicate only the occurrence of modification of crystal growth habit.

Infrared (IR) absorption spectra were recorded for the PEO-PNA composite film (50% PNA) as well as for the individual components (Fig.6.10). Table 6.6 gives the comparison of the IR data (obtained from the Fourier transform IR print out) for the PEO-PNA along with pure PEO and pure PNA. The underlined absorption bands clearly show changes in frequency

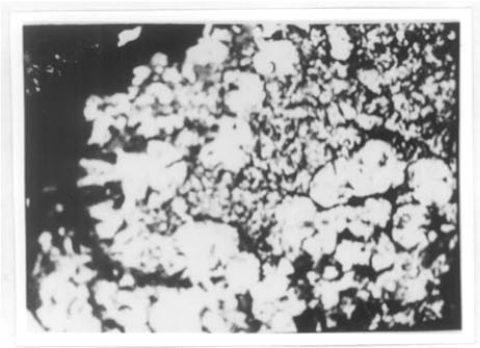

(a)

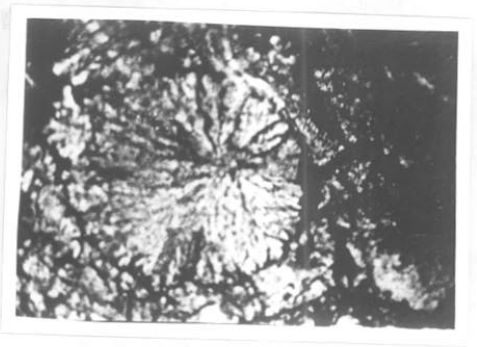

(b)

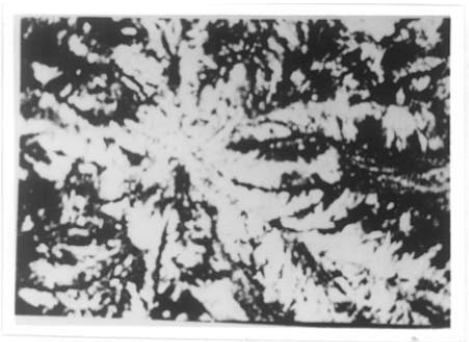

(c)

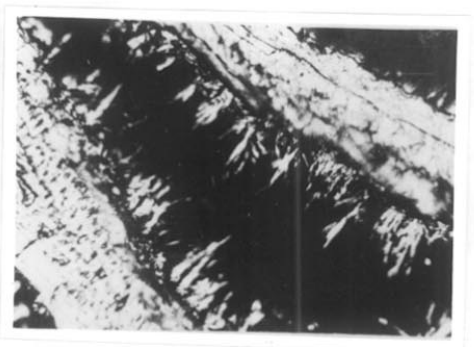

(d)

Figure 6.8 Optical micrographs for PEO-PNA (SC) films containing (a) 40% (b) 60% (c) 70% PNA respectively. (net magn. = 450x). Panel (d) is same as panel (c) but at higher magnification (net magn.= 700x).

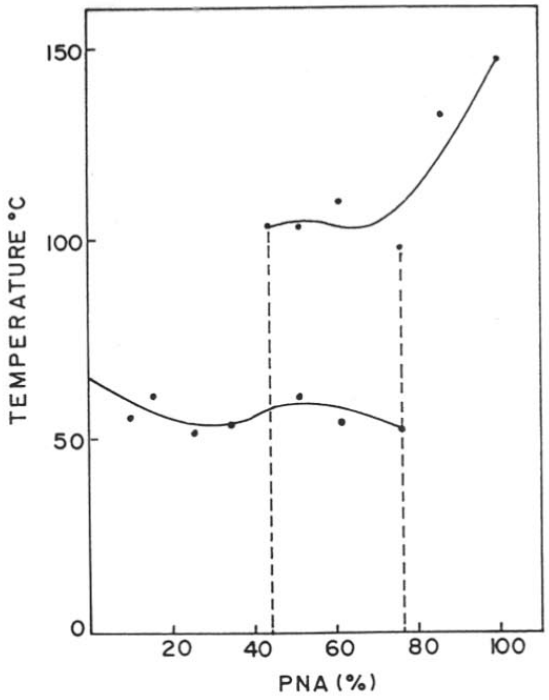

Figure 6.9 Melting behaviour of PEO-PNA composites for different compositions.

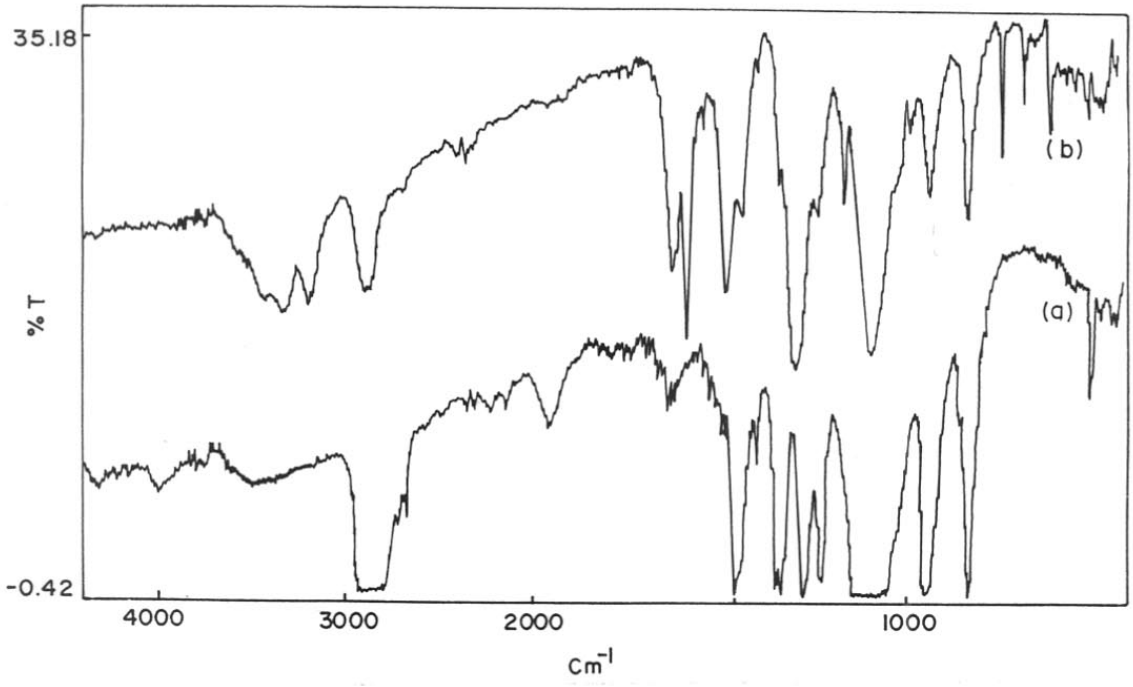

Figure 6.10 IR spectra of PEO-PNA film (b) as compared with pure PEO (a).

Table 6.6 IR absorption of PEO- PNA complex (50% PNA) as compared with pure components

PEO	PNA	PEO-PNA	Remarks
	3500 (ms)		
	3360 (s)	3380 (vs,br)	N—H stretch and hydrogen bonding
	3200 (vvw)	3200 (sh)	
	2900 (s)		
2830 (s,br)	2860 (sh)	2860 (s)	CH_2—O deformation
1950 (m,br)			
1645 (sh)			
1615 (m)	1625 (s)	1620 (sh)	
1585 (sh)	1590 (s)	1590 (vvs)	—R cissor NO_2
1500 (sh)	1490(sh)		
	1475 (s)	1475 (s)	NO_2 assynetric stretch
1435 (s)	1440 (sh)	1440 (sh)	
	1390 (sh)		C—NH_2 stretch
	1360 (sh)		
1340 (s)		1340 (sh)	CH_2 wagging
	1320 (sh)	1300 (vvs)	
1280 (s)	1280 (vvs)		
1235 (sh)		1240 (sh)	
	1180 (ms)	1175 (sh)	C—O—C deformation
1125 (s)	1130 (sh)	1130 (sh)	C—O—C deformation
1110 (vs)	1110 (s)	1100 (s)	
1080 (vs)		1050 (sh)	C—O—C deformation
1030 (ms)		1025 (sh)	
	995 (vvw)	990 (ms)	δ CH out of plane deformation aromatic ring
950 (s)	955 (vvw)	935 (ms)	
835 (s)	840 (ms)	840 (ms)	
	820 (sh)	810 (sh)	δ CH out of plane deformation aromatic ring
		780 (sh)	
	752 (ms)	750 (ms)	

s , strong; m , medium ; v, very ; br, broad ; sh, shoulder.

and intensity; there are shifts of the order 20-30 cm^{-1} in the N—H stretching (3360 cm^{-1}), C—N deformation (1320 cm^{-1}), C—O—C deformation (1080-1110 cm^{-1}), and CH_2— O symmetry (2830 cm^{-1}) modes. There is also strong absorption at 3380 cm^{-1}. These results indicate that PEO and PNA interact through hydrogen bonding which takes place at the NH_2 of PNA and the C—O—C moities of PEO. It may be noted that entirely new peaks are not observed in the IR spectra.

PEO and PNA both crystallize in a monoclinic type of structure[42-44], PEO having lattice parameters of a_p = 8.02 Å, b_p = 13.4 Å, c_p = 19.2 Å and β_p = 126° and PNA having a_{na} = 12.33 Å , b_{na}= 6.07 Å, c_{na}= 8.59 Å and β_{na} = 91.45° respectively. The PNA by itself is a centrosymmetric molecule that crystallizes in antiparallel configuration.[43-45] Hence, PNA does not exhibit NLO second order effects and has weak birefringence. According to the lattice mismatch theory[46,47], the lattice mismatch δ_l, between a_P of PEO and c_{na} of PNA ($|a_p-c_{na}|/(|a_p|)$ is 7.1%. Further, the mismatch between b_p of PEO and a_{na} of PNA is 7.9%. These are well within the limits of 15%. It may be mentioned here that PEO also has a strong tendency for complex formation with compounds containing NH_2 groups (for example urea), through hydrogen bonding between the oxygen atom of PEO and NH_2 group of urea.[48,49] Similar interactions can be expected for PEO with PNA as well. Figure 6.11 A, B and C illustrates schematically how the PNA planes are oriented. However, although a hydrogen bonding type interaction exists in these, there are no new crystalline structure observed in the WAXD scans as noted previously. Thus,the complex formed through hydrogen bonding does not appear to be crystalline in nature in this case. Nonetheless, the crystallization behaviour and resulting morphology are greatly affected by the presence of PEO in the solution or in the melt. One may consider that one component would be crystallizing out first and acting as a substrate for the other. However, the crystallization and growth of the first component itself are affected due to the interactive molecules present in the solution. Since there is a good lattice match between the {ab} planes of PEO and the {ac} planes of PNA, one expects large changes in the growth pattern along the same directions, leading to changes in intensities of the peaks corresponding to reflections such as (120) of PEO and (101) of PNA. This is observed in (SC) and (PC) samples wherein (120) reflection (peak II) of PEO and (101) reflection of PNA (peak III) exhibit large change in their intensities. Thus, the crystallites in PEO-PNA composite films are constrained to grow along a certain direction due to mutual interaction between them.

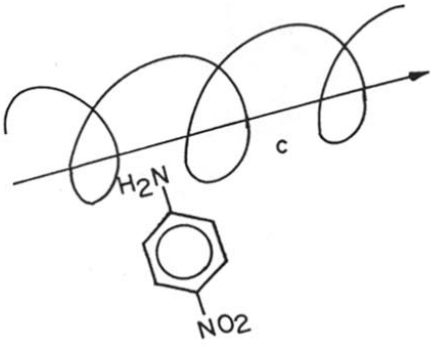

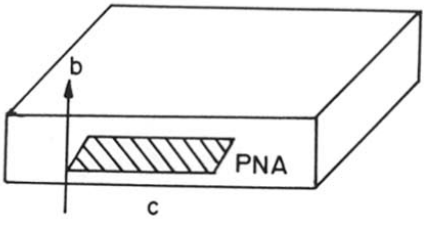

(C)

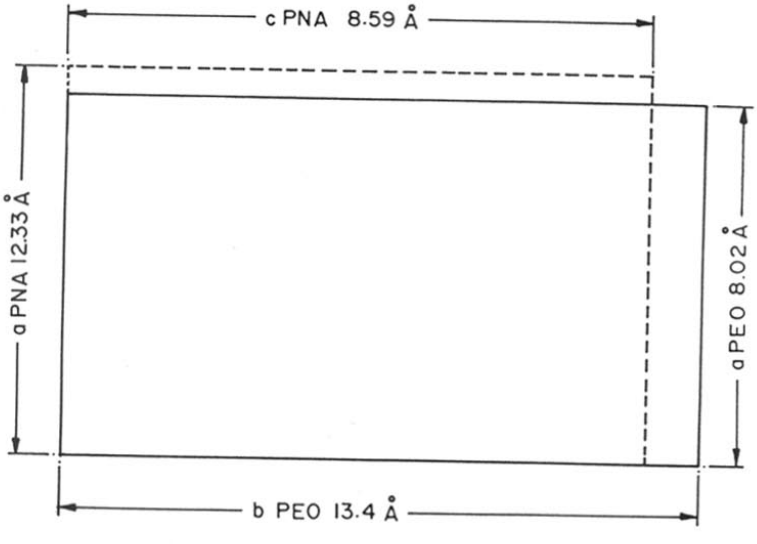

Figure 6.11 (A) Schematic sketch of molecular orientation between PNA and PEO
(B) Sketch of PNA planes along the film surface
(C) Sketch of orientation of PNA planes in PEO

From these various results obtained it can be concluded that there is interaction due to hydrogen bond formation between ether group of PEO and NH_2 groups of PNA. Due to close lattice mismatch between the crystallites of the two components, the former tends to align the molecules during the early stages of crystallization while the latter leads to preferential growth of crystals along certain planes.

6.3.2 Structure, Growth and Morphology of PMMA-PNA Composite System

The structure, growth and morphology of a composite made by dispersing para nitroaniline (PNA) in poly methylmethacrylate (PMMA) was investigated with respect to different crystallization methods, composition and application of electric field.

The PNA-PMMA composite films grown from solution casting technique were flexible and transparent up to a PNA concentration of 30% while those having high concentration of PNA were brittle and opaque. This suggests that the film having low concentration of PNA could be amorphous or their crystallite size was much less than 1000 Å. This was confirmed by optical polarising microscope, which showed very tiny dots less than 1 μm dispersed in amorphous matrix. The transparency and quality of the films depended very much on the technique and conditions used for growing them.

Figure 6.12 shows the WAXD scans for solution cast films of PNA-PMMA containing various concentration of PNA. Curves A to E correspond to PNA concentration of 10, 18, 30, 40 and 45 wt.%. On comparing this figure with the WAXD scan of pure PNA (see Fig. 6.2a) these curves clearly bring out the effect of the polymer on the structure and growth behaviour of PNA crystals. It is seen that with the increase of polymer content, the major reflections occurring in the 2θ region of 10 to 25° decrease considerably and the films become more amorphous. Interestingly, there are a few diffraction peaks appearing even at low concentration which become more prominent at a certain composition i.e. 30%. At lower concentration the size of the crystals are too small to be detected by X-ray. The comparison of relative intensities of various peaks and the estimated 'd' values derived from these scans is presented in Table 6.7. The detailed analysis of the results show that most of the reflections correspond to monoclinic crystalline phase of free PNA (PMMA being amorphous) with a = 12.33 Å, b = 6.07 Å and c = 8.59 Å and $\beta = 91.45°$. The new diffraction peaks, which become prominent at a certain composition above 30 wt.% of PNA, especially the peak at 2θ of 24.1° could not be assigned to any of the reflections from monoclinic structure of PNA. Hence,

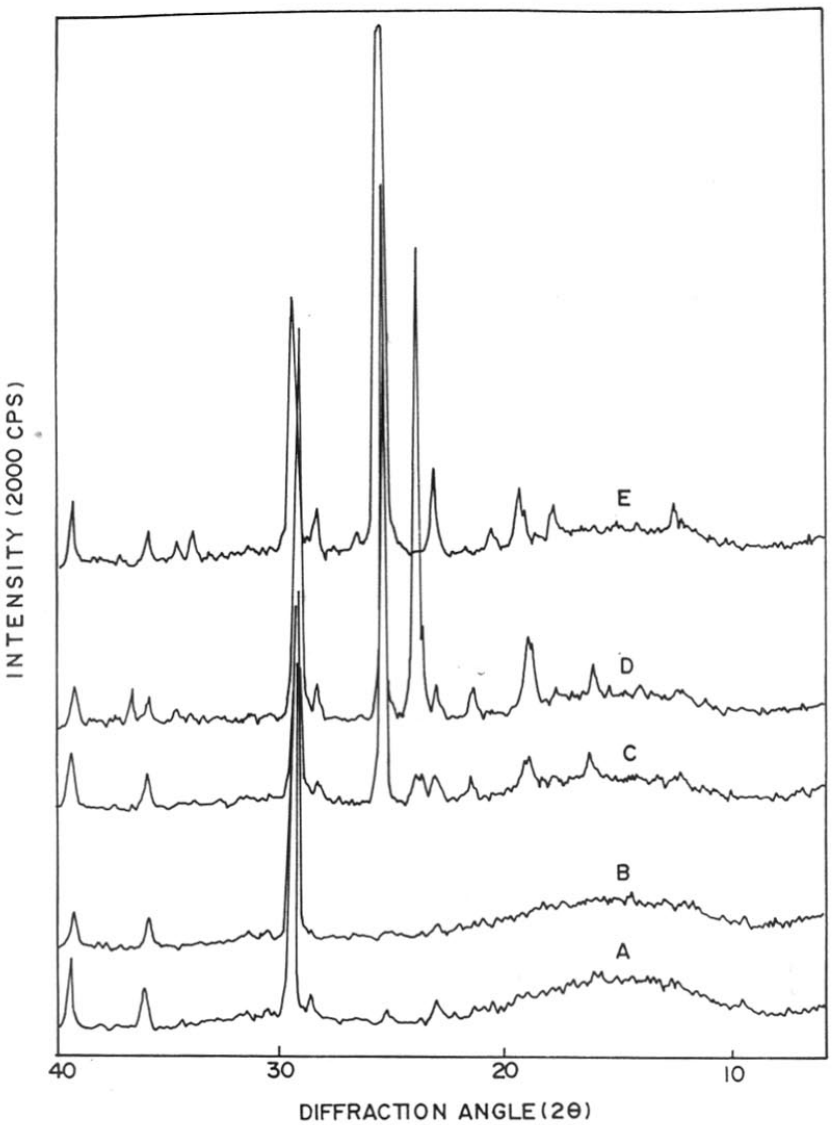

Figure 6.12 WAXD scans for PMMA-PNA (SC) samples with different concentrations of PNA. Curves A-E correspond to PNA concentrations of 10, 18, 30, 40 and 45 wt.% respectively.

Table 6.7 X-ray diffraction in PMMA-PNA composite film grown by solution cast technique

PNA 100%			10%		18%		30%		40%		45%			
d (obs)	I/I_0	hkl*	d (obs)	I/I_0	d (obs)	I/I_0	d (obs)	I/I_0	d (obs)	I/I_0	d (obs)	I/I_0	d cal**	hkl
7.19	15	101	7.08	7	7.08	11	7.08	8	7.19	8				
											6.97	3	6.97	011
6.23	7	200			6.11	16	6.23	8					6.29	111
									5.71	8			5.69	201
		110					5.41	12	5.47	12			5.50	020
4.98	25	011					4.95	7	4.98	8	4.92	3	4.95	300
							4.67	11	4.69	15			4.69	021
4.64	54	111					4.62	10	6.64	16				
											4.55	4	4.50	002
4.33	3	210	4.33	6										
		300					4.15	5						
							4.11	8	4.13	8			4.16	012
3.85	54	211	3.85	7	3.86	12	3.85	7	3.85	8	3.82	5	3.84	202
3.77	8	301					3.75	7	3.75	18				
							3.69	7	3.70	82			3.65	400
3.59	100	012	3.52	5			3.49	100	3.50	100	3.48	100	3.48	022
3.42	6	310												
3.37	6	112									3.33	2	3.38	122
3.16	52	311					3.14	6	3.15	8	3.14	3	3.15	222
3.08		212	3.12	9									3.08	231
3.04	29	020	3.03	100	3.04	100	3.04	55	3.06	67	3.03	15	3.05	420
		021	2.84	5	2.85	10								
2.77	8	121												
2.71	6	220												
2.65	9	411												
2.60	10	013/203							2.64	3	2.63	2	2.63	023/041
									2.59	4	2.58	1	2.58	141
			2.49	10	2.50	14	2.50	7	2.51	6	2.50	2	2.49	313

* As per monoclinic structure , a = 12.33 Å , b = 6.07 Å , c = 8.59 Å and ß = 91.45°

** As per new structure (orthorhombic) , a = 14.7 Å , b = 11.0 Å , c = 9.0 Å and ß = 90°

these peaks must correspond to a new crystalline structure formed possibly due to a complex between PNA and PMMA. The schematic representation of the structure of the complex in new crystalline form is shown in Fig.6.13. It should be noted that the interaction between PNA and PMMA can take place through C=O of PMMA and NH_2 of PNA. The calculations from lattice parameters indicate that the two PNA molecules have six repeat units between them. This tendency of the PNA molecule is encouraged by (a) considerable steric hindrance occurring between NO_2 groups of PNA and methyl groups of PMMA. (b) The hydrogen bond formation between C=O of PMMA and NH_2 of PNA is not a favourable interaction at right angles and the steric hindrance occurring between PNA and the adjacent side chain of the monomer. The detailed analysis of peaks in the table shows that the complex crystallizes in the form of orthorhombic crystalline structure with a = 14.7 Å, b = 11.0 Å , c= 9.0 Å and β = 90°. Thus, these films contain mixed crystalline phases. Also it can be seen from the Fig. 6.12 that there is a strong reflection occurring at low concentration of PNA at 2θ of 29.4° which corresponds to (020) reflection of monoclinic structure of free PNA. This reflection is normally much weaker in the case of pure PNA without any polymer. Such variation in the intensity of the diffraction peak could be due to either preferential growth of the crystallite along certain phase or orientation of crystallites with reference to the film surface.

Figure 6.14 depicts the WAXD scans of PMMA-PNA melt crystallized (MC) samples having PNA concentrations of 10, 18, 30, 40 and 45 wt.%. On comparing the figure with pure PNA structure (see Fig.6.2a) , it can be seen that in this case also, the presence of polymer matrix during the melt crystallization process has a profound effect on the intensities of different reflections especially those corresponding to (020) and (012) reflections from the monoclinic crystalline phase of PNA. At concentrations less than 10%, a broad amorphous background is seen with only one sharp reflection appearing at 2θ of 29.4°. Even in this case, new peaks are observed which do not correspond to the monoclinic crystalline phase of pure PNA. The new reflections have been assigned according to new crystal structure that is orthorhombic phase of the complex. The comparison of relative intensities of these various peaks and the 'd' values estimated is presented in Table 6.8. At high concentrations of PNA (45%), a new major diffraction peak at 2θ of 24.0° is seen which corresponds to (400) reflection from the crystallites having orthorhombic structure.

Figure 6.15 shows the X-ray diffraction scans for PNA-PMMA composite film having same concentration (40%) of the additive but grown in the melt (curve M), solution (curve S)

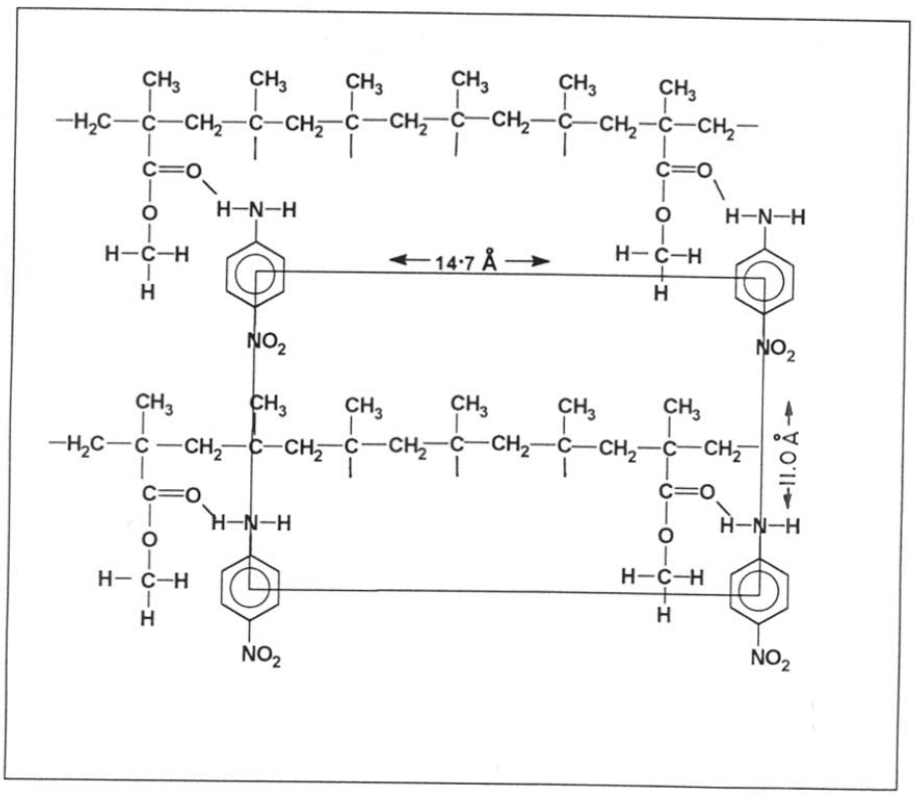

Figure 6.13 Sketch of PMMA-PNA complex crystallizing in new crystalline (orthorhombic) structure of PNA.

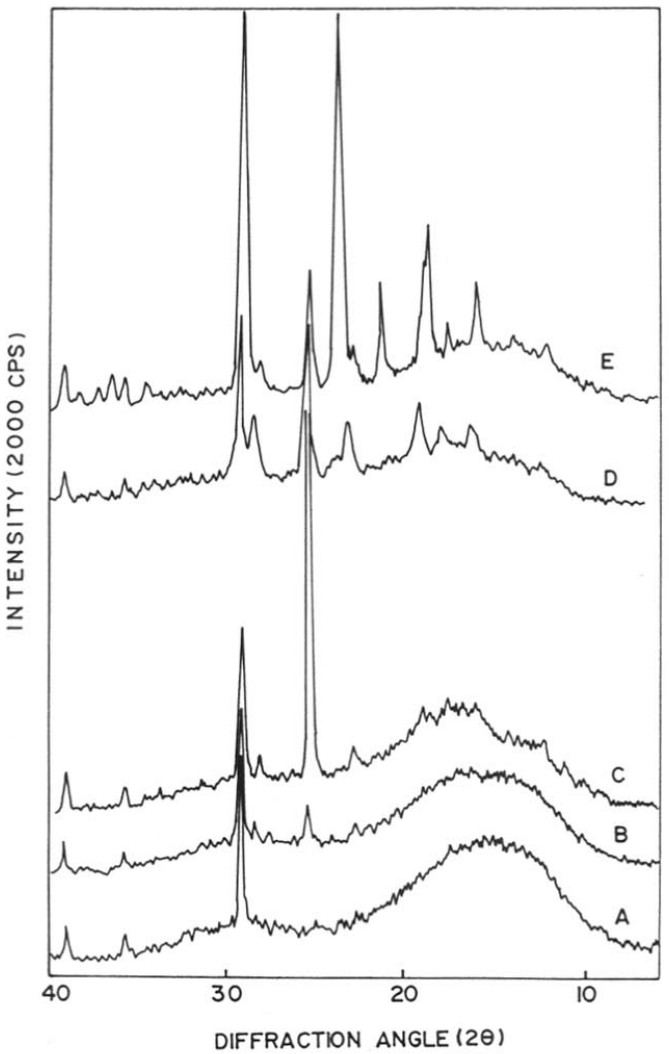

Figure 6.14 WAXD scans for PMMA-PNA (MC) samples. Curves A-E correspond to PNA concentrations of 10, 18, 30, 40 and 45 wt.% respectively.

Tables 6.8 X-ray diffraction in PMMA-PNA films grown by melt crystallized technique

PNA 100%			10%		18%		30%		40%		45%			
d (obs)	I/I_0	hkl*	d (obs)	I/I_0	d (obs)	I/I_0	d (obs)	I/I_0	d (obs)	I/I_0	d (obs)	I/I_0	dcal**	hkl
7.19	15	101					7.19	7	7.08	11	7.19	6		
6.23	7	200					6.15	7			6.23	6	6.29	111
5.47	28	110					5.47	10	5.37	25	5.47	16	5.50	020
4.98	25	011	5.03	18			4.98	11	4.90	22	4.98	10	4.95	300
											4.69	27	4.69	021
4.64	54	111	4.57	14			4.64	10	4.59	38	4.64	20		
4.33	3	210												
											4.13	18	4.16	012
3.85	54	211					3.85	7	3.81	38	3.85	11	3.84	202
3.77	8	301									3.75	44		
											3.69	100	3.68	400
		202	3.55	13										
3.49	100	012			3.48	38	3.48	100	3.48	93	3.49	23	3.48	022
3.42	6	310												
3.37	6	112												
		312			3.22	24							3.25	411
3.16	52	311					3.15	12			3.15	8	3.15	222
3.08	21	212			3.12	30	3.07	38	3.12	49	3.07	86	3.08	231
3.05	29	020	3.05	100	3.04	100			3.05	100			3.05	420
2.95	4	120												
2.77	8	121												
		410									2.73	4	2.75	412
2.71	6	220												
2.65	9	411					2.65	6	2.63	11			2.63	023/232
2.60	10	013/023							2.57	11	2.59	4	2.59	141
			2.50	14	2.50	14	2.50	6	2.50	12	2.50	5	2.49	313
2.43	6	122									2.46	5	2.46	502

* As per monoclinic structure , a = 12.33 Å , b = 6.07 Å , c = 8.59 Å and ß = 91.45°

** As per new structure (orthorhombic) , a = 14.7Å , b = 11.0 Å, c = 9.0 Å and ß = 90°

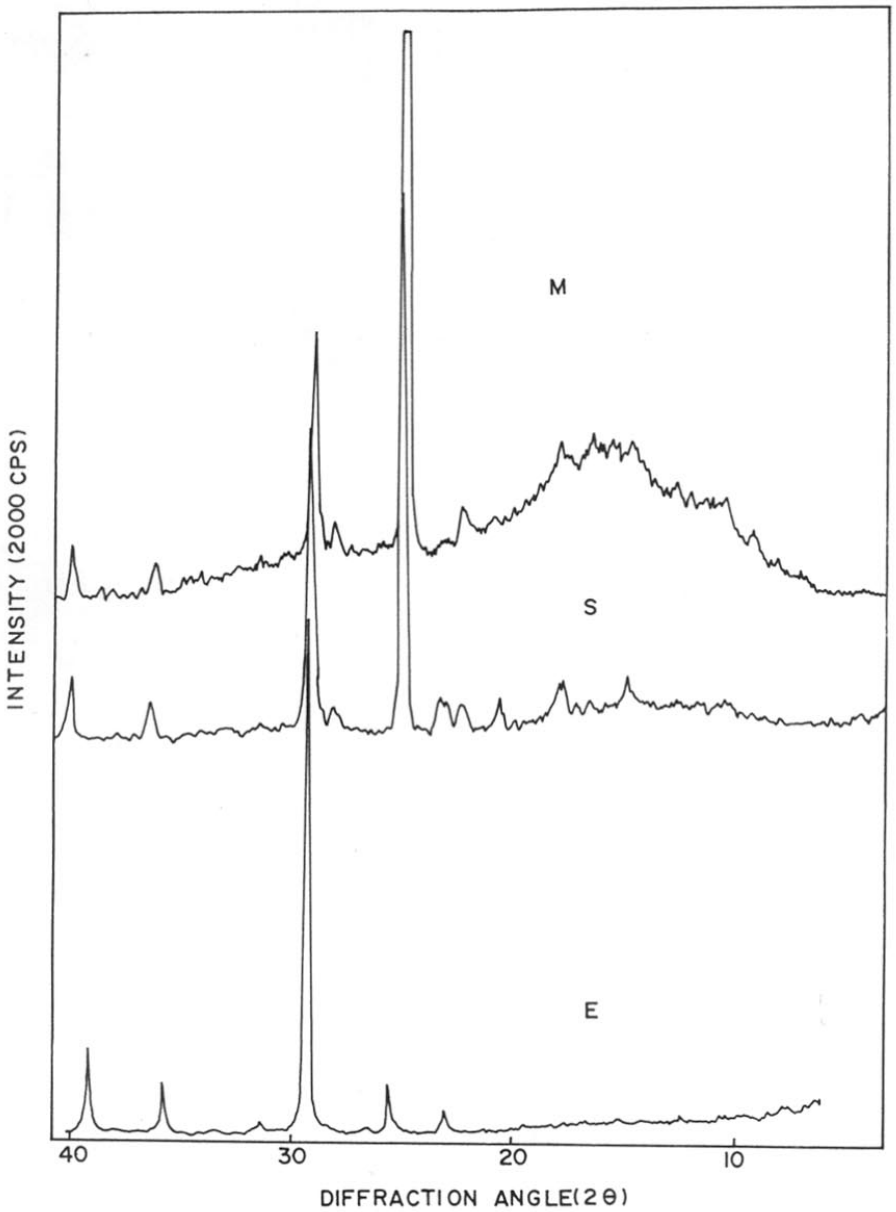

Figure 6.15 WAXD scans for PMMA-PNA composite film having same concentration of PNA (40%) grown under melt (curve M), solution (curve S) and with applied field (curve E)

and with applied field (curve E). The drastic reduction of reflection from (012) and tremendous increase of intensity from (020) reflection of monoclinic phase of PNA is noticed when the growth takes place in the presence of electric field. The detailed analysis of the relative intensities and the 'd' values etc. is presented in Table 6.9.

In order to investigate the type of interaction between PNA and PMMA, the IR absorption spectra of 30% PNA in PMMA composite film was carried out. The IR scans are shown for both composite film as well as for pure components in Fig. 6.16a, b, c and d. Table 6.10 gives the assignment of different IR bands for pure PMMA, pure PNA and PMMA- PNA. PMMA-PNA film shows additional bands occurring in the region of 3472 to 2346 cm^{-1} together with significant shift in the carbonyl band (1720cm^{-1} to 1710cm^{-1} or 1740cm^{-1}) which clearly suggests that there is hydrogen bonding between amino group of PNA and carbonyl group of PMMA. From the table and figure, we can see that there are three C=O bands occurring at around 1710cm^{-1}, 1720$cm^{-1}$and 1740cm^{-1} respectively. In addition to this, there is also a shift in the band corresponding to nitro group of PNA in the PMMA-PNA film (1498cm^{-1}) as compared to pure PNA(1490cm^{-1}). The occurrence of multiple C=O bands can be due to three types of C=O groups viz. complexed C=O in amorphous phase, complexed C=O in crystalline phase and free C=O groups away from PNA moieties. The shift in the band corresponding to the nitro group of the PNA also clearly suggests the formation of a complex. The assignment of other peaks are given in Table 6.10. Further, the peak intensities in the composite film are highly resolved compared to that of PNA. Thus, the complex formation between PNA and PMMA and its crystallization appears to be very strong possibility.

The most interesting result of the present study was seen in the effect of crystallization process on the transparency of the films. Figure 6.17 is a comparison of the transparency of the film having same composition (40% PNA) grown from solution (S), melt (M) and in presence of electric field (E). It can be seen that an underlying dark line is clearly seen through the E film, while the S film is totally opaque. Thus, the effect of oriented growth of crystals drastically changes the optical qualities of these materials.

In order to confirm the formation of complex, the DSC analysis was carried out. Figure 6.18 shows the DSC graphs of pure PNA and PMMA-PNA composite film of 45 wt.% PNA. From the figures it can be seen that pure PNA shows a sharp melting point at 150°C. On the other hand the the composite film exhibits two melting points at 78.6° and 138.2°C respectively which could be due to the formation of two types of crystalline phases. The higher melting

Table 6.9 X-ray diffraction in PMMA-PNA film (30% PNA) grown by various techniques

Solution cast			Melt crystallized			Electric field		
d (obs)	I/I_0	hkl	d (obs)	I/I_0	hkl	d (obs)	I/I_0	hkl
7.08	8	101	7.19	7	101			
			6.15	7	200			
5.40	11	020*	5.47	10	110/020*			
4.95	7	011/300*	4.98	11	011/300*			
4.67	11	021*						
4.62	10	111	4.64	10	111			
4.15	5	300						
4.11	8	012*						
3.85	7	211/202*	3.85	7	211/202*	3.86	5	211/202*
3.69	7	400/320*						
3.49	100	012/022*	3.48	100	012/022*	3.49	11	012/022*
						3.35	2	112/122*
3.14	6	311/222*	3.15	12	311/222*			
			3.07	38	212/231*			
3.04	55	020/420*				3.03	100	020/420*
						2.84	3	003
2.50	7	313*	2.50	6	313*	2.50	10	313*
						2.29	17	510

* As per new structure in Table 6.7.

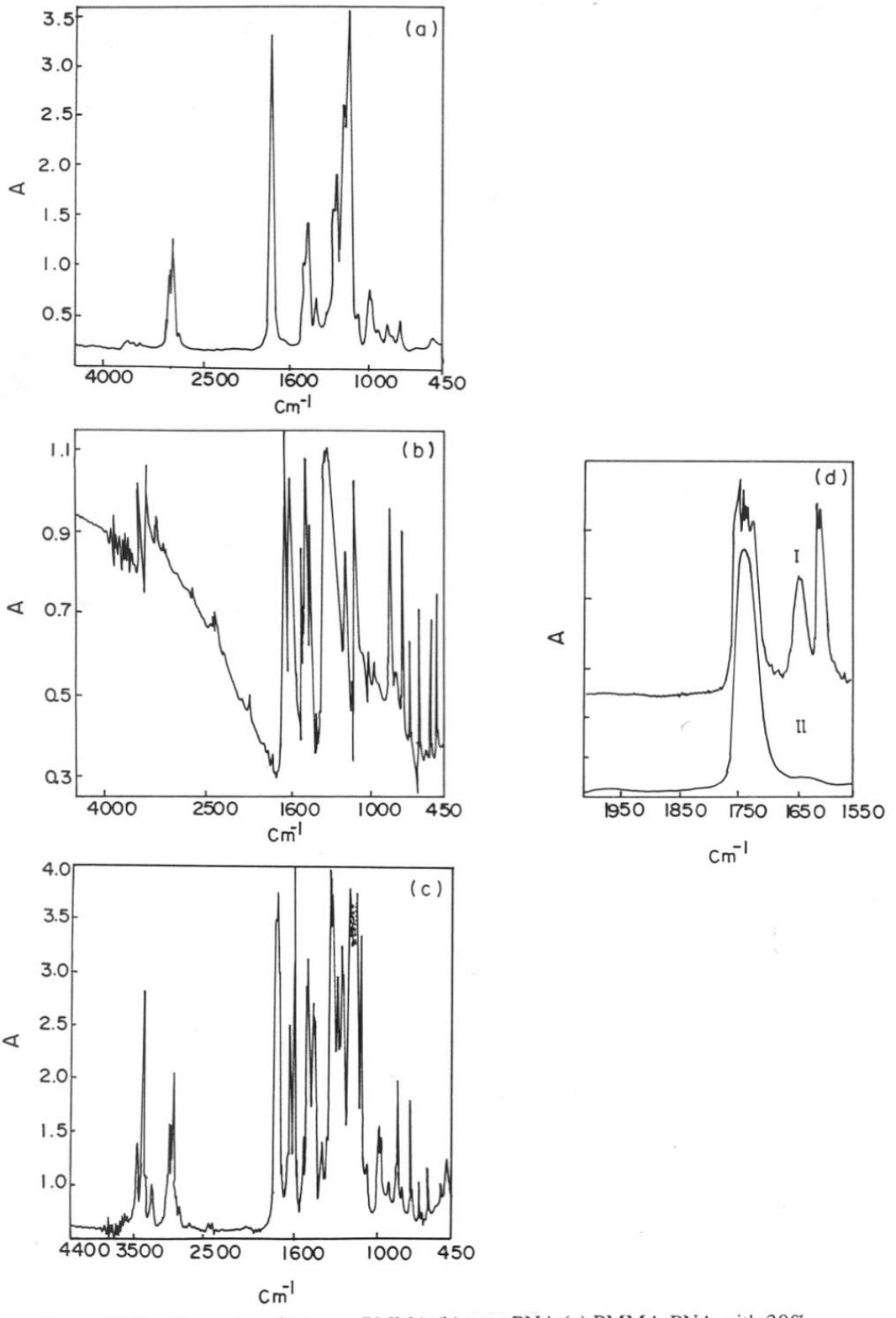

Figure 6.16 IR spectra of (a) pure PMMA (b) pure PNA (c) PMMA-PNA with 30% PNA (d) clearly showing three CO frequency bands for the composite film (I) compared to pure PMMA (II).

Table 6.10 IR absorption of 30% PNA in PMMA composite film as compared with pure components

PMMA	PNA	PMMA-PNA	Remarks
	3500 (ms)	3468 (ms)	
	3360 (ms)	3374 (vs)	N—H stretch and hydrogen bonding
	3267 (w)	3354 (w)	
3050 (w)	2900 (vvw)		
2995 (ms)		2996 (ms)	
2950 (ms)		2952 (vs)	CH_2—O deformation
		2842 (vvw)	
2372 (vw)			
1730 (vvs)		1742 (vvs)	
		1720 (vvs)	C=O
		1710 (vvs)	
	1634 (vvs)	1636 (ms)	Phenyl deformation
	1590 (vvs)	1598 (vvs)	
	1490 (ms)	1496 (ms)	NO_2 assymetric stretch
	1475 (s)	1490 (ms)	
1450 (ms)	1445 (ms)		CH_2 deformation, aromatic 1,4 disubstituted
1388 (w)	1390 (sh)	1388 (w)	
		1352 (sh)	CH_2 wagging
		1326 (vvs)	NO_2 assymetric stretch
1268 (sh)	1290 (vvs)	1274 (vs)	C—N stretch in aromatic
1242 (ms)		1246 (vvs)	
		1200 (vvs)	O
			C—OR stretch
1190 (s)	1182 (ms)	1184 (vvs)	
		1174 (vvs)	C—O—C deformation
1149 (s)	1136 (sh)	1144 (s)	CH_2 wagging , in plane phenyl deformation
	1110 (vs)	1110 (vvs)	
1065 (sh)		1064 (sh)	
985 (w)	995 (w)	990 (ms)	δ CH out of plane deformation of aromatic ring
	965 (w)	966 (ms)	
	955 (w)		
840 (w)	840 (ms)	860 (sh)	δ CH out of plane deformation of aromatic ring
823 (vvw)	820 (sh)		
810 (vvw)		816 (w)	CH_2 rock

s, strong ; m , medium ; w , weak; v , very ; sh , shoulder.

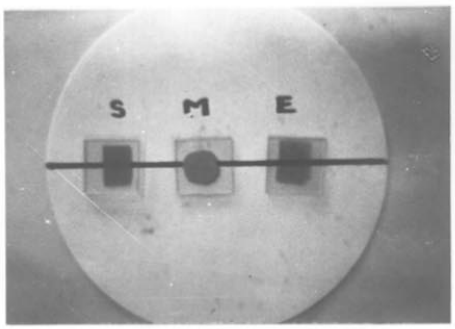

Figure 6.17 Photograph of PMMA-PNA film (40%) PNA showing transparency in presence of electric field (E) compared to that grown from solution (S) and melt (M).

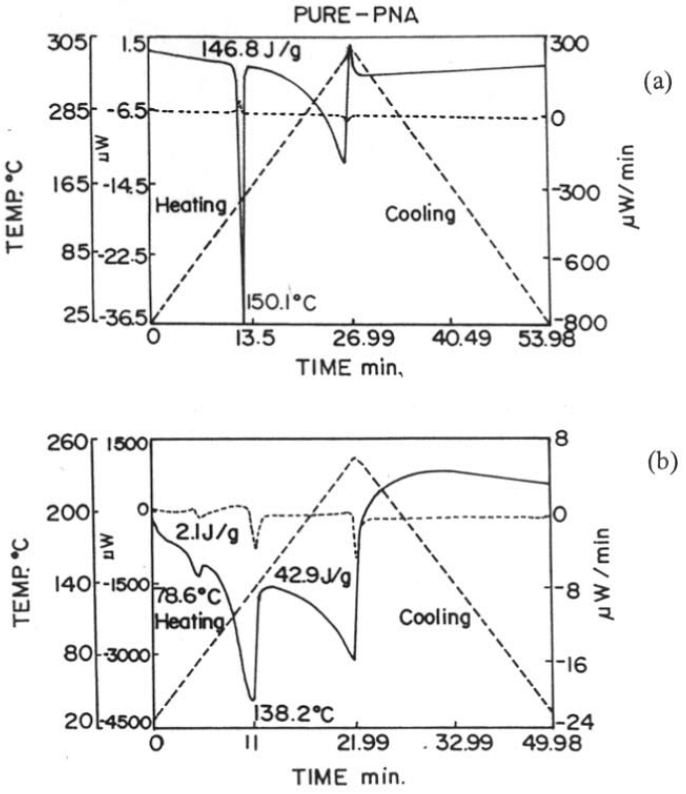

Figure 6.18 DSC curves for (a) pure PNA (b) 45% PNA in PMMA composite film.

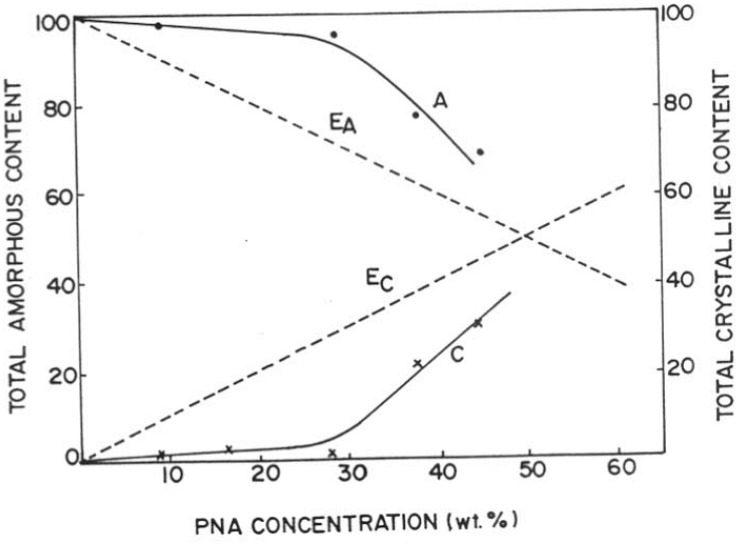

Figure 6.19 Graph of total crystalline content and total amorphous content with respect to concentration of PNA.

point of 138.2°C corresponds to that of free PNA in the films. The lowering of melting point of PNA in the composite as compared to pure PNA can be attributed to dilution effects which presumes large interaction and good miscibility of components. The presence of another new peak (78.6°C) clearly suggeststhe formation of new crystalline phase. These findings together with earlier discussions on XRD and IR clearly indicate the formation of a complex between PNA and PMMA above certain concentration of PNA, which crystallizes in orthorhombic structure.

The total crystalline content and total amorphous content was also determined from the observed heat of fusion (J/g) values from the melting curve and the J/g for pure PNA (PMMA being amorphous). Figure 6.19 shows the graph of total crystalline content and total amorphous content with respect to the concentration of PNA. The solid line shows the observed total crystalline (C) and amorphous content (A). The dashed lines represent the expected total crystalline content (E_C) and amorphous content (E_A). The expected curves represent total crystalline and amorphous content when the whole of PNA crystallizes out in one phase similar to that of original PNA without complexation. The experimental curve shows that the material exists in three phases. At low concentration (< 5%) it is purely in one phase. At intermediate concentration it is composed of three phases while at very high concentration (> 45%) it exists predominantly in one crystalline phase. At 50% concentration of PNA, the expected total crystalline and total amorphous content coincide with each other showing that at this concentration of PNA both crystalline and amorphous phases are present in equal amounts. At low concentration of PNA (< 5%), the observed total crystalline content is almost negligible that is it is totally amorphous. This shows that the complex formed between PNA and PMMA is in the amorphous phase. At intermediate concentration (> 10 %), the observed crystalline content starts increasing with increase of PNA showing a corresponding decrease in the observed amorphous content. Here the material exists in three phases. One phase is due to the complex in the amorphous phase, the second is due to a complex between PNA and PMMA in the crystalline phase and third is due to free PNA also in the crystalline phase. With further increase of PNA concentration, the crystalline content due to free PNA increases and becomes predominant at very high concentration of PNA. At this concentration, it is quite likely that the crystalline phase in the composite contains predominantly one component. Thus, one can conclude from the results of XRD, IR and DSC that the PNA in PMMA crystallizes in two crystalline phases in most range of composition

studied. One due to a complex crystallizing in orthorhombic configuration and the other due to free PNA crystallizing in original monoclinic phase.

Figure 6.20 shows the TGA of composite films of (a) 30% and (b) 40% concentration of PNA. The first transition corresponds to the weight loss of PNA, which is 27.9% and 37.78% by weight for PMMA-PNA films with PNA concentration of 30% and 40% respectively. This clearly indicates that no PNA escapes the film by diffusion at room temperature and PNA loaded in PMMA is fully retained. The proportion of PNA in the form of amorphous complex and as crystalline state was estimated from the DSC and TGA data. The observed J/g (ΔH) value from the melting curve was subtracted from the expected ΔH value. The difference of ΔH value gave amount of PNA remaining in the amorphous phase. The percentage of PNA in amorphous complex can then be calculated by taking the remaining ΔH value and taking into account the ΔH value for 100% PNA. Thus, the percentage PNA in amorphous complex and the crystalline state was calculated. This is represented in Fig. 6.21 and it is immediately clear that these curves are similar to Fig.6.19 and same conclusions can be drawn from them.

Figure 6.22 shows the morphology of the PMMA-PNA composite films investigated by optical polarising microscopy. The pure PMMA film is totally isotropic and amorphous. On the other hand, with the incorporation of PNA, the films show increasing degree of transmittance under cross polar condition suggesting presence of birefringence and anisotropy. At low concentration of PNA (30%) in PMMA-PNA film, the sample consists of very small crystals ($<1\mu m$) which appear as dots in the microscope and the other consisting of large elongated crystals (Fig.6.22a). The smaller crystals are due to the complex crystallizing in the orthorhombic phase of PNA. At a certain critical concentration (40%) both small and large spherulites are observed (Fig.6.22b). The small spherulites with intense colours correspond to orthorhombic crystals while the large spherulites have monoclinic crystals. For very high concentrations of PNA (45%), both spherulitic as well as dendritic crystals are seen (Fig. 6.22c). These various results clearly indicate that the PMMA-PNA composite film crystallizes in two distinct crystalline structures. At low concentration of the additive, the orthorhombic phase is predominant while at high concentration, the monoclinic phase become major component.

At low concentration of PNA, the films exhibited very small dots, which could not be distinctly seen by optical microscopy. Hence TEM studies were carried out. Figure 6.23 shows

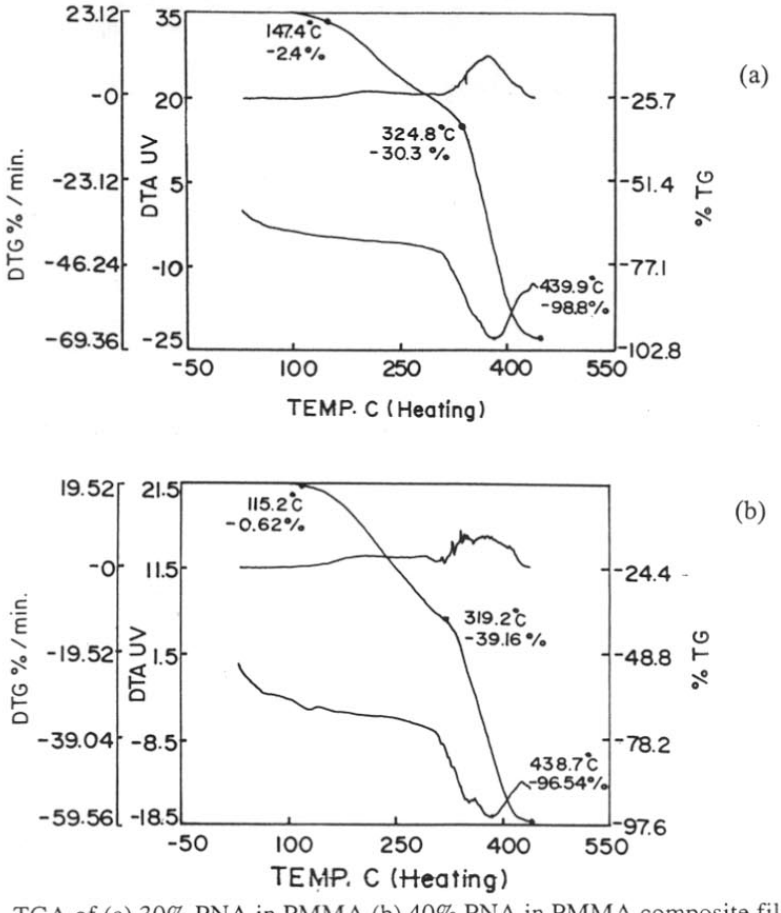

Figure 6.20 TGA of (a) 30% PNA in PMMA (b) 40% PNA in PMMA composite film.

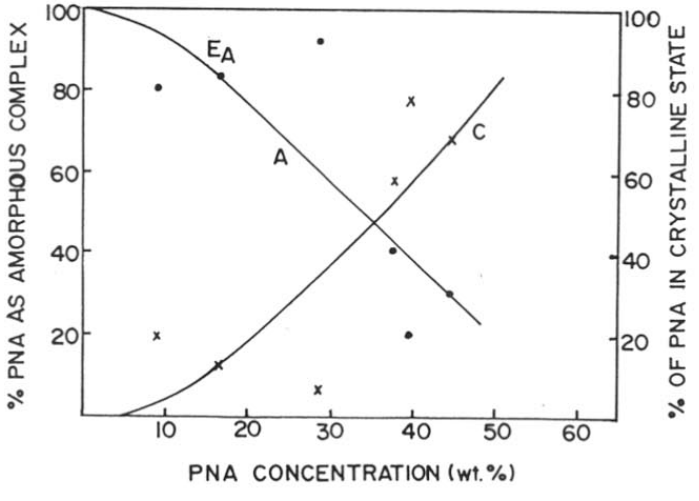

Figure 6.21 Graph of % of PNA as total amorphous complex and in crystalline state as a function of concentration of PNA.

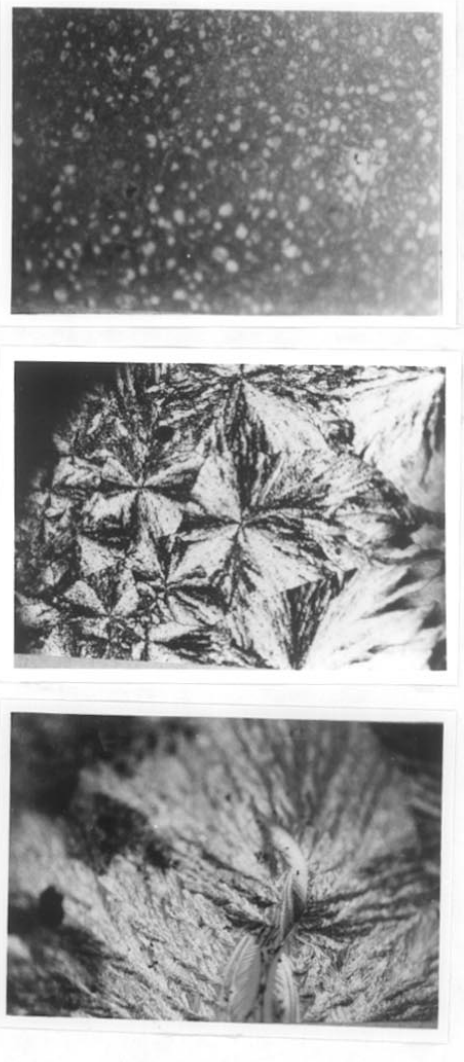

(a)

(b)

(c)

Figure 6.22 Optical micrographs for PMMA-PNA (SC) films containing (a) 30% (b) 40% and (c) 45wt.% PNA respectively . (net magn.= 450x)

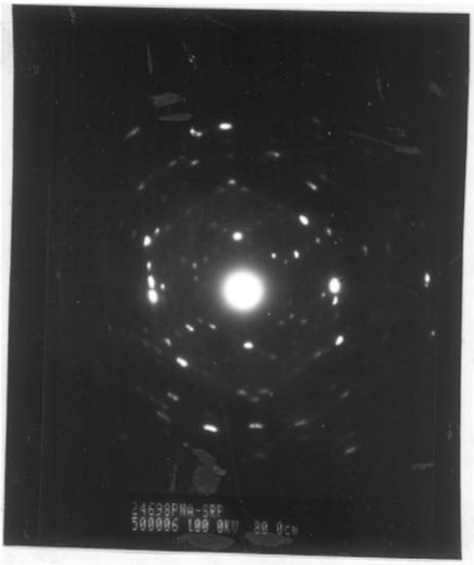

(a)

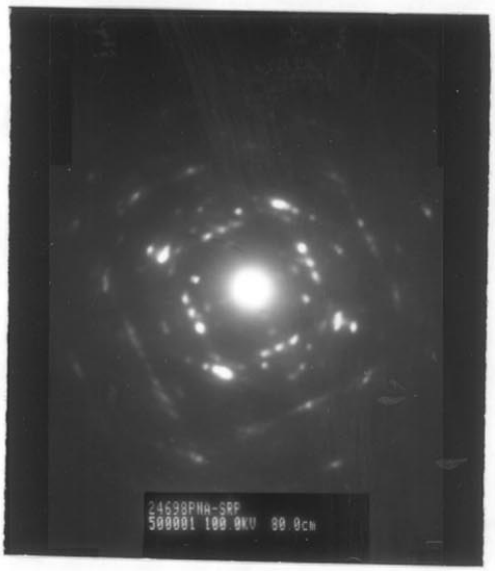

(b)

Figure 6.23 TEM micrographs of (a) monoclinic structure of free PNA. (b) PMMA-PNA complex crystallizing in new orthorhombic structure of PNA.

the electron diffraction patterns of such PMMA-PNA films. The selected area diffraction exhibited monoclinic crystalline structure in one region (a) and the complex structure crystallizing in the orthorhombic crystalline phase in another region (b). The size of the crystallites in PMMA matrix were estimated to be of the order of 40 nm.

From the preceding experimental evidence, one can conclude that large interaction between the polymer matrix and the additive is occurring. In a non-interactive system, where the polymer and the additive are inert little influence would be expected on the crystallization behaviour of either component. PNA is centrosymmetric with no second order nonlinearity and has a strong dipole moment (13.4D)[50] due to positively charged amino group placed at the para position of the newly charged nitro group in the PNA molecule. On the other hand, PMMA has comparatively weak dipole moment associated with its acetate group (6.0D).[51] Thus, one expects the interaction between these moieties only through the amino group of PNA and the carbonyl group of PMMA. Such an interaction is sufficient to cause the displacement of PNA molecules during their crystallization. In pure PNA having monoclinic crystal structure, all the benzene rings are placed in a planar configuration along the plane parallel to 'b' axis and any change in these can cause preferential growth, occurrence of new reflections, modification of growth habit and orientation. This has been observed by us as indicated in the preceding sections. Interestingly the application of an electric field during crystallization can also cause orientation of these molecules because of their strong dipole moment. Such an orientation induced by electric field will subsequently lead to oriented growth of crystallites. The presence of one strong reflection (020) plane of monoclinic phase of PNA clearly shows the orientation along b-axis. It is also interesting to note that at a certain critical concentration, spherulitic morphology was observed which would be normally expected for semi-crystalline polymers as for example PEO dispersed with PNA.[52] In such polymers, the same molecule passes through the crystalline and amorphous domains. However, in the present case, PNA forms the crystallizing component with PMMA inclusions in the monoclinic phase of PNA constituting the amorphous region. As seen from the above results PNA forms a complex with PMMA and this complex crystallizes in the spherulitic morphology first. Such a crystallization behaviour has been reported for a number of PEO-complexes with inorganic salts or urea etc.[49] These exhibit spherulitic morphology, different melting points and new crystalline structure.

6.3.3 Structure, Growth and Morphology of PMMA-MNA Composite System

MNA by itself is non-centrosymmetric and exhibits a high nonlinear susceptibility coefficient β of $6x10^{-30}$ esu.[50] Interesting structural and morphological features were observed when MNA was dispersed in PMMA polymer matrix as host. These are described in the following section.

The PMMA-MNA films were amorphous and transparent yellow in appearance up to MNA concentration of 35%. With increase of MNA content above 38%, the films were opaque suggesting the samples were highly crystalline. Figure 6.24 (a) represents the WAXD scans of solution cast PMMA-MNA composite films. Curves A to F correspond to MNA concentration of 30%, 35%, 40%, 42%, 45% and 50% respectively with respect to PMMA matrix. On comparing these curves with solution crystallized pure MNA (see Fig.6.24 b), it can be seen that there is a pronounced change in the intensities of various diffraction peaks which clearly brings out the effect of polymer on the growth and morphology of these crystals as compared to pure MNA. The pure MNA shows a major intense peak in its XRD at 2θ of 18.0°, which corresponds, to (011) reflection. In the solution cast PMMA-MNA film, this intense diffraction peak of (011) reflection is totally suppressed. At low concentration of MNA film (30%), the film is totally amorphous and does not show any of the peaks corresponding to pure MNA, which shows major intense peaks at 2θ of 10° to 26°. However, with increase of MNA concentration to 40% intense diffraction peaks are observed. At higher concentration (>45%), new reflections appear that become even more prominent at high concentration (>40%). The comparison of relative intensities of various peaks and the estimated 'd' values derived from these scans is presented in Table 6.11. Although there are changes in the intensities of various diffraction peaks, most of the peaks of XRD can be assigned to various reflections from MNA which crystallizes in orthorhombic crystalline phase[44] with lattice parameters of a = 6.505 Å, b = 19.346 Å and c = 5.074 Å. There are a few new diffraction peaks, which become more prominent at high concentration of MNA (40%) especially the peak at 2θ of 17.8° and which could not be assigned to any of the reflections from orthorhombic crystalline phase of MNA. Hence, these peaks must correspond to a new crystalline structure formed possibly due to a complex between PMMA and MNA. The detailed analysis showed that this was monoclinic one with lattice parameters of a = 13.01Å, b = 19.346Å and c = 10.148Å and $\beta = 64^{\circ}$. The structure of complex in new crystalline form is schematically shown in Fig. 6.25. The calculations from lattice parameters indicate that MNA

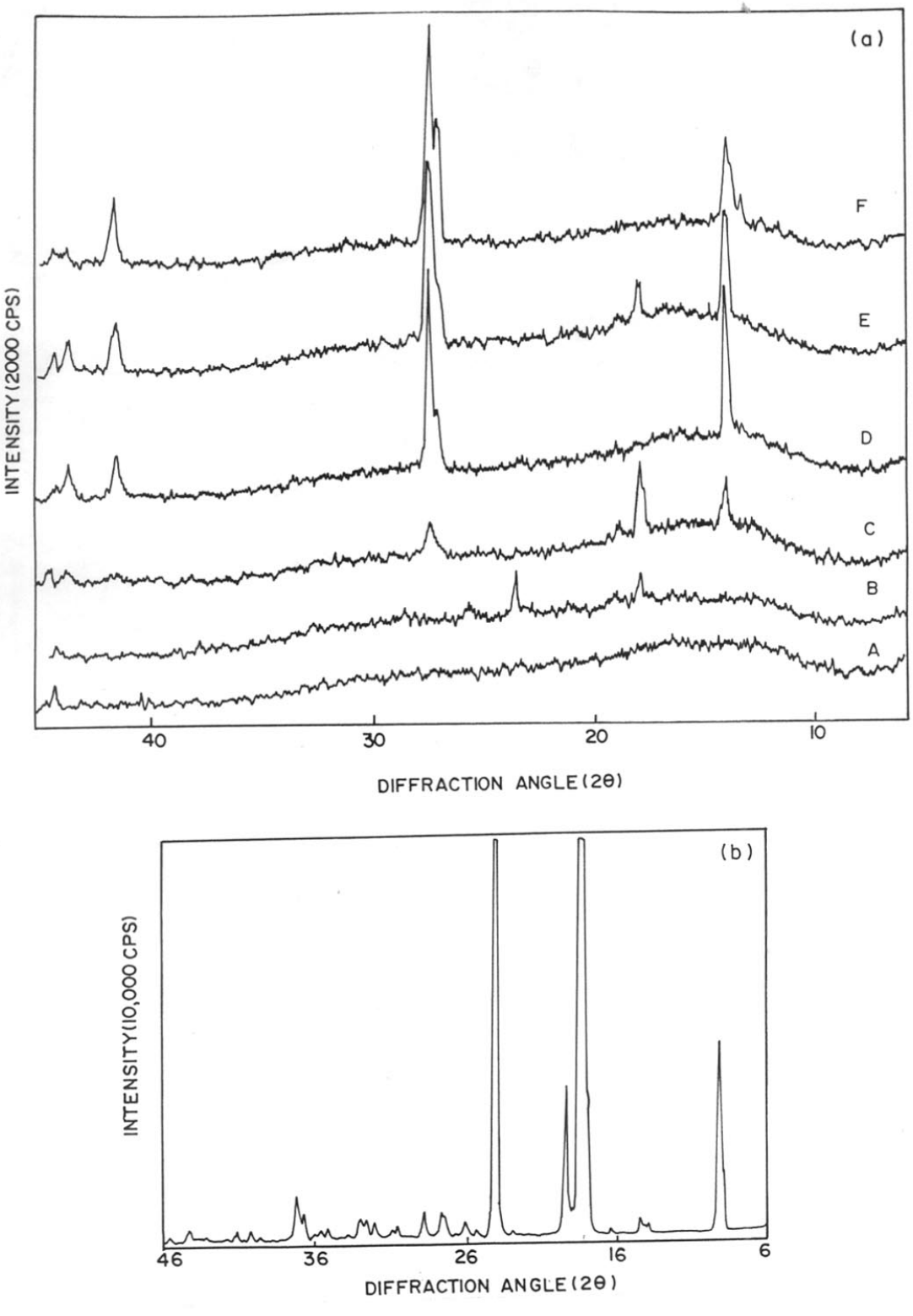

Figure 6.24 (a) WAXD scans for PMMA-MNA (SC) samples with different concentrations of MNA. Curves A-F correspond to MNA concentration of 30, 35, 40, 42, 45 and 50wt.% respectively.
(b) WAXD scan for solution crystallized pure MNA.

Table 6.11 X-ray diffraction in PMMA- MNA films grown by solution cast technique

MNA 100%			35%		40%		42%		45%		50%			
d (obs)	I/I_o	hkl*	d (obs)	I/I_0	d (obs)	I/I_0	d (obs)	I/I_0	d (obs)	I/I_0	d (obs)	I/I_0	d (cal)**	hkl
9.66	11	020												
											6.60	20	6.64	021
					6.33	71	6.33	79	6.33	64	6.33	45	6.34	201
6.11	1	110												
									6.03	17			6.03	$211/10\bar{1}$
5.40	9	120												
					4.98	100							5.00	220
4.92	100	011	4.90	82					4.92	3			4.90	112
4.82	9	040												
					4.72	38							4.74	202
			4.62	53			4.67	13	4.67	14			4.61	212
4.57	9	130												
			4.17	42							4.19	10	4.13	022
3.88	1	050												
			3.73	100									3.73	$10\bar{2}$
3.70	29	121												
3.52	1	041												
			3.45	42									3.49	142/003
3.41	1	131												
		200			3.26	47	3.26	33	3.29	37	3.29	56		
3.24	1	060					3.23	100	3.24	100	3.24	100	3.22	060
3.08	1	220												
3.92	1	230												
2.89	1	160												
2.78	1	070/151												
2.73	1	201												
2.71	1	211												

*As per orthorhombic structure , a = 6.505 Å, b = 19.346 Å , c = 5.074 Å

** As per new structure (monoclinic) , a = 13.01Å , b = 19.346 Å , c = 10.148 Å and ß = 64°

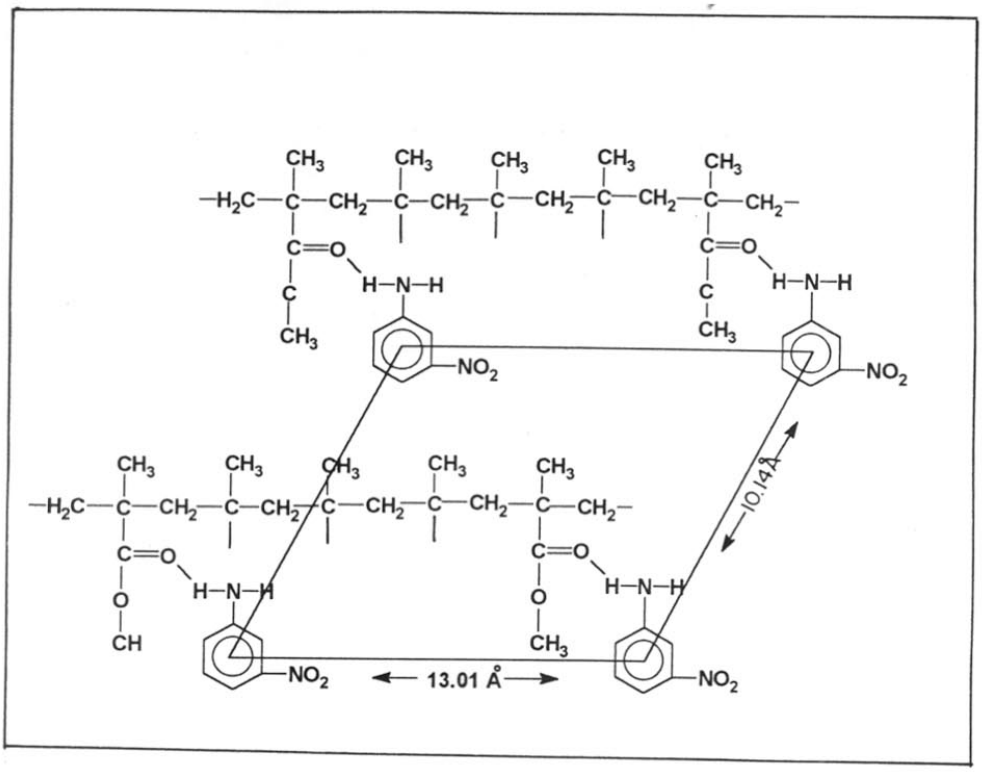

Figure 6.25 Sketch of PMMA-MNA complex crystallizing in new crystalline (monoclinic) structure of MNA.

molecule is placed at every 4th C=O group of the PMMA chain. It can be seen from the figure that there is a strong reflection occurring at high concentration of MNA (>40%) at 2θ of 27.5° which corresponds to (200) reflection of orthorhombic structure of free MNA. This reflection is normally weaker in the case of pure MNA without any polymer. Such variation in the intensity of the diffraction peak could be due to either preferential growth of the crystallite along certain phase or orientation of crystallites along the film surface.

Figure 6.26(a) shows the WAXD scans of melt crystallized samples of PMMA-MNA films. Curves A to F correspond to MNA concentrations of 30%, 35%, 40%, 42%, 45% and 50% with respect to PMMA matrix respectively. On comparing this figure with the WAXD of pure MNA (sublimed crystals) which is depicted in Fig. 6.26 (b), it can be observed that even in this case a major change in the intensities of various diffraction peaks occur with the suppression of most of the peaks which are seen in the WAXD of pure MNA and the enhancement of one strong intense peak at 2θ of 18.1° which corresponds to (011) reflection. These observations are very similar to those of PMMA-PNA composites and hence same conclusions can be drawn from them regarding crystalline structure. The comparison of relative intensities of these various peaks and the 'd' values estimated from these scans is presented in Table 6.12 and in this case too, the new structure is seen to occur.

Some of the composite films were investigated for the long time stability. Figure 6.27 shows the WAXD scans of solution cast 45% MNA in PMMA film where the curve A represents the WAXD scan of fresh film and the curve B represents the WAXD scan of film stored over a long period of time termed as an aged film. On comparing these curves, it can be seen that the high intense peak at 2θ of 27.5° corresponding to (060) reflection for fresh film gets suppressed or weak while the low intense peak at 2θ of 18.0° corresponding to reflection (011) gets enhanced in case of aged film. These variations in the intensities of various peaks occur due to structural changes over a period of time. This can be explained as follows:
PMMA matrix is flexible enough and has enough free volume to allow the rotational movement of MNA. This relaxational behaviour of PMMA chains is enough to cause reorientation in the molecule/crystallites giving changes in certain reflections.

Figure 6.28 (a), (b) and (c) shows the IR spectra recorded for PMMA-MNA composite film containing 30% MNA along with their individual components. Table 6.13 gives the assignment of different IR bands for pure PMMA, pure MNA and PMMA-MNA composite. The PMMA-MNA shows additional bands occurring in the region 3472 cm^{-1} to 2346cm^{-1}

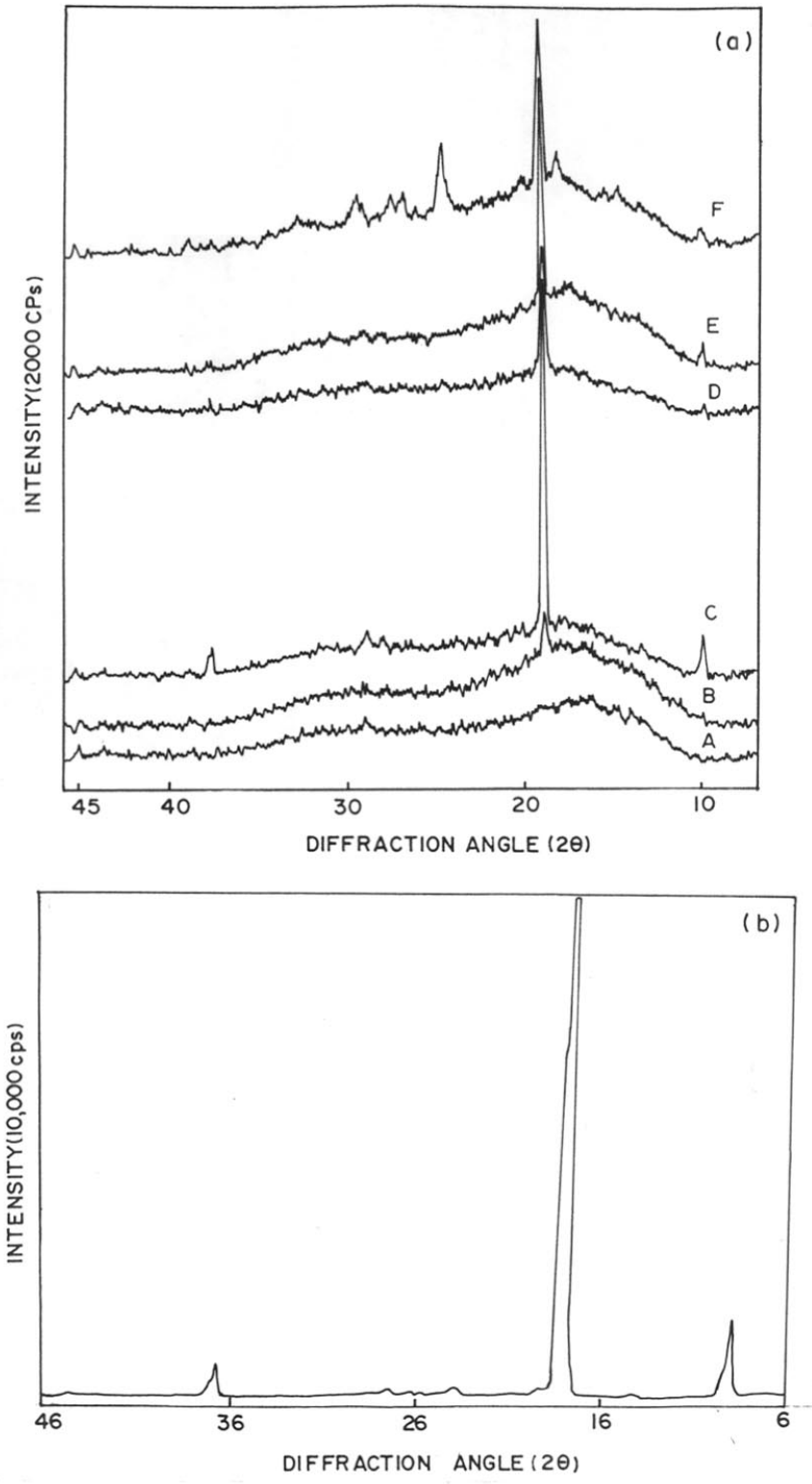

Figure 6.26 (a) WAXD scans for PMMA-MNA (MC) samples . Curves A-F correspond to MNA concentrations of 30, 35, 40, 42, 45 and 50wt.% respectively. (b) WAXD scan for pure MNA (sublimed crystals).

Tables 6.12 X-ray diffraction in PMMA-MNA films grown by melt crystallized technique

MNA 100%			30%		35%		40%		42%		45%		50%			
d (obs)	I/I_0	hkl*	d (obs)	I/I_0	d (obs)	I/I_0	d (obs)	I/I_0	d (obs)	I/I_0	d (obs)	I/I_0	d (obs)	I/I_0	d (cal)**	hkl
9.93	9				9.93	15	9.93	7	9.93	9	9.93	10			10.0	110
9.61	5	020											9.71	10		
					7.43	24									7.45	120
			6.70	100											6.77	121/021
													6.41	11	6.44	030
													6.07	11	6.03	211
					5.57	53			5.57	15					5.59	210
													5.12	23	5.06	102
4.92	100	011			4.90	100	4.87	100	4.90	100	4.92	100	4.87	100	4.90	112
4.84	40	040														
4.59	2	130									4.59	10			4.60	212
3.75	2								3.72	15			3.74	40	3.72	$032/10\bar{2}$
3.69	2	121														
3.50	1	041											3.52	10		
3.40	1	131											3.41	16	3.38	242/203
													3.33	16	3.33	330
3.26	2	200					3.26	3								
			3.15	80	3.14	14	3.16	5			3.15	8	3.16	14	3.16	303
													3.12	20	3.12	313
3.08	1	141														
2.78	1	151											2.79	11	2.75	033
2.72	1	201/211														
2.44	4	022														
2.42	2	080					2.43	6							2.41	080
					2.36	24									2.36	072/053
2.03	1	202	2.04	70												

* AS per orthorhombic structure , a = 6.505 Å , b = 19.346 Å , c = 5.074 Å

** As per new structure (monoclinic) , a = 13.01Å, b = 19.346 Å , c = 10.148 Å and ß = 64 °

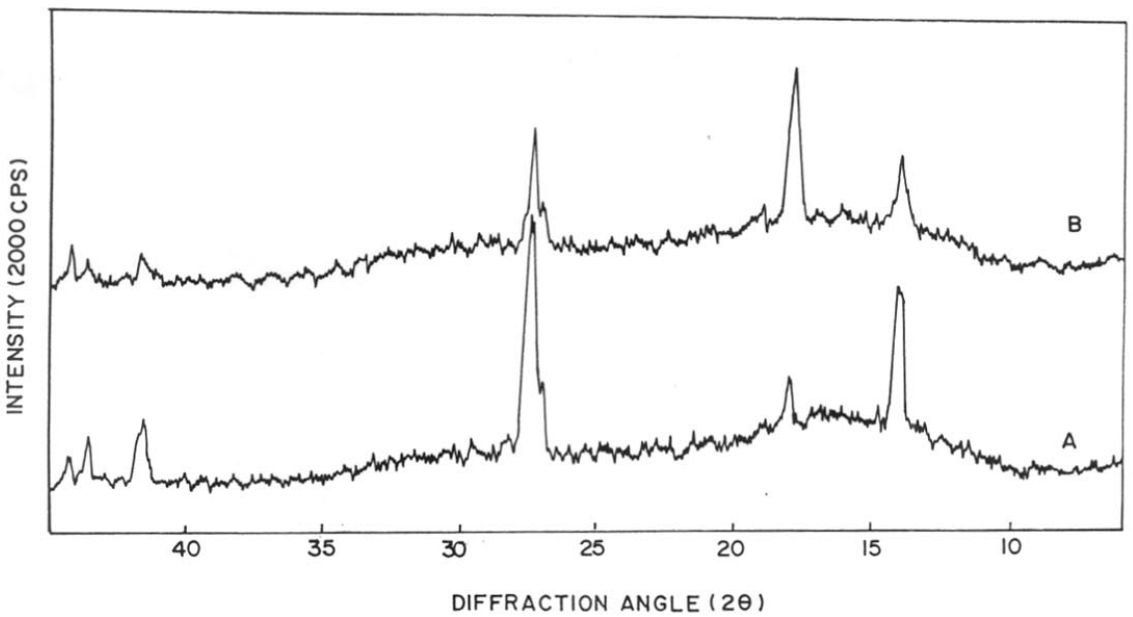

Figure 6.27 WAXD scans for PMMA-MNA solution cast films containing 45% MNA to determine stability. (A) fresh film (B) aged film.

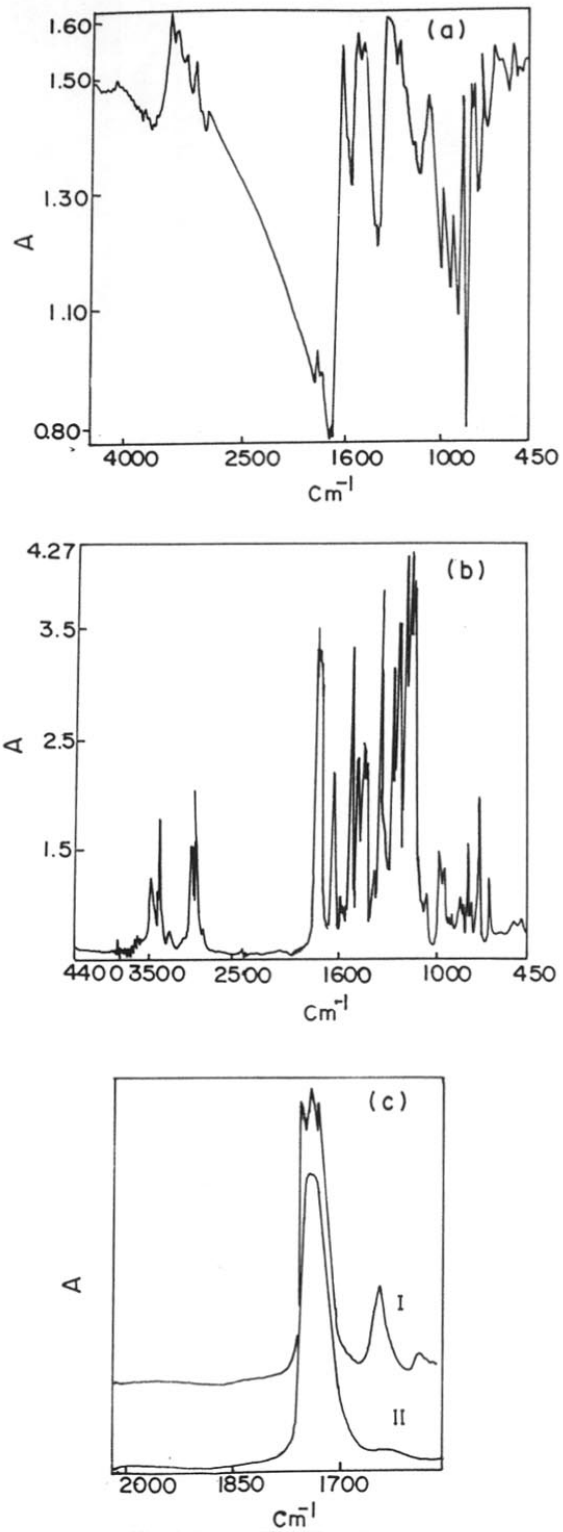

Figure 6.28 IR spectra of (a) PMMA-MNA film (b) MNA and (c)clearly showing three CO bands for composite film (I) compared to pure PMMA (II).

Table 6.13 IR absorption of 30% MNA in PMMA composite film as compared with pure components

PMMA	MNA	PMMA-MNA	Remarks
	3428 (ms)	3472 (w)	
	3374 (ms)	3380 (ms)	N—Hstretch and hydrogen bonding
		3244 (w)	
2994 (ms)		2998 (ms)	CH_2— O deformation
2950 (ms)		2950	
2372 (vvw)			
1730 (vs)		1710 (vvs)	
		1726 (vvs)	C = 0
		1740 (vvs)	
	1624 (vs)	1634 (ms)	Skeletal out of plane of phenyl deformation
	1522 (vs)	1578 (vvw)	
1444 (ms)	1460 (vs)	1486 (ms)	NO_2 assymetric stretch
		1452 (ms)	CH_2 deformation
1388 (w)	1376 (ms)	1388 (w)	CH_2 wagging, in plane phenyl deformation
	1348 (vs)	1354(vvs)	
		1350(sh)	
1268 (sh)	1262 (ms)	1274(vvs)	C—N stretch in aromatic
1242 (ms)		1244(vvs)	O
			C-OR stretch
		1198 (vvs)	
1191 (ms)	1180 (sh)	1182 (vvs)	C—O—C deformation
		1162 (vvs)	
1149 (vs)		1146 (vvs)	CH_2 wagging ,in plane phenyl deformation
1064 (sh)	1090 (ms)	1064 (w)	δ CH out of plane defomation
988 (w)	990 (vvw)	994 (w)	of aromatic ring
	930 (ms)	966 (w)	
912 (vvw)			
	866 (vs)	866 (vvw)	δ CH out of plane deformation
842 (w)			of aromatic ring
826 (vvw)	816 (ms)	816 (vvw)	CH_2 rock
810 (vvw)	790 (w)	794 (ms)	
		750 (w)	

together with significant shift in the carbonyl band (1726cm^{-1} to 1742cm^{-1} or 1710 cm^{-1}) which clearly suggests that there is hydrogen bonding between the amino group of MNA and CO group of PMMA. In addition to this there is also a shift in the band corresponding to nitro group of MNA in the PMMA-MNA film (1486cm^{-1}) as compared to pure MNA(1460cm^{-1}). Thus, same explanation holds good here also as explained in the case of PMMA-PNA film in section 6.3.2. These results clearly bring out that the complex formation between MNA and PMMA and its crystallization appears to be a very strong possibility.

In order to investigate the type of interaction or complex formation, etc. The DSC analysis was carried out for these films. Figures 6.29 a, b and c shows the DSC curves for pure MNA, 30%MNA in PMMA and 50% MNA in PMMA respectively. Pure MNA shows a sharp melting point at 114.2°C with 14.4 J/g. On the other hand, the films show two melting points. The lower melting point occurring at around 67-72°C is quite intense at low concentration of MNA (30%) which decreases with the increase of MNA concentration (50%) while the higher melting point occurring at around 92-94°C becomes more prominent at high concentration of MNA (50%). From these observations, we can conclude that the lower melting point is due to the formation of complex, which crystallizes in new monoclinic configuration, while the higher melting point is due to free MNA crystallizing in orthorhombic crystalline phase. However, it should be noted that the lowering of melting point of free MNA in the composite film as compared to pure MNA is observed which can be associated with the dilution effect.

The TGA analysis were carried out for these composite films to determine the amount of MNA actually present in these films. Table 6.14 below shows the data in the composition range 30% to 50% MNA in PMMA respectively.

Table 6.14 TGA data of different compositions of MNA in PMMA composite films.

Composition (%)	Diffusion of free MNA (%)	Actual concentration of MNA present (%)
30	7.99	20.58
35	9.33	24.0
40	10.49	27.01
42	11.52	29.65
50	13.26	34.1

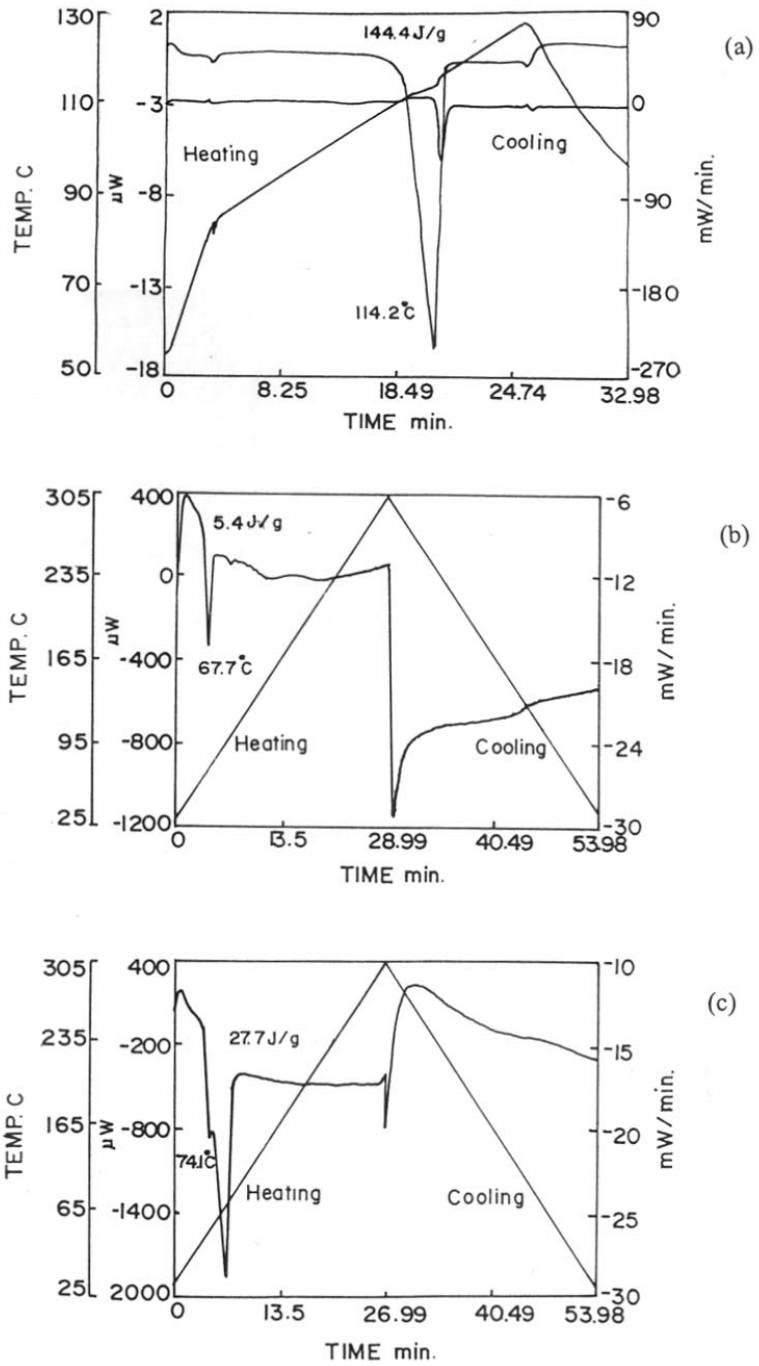

Figure 6.29 DSC curves for (a) pure MNA (b) 30% MNA in PMMA film (c) 50% MNA in PMMA film.

It is clear from the values in the table that there is some diffusion of free MNA out of the composite at room temperature and it increases with increase of MNA concentration. The table also gives the percentage of actual MNA present for each composition. This can be due to lower melting point of MNA as compared to PNA.

The total crystalline and total amorphous contents were determined from the DSC curves. Figure 6.30 shows the graph of total crystalline and total amorphous content with respect to actual concentration of MNA present taken from TGA data. The solid line shows the observed crystalline and amorphous content. The dashed lines represent the expected total crystalline (E_C) and amorphous (E_A) content. The expected curves represent total crystalline and amorphous content when the whole of MNA crystallizes out in one phase similar to free MNA irrespective of the concentration. The experimental curve shows that the material exists in three phases. These are very similar to those observed in the case of PMMA-PNA composites and hence, similar conclusions can be derived from them. The DSC data also yields similar results (Fig. 6.31) which support the hypothesis.

Fig.6.32 shows the optical micrographs for PMMA-MNA composite films along with pure MNA. Pure MNA shows elongated crystals and it is highly birefringent (Fig.6.32a). At low concentration of MNA (30%), very tiny crystals are seen (Fig.6.32b). These smaller tiny crystals correspond to a complex in crystallizing in new monoclinic crystalline phase. At high concentration of MNA (40%), spherulitic morphology is observed which are radiating from the central nucleus(Fig.6.32c). The internal structure of the spherulites consists of long fibrils in which the highly birefringent crystals of MNA are embedded. In addition, some free elongated crystals are also seen. The photomicrographs of melt crystallized PMMA-MNA films also show interesting feaures. The low concentration of MNA (30%) is more amorphous with very few tiny crystals (< 1 μm) (Fig.6.32d). With increase of MNA concentration (40%), very tiny spherulites in clusters are observed (Fig.6.32e). In addition, some elongated MNA crystals are also seen. These various observations clearly show that the PMMA-MNA composite films crystallizes in two different types of crystalline structures.

In order to determine the size of crystallites, these composite films were investigated by TEM and it was found to be of the order of 15nm. This could be the reason for the high transparency of PMMA-MNA composites at 30% concentration of additive.

From the preceding experimental evidence, one can conclude that an interaction between MNA and PMMA matrix is occurring. It should be noted that the pure MNA has a

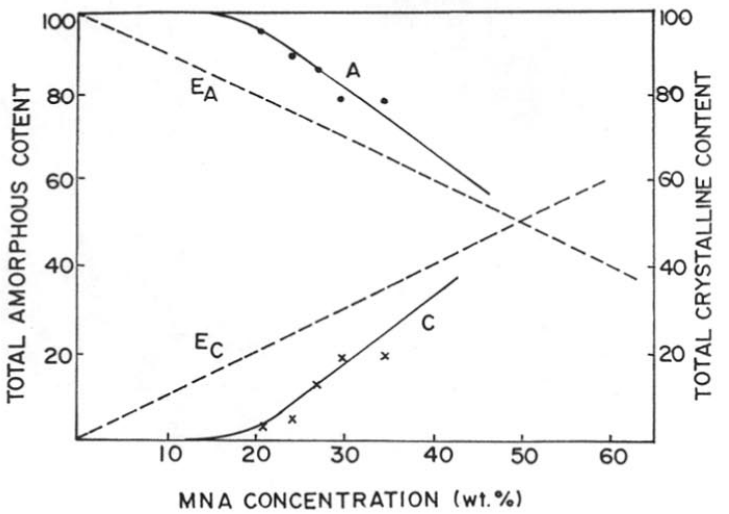

Figure 6.30 Graph of total crystalline content and total amorphous content with respect to concentration of MNA.

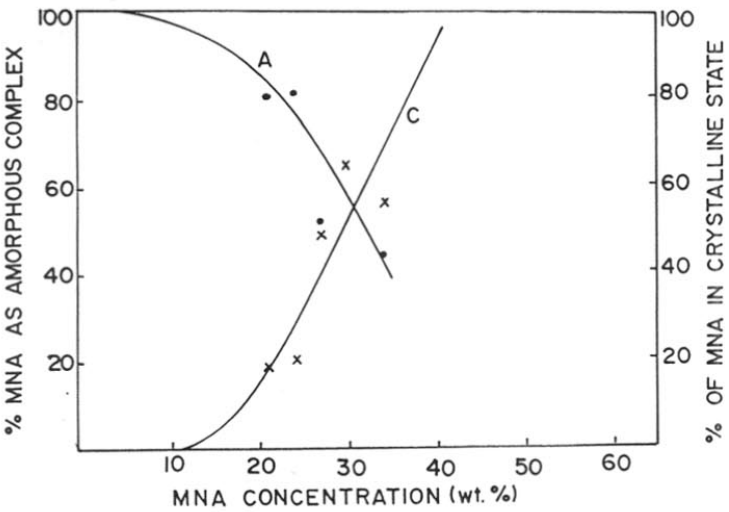

Figure 6.31 Graph of % of MNA as amorphous complex and in crystalline state with respect to concentration of MNA.

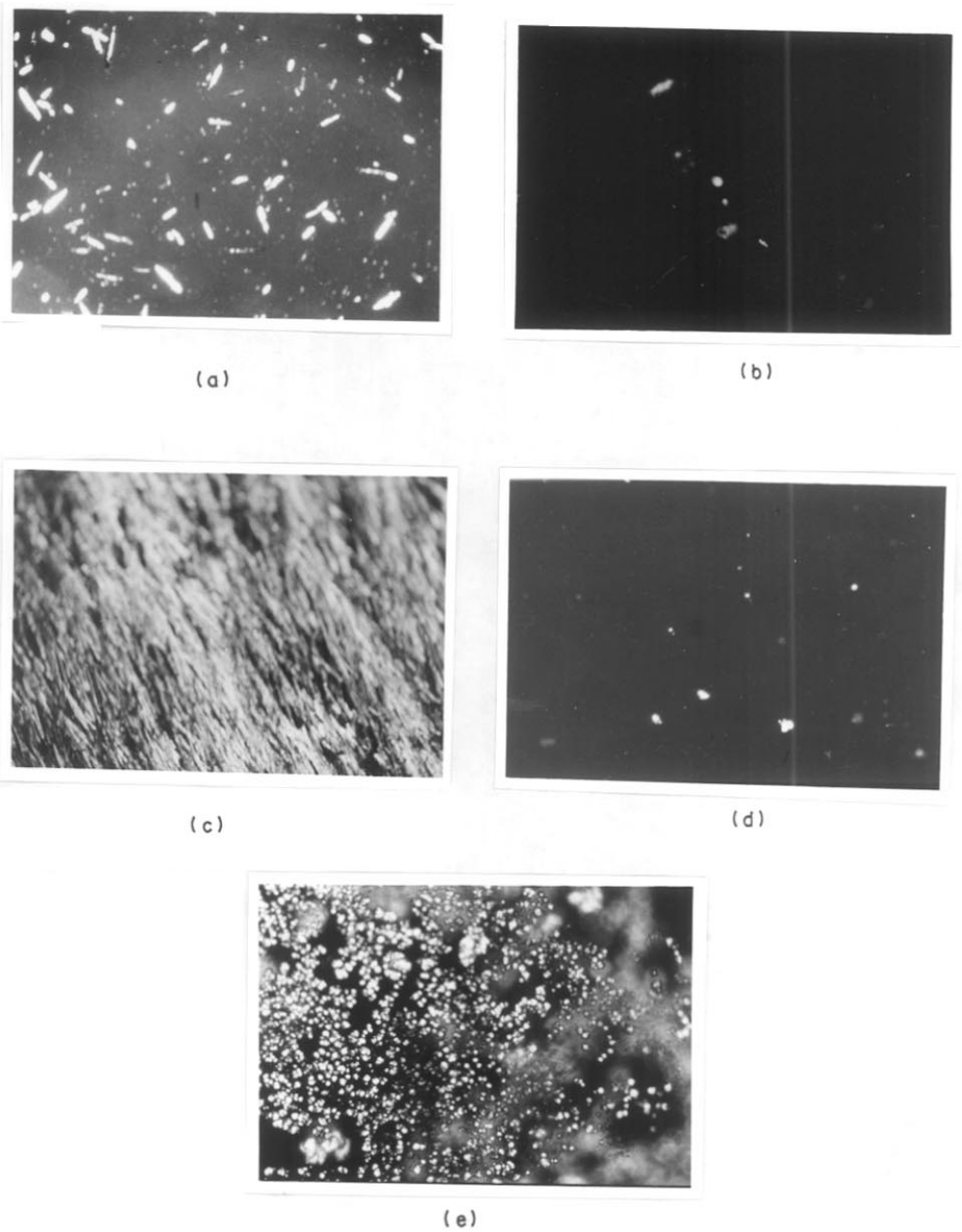

Figure 6.32 Optical micrographs for (a) pure MNA . Solution cast PMMA- MNA film of MNA concentration of (b) 30% (c) 70%respectively.
Melt crystallized composite films of MNA concentration of (d) 30% (e) 40% respectively. (net magnification= 450x)

strong dipole moment of 11.9D[53] due to negatively charged nitro group placed at meta position of positively charged amino group in the MNA molecule while PMMA as already observed has a comparatively weak dipole moment of 6.0D associated with its acetate group as mentioned earlier. Thus, one expects the interaction between these two moieties only through amino group of MNA and C=O group of PMMA. Such an interaction is sufficient to cause displacement of molecules during crystallization. In pure MNA, having orthorhombic crystalline structure, the planes of benzene rings are parallel to c-axis with all the nitro groups pointing in the similar direction.[54] It shows a major intense peak corresponding to (011) reflection. Hence, any change in these can cause preferential growth, occurrence of new reflection, modification of growth habit and/or orientation. This has been observed by us in the solution crystallized samples which shows a major intense peak corresponding to reflection (060). This clearly shows that the crystallites have got oriented along the b-axis. Also the formation of complex due to the presence of new reflection has given rise to changes in the crystalline structure to new monoclinic configuration.

6.3.4 Structure and Morphology of PNA in Different Polymer Matrices

In the last section of this chapter, we have studied the matrix mediated control of morphology in para-nitroaniline dispersed in various polymer matrices such as PMMA, PVAc, PVA, PEO, Pc etc.

Figure 6.33 shows the WAXD scans for solution cast samples containing same concentration of PNA (45%) but with different polymer matrices. Curves A, B, C and D correspond to PMMA, PVAC, PVA and PEO as the matrix respectively. There are clearly large differences in the intensities of various peaks with the change of the polymer matrix. The PNA crystallizes in the same monoclinic structure in all the polymeric media used (except PMMA where it shows some new peaks, which crystallizes in new orthorhombic crystalline phase due to complex formation as seen earlier). However, from all these cases it can be seen that different peaks become more prominent in some polymers than in others. For example, the (012) peak of PNA has highest intensity in PMMA and PVAC while the (202) peak becomes strongest in the presence of PVA or PEO. It may be mentioned here that except for PEO, all other polymers used are predominantly amorphous and hence the crystallizing component is only PNA. It is interesting to note that the polymer-PNA interaction in the case of PMMA and PVAC is expected through C=O and NH_2 groups while that for PVA is through OH with NO_2

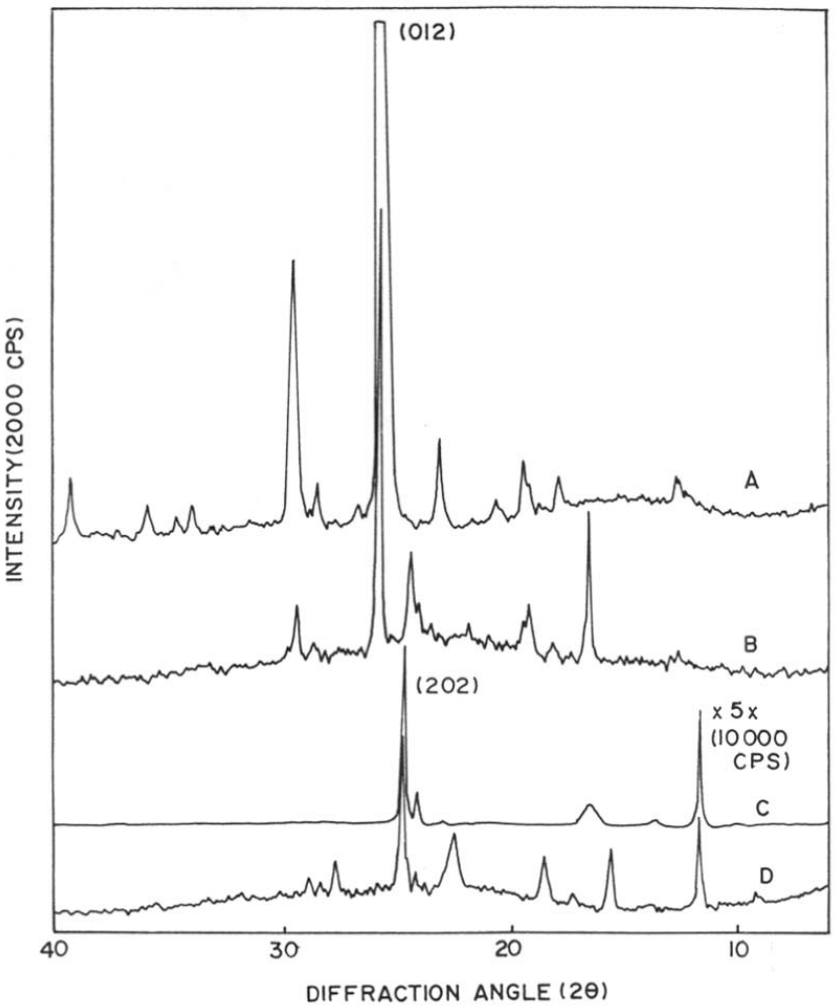

Figure 6.33 WAXD scans for (SC) samples containing same concentration of PNA (45%) grown in different polymer matrices. Curves A, B, C and D correspond to PMMA, PVAc , PVA and PEO as matrix respectively.

group of PMA. On the other hand, PEO is known to form complexes with NH_2 containing compounds such as urea and one may expect a similar type of interaction in PEO-PNA.

Figure 6.34 shows the optical micrographs for the PNA-polymer composite films having 45% concentration of PNA but different polymer matrices: (a) PMMA, (b) PEO, (c) PVA and (d) PVAC respectively. The distinctly different morphological features obtained in each case are clearly revealed in these micrographs. These observations clearly demonstrate the important role of the polymer matrix together with its specific interaction in controlling the growth and morphology of the crystallizing component dispersed in it. The changes in the relative intensities in the XRD scans can be understood in terms of the placement of the crystallites with respect to the sample surface. It may be noted that these samples were in the form of films and XRD scans recorded in the reflection mode. Changes in the intensities of certain reflections will be expected when the crystallites have preferred growth direction/orientation with respect to the film surface.[55,56] The placement of the crystallite phases will be more randomly oriented in the case of spherulites than in the case of long needle shaped crystallites. In the latter case, the long axis would preferentially lie along the film surface. In the case of platelet morphology, the flat crystallite phases would tend to be along the film surface. It appears from the XRD scan in the present case that (bc) plane of the crystal is preferably along the film surface in PMMA-PNA and PVAC-PNA systems giving rise to a large increase of the (012) reflection while the (ac) plane of the crystals is along the film surface for PVA-PNA composite.

The exact mechanism by which the morphology of the crystals of the additives when grown in different polymers, is not yet fully understood. In the first instance, it may appear that the changes observed in the present studies could be due to the different solvents used. Recently Liu et al.[57] have reported the effect of solvents on the growth morphology of crystals. However, it can be seen that in the case of PEO and PVAC, the solvent used was the same (viz. methanol) but the X-ray diffraction shows large changes in the intensities of some peaks in the two cases. Similarly in the case of PMMA, the solvent used was acetone while that for PVA was acetone/water mixture but in these cases also no similarity is observed in the X-ray diffraction or morphology. Hence, it is confirmed that the effect of solvent cannot be the main cause for the changes observed in the present case. On the other hand, if one considers the molecular interactions between the guest and the host molecules, PMMA and PVAC both have C=O groups which can interact with the NH_2 groups of PNA and both the PMMA-PNA as well

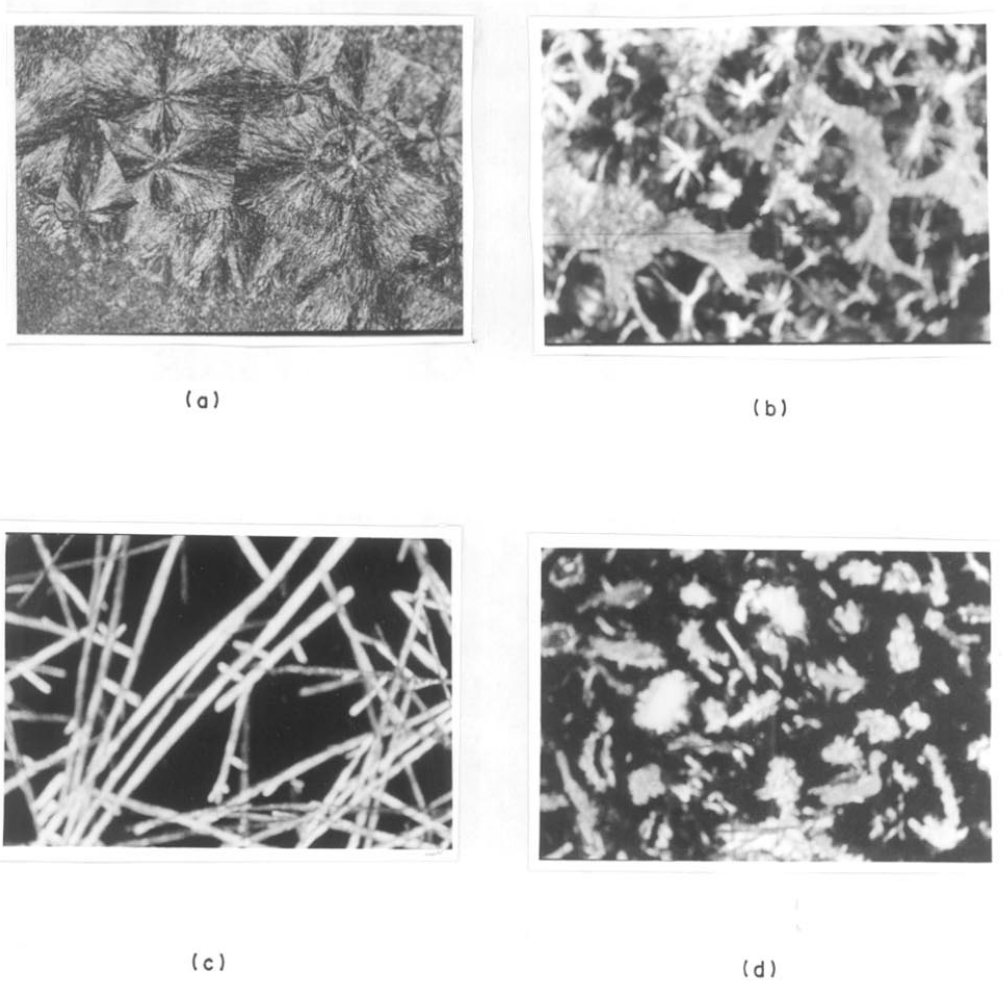

Figure 6.34 Optical micrographs for the polymer - PNA composite films with 45% PNA: (a) PMMA (b) PEO (c) PVA and (d) PVAc matrix respectively. (net magnification = 450x)

as PVAc-PNA composites exhibit very similar X-ray diffraction scans. These WAXD scans are quite different from those observed from PVA-PNA and PEO-PNA which have few common features. We have also used Pc as the matrix for dispersing PNA and in this case too, a single strong (012) peak of PNA was observed to emerge prominently at a concentration of 20% of PNA. This certainly points to the interaction between C=O and NH_2 groups as the source for the modification of growth pattern and /or the changes in the X-ray diffraction scans for these samples. Tentatively, one may consider that in the initial stages of film formation, PNA molecules are attracted selectively to the C=O groups of PMMA and juxtaposed in the perpendicular position of the main PMMA chain. The subsequent arrival of PNA molecules is constrained by this initial molecular recognition effect. Hence , only restricted growth of the crystals takes place constrained to certain directions. Such molecular recognition effects have been reported in the past for organic crystals (benzamide, glysine, cinnamic acid, etc).[58,59] It should be pointed out that the polymer used can also affect the rate of evaporation of the solvent. It may also contribute to the restriction in the diffusion of PNA molecules as the polymer solution thickens (possibly forming gel) during the film formation process.

6.4 Conclusions

In this study, dramatic changes on the structure and morphology of NLO crystals are seen to occur due to polymer induced crystallization. In the first section the molecular interaction between PNA and PEO occurring through hydrogen bonding between the ether group of PEO and the NH_2 group of PNA played an important role in the crystallization of NLO crystals. The good lattice match between the crystallizing components led to preferential growth of crystals along a certain direction. The same type of interaction (hydrogen bonding between C=O and NH_2) gave rise to formation of complex between PNA and PMMA as well as MNA with PMMA which gave rise to formation of new crystalline structure. In the last section, the role of polymer in modifying growth of crystals in constrained morphology for the same NLO crystal (PNA) dispersed in different polymer matrices is clearly brought out. Therefore, it is possible to enhance the optical properties (especially transparency) in NLO guest/host materials by choosing correct polymers as the growth media. Thus, polymer induced crystallization or polymer mediated growth can be effectively used for developing new materials with improved performance.

6.5 References

1. F. Hanson and D. Dick , Opt. Lett., **16** (1991) 205.
2. K.D. Singer, D. Kenneth , Opt. Eng., **32** (1992) 321.
3. K. Anderle, H. Bach , Th. Fuhrmann, J. H. Wendorff, Macromol. Symp., **101** (1996) 549
4. Baird , G. Donald , ACS Symp. Ser, **435** (1990) 416.
5. I. Ledoux , J. Badan , J. Zyss et al. , J. Opt. Soc. Am., $\mathbf{B_4}$ (1987) 987.
6. G.T. Boyd , J. Opt. Soc. Am., $\mathbf{B_6}$ (1989) 685.
7. S. R. Marder, J.E. Sohn and G.D. Stucky (eds) " Materials for Nonlinear Optics" (ACS, washington, DC, 1991).
8. C. Chen , Y.X. Fan, R.C. Eckardt and R.L. Byer , SPIE . Proc., **681** (1986) 12.
9. A.J. Campillo and C.L. Tang, Appl. Phys. Letts., **16** (1970) 242.
10. R.C. Eckardt , H. Masuda , Y. X. Fan and R.L. Byer , J. Quantum Electron. **26** (1990) 922.
11. S. Tripathy, E. Cavicchi , J. Kumar, R.S. Kumar, Chemtech , **19** (1989) 620; S. Tripathy , E. Cavicchi , J. Kumar , R.S. Kumar , Chemtech, **19** (1989) 747.
12. J. F. Nicoud , R. J. Twieg , Nonlinear Optical Properties of Organic Molecules and Crystals; Acedemic , Orlando, FL, **1** (1987) chapt.3.
13. D.F. Eaton, Science, **253** (1991) 281.
14. D. Morichere, V. Dentan, F. Kajzar, P. Robin, Y. Levy, M. Dumont, Optics Commun., **74** (1989) 68.
15. R. J. Twieg , K. Jain , Non linear Optical Properties of Organic and Polymeric Materials, ACS Symp. Ser., **233**; ACS Washington DC, (1982) chapt.3.
16. J. Zyss, I. Ledoux , Chem. Rev., **94** (1994) 77.
17. D. M. Walba , M. B. Ros , N. A. Clark , R. Shao, M. G. Robinson, J. Y. Liu. K. M. Johnson, D. J. Doroski , Am. Chem. Soc. **113** (1991) 547.
18. G. R. Meredith, J. G. Vandusen , D. J. Willams, Macromolecules, **15** (1982) 1385.
19. K. D. Singer, D. G. Sohn and S. J. Lalama , Appl. Phys. Lett. **49** (1986) 248.
20. M.G. Kuzyk, R. C. Moore and L. C. King, J. Opt. Soc. Am., $\mathbf{B_7}$ (1990) 64.
21. Y. Karakus , D. Bloor and G. H. Cross, J. Phys. D, Appl. Phys., **25** (1992) 1014.

22. J. R. Hill, P. L. Dunn, G.J. Davies, S.N. Oliver, P. Pantelis, J. D. Rush, Electronic Letts., **23 (13)** (1987) 700.

23. G. Khanarian et al., SPIE Proc., **682** (1987) 153.

24. M. J. Goodwin, G. Edge, C. Trundle and I. Bennion , J. Opt. Soc. Am., **B5** (1988) 419.

25. P. Pantelis , J. R. Hill, S.N. Oliver and G.J. Davies, Br. Telecom. Tech. J., **6** (1988) 5.

26. R. D. Small , K.D. Singer, J.E. Sohn. et al., SPIE Proc., **682** (1986) 160.

27. S. Esselin et al., SPIE Proc. **971** (1988) 120.

28. R. Glenn, M.J. Goodwin and C. Trundle, J. Mol. Elec., **3** (1987) 59.

29. N. Azoz, P. D. Calvert, M. Kadim, McCaffery, J. Anthony, R. Kenneth, Nature, **344** (1990) 49.

30. F. Wan, G.O. Carlisle, K. Koch and D.R. Martinez, J. Mater. Sci. Mater. Elec., **6** (1995) 228.

31. A. Suzuki , Y. Matsuoka , A. Ikushima, Nonlinear Opt. Proc. ,Toyota Conf. Nonlinear Opt. Mater. 5th (1992) 207, edited by S. Miyata.

32. T. Watanabe , K. Yoshinaga , D. Fichou and S. Miyata, J. Chem. Soc., Chem. Commun., **4** (1988) 250.

33. S. Miyata, E , Kachiki , M. Kagami , Watanabe, Toshiyuki, Japan Pat. 03,276,131 (91,276,131) 6 Dec. (1991).

34. S. Miyata , K. Yoshinaga, T. Miyazaki, Jpn. Pat. 6400,523 (89,00,523) 5 Jan. (1989).

35. B.K. Mandal, Y.M. Chen , R.J. Jeng , T. Takahashi, J.K. Huang, J. Kumar, S. Tripathy , Eur. Polym. J., **27** (1991) 735.

36. G. Cheng , Y. Xu , W. Wang , Z. Feng , Polym. Int., **35(3)** (1994) 273.

37. H.L. Hampsch , J. Yang , G. K. Wong , J.M. Torkelson , Polym. Comm., **30** (1989) 40.

38. A. Tracz, J..K. Jeska, E.I. Shafee, J. Ulanski and M. Kryszewski , J. Phys. D. (Appl. Phys), **19** (1986) 1047.

39. C.H. Choi, A. Tracz, J..K. Jeska, G. Boiteux , G. Seztre , J. Ulanski and M. Kryszewski , Synth. Met. **37** (1990) 181.

40. B. Wunderlich , Macromolecular Phys. **182**, Acedemic Press, New York (1976).

41. J. L. Thompson and A. A. VanRooyen , J. Mater. Sci. **27** (1992) 889.

42. H. Tadokoro, F. Yoshihara, Y. Chatani , S. Tahara and S. Murahast, Makmol. Chem. , **73** (1964) 104.

43. W. G. Wykoff, Crystal Structure, **6,** Wiley, New York (1969).

44. J. Schmierer , G. Jeffrey and G. J. Mc Carthy, Powder Diffr. **3** (1988) 98.

45. R.A. Hann and D. Bloor , Organic Materials for Non-linear Optics , Royal Soc. Of Chem., London (1989).

46. A. G. Walton , in Nucleation , Zettle Moyer , Ed; Marcel Dekker , New York (1969).

47. K. A. Mauritz , E. Baer and A.J.Hopfinger , J. Poly. Sci. Macromol. Rev.,**13** (1978) 1.

48. F. E. Bailey and H. G. France , J. Poly. Sci. , **49** (1961) 397.

49. H. Tadokoro , T. Yoshihara , Y. Chatani and S. Murahashi , J. Polym. Sci. **pt. B** (1964) 363.

50. R. W. Munn and C. N. Ironside , Principles and Applications of Non linear Optical Materials , Blackie Acedemic , London (1993) Chapt.7 p. 149.

51. A. R. Blythe , Electrical Properties of Polymers , Cambridge Univ. Press. (1979) p.130.

52. C. Saujanya , S. Radhakrishnan , J. Appl. Polym. Sci., **65** (1997) 1127.

53. H.K. Sinha and K. Yates, J. Am. Chem. Soc, **113** (1991) 6062.

54. C. S. Andrzej , J. of Chemical Society Perkin II, (1973) 1197.

55. L.E. Alexander, X-ray diffraction Methods in Polymer Science (Wiley, New York, 1969).

56. E. F. Kaelble , Handbook of X-rays, (Mc Graw Hill , New York, 1967).

57. X.Y.Liu , E.S. Boek , W. J. Briels and P. Bennema , Nature , **374** (1995) 342.

58. L. Weissbuch , L.Addadi , M. Lahav and L. Leiserowitz , Science , **253** (1991) 637.

59. J.D. Wright, Molecular Crystals, (cambridge Univ. Press, 1989) p. 108.

Chapter 7

Summary and Conclusions

There has been a tremendous surge of activity in the recent years for the synthesis of novel composites by *in situ* precipitation technique so as to mimic the naturally available composites as closely as possible. One of the methods for achieving the above objective has been based on polymer induced crystallization - a phenomenon observed recently by various researchers. Polymer induced crystallization plays a vital role in structure development through modification of crystal structure, domain size and morphology. Thus, it has become an important area in the context of production of smart materials, high- tech composites, nano technology, etc.

In the present studies, we have investigated the role of polymer matrix on the structure development in conventional composites such as PP filled with $CaSO_4$, glass fibres, thermoplastic elastomers, polyseter fibres as well as novel composites containing NLO crystals. The important role of matrix in controlling the structure and morphology of the composites has been clearly observed in all the systems studied.

The growth of an inorganic crystal in an organic polymer has been discussed in Chapter 3. The preparation of filler i.e. $CaSO_4$ by *in situ* deposition technique within a polymer matrix (PEO) and its effects on the crystallization behaviour and properties of PP have been given in section 3.3. The presence of PEO, when used as a growth medium for $CaSO_4$ shows remarkable changes on the crystal structure and morphology of the $CaSO_4$ crystals grown from PEO-$CaCl_2$. The dihydrate type with monoclinic configuration is obtained as compared to the anhydrite type with orthorhombic structure for commercial $CaSO_4$ sample without PEO. The crystal morphology consists of sharp needle shape having aspect ratio of 10. The concentration of polymer used during the *in situ* deposition technique shows a profound effect on the crystal size and distribution. The crystal size becomes narrow and the average crystal size reduces with the increase of polymer (PEO) concentration. The sheared samples show a high degree of orientation of needle shaped $CaSO_4$ crystals.

The effect of *in situ* formed $CaSO_4$ on the crystallization of PP revealed distinct features quite different from the commercial $CaSO_4$. The latter containing mainly the anhydrite form gives the α form of PP while the former $CaSO_4$ prepared by *in situ* method gets itself transformed from dihydrate to anhydrite γ form of $CaSO_4$ which in turn nucleates β form of PP during the isothermal crystallization from melt at 115°C. The presence of PEO, which is used for the *in situ* preparation of $CaSO_4$, is found to hinder the rate of crystallization of and nucleation of β form of PP. However, it gives a high degree of orientation in the $CaSO_4$ needle

like crystals during extrusion of PP-$CaSO_4$ composites. The comparison of skin and core layer of section of injection moulded specimens, reveals an enhancement of β phase in the core layer which is due to the presence of fibrous or needle shaped component.

The mechanical properties i.e. impact strength increases together with high crystallinity and high tensile modulus for one of the grades of $CaSO_4$ i.e. PP-CaS(ISW) as compared to pure PP. Thus, the $CaSO_4$ prepared by polymer induced growth is different in behaviour as additive in PP than the commercially available material.

The *in situ* fibre formation in PP/SBS has been distinctly observed and extensive fibre formation is found to occur at a certain composition (30% SBS). This was correlated with the polymer/polymer interaction, which was reflected by crystallization behaviour and nucleation. Enhanced crystallization rate and large changes in the intensities of XRD peaks are noted in the PP/SBS blends. The morphology of PP/SBS shows two types of spherulites: one similar to PP and the other much smaller in size having different internal morphological features. The mechanical properties show variation in association with the structure development in these blends. The impact strength increases to almost 8 times than that of pure PP at 40% SBS. The tensile modulus also improves considerably than that of expected modulus. These observations were associated to the fibrous morphology obtained at these compositions. Although a tremendous increase in the impact strength is observed in these blends, the corresponding tensile modulus decreases due to the presence of SBS. In order to improve the Young's modulus together with enhancement of impact strength, a hybrid composite using glass fibres was studied.

The studies on the structure and properties of PP/SBS/glass hybrid composites show both SBS and glass as good nucleating agents for PP. Further, the nucleation efficiency of glass fibres which is generally high, is seen to decrease at high concentration of SBS (≥30%) for PP which is explained on the basis of an intermediate layer formation of SBS between glass fibre and PP matrix. The morphology of fracture surface of injection moulded PP/SBS/glass shows good bonding between SBS and glass. The orientation of glass fibres is also seen in some of the injection moulded samples. The mechanical properties i.e. impact and tensile modulus in these hybrid composites show synergistic behaviour i.e. enormous elongation and toughness at certain composition of 30% SBS and 20% glass fibres in PP.

The investigations on the structure development at PP/PET interface and modification of properties in PET fibre filled PP composite revealed the crystallization and growth is

accompanied by transcrystalline morphology of PP at PET interface. The crystallization process in the transcrystalline zone is much faster than that in the bulk, showing lower $t_{1/2}$ values and higher crystallites at PP/PET interface. The presence of transcrystalline zone is associated with the row nucleation and growth of oriented crystallites of PP along PET fibre giving rise to large increase in the intensity of (040) reflection in the XRD pattern. However, the crystalline phase of PP remains monoclinic α type. The crystallinity (C_I) determined from the XRD graphs show higher values of the order 75% as compared to virgin PP (62%). The crystallization kinetics using Avrami equation, revealed a high value of Avrami constant n = 4 to 4.5 for transcrystalline phase which suggests heterogeneous nucleation and linear growth of crystallites.

The use of maleic anhydride as compatibilizer in these PP/PET composites on the other hand, shows no transcystalline morphology and gives α form of PP. However, the average spherulite size reduces considerably to almost 15μm as compared to pure PP (50 - 60 μm). The XRD patterns do not exhibit the high intensity of (040) peak and DSC studies clearly reveals the presence of transcrystalline layer for PP/PET as compared to PP-g-MA/PET. The SEM studies on fracture surface show strong fibre -matrix bonding for PP/PET containing MA but fibre pull out is noted for PP/PET without MA. The mechanical properties were also investigated for these composites. The tensile modulus increases for PP/PET composites due to high crystallinity, transcrystalline morphology and reinforcement effect of PET fibres. On the other hand, for PP-g-MA/PET, there is a slight increase, which can be explained on the basis of strong adhesion between the fibre and the matrix and high aspect ratio of the fibre. The impact strength also show improvement to almost 1.4 times that of pure PP for both PP/PET and PP-g-MA/PET composites.

The structure, growth and morphology of NLO crystals dispersed micro composites have been investigated with a view to understand the phenomena of matrix mediated growth of low molecular weight compounds. Many polymers were used as growth media as for example, PEO, PMMA, PVA, PVAc , etc and two low molecular weight organic compounds viz. PNA and MNA were used. All of these gave two phase morphology suggesting formation of microdispersed composites. In PEO-PNA composite system, the crystallization behaviour of PEO-PNA composites show large variation in the intensities of certain peaks in the XRD scans with respect to composition and method of crystallization used. In case of solution crystallized samples, the (101) reflection from PNA becomes high while the (012) reflection is suppressed especially at high concentration of PEO. The intensities of two major

peaks from the polymer crystallites, is also affected considerably. The melt crystallized samples show (012) reflection of PNA as the most intense while the (101) reflection is of medium level. The powder blended samples reveals birefringent crystallites dispersed in the spherulitic morphology of the PEO matrix in contrast to the weakly birefringent crystals of the additive itself. The results have been explained on the basis of intermolecular interaction as well as good lattice match between the crystallizing compounds leading to preferential growth of crystallites along a certain direction. The DSC thermograms show the presence of two distinct phases of composites. The IR spectroscopic studies reveal complex formation between PNA and PEO molecules.

The studies on PMMA containing PNA and MNA also revealed interesting features in the XRD patterns i.e. large variations in the intensities of various peaks. This can be associated with preferential direction of growth of these crystals. Both PNA and MNA in PMMA composite show transparency at low concentration of the additive up to 30% but it depends very much on the conditions of growth. The composite films crystallize in two crystalline forms: one containing original PNA or MNA crystals and the other consisting of a complex between the polymer and the dopant molecules. The latter has a new crystalline phase, which can be ascribed to the constrained growth due to bonding between PNA or MNA with PMMA chains. The DSC and IR analysis confirms complex formation. The morphological features are interesting wherein spherulitic morphology is seen at a critical concentration of PMMA-PNA (40% PNA) which could be due to the incorporation of amorphous component in the intercrystalline domains. The presence of strong intensity (020) reflection of monoclinic phase of PNA suggests strong orientation along ' b' axis for samples crystallized under electric field. The TEM analysis shows the crystallite size of 40nm for PNA and 15nm for MNA in PMMA matrix respectively.

The outstanding results in the present investigations were obtained when the growth of PNA dispersed in different polymer matrices was studied. These unequivocally brought out the role of polymer in matrix mediated growth. Distinctly different morphological features are seen in each case depending on the polymer matrix used. The crystal growth habit changes from globular to spherulitic or even fibre like, when the polymer matrix was changed from PVAc to PMMA, PEO or PVA. The changes in crystalline morphology were accompanied by very large variations in their XRD scans. The intensities of (202) and (012) reflections were found to vary considerably when the polymer used for growth medium was changed.

From these different investigations on various types of composites studied, it can be concluded that polymer induced crystallization plays a very important role in the structure and properties of different types of composites. It can act as a growth medium for the filler/additive; it can influence the crystallization at fibre-matrix interface or it can be a growth matrix for the guest/host systems. In all the systems studied, the importance of the interaction between the polymer matrix and the additive is clearly bought out. This interaction may be of different nature depending upon the type of additive and the polymer. For example, it may be hydrogen bonding type, it can be co-ordinated complex formation, donor- acceptor type or simply crystal lattice type. In each of the systems studied, one of these interactions plays more important role. Unusual morphological features and growth habits of crystals have been obtained due to this. These various changes in the supermolecular structure gives rise to prominent changes in the mechanical properties, optical and other properties of the composites which has been observed by us. Thus, polymer mediated crystallization can be effectively used for developing new materials with value addition and improved performance.

List of Publications

1. Matrix mediated control of morphology in PNA dispersed polymeric composites, S.Radhakrishnan and **C.Saujanya**, ***Material Letters,*** **28** (1996) 341.
2. Crystallization behaviour of polyethylene oxide/PNA microdispersed composites, **C.Saujanya** and S.Radhakrishnan , *J. Appl. Polym. Sci*, **65** (1997) 1127.
3. Structure development in PP/$CaSO_4$ composites Part I: Preparation of the filler by *in situ* technique, **C.Saujanya** and S.Radhakrishnan, *J.of Mater.Sci.,* **33** (1998) 1063.
4. Structure development in PP/$CaSO_4$ composites Part II: Effect of filler on the crystallization and morphology, S.Radhakrishnan and **C.Saujanya**, *J. of Mater. Sci* , **33** (1998) 1069.
5. Development of transcrystalline phase in PP at PET interface, **C.Saujanya** and S.Radhakrishnan, *Polymer*(1998) (communicated).
6. Structure and Properties of PP/$CaSO_4$ composites PartIII: Effect of filler grade on properties, **C.Saujanya** and S.Radhakrishnan, *J. of Mater. Sci.*, (1998) (communicated).
7. Structure, Growth and Morphology of PNA dispersed PMMA composite, **C.Saujanya** , A. Mitra and S. Radhakrishnan, *J. of Appl. Polym. Sci.* ,(1998) (communicated).

Patents

1. A process for preparation of modified PP moulding compound having high impact strength, S.Radhakrishnan, Anand Khare and **C.Saujanya**, Indian Pat. Appl. 2626/DEL/ 96 dated 29.11.96.
2. A process for preparation of PP moulding compound having high impact and tensile strength, S.Radhakrishnan and **C.Saujanya** , Indian Pat. Appl. NF 226/97 dated 1.9.97.
3. An improved process for preparing PP moulding compound having high impact strength, tensile strength and toughness value, S.Radhakrishnan and **C.Saujanya**, Indian Pat. Appl. NF 274/97 dated 9.10.97.